

OBSERVATOIRE DE PARIS

DOCTORAL SCHOOL

ASTRONOMY and ASTROPHYSICS OF ILE DE FRANCE

Observatoire de Paris-Meudon

Laboratoire Galaxies, Etoiles, Physique et Instrumentation - UMR 8111

THE S I S

presented to obtain the degree of

PhD of the Observatoire de Paris

Specialty : ASTRONOMY AND ASTROPHYSICS

by

Rodney DELGADO SERRANO

The Evolution of the Hubble Sequence: morpho-kinematics of distant galaxies

Examination board:

<i>President :</i>	Ana GOMEZ	Observatoire de Paris-Meudon
<i>Reviewers :</i>	Sidney VAN DEN BERGH	Dominion Astrophysical Observatory
	Denis BURGARELLA	Observatoire de Marseille Provence
<i>Examiners :</i>	Lia ATHANASSOULA	Observatoire de Marseille Provence
	Thierry CONTINI	Observatoire Midi-Pyrénées
<i>Supervisors :</i>	Francois HAMMER	Observatoire de Paris-Meudon
	Hector FLORES	Observatoire de Paris-Meudon

October 06, 2010

OBSERVATOIRE DE PARIS

DOCTORAL SCHOOL
ASTRONOMY and ASTROPHYSICS OF ILE DE FRANCE

Observatoire de Paris-Meudon
Laboratoire Galaxies, Étoiles, Physique et Instrumentation - UMR 8111

THESIS

presented to obtain the degree of
PhD of the Observatoire de Paris
Specialty : ASTRONOMY AND ASTROPHYSICS

by

Rodney DELGADO SERRANO

The Evolution of the Hubble Sequence: morpho-kinematics of distant galaxies

Examination board:

<i>President :</i>	Ana GOMEZ	Observatoire de Paris-Meudon
<i>Reviewers :</i>	Sidney VAN DEN BERGH	Dominion Astrophysical Observatory
	Denis BURGARELLA	Observatoire de Marseille Provence
<i>Examiners :</i>	Lia ATHANASSOULA	Observatoire de Marseille Provence
	Thierry CONTINI	Observatoire Midi-Pyrénées
<i>Supervisors :</i>	François HAMMER	Observatoire de Paris-Meudon
	Hector FLORIS	Observatoire de Paris-Meudon

October 06, 2010

Abstract

The main objective of my thesis was to provide us, for the first time, with a reliable view of the distant Hubble sequence, and its evolution over the past 6 Gyr. To achieve this goal, we have created a new morphological classification method which (1) includes all the available observational data, (2) can be easily reproduced, and (3) presents a negligible subjectivity. This method allows us to study homogeneously the morphology of local and distant galaxies, and has the main advantage of presenting a good correlation between the morphological type and dynamical state of each galaxy.

The first step has been to study the evolution of galaxies using the IMAGES survey. This survey allowed us to establish the kinematic state of distant galaxies, to study the chemical evolution of galaxies over the past 8 Gyr, and to test important dynamical relations such as the Tully-Fisher relation. The information gained from kinematics is, indeed, crucial to guarantee a robust understanding of the different physical processes leading to the present day Hubble sequence. Using Integral Field Spectroscopy, which provides a complete kinematic diagnosis, we have been able to test our new morphological classification against the kinematic state of each galaxy. We found that the morpho-kinematic correlation is much better using our classification than other morphological classifications. Applying our classification to a representative sample of galaxies at $z \sim 0.6$, we found that 4/5 of spiral galaxies are rotating disks, while more than 4/5 peculiar galaxies are not in a dynamical equilibrium.

Applying our morphological classification to a representative sample of both local and distant galaxies, having equivalent observational data, we obtained a Hubble sequence both in the local and distant Universe. We found that spiral galaxies were 5/2 times less abundant in the past, which is compensated exactly by the strong decrease by a factor 5 of peculiar galaxies, while the fractional number of elliptical and lenticular galaxies remains constant. It strongly suggests that more than half of the present-day spirals had peculiar morphologies, 6 Gyr ago.

Finally, I present further studies concerning the history of individual galaxies at $z < 1$, combining kinematic and morphological observations. I also present the first ever-estimated distant baryonic Tully-Fisher relation, which does not appear to evolve over the past 6 Gyr. In the coming years, our morphological classification and these studies will be extended to galaxies at $z \gg 1$, thanks to the future ELTs.

Keywords: Galaxy Formation and Evolution - Galaxy Morphology and kinematics.

Abstract

L'objectif principal de ma thèse était de fournir, pour la première fois, une vision fiable de la séquence de Hubble distante, et de son évolution au cours des dernières 6 milliards d'années. Pour atteindre cet objectif, nous avons construit une nouvelle classification morphologique qui (1) prend en compte toutes les données observationnelles disponibles, (2) peut être facilement reproduite, et (3) présente une subjectivité négligeable. Cette méthode peut être appliquée à l'étude morphologique des galaxies locales et distantes, et son principal avantage est de présenter une bonne corrélation entre le type morphologique et l'état dynamique de chaque galaxie.

La première étape a été d'étudier l'évolution des galaxies grâce au relevé IMAGES. Ce relevé nous a permis d'établir l'état cinématique des galaxies lointaines, d'étudier leur évolution chimique depuis 8 milliards d'années, et de tester des relations dynamiques importantes telles que celle de Tully-Fisher. La cinématique est, en effet, une information cruciale nécessaire pour garantir une compréhension solide des différents processus physiques conduisant à la séquence de Hubble actuelle. En utilisant la spectroscopie intégrale de champ, qui fournit un diagnostic cinématique complet, nous avons été en mesure de tester notre méthode de classification morphologique en fonction de l'état cinématique de chaque galaxie. En utilisant notre classification, nous avons trouvé une corrélation morpho-cinématique bien meilleur qu'avec d'autres classifications. En appliquant notre classification à un échantillon représentatif de galaxies à $z \sim 0.6$, nous avons constaté que 4/5 des galaxies spirales sont des disques en rotation, tandis que plus de 4/5 des galaxies particulières ne sont pas en équilibre dynamique.

En appliquant notre classification morphologique à deux échantillon représentatif de galaxies locales et distants, disposant des données observationnelles équivalentes, nous avons obtenu une séquence de Hubble dans l'Univers local et dans l'Univers distant. Nous avons trouvé que les galaxies spirales étaient 5/2 fois moins abondantes dans le passé, ce qui est compensé exactement par la forte diminution, par un facteur 5, des galaxies particulières, alors que la fraction de galaxies elliptiques et lenticulaires reste constante. Ce résultat suggère fortement que plus de la moitié des spirales d'aujourd'hui avait des morphologies particulières, 6 milliards d'années auparavant.

Enfin, je présente de nouvelles études concernant l'histoire de galaxies individuelles à $z < 1$, en combinant des observations morphologiques et cinématiques. Je présente aussi la première étude concernant la relation Tully-Fisher baryonique lointaine, qui montre une absence d'évolution depuis 6 milliards d'années. Dans les années à venir, notre classification morphologique et ces études seront étendues aux galaxies à $z \gg 1$, grâce aux futurs ELTs.

Keywords: Formation et Évolution des Galaxies - Morphologie et Cinématique des Galaxies.

Acknowledgment

First of all, I want to thank my parents, Wilfredo Delgado and Ana Matilde Serrano, my brother, Will, and my best friend (and now my wife), Jossela Calderón, for being unconditionally there with me.

I would like to also thank very much Francois Hammer and Hector Flores. Thank you for everything, for giving me the opportunity to be in this team, for trusting me the job I have done during these past few years, which finally succeeded to derive the first Distant Hubble Sequence with a highlighted A&A article and an ESA/NASA press release. Evidently, it was not so easy, but finally we could probe what we were looking for. Thank you very much Masters for all the knowledge you have shared with me and for teaching me all the meticulous details of the astronomical observations, which are not only "observations" but astronomical analytic examinations. Furthermore, thank you for giving me the opportunity to do observations at ESO in Chili. Anyway, you know this is not a goodbye.

Thanks to the DU at the Paris Observatory for letting me participate and help in such a formation, offering to students of different ages the opportunity to learn more about the world of astronomical analysis.

Thanks to my PhD friends: Raphael Galicher, Myriam Rodrigues, Loïc Le Tiran, Manuel González, Noah Schwartz, Pierre Inizan, Sandrine Guerlet, Jean Coupon, Carlos Correia, Pierre Guillard, with whom the idea of organizing conferences "by the PhD students, for the PhD students" of Île-de-France was born, creating thus the first Elbereth conferences (Elbereth 2008) with the help of the Paris Observatory (Gepi), IAP, ONERA, and Phase. Moreover, thanks to Jacqueline Plancy, Myriam Rodrigues, Raphael Galicher, Loïc Le Tiran, Daniel Rouan, Manuel González and Ivan Debono for letting me also participate and organize with them the "parrainage" of foreign PhD students at the doctoral school of Île-de-France. I hope such efforts will continue producing great results.

Special thanks to the "Uranoscope de France", the French Embassy in Panama, and the Technological University of Panama for their efforts in giving to Panama the first Panamanian Astronomical Observatory. It has been 10 long years, but we have finally succeeded. As the first director of the new Panama's Observatory, I will put all of my best to make it as good as everyone is expecting.

Thanks to the post-docs Mathieu Puech, Yanbin Yang, Paola di Matteo, Benoit Neichel, Isaura Fuentes and Sébastien Peirani, for the numerous rich discussions, and with whom I have learned a lot. In a similar way, thanks to Chantal Balkowsky, David Valls-Gabaud, Marc Huertas and Matthew Lehnert. Mathieu and Yanbin, who are not post-docs any more, thank you very much for your patience and for always having time for me.

Thanks to the PhD students Myriam Rodrigues, Loïc Le Tiran, Irene Balmes, Anand Raichoor, Rami Gasmi, Sylvain Fouquet and Yan Qu, the post-docs Jianling Wang and Susanna Vergani, the master student Karen Disseau, for the great moments we shared together, including the "tea time". Thanks to all the PhD and post-doc students of the

"Observatoire de Paris" I had the great opportunity to know and share quite important recreation times. Thanks to my thesis sister Myriam Rodrigues, with whom I have shared the office during these three years of PhD. Furthermore, thanks to the summer football team with whom I had great moments in our Observatory football field: Juan Cabrera, Xuhui Han, Rui Pinto, Joao Marques, Juan Gutierrez, Nicolas Vasset, Matteo Cerruti, Lorenzo Matteini, Julio Ramirez, Alberto Escalante, Alvaro Alvarez, and all the others. I also want to thank Vivienne Wild and Jaime Fields for having the kindness of reading my thesis and correcting the grammar and orthographic mistakes.

Of course I cannot forget to thank the incredible help of the Gepi and PhD school secretaries. I am thinking especially about Sabine Kimmel, Laurence Gareaux, Pascale Hammès, Pascale Lainé, Daniel Michoud, Jacqueline Plancy. Thank you for your friendship and your patience each time I went to ask for your help. Thanks also to Nadine Denis for all the support in the administration procedures during these last months of PhD.

I have also a very special thought for Ana Gomez, Christophe Sauty, Jacqueline Plancy and Sébastien Fontaine, whose great help and support was essential since I came to Paris for the first time. I cannot hide the sadness that leaving Paris, and the Paris Observatory, causes me. There are, a lot, a lot of things I am leaving here. It has been five years since I met Ana Gomez, Christophe Sauty and Jacqueline Plancy for the first time, during the reception for the new M1 students of the Paris Observatory, and six years since I met Sébastien. Do you remember that? Nevertheless, within this sadness, I am also very happy because I am going back to my country, with a lot of projects and responsibilities, to try to make a better Panama.

Thanks to SENACYT-IFHARU and the Technological University of Panama for the financial support during these five years. Of course, without it, I could not have come to the Paris Observatory, nor gained my PhD. A special thanks to Bernardo Fernandez, who has supported and helped me since I was a student at the University of Panama.

Finally, but no less importantly, I want to express my most sincere gratefulness to the members of my thesis jury for their comments and great interest. Please, let me give a special thanks to my reviewers, Sidney van den Bergh and Denis Burgarella, whose interest in my thesis was evidently enormous and with whom I had the great pleasure to share a lot of rich discussions through the numerous emails we interchanged.

I hope I did not forget anyone of those who were important during my five years in Paris. If I did, sorry for that, and be sure I will make it known.

Acknowledgment to http://olivier.commowick.org/thesis_template.php for providing the thesis template used here.

Contents

Abstract (English)	i
Abstract (French)	iii
Acknowledgment	v
I Galaxy evolution in a cosmological context	1
1 Cosmology and galaxy classification	3
1.1 From the Big-Bang to the formation of galaxies	3
1.1.1 The cosmological principle	5
1.2 Morphological classification of galaxies	8
1.2.1 Considerations on the classification of a galaxy sample . . .	9
1.2.2 The local Hubble sequence	12
1.2.3 De Vaucouleurs's Revised Classification Scheme	15
1.2.4 Yerkes's Classification Scheme	17
1.2.5 van den Bergh's Classification Scheme (DDO)	19
1.2.6 Discussion about the physical Hubble sequence	21
2 The galaxy formation and evolution	25
2.1 Downsizing: a scenario of galaxy formation or a natural consequence of the primordial collapse model?	26
2.2 Secular evolution	29
2.3 Violent encounters: major mergers	33
2.3.1 An observational scenario: "The Spiral Rebuilding"	34
2.4 Discussion	37
II Shape and evolution of galaxies as a witness of the Hubble sequence	39
3 Observables in galaxy morphology	41
3.1 The standard morphological classification method	41
3.2 Modern methods for the morphological analysis	43
3.2.1 The non-parametric methods	44
3.2.2 The parametric methods	47
3.2.3 The color information	50

4	Studying the morphological evolution	53
4.1	Morphological studies in the distant universe	53
4.1.1	Local universe	53
4.1.2	Distant Universe ($z \gtrsim 0.3$)	55
4.2	Need of representativeness	56
4.2.1	Sample representativeness and luminosity function	57
4.2.2	What are the galaxies responsible for the evolution?	58
III	Our approach: Looking for the evolution at $z < 1$	61
5	IMAGES	63
5.1	Introduction	63
5.2	The survey	70
5.3	Sample selection and representativeness	73
5.4	Results of the IMAGES survey	75
5.4.1	Kinematic evolution of galaxies since $z=1$	76
5.4.2	The morpho-kinematic correlation 6 Gyr ago	76
5.4.3	Chemical evolution of intermediate-mass galaxies since $z \sim 0.7$	77
5.5	Beyond the IMAGES survey	77
6	Reconstructing the distant Hubble sequence	79
6.1	Our galaxy sample	82
6.2	The parameters retrieval: analysis of the observables	82
6.2.1	The light profile analysis	83
6.2.2	Structural parameters	89
6.2.3	The color information	91
6.2.4	Bar inspection	94
6.2.5	Color determination	95
6.3	The morphological classification method	97
6.4	Results	98
6.4.1	Galaxy number density	98
6.4.2	Bar fractions	99
6.4.3	Color distribution	100
7	Conclusion and Discussion	105
7.1	Merger events and the baryonic Tully-Fisher relation	107
7.2	Prospectives	108
	Publication list	111

Appendix	115
A Cosmology: The history of the Universe and the formation of structures	115
A.1 The primordial collapse model	116
A.2 The hierarchical model	119
B Basic and short introduction to modern imagery and photometry	131
B.1 Filters and photometric calibration	132
B.2 The magnitude systems	134
C Kinematic studies of distant galaxies using integral field spectroscopy	137
C.1 Toward a kinematic classification of distant galaxies	137
C.2 The kinematic analysis using GIRAFFE	138
C.3 Some preliminary results	141
D Building an Observatory in Panama	149
D.1 A very short history	149
D.2 Location	150
D.3 General description	150
D.4 The Instruments	151
D.5 The Projects	151
Bibliography	155

List of Figures

1.1	Universe history: from the Big-Bang to the present galaxies	4
1.2	Λ CDM model simulation	5
1.3	Redshift galaxy distribution from the 2dFGRS	6
1.4	Comparison of galaxy redshift distribution between simulations and observations	7
1.5	Comparison between the power spectrum derived from a Λ CDM model and the values obtained by observations	8
1.6	Images of the same object with difference depth	12
1.7	Images of the Milky Way in different wavelength bands	13
1.8	Different appearances a galaxy could have if observed at different wavelengths	13
1.9	Hubble tuning-fork diagram (1936)	14
1.10	de Vaucouleurs morphological scheme (1959)	15
1.11	Table comparing Hubble's morphological types and de Vaucouleurs's ones	16
1.12	Images of NGC 6753 in different bands and with different instruments	17
1.13	Images of NGC 300 in different bands and with different instruments	19
1.14	Images of NGC 1300 in different bands and with different instruments	19
1.15	van den Bergh scheme of galaxy morphology	20
2.1	Evolution of the ETGs luminosity function with redshift	27
2.2	Morphological types of galaxies as a function of their rest-frame V-band absolute magnitude and U-V color	28
2.3	Schematic scenario of two bar episodes, and the corresponding phases for the AGN fueling	30
2.4	Bar fraction evolution with redshift	31
2.5	Major merger simulation	33
2.6	Spiral rebuilding scenario diagram	35
3.1	Example of images for the morphological classification by eye	43
3.2	Expected distribution of the different morphologies within the A-C plane	45
3.3	Distribution of a galaxy sample in the A-C plane from observations	46
3.4	Expected distribution of the different morphologies within the G-M ₂₀ plane and observations	47
3.5	Examples of bulge+disk decomposition	48
3.6	Example of color maps	50
4.1	SDSS 3-dimensional map of the galaxy redshift distribution	54

4.2	Number fraction of different morphologies vs redshift	56
4.3	Intermediate mass galaxies definition from a MDLFs plot	59
5.1	SFR evolution with redshift	65
5.2	TFR scatter at low and high redshift	67
5.3	Detection of anomalous rotating curves in local galaxies	68
5.4	Rotating curves with the respective galaxy images and its long-slit arrangement	69
5.5	GIRAFFE line analysis interface to measure the line wavelength and its FWHM	70
5.6	Illustration of FLAMES/GIRAFFE, installed on the UT2 at VLT .	71
5.7	Instruments used by IMAGES and the related observed quantities .	72
5.8	Schematic view of the Chandra Deep Field-South survey	72
5.9	EW[OII] histogram of the GTO galaxy sample	73
5.10	IMAGES galaxy sample representativeness	74
5.11	Kinematic evolution of galaxies over the past 6 Gyr	76
6.1	Color images of distant galaxies showing their huge variety of shapes and physical properties	81
6.2	Illustration of different galaxy parameters	84
6.3	Examples of bulge+disk Sersic profiles	85
6.4	Example of a galfit simulation for one galaxy in our sample	87
6.5	HST/ACS GOODS image from the ESO/GOODS project	88
6.6	Comparison of the χ^2_{red} parameter of two different galaxies	90
6.7	Example of Galfit result parameters from our morphological analysis	90
6.8	Display of our methodology to measure $R_{1/2}$	92
6.9	Example of color maps for two different galaxies in our morphological analysis methodology	93
6.10	Examples of color images we use in our morphological analysis methodology	94
6.11	IRAF/Ellipse analysis showing a bar detection	96
6.12	Scheme of the local Hubble sequence	97
6.13	Our morphological classification decision tree	98
6.14	Galaxies database created to gather all the galaxies information used during our classification methodology	99
6.15	Bar fraction density results from our local and distant representative samples	100
6.16	Morphological contamination in the so called "red sequence" shown by a 3D plot of the color distribution of our representative distant and local samples	102
6.17	Distant and Local Hubble sequences derived from our morphological study	103

7.1	IMAGES results diagram from different instrument observations . .	106
A.1	Illustration of the Top-Down model	116
A.2	CMB map observed by COBE	117
A.3	Photo of one part of the Super-Kamiokande	118
A.4	CDM model simulations	121
A.5	Different CDM models simulations at $z=0$	122
A.6	Illustration of the Millenium simulation	123
A.7	3D dark matter simulation showing the structure formation in the gaseous component of the universe	124
A.8	Illustration of the primordial scalar field fluctuations	125
A.9	The abundance of the main four light elements vs. baryon density in the Universe, as predicted by the theory	126
A.10	CMB observations from WMAP5	127
A.11	Simulated galaxies in the Λ CDM model	128
A.12	Artistic view of the Universe history	129
B.1	CCD diagram to illustrate how it works	132
B.2	Response curve for different filters	133
C.1	Examples of different kinematic classes	138
C.2	OII GIRAFFE detection data-cube	139
C.3	Spatial data-cube for a low redshift galaxy ($z=0.14$)	140
C.4	Example of a velocity field from FLAMES/GIRAFFE	141
C.5	HST/ACS image, velocity field, FWHM map (sigma-map), and S/N map for one galaxy	142
C.6	Preliminary results: Tully-Fisher relation	143
C.7	3D kinematic analysis of $M_B < -16.40$ galaxies	143
D.1	Panama observatory - Location	150
D.2	Panama observatory - Architectural scheme	151
D.3	Observatories international network	152
D.4	Panama observatory - on March 2010	153
D.5	Panama observatory - on July 2010	154

List of Tables

1.1	Galaxy properties vs morphology	22
B.1	Magnitude AB of the star Vega	136

Part I

Galaxy evolution in a cosmological context

Cosmology and galaxy classification

Contents

2.1	Downsizing: a scenario of galaxy formation or a natural consequence of the primordial collapse model?	26
2.2	Secular evolution	29
2.3	Violent encounters: major mergers	33
2.3.1	An observational scenario: "The Spiral Rebuilding"	34
2.4	Discussion	37

1.1 From the Big-Bang to the formation of galaxies

In appendix A, I make a more detailed explanation of the different approaches attempting to explain the evolution of the Universe from its "beginning" until the present (see figure 1.1), as well as the principal models explaining the formation of the different structures of the Universe. In this section (and in appendix A), I refer especially to a framework based on the Big-Bang theory, which generally explain the evolution of the Universe beginning by a big "explosion", and a subsequent expansion (which continues infinitely, or later becomes a contraction with a Big-Crunch end). This theory is the more accepted within the scientific community until the present days.

There are two principal model developed in order to explain the formation of large and small structures in the Universe: the "primordial collapse model" (PCM), and the "hierarchical model" (HM). Both of them confront each other. The PCM proposes a *top-down* configuration, with the larger structures forming first and evolving to form the smaller ones. The HM has been developed with a *bottom-up* configuration: the smaller structures form first, and evolve to form the largest ones. However, it is the observational cosmology which has the last word. It seems that a large part of observational results support the hierarchical model (see appendix A). Nonetheless, such a theoretical scenario has evolved significantly since its creation (in the 60s) until the present days, in order to establish the best possible combination of parameters in agreement with the existing observational

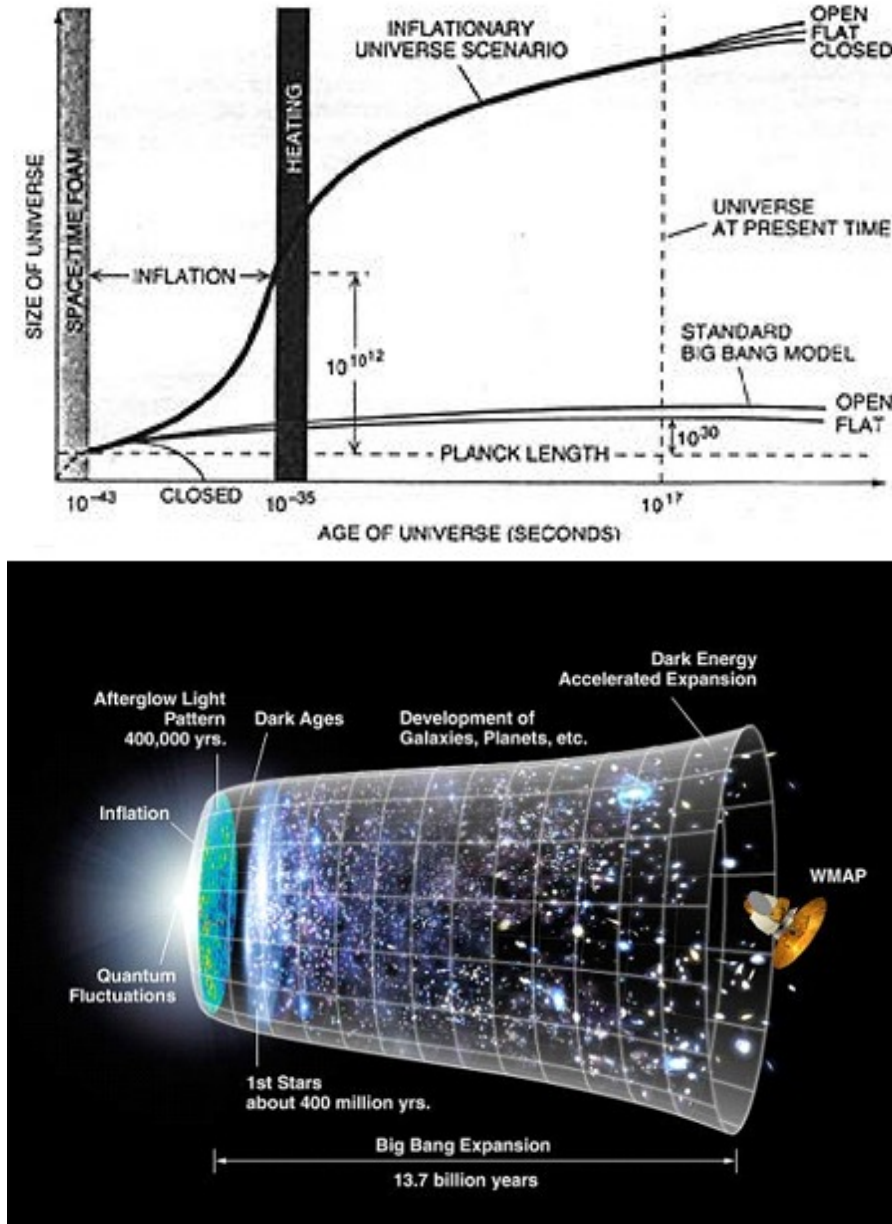


Figure 1.1: *Top*: plot showing the Universe evolution scenario (see details in appendix A). *Bottom*: an artistic view of the Universe history, from the Big-Bang, through the inflation and the emission of the present Cosmic Microwave Background (CMB), until the present galaxies (Credit: NASA/WMAP Science Team).

data.

Nowadays the most accepted model, adopted by a large part of the scientific community, is the so called Λ CDM (Lambda-Cold Dark Matter) model (see figure 1.2). It is an extension of the original CDM model proposed in the 80s (e.g., Primack & Blumenthal, 1984), even though it includes new parameter values to

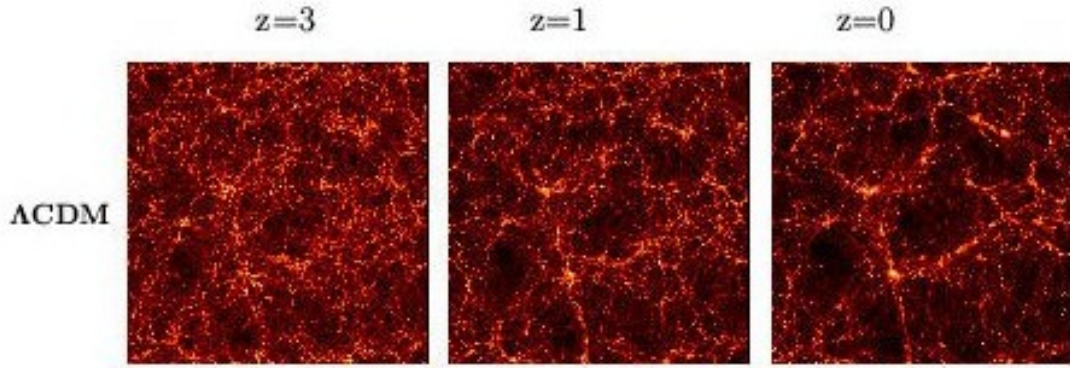


Figure 1.2: Λ CDM model simulation on the Virgo cluster (Jenkins *et al.*, 1998; Thomas *et al.*, 1998, for the Virgo Supercomputing Consortium).

be in agreement with the most recent observations. The Λ CDM model supposes an expanding Universe composed of baryonic and cold dark matter (see appendix A). Such an expansion is accelerating thanks to a certain dark energy, which is represented by the cosmological constant Λ . This scenario predicts that the first baryonic structures to be formed have a typical size of the present globular clusters (10^5 - $10^6 M_\odot$). Interestingly, these are also known to be amongst the oldest objects in the Universe. Inside these halos of baryonic matter, the first stars are formed. Then, such structures evolve to form the largest ones (see more details in appendix A).

1.1.1 The cosmological principle

This principle states that the Universe is homogeneous and isotropic. The first property refers to the fact that, at a given time, all points in the Universe are equivalent to each other. The second one means that the Universe looks the same in all directions. These two properties drive us to the original statement of the cosmological principle: "we do not live at a privileged location in the Universe". Even if, at first glance, the Universe is not strictly homogeneous and isotropic (for example, if we only consider the Solar System, or the Galaxy), it appears to be so, with a good approximation, on sufficiently large scales.

However, the last affirmation in the precedent paragraph does not seem to be the case either. During decades, astronomers have been compiling catalogs giving the positions and magnitudes of galaxies. The result is showed in figure 1.3. As we can see galaxies appear to lie along filaments or within flattened structures (sheets) separated by voids. Moreover, concerning the isotropy of the Universe, one can well imagine that an observer traveling very fast with respect to the local

matter will see galaxies (until a certain scale) moving toward him in one direction and away from him in another direction. The isotropic property of the Universe is thus not true for all observers. In addition to the above, one must consider that the Universe evolves, while we are observing it at different epochs.

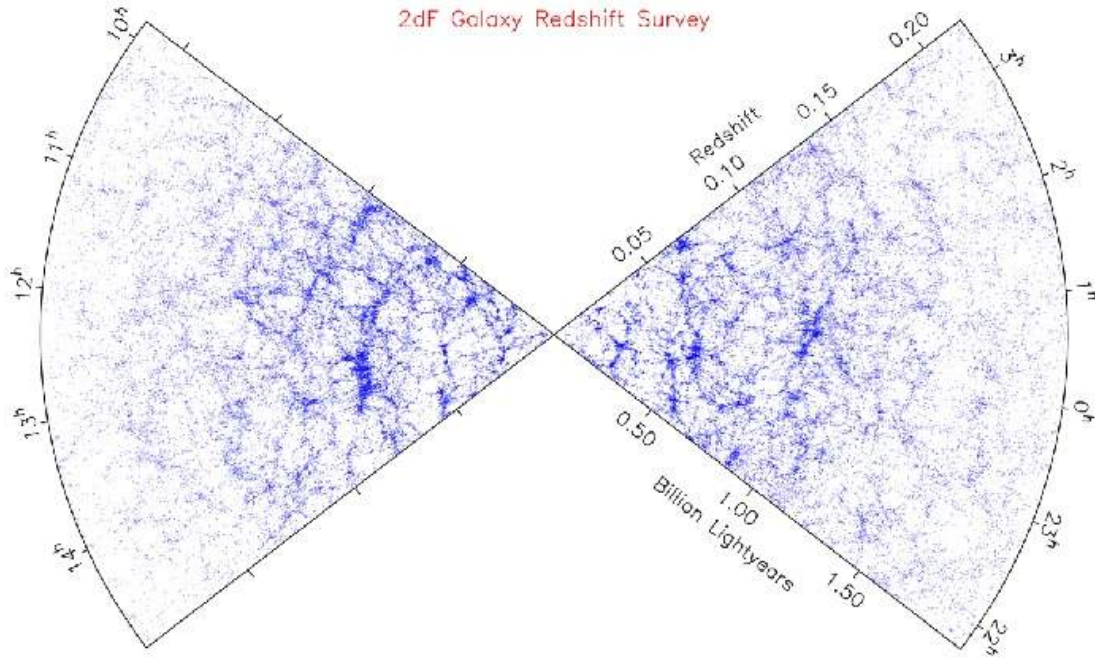


Figure 1.3: Image showing the distribution of galaxies in a redshift cone from the 2dFGRS (2 degree Field Galaxy Redshift Survey)(Colless *et al.*, 2001).

Is therefore the cosmological principle wrong? No, because of the following reasons. On the one hand, one must replace the classic idea of homogeneity by the notion of "statistical homogeneity" (whereby the distribution is smooth only in an average sense), as well as understand how the Universe deviates from perfect smoothness. In this context, if we have a homogeneous distribution and we add deviations on it, which we could call inhomogeneities, then this will cause differences between locations to appear by chance, and any statistical measure of the inhomogeneities is independent of position (Liddle & Loveday, 2008). As an example, we can consider two people rolling two dice (each one) a large number of times. Even if their individual sequences will differ, they will still share statistical properties such as the mean value and its standard deviation (Liddle & Loveday, 2008). On the other hand, one also must consider that random velocities of galaxies, as well as the velocities of the stars inside them, are small if we compare these velocities to the relative velocities of galaxies separated by larger distances (\sim several tens of Mpc). Thus, any observer looking at the Universe at sufficiently large scales is, in a good approximation, a fundamental observer.

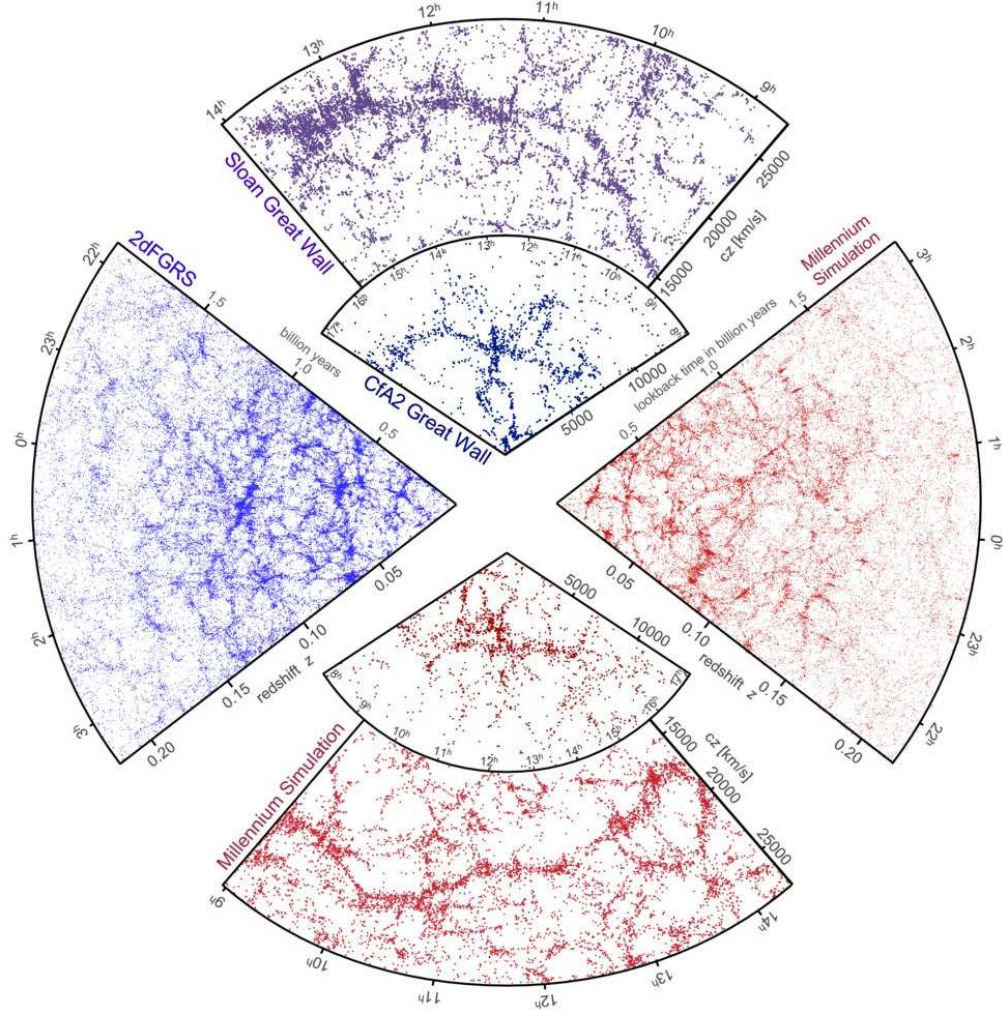


Figure 1.4: Comparison of galaxy redshift distribution between simulations (in red) and observations (in blue) (Springel *et al.*, 2006).

Therefore, based on Gunn (1978), we can rewrite the cosmological principle as follows: the Universe appears statistically homogeneous and isotropic to all fundamental observers at a given cosmic time. Two important observations in agreement with this are the CMB (see figure A.10) and the fact that the Hubble law seems to be independent of the direction of observation. Furthermore, the well known Λ CDM model simulations (see section A.2) are in good approximation with observations of large scale structures (see figure 1.4 and 1.5).

This fundamental principle thus allows us to connect distant objects to local ones. This is a key condition for the goal I wanted to reach with my thesis, which assumes that galaxies seen at a look-back time of ~ 6.5 Gyr are the progenitors of the present-day Hubble sequence (see chapter 6). Therefore,

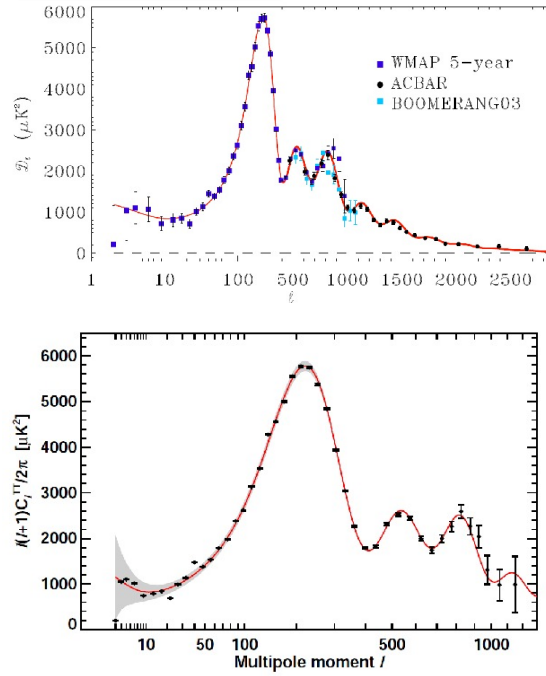


Figure 1.5: *Left*: Comparison between the temperature anisotropy power spectrum derived from the Λ CDM model and values from WMAP5, BOOMERANG and ACBAR observations (Reichardt *et al.*, 2009)(see also Challinor & Peiris, 2009, for a general explanation). *Right*: Comparison between the temperature anisotropy power spectrum derived from the Λ CDM model and values determined from seven years of WMAP data (Larson *et al.*, 2010).

the cosmological principle allows us to link these two epochs independently of the line of sight¹, establishing that one can compare distant galaxies and local ones.

1.2 Morphological classification of galaxies

Galaxies are complex objects containing several tens of billions stars, as well as gas and dust. Present-day galaxies are regular and relaxed systems, and are made of a dispersion-supported bulge surrounded by a rotationally-supported disk. They all fit into the initial morphological scheme proposed by Hubble (1926), which is called the Hubble sequence and will be described below.

A morphological classification of galaxies lies in classifying galaxy shapes on the basis of their images. Looking for some similar features, we can separate galaxies into different groups. However, if we want to catch a physical meaning, this task is much more complicated than it could be expected at first glance.

¹However, the problem of the cosmic variance still remains to be solved.

Before starting to talk about the morphological classification of galaxies some questions need to be answered: how we define the sample?, is this sample representative of one or all kinds of galaxy populations?, which methodology should be used to classify the galaxy morphologies?, which parameters will be included in such methodology?, can it be reproduced in other samples?, and can it be independent of human judgment (opinion)?

1.2.1 Considerations on the classification of a galaxy sample

Since the beginning of the past century, astronomers have been gathering images of galaxies from the Local Universe (and very recently from the Distant Universe). The number of Local galaxies being photographed have thus increased enormously from a few hundreds in the 1920s (Hubble, 1926)² to almost a million in the 2000s (e.g., de Vaucouleurs *et al.*, 1991,³ and the SDSS catalog). We can then infer that compared to the "sample" of local galaxies existing in the 1920s, at present we now have available a truly exhaustive "library" of Local galaxies.

The methodology followed by Hubble to classify the morphology of galaxies was the simplest one. He first separated objects with regular forms from those with irregular ones, these last representing 2 or 3 per cent of his sample. He then separated the regular objects in different groups, each one following a common feature. This gave two main groups: elliptical and spiral galaxies. Finally, he subdivided each group in subgroups (see subsection 1.2.2). At this stage, one can ask oneself if there could be some kinds of galaxy morphology that could be missed in the relative small Hubble's sample, as he did not have access to the whole library of the local galaxies. Indeed, if we consider that lenticular galaxies were added after Hubble papers, we could consider so. However, it was just a problem of definition (Sandage *et al.*, 1975; van den Bergh, 2009). Then, we can conclude that, thanks to the cosmological principle, the probability of missing some morphological types is very small (even if the size of the sample is relatively small and the sky zone being observed is limited)⁴. Nonetheless, Impey *et al.*

²I refer here to galaxy images with enough resolution and surface brightness to be morphologically classified. Galaxies have been photographed since the 18th century, as they were among the objects known as "nebulae" in the Messier catalog (1784). Furthermore, Sir William Herschel (1738-1822) and his son, Sir John (1792-1871), constructed a larger catalog (the first of the entire -north and south- sky) of about 4 630 nebulae (1864), which was replaced later by the Dreyer's New General Catalog (NGC) in 1890.

³The Third Reference Catalog of Bright Galaxies.

⁴For example, if we consider only the elliptical galaxies, which represent the smallest fraction ($\sim 3\%$) of the local galaxy population (see chapter 6), the probability of Hubble (1926), using a sample of 400 galaxies, to miss the elliptical population is roughly 0.000005. Note that if we consider the elliptical/lenticular population with a fraction of $\sim 17\%$, following the Shapley-

(1996), by studying a sample of faint galaxies, concluded that when samples are limited by a selection bias (the flux in this case), they can exclude large number of objects having structures which may be important for the understanding of the galaxy evolution (rings, bars, etc.). Taking into account that the main selection bias during the beginning of the past century was the surface brightness limit imposed by the small telescope diameters at such epochs, it explains the evolution of the local Hubble sequence diagram from 1936 (*The Realm of the Nebulae* by Hubble⁵) to the revised one by de Vaucouleurs (1959) (see subsections 1.2.2 and 1.2.3).

A fundamental consideration when studying a sample of galaxies is therefore: "**the selection criteria**". Rather than being only concerned by the number of galaxies in the sample, could a selection criterion lead to a representative sample⁶ that misses a galaxy type population (e.g., E/S0 galaxies)? Yes, it does. One example I experienced myself during my thesis is the comparison of the work we made in Neichel *et al.* (2008) and that in Delgado-Serrano *et al.* (2010) (see chapters 5 and 6). By taking a selection criterion (equivalent width of the O[II] emission line larger than 15\AA), which is not related to the morphology of galaxies, we found in Neichel *et al.* only spiral and peculiar galaxies. This further influenced the methodology used to classify the galaxies defined in both papers, which was limited in the first one. Therefore, the definition of a specific selection criterion can lead to a specific sample of galaxy images, which could miss some morphological types populations, and even could affect the methodology defined for the galaxy classification.

The classification methodology could also be affected by the observational data available. One example is the comparison between a sample of galaxies where each galaxy has images with different filters, and another sample where each galaxy has only one filter observation. In the first case, the color of each galaxy could play an important role in the classification process, while in the second case, the color is not taken into account.

Additionally to the above reflections, I want to draw the reader's attention to the characteristics of the images used to classify galaxies. Images play the main role for the morphological classification process, and should be considered seriously:

- Depth: Figure 1.6 shows two images of the same galaxy with identical scale

Ames Catalog, the probability of missing such a population by Hubble goes down to 4.28×10^{-33} . I assumed here that galaxies are randomly distributed over the whole sky.

⁵Hubble (1936).

⁶see subsection 4.2 for a discussion about the representativeness of a sample, and its possible effects on the galaxy evolution studies.

and orientation. Nevertheless, as we can see, one could think that these two images illustrate two different objects. Thus, morphological classification strongly depends on depth.

- **Wavelength range:** Observations of the same galaxy in different wavebands reveals different information, as it is shown in figures 1.7 and 1.8. Therefore, even if each band image is very useful to study and to better understand all the components of a particular galaxy, there is no meaning in comparing two galaxies using different bands. If such was the case, one could classify nearly identical objects in different classes just because we are not comparing the same information. This problem should be treated carefully when comparing galaxies at different redshifts, since the Doppler effect⁷ shifts the observable wavelength compared to the rest-frame wavelength. For example, an R-band (SDSS) image for a local galaxy and a z-band (ACS/HST) for a galaxy at $z=0.7$ allows us to sample the same rest-frame wavelengths.
- **Resolution:** The spatial resolution of the images can also change the way we can see a galaxy. It depends on the PSF (FWHM), which gives the smallest resolution element of the observation. Evidently, for a given galaxy, the better the spatial resolution of its images, the better the details we can distinguish on it. Therefore, if we compare two different galaxies with different spatial resolution images, we are not looking at the same degree of details⁸. As a consequence, we may not be "measuring" the same information. Furthermore, if the galaxies are at different redshift (distances), one must pay attention to make the difference between the angular spatial resolution (arcsec/pixel) of the instrument, and the linear proper spatial resolution (kpc/resolution element) of the galaxy being observed.

The last considerations to be evoked here is the reproducibility and subjectivity of the morphological classification method. For this, I just want to draw the reader's attention on the study carried out by Naim *et al.* (1995). They took 831 galaxies to be morphologically classified (by eye) by six astronomers, investigating the question whether different astronomers place a given object in the same class when they work from identical material. Interestingly, in many cases, two astronomers placed the same galaxy in different classes with a non-negligible scatter. I could call this the *Human Feeling (HF) bias*. Such a HF bias makes advisable to look for a quantitative analysis which could verify the qualitative one.

Finally, according to the above considerations for a morphological classification of galaxies, I can cite the following conclusions:

⁷Note: "Doppler effect" isn't really correct, as the "cosmological redshift" has the same effect as the Doppler effect but the cause (an expanding Universe) is completely different.

⁸such details will also depend on the number of photons by element of resolution, which depend on the exposition time, and is defined by the "Depth" of the image.

- (1) any galaxy sample must be homogeneous, in the sense that all galaxies in it must have the same kind of information,
- (2) the criteria used to separate the galaxy morphologies into classes must lead to a unique classification, making it a reproducible process. When different parameters are used, the order of their application must be carefully established to reduce its inherent subjectivity (to avoid that a same galaxy could be placed into more than one class). With this objective, the parameters should also be quantifiable.
- (3) Such parameters should be as close as possible to physical properties (e.g., D/T , which represents the ratio of the disk flux to the total galaxy flux, is correlated with the amount of rotational support).

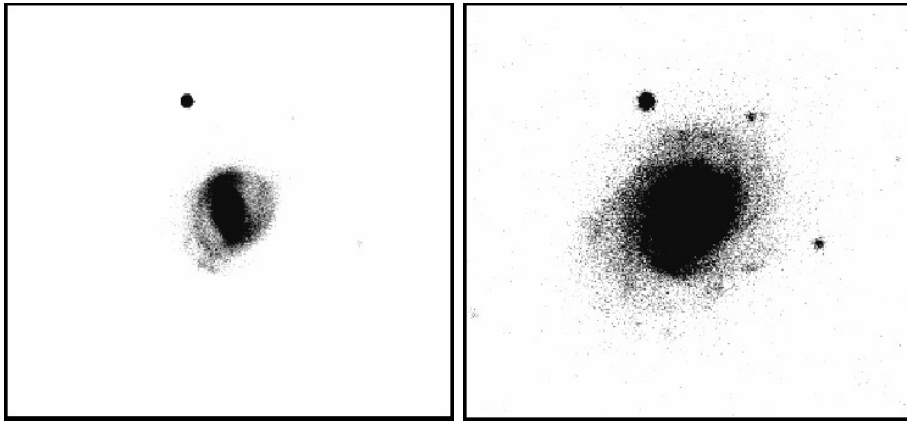


Figure 1.6: The difference in depth of images of the same object could imply a different morphological classification. As an example, I show here the same galaxy image from the SDSS. Only by playing with the contrast, we could think they are two different galaxies.

Since the last century, different propositions for the morphological classification of galaxies have been built up. Even if they all share Hubble's original notion⁹, each of them has its special characteristics. The most relevant ones are presented below.

1.2.2 The local Hubble sequence

The most used morphological classification scheme is the "Hubble sequence", which was initially introduced by Hubble (1926). In his first version, based on the optical appearance of galaxy images on photographic plates, Hubble proposed three general classes: ellipticals (En^{10}), spirals (S or SB¹¹), and irregulars (Irr).

⁹the morphological sequence should attest to an underlying sequence of numerous physical processes

¹⁰ $n=1,2,\dots,7$ indicates the ellipticity of the galaxy

¹¹B identifies a spiral galaxy with a bar in the center

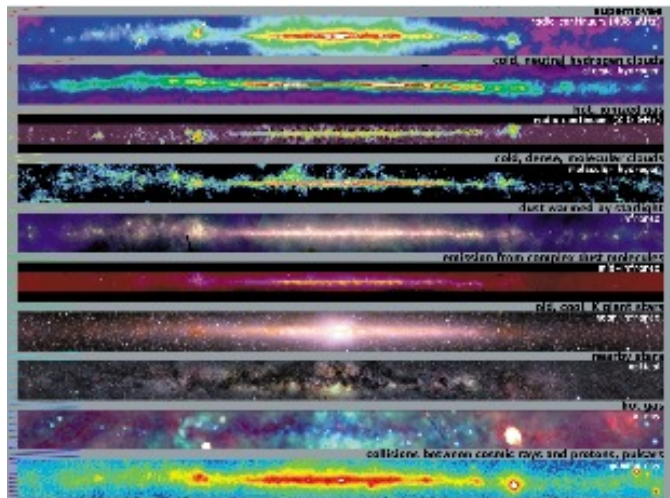


Figure 1.7: Images of the Milky Way in different wavelength bands. As we can see, each band gives us different information about a galaxy. (Credit: <http://www.astro.wisc.edu/>).

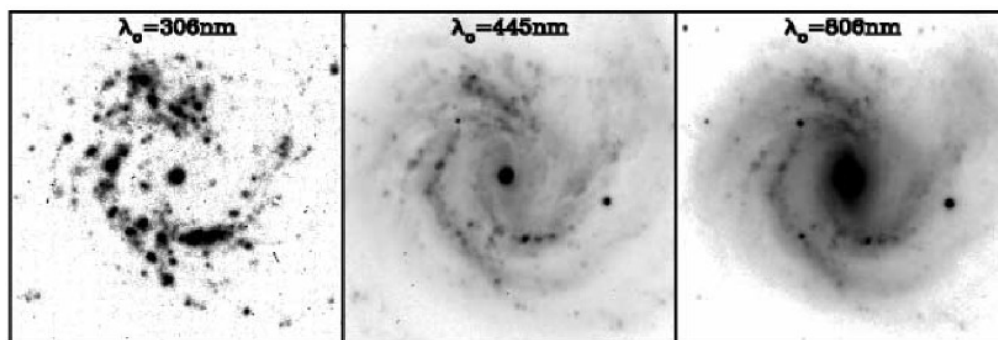


Figure 1.8: Different appearances a galaxy could have if observed at different wavelengths from Sheth *et al.* (2003). From left to right: NGC 4303 in UV, B-band, and I-band, respectively.

In 1936¹², he presented the first "Hubble tuning-fork diagram", as it is shown in figure 1.9. Here, Hubble added the "more or less hypothetical type S0", presented as a necessary intermediate state between early type galaxies (ellipticals) and late types galaxies (spirals). The final Hubble sequence thus consisted of four galaxy types: elliptical (E), lenticular (S0), spiral (S or SB), and irregular (Irr). However, this last type of galaxies (irregulars) was considered at that time as not finding a "place in the sequence of classification" because they "show no evidence of rotational symmetry". For this reason it does not appear in the original diagram (figure 1.9). It is important to note that in 1936 scientists believed that the Hubble diagram revealed a time evolution of galaxies, and it was thus called "a sequence". Indeed, it was believed that "elliptical galaxies formed first in the

¹²in his book *The Realm of the Nebulae*

universe history and becomes spirals with time, but after being lenticulars". We keep calling elliptical galaxies as early type galaxies and spiral galaxies as late type galaxies for this reason.

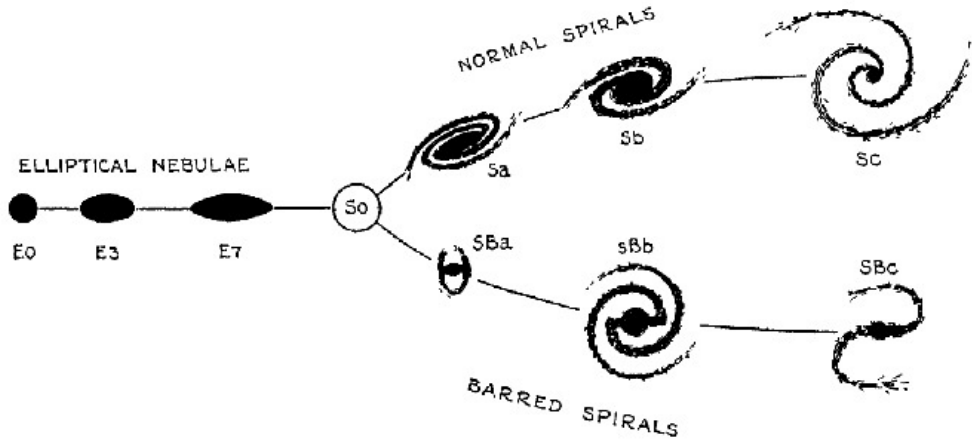


Figure 1.9: This is "The Sequence of Nebular Types" diagram published by Hubble (1936).

Later studies developed a more detailed Hubble diagram (e.g., Sandage *et al.*, 1975; Sandage & Tammann, 1981; Sandage & Bedke, 1994) using larger catalogs of galaxies. However, they all follow the same principle: galaxies are organised from pure bulges (ellipticals) to increasing disk contribution to their light or mass (S0 to Sc). Contrary to figure 1.9, in these later diagrams real examples of S0 galaxies are found.

The main types in this classification are the following:

- Ellipticals: these galaxies are characterized by their ellipticity $e=(a-b/a)$, where a and b are respectively the major and minor axes of the ellipse formed by the projection of the galaxy on the sky's plane. They are also noted as E_n , where $n=10e$ (n value goes from 0 to 7).
- Lenticulars: S0 galaxies guarantee the transition between elliptical and spiral galaxies. They have a bulge and a disk. Nevertheless, they don't present spiral arms.
- Spirals: they are composed by a bulge and a disk, and this latter (the disk) could present spiral arms which are attached to the bulge. For instant, this type of galaxies can be divided in subclasses (Sa to Sd) according to the increase resolution of spiral arms and the decrease importance of the bulge compared to the disk.

- Irregulars: Originally, these galaxies were separated from the others mainly because of the absence of a rotational symmetry (Hubble, 1936). Morphologically, these objects are characterized by a lack of a conspicuous nuclei and/or by a non symmetric shape.

1.2.3 De Vaucouleurs's Revised Classification Scheme

de Vaucouleurs (1959)¹³ classification keeps the basic division of Hubble one. However, he introduced a more detailed classification for spiral galaxies, since there are at least three more characteristics which deserve more attention: bars, rings, and the spiral arms. It is a consistent scheme which includes all or most of the recent revisions and additions to the standard classification. While the Hubble's diagram is two dimensional, de Vaucouleurs developed a classification that can be seen as three dimensional (see figure 1.10). This new "classification volume" is explained in the following.

The presence of a bar is noted by a "B", while its absence by an "A". Then, a spiral galaxy is represented by "SB" or "SA" when it has or not a bar in its center, respectively. An "SBA" representation is adopted as intermediate class, when the galaxy has mixed characteristics (weakly barred). Similarly, lenticular galaxies could be "SA0" (unbarred), "SB0" (barred) or SAB0 (intermediate class). However, when it is impossible to tell if the galaxy has a bar or not, it is noted only by an "S" in the case of a spiral galaxy or by "S0" if the galaxy is lenticular.

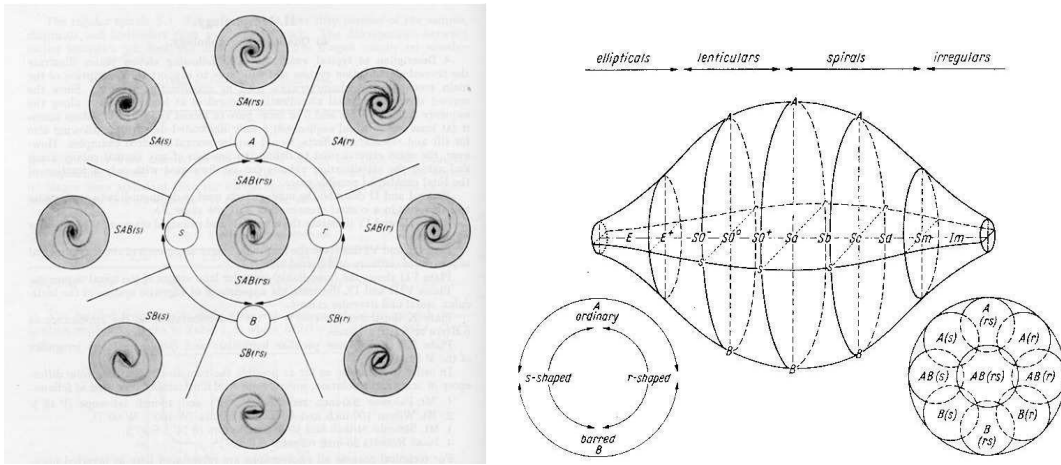


Figure 1.10: This is "The Sequence of Nebular Types" diagram published by de Vaucouleurs in 1959 as part of his article *Classification and Morphology of External Galaxies*.

¹³"Classification and Morphology of External Galaxies", where he also makes a remarkable summary of almost all the galaxy classification history until 1959.

The presence of a ring is distinguished with an "(r)", while its absence with an (s). An intermediate type is noted (rs). Nevertheless, de Vaucouleurs expressed himself that the "(s)" symbol warns, more exactly, about the presence of spirals (an "S-shaped" type). Then, the "distinction between the two families A and B and between the two varieties (r) and (s) is most clearly marked at the transition stage S0/a between the S0 and S classes. It vanishes at the transition stage between E and S0 on the one hand, and at the transition stage between S and I on the other" (see figure 1.10).

Taking into account the tightness of the spiral arms, de Vaucouleurs extends the Hubble's diagram. After de Vaucouleurs, we can distinguish four stages along each of the four spiral principal sequences SA(r), SA(s), SB(r), SB(s), noted a, b, c, d for "early", "intermediate", "late" and "very late". Intermediate stages are Sab, Sbc, Scd. We can thus have, for example, a SB(s)c or a SA(r)ab types. For the transition to the magellanic irregulars the notation Sm is used (e.g., the Large Magellanic Cloud is a SB(s)m type). In the case of elliptical or lenticular galaxies, the signs "+" and "-" are used to denote "early" and "late" subdivisions. "In both the SA0 and SB0 sub-classes three stages, noted S0 -, S0 deg, S0 + are thus distinguished; the transition stage between S0 and Sa, noted S0/a by Hubble, may also be noted Sa-".

Hubble stage T	-6	-5	-4	-3	-2	-1	0	1	2	3	4	5	6	7	8	9	10
de Vaucouleurs class ^[4]	cE	E	E	S0	S0 ⁰	S0 ¹	S0/a	Sa	Sab	Sb	Sbc	Sc	Scd	Sd	Sdm	Sm	Im
approximate Hubble class ^[5]	E			S0			S0/a	Sa	Sa-b	Sb	Sb-c	Sc	Sc-irr		Irr I		

Figure 1.11: Table comparing Hubble's morphological types and de Vaucouleurs's ones.

Finally, irregular galaxies, as the Small Magellanic Cloud, are noted Im. Figure 1.11 shows a table comparing Hubble's and de Vaucouleurs's classes. In here, as well as in figure 1.10, there is no mention of the (R) "type" galaxies (e.g., an (R)SA galaxy). This (R), preceding the symbol of the class, was used by de Vaucouleurs to distinguish those galaxies with an outer ring-like structure which appears in all four sequences near the transition stage S0/a. However, this particularity was considered as not so important along any definite line of evolution. It was more characteristic of a certain stage of evolution. One example of galaxy having an outer and an inner ring could be NGC 6753, which is noted an (R)SA(r)ab galaxy by de Vaucouleurs (see figure 1.12).



Figure 1.12: Images of NGC 6753. *Left*: band blue ($\lambda = 440$ nm) from dss. *Middle*: band red ($\lambda = 640$ nm) from dss. *Right*: band i ($\lambda = 801.2$ nm) from HST/WFPC2.

1.2.4 Yerkes's Classification Scheme

This is a classification of galaxies introduced by W.W. Morgan (Morgan, 1958, 1959), who worked in the Yerkes Observatory in Wisconsin (University of Chicago). It is based on the central luminosity of galaxies and its spectral features. These allow to derive the stellar populations locked in the inner region of the galaxy, using the MKK system (Morgan *et al.*, 1943; Morgan & Keenan, 1973). At that time, the main idea was to distinguish each galaxy by their stellar composition, which was not taken into account by the Hubble classification alone. Was this new classification really necessary? Let Morgan answer that question himself: "*a valid and precise definition of an empirical system of classification can only be in terms of the observed properties of the specimens classified in each category. As the amount of observational evidence increases, the ideas on which the new classification is based are subjected to increasingly critical tests.*" (W.W. Morgan, 1959). In the same article, he pointed out that the final answer will depend on the usefulness it would prove in the next decades.

The Morgan's classification was based on the work of Morgan & Mayall (1957). Here, the authors made a classification of a group of galaxies by their spectroscopic categories from A to K (systems A-F-G-K). Galaxies with a strong contribution of A star in their integrated light (galaxies with an earliest spectral type) were called A-systems, galaxies where the principal contributors are F stars are called F-systems, and so on. We can also find mixed systems as AF or FG, for example. They find in this study that most of the galaxies follow an interesting correlation between the spectral classification and the degree of central concentration of light in the system. In other words, irregulars and spirals galaxies with little or no central concentration of light appears to be A or F systems, while spirals with large nucleus light concentration, lenticular and elliptical galaxies have G and K spectral types. Galaxies with a relative intermediate stage of central light concentration are in the F-G categories.

Because one of the principal criteria used by Hubble for his morphological classification is the degree of central concentration of light, we can therefore consider the new Morgan classification as a modification of that made by Hubble. However, the new classification makes a remarkably distinction between the different central stellar populations in the different morphological types. *"The value of a system of classification depends on its usefulness; the justification of the present attempt must lie in the direction of furnishing information additional to that of the classical Hubble system. It should be emphasized that the present system is put forward for the purpose of giving information additional to that included in Hubble's system"* (W.W. Morgan, 1958).

Finally, the Yerkes classification can be detailed as follows. It is described by three parameters. The fundamental one is noted by seven categories which are "a", "af", "f", "fg", "g", "gk", and "k". An "a" galaxy has a contribution to its central luminosity principally due to B-, A-, and F-types stars, while a "k" galaxy has a principal contribution coming from giant K-type stars¹⁴. The second parameter called "form family" is denoted by the initials S, B, E, and I, for Spiral, Barred spiral, Elliptical, and Irregular galaxy, respectively. Moreover, four additional morphological type were added: Ep systems which are elliptical galaxies with well-marked dust absorption; D galaxies which have a characteristic rotational symmetry but no spiral or elliptical structures, or non-spiral with symmetrically distributed absorption from dust clouds; L systems have low surface brightness; and N galaxies contain a small and bright nucleus superimposed on a considerably fainter background. Intermediate stages for the "form family" are also possible. Finally, we have the purely geometrical inclination parameter or "inclination class", which goes from 1 to 7. A face-on galaxy is noted by 1, and an edge-on galaxy by 7. Zero is not used for this parameter to avoid any ambiguity with class S0 in the Hubble classification. A "p" letter is used in the case of peculiar systems (I, L), where an inclination is difficult to determine.

As an example, I can mention galaxies NGC300 and NGC1300. The first was classed as Sc by Hubble, while in the new system is an aS4 (see figure 1.13). The second is a SBb in Hubble's classification, and a fB2 in Morgan's classification (see figure 1.14). As we can notice, no diagram has been created to show Morgan's classification as it was the case for Hubble and de Vaucouleurs (see figures 1.9 and 1.10). Maybe because the Morgan's classification is a bit more difficult to organize in a sequence?

¹⁴Morgan (1958) clarifies that such contributions are studied in the violet spectral region.

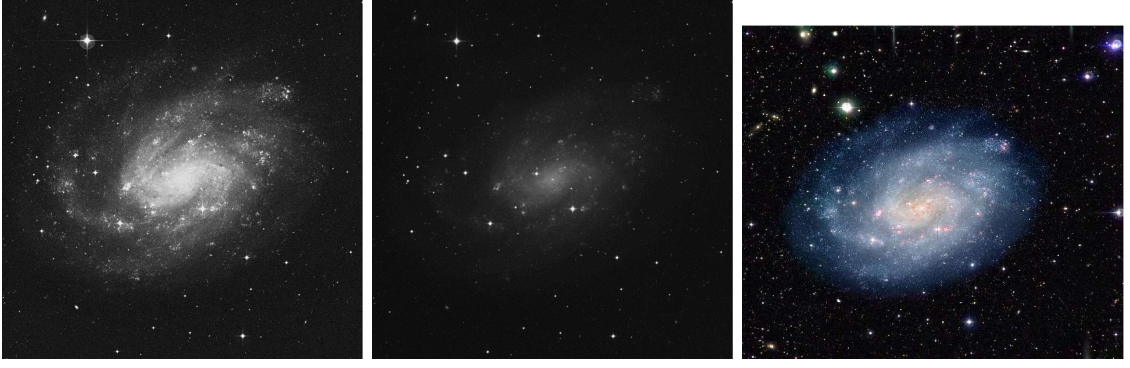


Figure 1.13: Images of NGC 300. *Left*: band blue ($\lambda = 440$ nm) from dss. *Middle*: band red ($\lambda = 640$ nm) from dss. *Right*: color image from the Wide-Field Imager (WFI) on the MPG/ESO 2.2-m telescope at the La Silla Observatory (Image Credit: ESO).

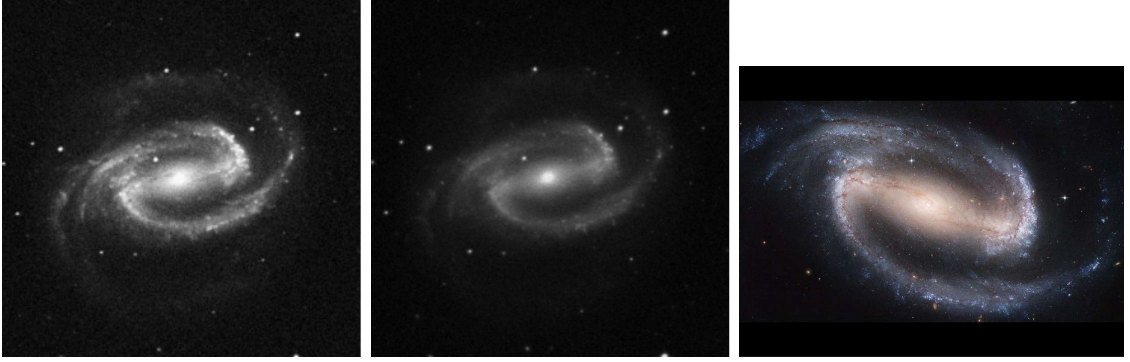


Figure 1.14: Images of NGC 1300. *Left*: band blue ($\lambda = 440$ nm) from dss. *Middle*: band red ($\lambda = 640$ nm) from dss. *Right*: color image from HST/WFPC2 (Image Credit: NASA, ESA, The Hubble Heritage Team - STScI/AURA. Acknowledgment: P. Knezek - WIYN).

1.2.5 van den Bergh's Classification Scheme (DDO)

This is another extension of the Hubble morphological classification developed by Sidney van den Bergh at the David Dunlap Observatory (DDO). In this case, the classification is based on the correlation between absolute magnitude and the degree of development of spiral arms. Thus, it was, since the beginning, employed on spiral and irregular galaxies. [van den Bergh \(1960b\)](#) found that galaxies with the highest luminosity are also those with the most strongly developed spiral structures. He then concluded that one limitation of the Hubble system is the existence of luminosity effects on the contrast and development of spiral arms.

This finding allowed [van den Bergh \(1960b,a\)](#) to classified galaxies following two

criteria: (1) the galactic type, and (2) the luminosity class. The first one follows the Hubble morphological classification, recognizing Sa, Sb, Sc, and Irr types. The second one divides galaxies from I to V by decreasing luminosity. Luminosity classes were chosen to agree with those used to classify stellar luminosities in the Yerkes system. Type I refers to super-giant galaxies, type II to bright giant galaxies, type III to normal giant, type IV to sub-giant galaxies, and type V to dwarf galaxies. Super-giant galaxies could have, approximately, an absolute blue magnitude of -20.5 and dwarf galaxies a blue magnitude of -14.

The DDO scheme adds further notations. Sub-giant spirals with low and high arms resolution¹⁵ are noted "S-" and "S+", respectively. Objects between barred and not barred spirals, corresponding approximately to the SAB type in de Vaucouleurs diagram, are noted "S(B)". When a galaxy has fuzzy or nebulous arms an "n" is added to the galactic type, while an "*" is added if the spiral arms have a patchy structure. The letter "t" at the end of the galactic type indicates distorted spiral arms, which are maybe coming from past or present tidal interactions. In extreme cases, "nn", "***", "tt" could be also used. Finally, the symbol "SD" represents the disk-shaped galaxies. In the DDO classification, the irregulars galaxy type exclude colliding and interacting galaxies, deformed elliptical galaxies, and ellipticals exhibiting dust patches.

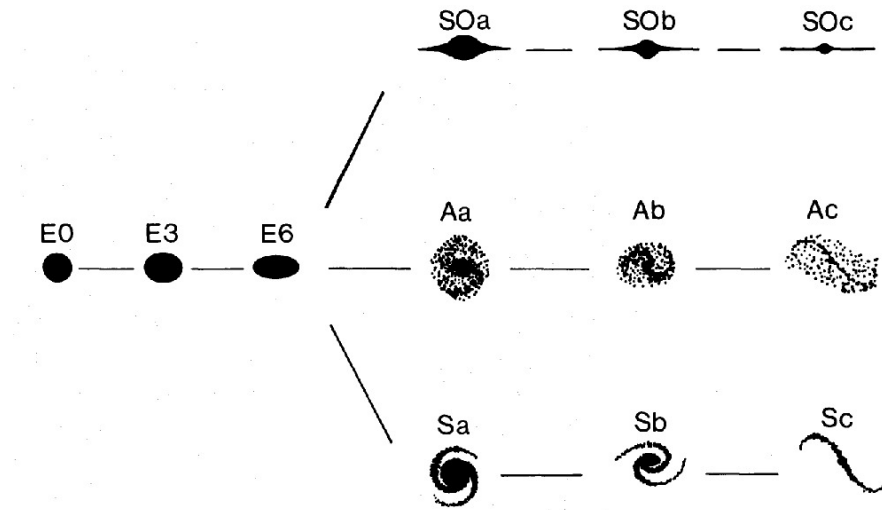


Figure 1.15: van den Bergh scheme of galaxy morphology from [van den Bergh \(1976\)](#).

A later revision of the classification led van den Bergh to identify transition cases between S0 and spiral galaxies. These transitions appeared to be spiral galaxies with little star formation in their arms. Such detections and other reasons (e.g.,

¹⁵It refers to the degree the arms are resolved.

flattening and B/D ratio) made [van den Bergh \(1976\)](#) disagree with the placement of S0 galaxies in the Hubble sequence (see figure 1.9). For van den Bergh, S0 galaxies must be placed in a sequence parallel to spirals, instead of being in the "transition region" between ellipticals and spirals (see figure 1.15). It was called the RDDO (Revised DDO) system¹⁶.

1.2.6 Discussion about the physical Hubble sequence

In the previous section, I have cited the most known morphological classification systems. Noteworthy, other morpho-classifications have been also developed. Amongst them we have: a.) the Vorontsov-Velyaminov classification, which is a purely descriptive (or MCG) system ([Sandage *et al.*, 1975](#)); b.) the arm classes system of [Elmegreen & Elmegreen \(1982, 1987\)](#); c.) the [Kormendy & Bender \(1996\)](#) revised system of Hubble classification for elliptical galaxies, based on their inclination and structures rather than any intrinsic property; and d.) [Conselice \(2006\)](#) system, taking into account the star formation, galaxy interaction and mass.

All these systems make reference to the different "species" of galaxies we can find using a morphological classification. However, one might wonder whether this is even important for understanding galaxy evolution. First, only with the intention of starting the discussion, I will dare to make a light analogy (if there could be any) with paleontology. Even if living beings could have many intrinsic individual characteristics, their shapes and structures have been an essential, and maybe the most important feature to trace the evolution of organisms on earth (e.g., see "On the Origin of Species" by Charles Darwin¹⁷).

As a result, we are essentially in agreement with [de Vaucouleurs \(1994\)](#) who says that "taxonomy ... is nevertheless an essential first step in all fields of science". Now, we could also say that galaxy taxonomy through the morphological sequence attests to an underlying sequence of numerous physical processes (see table 1.1). As we have seen, this notion has been widely accepted for the past decades, making morphological classification of large numbers of galaxies important for better modeling and understanding the galaxy structure and evolution.

We can say that galaxy morphology is useful because it does not only succeed, to some extent, in distinguishing galaxies which are physically different. The basic

¹⁶The separation of S0 and Sp galaxies by van den Bergh is based on the B/D ratio as a classification criterion. Further studies by [Simien & de Vaucouleurs \(1986\)](#) on the bulge/disk decomposition and correlation between B/T ratio and Hubble type found that B/T of S0 galaxies is generally intermediate between pure spheroidal systems and spirals, supporting the placement of S0 galaxies between ellipticals and spirals.

¹⁷[Darwin \(1859\)](#)

Parameter/property	from early to late type
V/σ	\nearrow
R_{disk}	\searrow
B/T	\searrow
(B-V) color	\searrow
HI abundance	\nearrow
HII abundance	\nearrow
H ₂ abundance	\searrow
Metal abundance	\searrow
K/A*	\searrow
Luminosity	\searrow
Dynamical mass	\searrow
Baryonic mass	\searrow

Table 1.1: Galaxy properties vs morphology. Relation between different physical parameters/properties of galaxies and their morphology (from elliptical/lenticular to spiral/irregular galaxies, see figures 1.9 and 1.10). These relations have been studied amongst the local galaxies by Roberts & Haynes (1994a,b), Nakamura *et al.* (2004), Shen *et al.* (2003), Springob *et al.* (2005), Kauffmann *et al.* (2003), Strateva *et al.* (2001), Shimasaku *et al.* (2001), Kennicutt (1992), Kent (1985), Tinsley (1981), Roberts (1969), Pizzella *et al.* (2004), Vega Beltrán *et al.* (2001), Conselice (2006). Nevertheless, due to the considerable scatter in some of the relations, these trends may not be evidence of causal connection, until new results provide better understanding of both trends and scatter. One example is the integral galaxy color, which scatter is still under discussion (see section 6 in Cirasuolo *et al.*, 2007). Another consideration to be taken into account is the existence of exceptions to generalities, as it is the case for the R_{Disk} or the total mass. The general trend of the relation between these two properties with the morphology is affected by the existence of elliptical dwarf galaxies, for example. (* K/A represents the ratio between the *old stellar population (K) fraction and the young stellar population (A) fraction*).

classification scheme (Hubble scheme) succeeds, although with some caveats¹⁸, in separating galaxies according to their physical and kinematic properties. Furthermore, galaxy morphology is a direct consequence of the underlying physics governing their formation and evolution.

After establishing the main importance of galaxy morphology, we are now

¹⁸even if properties are generally well correlated with the morphological types, in some cases the considerable scatter must be carefully considered (see legend of table 1.1). Somehow such scatter should be pondered when using them to morphologically classify galaxies.

confronted with a new paradigm: how many morphological details do we need to include in a morphological classification? As we saw in the above sections, each morphological classification took the basis of the Hubble sequence. However, each one takes, more or less, different physical details to achieve the classification of galaxies because "there are several possible approaches to the problem of the classification of galaxies: morphologic, photometric, colorimetric, spectroscopic" (de Vaucouleurs, 1963)¹⁹.

Details are important in the description of the evolution of individual systems. However, how much importance do they deserve when trying to unravel the evolution of galaxies in the Universe? It depends on the scale at which we are looking at, as well as the interrelation that could have the different scales. On the one hand, we have the morphological/physical details to be taken into account for the morphological classification. On the other hand, we have the physical/dynamical properties that correlate with such morphologies. Where is the limit between the two? A key point will then be the definition of the methodology to be followed during the morphological classification (see chapters 3 and 6). This methodology, in the ideal case, must be easily reproducible and not subjective, must take into account a reasonable number of principal morphological/physical details, and must result in the best possible correlation with the main galaxy properties (for example, the kinematics, the important role of which to understand the evolution of galaxies is well established). *"As Long as only a few criteria define a system, and if image material of a similar quality to that which formed the basis of the system is used, then there will be a greater ease of applicability and reproducibility of that system by independent observers. If one later finds correlations between fundamental observables and classifications, then the system could lead to physical insight ..."* Buta (1992a). Finally, a good classification must drive morphology to the physical/dynamical properties (e.g., table 1.1), but such properties must not be used to drive (make) the classification²⁰ (see subsections 6.2.5 and 6.4.3 for an example).

Since the past century, morphological classification has had great success in helping us to understand local galaxies. One of the objectives of my thesis is to extend this successful analysis technique into the distant Universe, and look for a possible time evolution of the Hubble sequence.

¹⁹even if de Vaucouleurs (1994), referring to the "low" number of morphological features taking into account in the original Hubble sequence, argued that "this would be erudition, but not science which aims at the general, not the particular", sometimes science can be lost in so many details.

²⁰this is a modification to words by Sandage (2005).

The galaxy formation and evolution

Contents

3.1	The standard morphological classification method	41
3.2	Modern methods for the morphological analysis	43
3.2.1	The non-parametric methods	44
3.2.2	The parametric methods	47
3.2.3	The color information	50

Scenario of galaxy formation and evolution

How can we obtain the different shapes of galaxies we see in the local Universe? How do galaxies get different components with different dynamics? Why some galaxies appear flattened like disks while others are spheroidal? These questions remains a major unsolved problem in galaxy formation.

Some attempts have been made in the past and continues in the present. The principal idea presents this problem as a 'nature' versus 'nurture' dichotomy: is the morphology of a galaxy imprinted in the initial conditions, or does it result from environmental processes such as mergers, tidal interactions, or gas infall? On the one hand, it has been proposed that the determining factor of the galaxy formation process is the protogalactic angular momentum (Sandage *et al.*, 1970). On the other hand, different mechanisms that could transform one morphology type into another have been studied. Amongst them we can mention ram-pressure stripping by the hot intracluster medium (Gunn & Gott, 1972), or galaxy 'harassment' by impulsive encounters in clusters (Moore *et al.*, 1996). Furthermore, other studies (Hammer *et al.*, 2009a, and references therein) support the idea that galaxy mergers are a possible explanation for the origin of the Hubble types.

In the following, I describe the principal scenarios of galaxy formation.

2.1 Downsizing: a scenario of galaxy formation or a natural consequence of the primordial collapse model?

Downsizing was introduced by [Cowie *et al.* \(1996\)](#). Studying the redshift, mass (through M_K) and star formation of 280 galaxies since redshift 1.6, they concluded that the maximal mass of galaxies having a burst of star formation increases with redshift, and that most of the galaxy formation process took place between redshift 0.8 and 1.6. This led them to suggest that the galaxy mass assembly occurred in a 'downsizing' way (referring to a top-down universe evolution) with the most massive galaxies forming at higher redshift, while less massive ones formed at later cosmic times.

According to this downsizing effect, massive galaxies are thus expected to exist at high redshifts ($z \gg 1$). Observations show that it is the case ([Elston *et al.*, 1988](#); [Dey *et al.*, 1999](#); [Dickinson *et al.*, 2000](#); [Im *et al.*, 2002](#); [Cimatti *et al.*, 2004](#); [Daddi *et al.*, 2005](#); [Saracco *et al.*, 2005](#); [Kriek *et al.*, 2006](#); [Cimatti *et al.*, 2008](#)). Those large systems have been detected by their red colors or their bright emission at sub-millimeter wavelengths. Some of them already have old stellar populations, some with significant recent star formation.

The downsizing picture has been widely debated because of the apparent contradiction between downsizing and the hierarchical evolution expected from the Λ CDM cosmological model (see chapter 1). Nevertheless, this contradiction is only apparent. While the downsizing picture describes only the evolution of baryonic structures, the Λ CDM model focuses on the dark matter halos evolution. Moreover, the interactions between baryons and dark matter remains largely uncertain. The hierarchical evolution of dark matter halos does not imply, "a priori", a hierarchical evolution of baryonic structures.

Actually, the first fluctuations of baryonic mass to be condensed are those inside the most massive dark matter halos, because these last are the catalysts of the formation of the first baryonic structures ([Neistein *et al.*, 2006](#); [Mouri & Taniguchi, 2006](#)). It is in these halos where the stellar formation activity would first begin. Consequently, the apparent paradox between downsizing and Λ CDM model is mostly due to a confusion in the literature between the evolution of dark matter halos (hierarchical) and the evolution of baryonic structures (anti-hierarchical).

After the finding of the downsizing effect by Cowie *et al.*, other works seemed to point in the same direction. One example is the finding of lack of density evolution of large elliptical and spiral galaxies between redshift 1.3 and 0 ([Lilly](#)

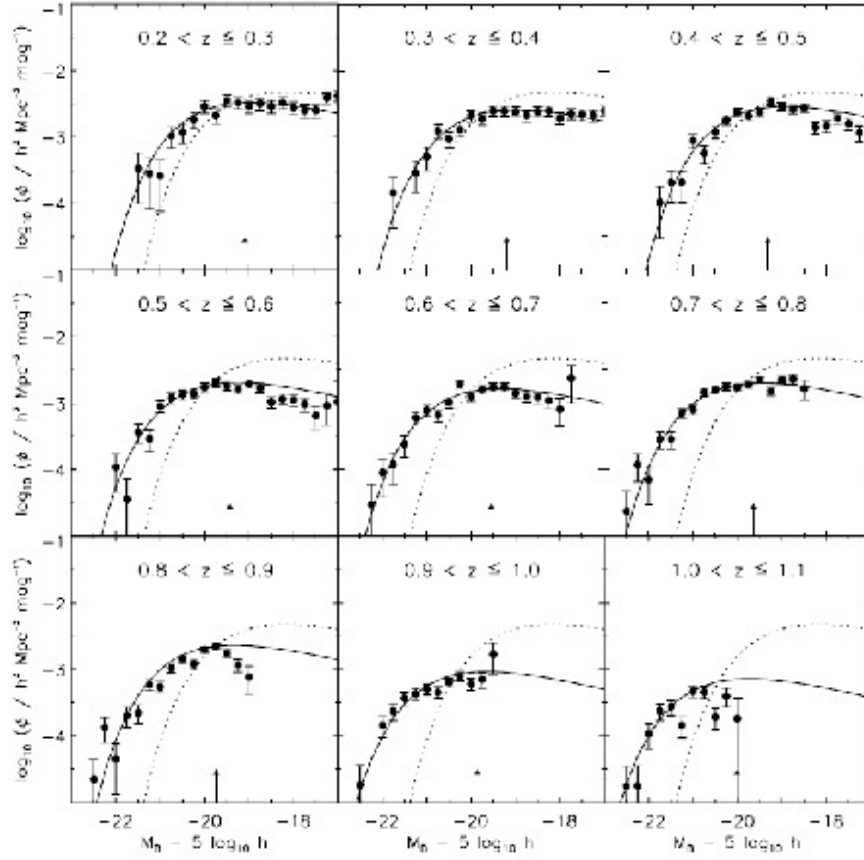


Figure 2.1: Redshift evolution of the red-sequence luminosity function, in straight line, from [Bell *et al.* \(2004b\)](#). Here, we notice the increasing faint end from $z \sim 1$ to $z \sim 0.25$. For comparison they plot, in dotted line, the LF of a local sample they select from the SDSS EDR (Early Data Release, [Stoughton *et al.*, 2002](#)).

et al., 1998; [Schade *et al.*, 1999](#)). Moreover, [Brinchmann & Ellis \(2000\)](#), using a sample of 321 galaxies morphologically classified (visually and with automated classifiers), showed how the stellar mass density changes by morphological type as a function of redshift. They found that spiral galaxies do not present any change in their stellar mass density between redshift 1 and 0. However, that of irregular galaxies has a remarkable decline, while that of elliptical galaxies present a modest increase. Later, [Bundy *et al.* \(2005\)](#) found that spiral and irregular morphologies dominate among galaxies of low mass in all redshifts, while the E/S0 dominate among galaxies of larger mass range. They then suggest a morphological extension of the downsizing principle: galaxies that form at high redshift are the most massive ones and have elliptical morphology. They also found that the fraction of massive galaxies at lower redshifts are dominated by elliptical types, which could suggest an evolution to this morphological type. Another important fact that supports the downsizing effect is the extrapolated evolution of the faint end of the red sequence luminosity function (LF) since $z \sim 1$ (see figures 6 and figure 3 in

Cirasuolo *et al.*, 2007; Bundy *et al.*, 2006; Bell *et al.*, 2004b, respectively; see also figure 2.1), which supposes that the population of dwarf ellipticals (dE) galaxies increases from the past to the present.

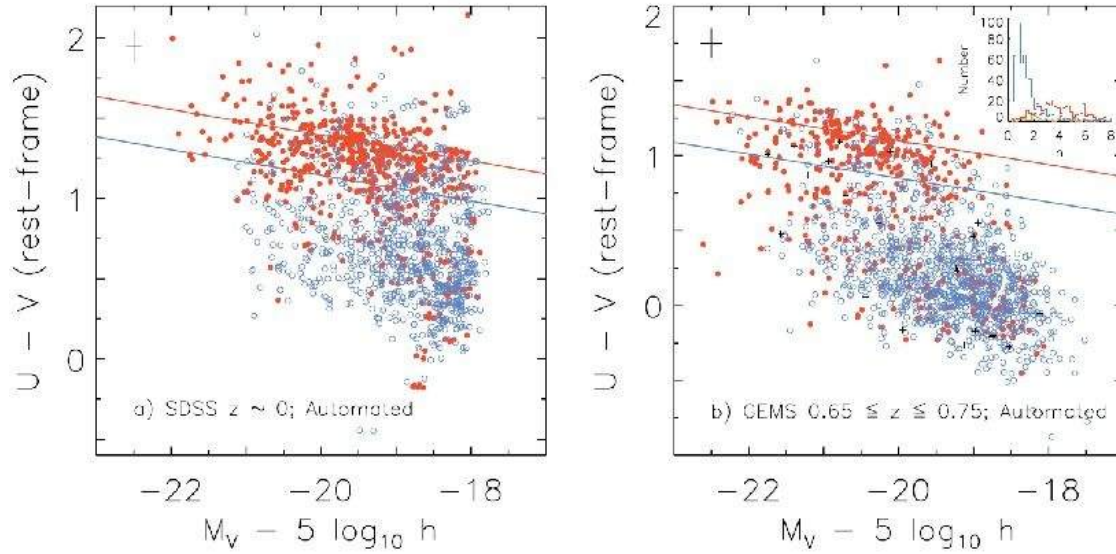


Figure 2.2: Color contamination from Bell *et al.* (2004a). This figure shows the morphological types of galaxies as a function of their rest-frame V-band absolute magnitude and U-V color over the last half of the cosmic history. Blue open circles denote morphologically classified late-type galaxies, whereas red solid symbols show early-types. The red line shows a fit to the red sequence and the blue line the adopted cut between red and blue galaxies. As we can easily notice just by looking to the fainter galaxies in both plots, the contamination of late-type galaxies into the red-sequence for local fainter galaxies (left plot) is higher than those at intermediate redshift (right plot). Could it be the cause of the evolution inferred from figure 2.1?

These observational results have led to the downsizing effect being considered as a real scenario of galaxy formation¹, predicting that the galaxy population which would be formed in the present is mostly composed of dE types. However, such a scenario would present some problems in a cosmological frame. First, the formation of small galaxies (principally, dE galaxies) at present epochs, and a passive evolution of intermediate mass spiral and elliptical galaxies since $z \sim 1$, can not explain the high stellar mass fraction ($\sim 50\%$) formed since $z \sim 1$ (Dickinson *et al.*, 2003), and could be in contradiction with the fact that most of the present-day stars are in structures more massive than dE galaxies (elliptical and bulge of spiral galaxies; Fukugita *et al.*, 1998; Brinchmann & Ellis, 2000). It

¹by a dissipative collapse of baryons in dark matter halos.

is also in contradiction with the fact that the bulk of the star formation density at intermediate redshift is mainly in intermediate mass galaxies (Heavens *et al.*, 2004; Hammer *et al.*, 2005a; Bell *et al.*, 2005), and with the metal evolution found since $z \sim 1$ (Liang *et al.*, 2006). In addition the application of the downsizing scenario seems to be in disagreement with the increasing frequency of mergers with redshift (Le Fèvre *et al.*, 2000; Conselice *et al.*, 2003; Bundy *et al.*, 2004; Lotz *et al.*, 2006; Rawat *et al.*, 2008), as mergers form bigger structures rather than smaller ones. Finally, we could go even further, and argue that the assumption of the evolution of the faint end of the red sequence LF are based on the hypothesis that such a LF corresponds to the LF for early-type galaxies (ETGs). Making the hypothesis that all red color galaxies are ETGs could be too rough, as it is well known, even for local galaxies, that there is a non-negligible "contamination" of late-type galaxies amongst red color galaxies: Strateva *et al.* (2001) found that ~ 20 per cent of late-type galaxies have red colors compatible with the red sequence in the local Universe (see also Bell *et al.*, 2004a, and figure 2.2). This contamination becomes even stronger with redshift (~ 35 per cent at $z \sim 1$; Franzetti *et al.*, 2007)(see also Bell *et al.*, 2004a, and figure 2.2 for $z < 1$). This could be related to the discussion, about the correlation between morphology and different physical galaxy properties, started in subsection 1.2.6, and will be further detailed in subsection 6.2.5.

Now, we may distinguish between the *downsizing effect*, which is a real tendency, and the *downsizing scenario*, which disagrees with a number of observations.

2.2 Secular evolution

In the 1960s-70s, observations of the Milky Way (MW) suggested a scenario in which spiral disks acquired their angular momentum at early epochs (Peebles, 1969a, and references therein), and then evolved in a slow, "secular" manner by gradual accretion of material from their environment. In this secular evolution process, galaxies are hence considered as open systems which can get, by accretion, the gas coming from the intergalactic medium. This gas is then transformed into stars through time, while the various galaxy components interact with each other. For example, the bulge is formed slowly from the disk (and external gas) through the bar action (Athanasoula, 2005; Kormendy & Kennicutt, 2004; Athanasoula, 1992b; Combes *et al.*, 1990). The total accretion process happens in a nonviolent way. The redistribution of energy and angular momentum inside the system could be also driven by nonaxisymmetries other than a bar. These are the spiral arms, which can also cause an internal, slow secular evolution rearranging the disk structure.

This is useful to distinguish between internal secular evolution and environ-

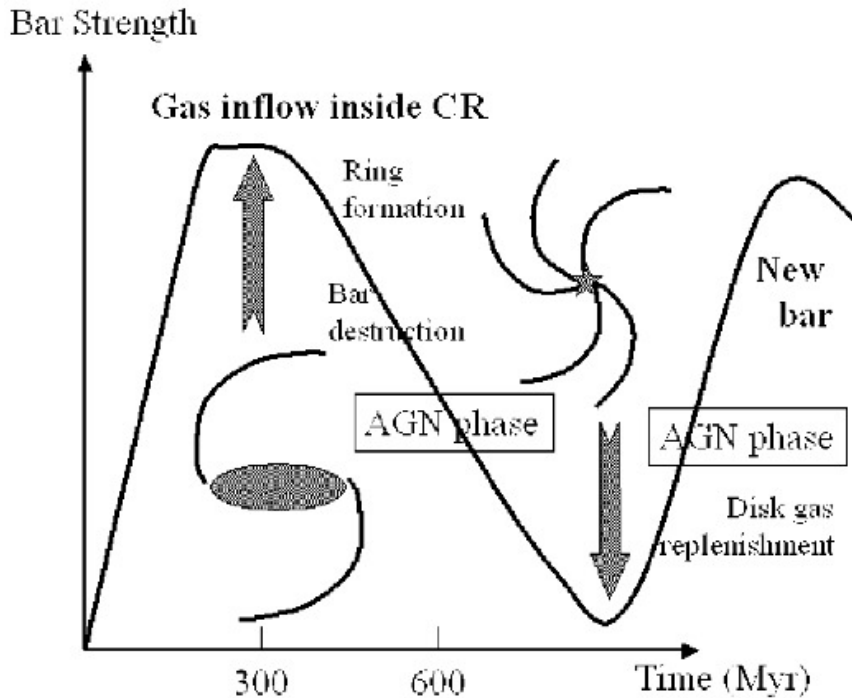


Figure 2.3: Schematic scenario of two bar episodes, and the corresponding phases for the AGN fueling (Combes, 2005). It shows the relatively short lifetime of the bar.

mental secular evolution. The first is responsible for the formation of pseudobulges in disk galaxies (Kormendy & Kennicutt, 2004) and could explain the abundance of pure disk galaxies with no evidence for merger-built bulges in the local Universe (Kormendy & Fisher, 2008). The second is responsible for the formation of spheroidal galaxies whose observable parameters are similar to those of late-type galaxies, even if they are morphologically similar to ellipticals. These authors suggest that spheroidals are defunct late-type galaxies transformed by internal processes such as supernova-driven gas ejection and environmental processes such as secular harassment and ram-pressure stripping.

One piece of evidence in support of secular evolution is showed by Gadotti & dos Anjos (2001). They studied the color gradients, and the correlation between bulge and disk colors, in 257 late-type barred galaxies, reaching the conclusion that their results could be only explained if the bulge of those barred objects are formed from a secular evolution. Bournaud *et al.* (2005) (and Bournaud & Combes, 2002) also showed that if, during the formation of the bulge, the central concentration of matter exceeds a few percents of the total mass, it could even destroy the bar, which would have a lifetime of a few (1-2) Gyr (see figure 2.3). Given the roughly constant fraction of barred galaxies from the local Universe to the distant one (Zheng *et al.*, 2005; Jogee *et al.*, 2004; Sheth *et al.*, 2003), it would

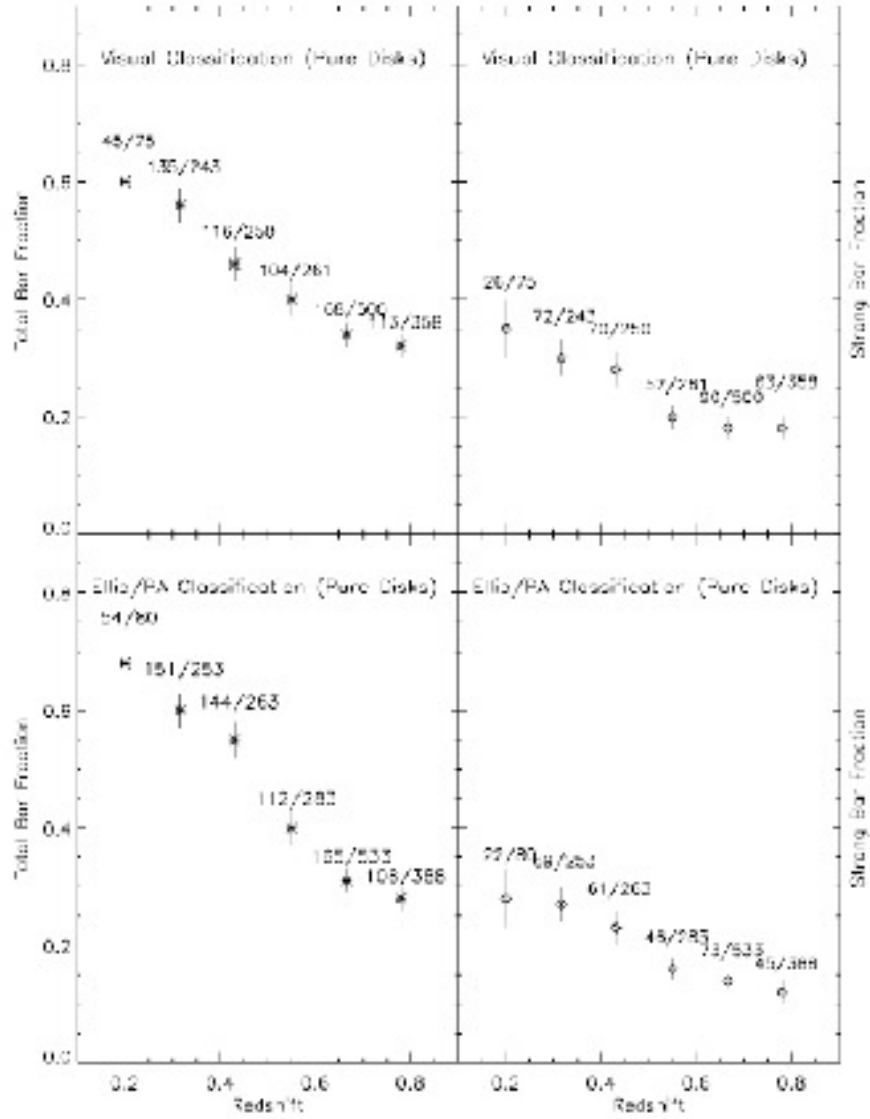


Figure 2.4: Bar fraction evolution with redshift from [Sheth *et al.* \(2008\)](#).

imply that bars are continuously reconstructed. Such periodic reconstructions could only be possible through gas infall ([Combes, 2005](#); [Block *et al.*, 2002](#)) coming from filaments ([Semelin & Combes, 2005](#), see also figures A.4, A.5, A.6). Nevertheless, [Athanassoula *et al.* \(2005\)](#) propose that bars are not sporadic events, but instead their lifetime could be larger than 5 Gyr, even with an increase of the galaxy central mass of a few percents of the total mass. This is supported by recent studies that show, indeed, a quite important evolution of the fraction of barred galaxies since $z \sim 0.8$ ([Sheth *et al.*, 2008](#); [Athanassoula, 2008](#), see figure 2.4).

The secular evolution scenario is challenged by observations of distant galaxies, which emitted their light 6 Gyr ago. They reveal that nearly half of them had peculiar morphologies and anomalous kinematics ([van den Bergh, 2002](#); [Flores](#)

et al., 2006). In other words, they are not yet dynamically relaxed. This is at odds with the hypothesis of secular evolution of most of spiral galaxies during the past 6 Gyr (for further drawbacks of the secular scenario see also subsection 2.4). Additionally, contrary to the early predictions that a secular evolution leads to a transformation of late-types to early ones, Sheth *et al.* (2005) studied the gas inflow induced by the bar in spiral galaxies, and concluded that *"despite the evidence for bar-driven inflows in both early and late Hubble-type spirals, the data indicates that it is highly unlikely for a late-type galaxy to evolve into an early type via bar-induced gas inflow. Nonetheless, secular evolutionary processes are undoubtedly present, and pseudobulges are inevitable; evidence for pseudobulges is likely to be clearest in early-type galaxies because of their high gas inflow rates and higher star formation activity."*

Finally, an important issue is the origin of the gas accreted during the secular evolution process. Bertola *et al.* (1992) showed that in some S0 galaxies the gas rotates in the opposite direction of stars, which led them to predict an external origin of the gas. Possible origins are filaments (see figure A.4) or a high occurrence of minor mergers during Hubble time. However, could it be just the infall of gas due to major merger systems? In any case, identifying from where the gas was lying before being transformed into present day stars, as well as determining its momentum, could solve the issue of the high angular momentum observed in present-day disks which can not be reproduced by a large number of simulations. It has been called "the angular momentum catastrophe".

Minor mergers

The infall of low mass satellite galaxies has been consider as an extension of the secular evolution scenario in order to solve its disadvantages. Indeed, the first numerical simulations showed that minor mergers (generally having progenitors with a mass ratio smaller than 1:5) do not destroy the disk of the largest progenitor, but this last undergoes a morphological evolution to an earliest type by the increase of the velocity dispersion and height of the disk (Walker *et al.*, 1996; Velazquez & White, 1999). Later, Abadi *et al.* (2003) showed that the thick disk obtained in their simulations was mainly composed of remains of satellite galaxies, while the thin disk was composed of stars formed "in situ" after the last merger. In addition, Berentzen *et al.* (2003) showed that the interactions between a satellite galaxy with a barred galaxy could drive to the formation of structural features such as rings, as well as a faster displacement and destruction of the bar. Depending on the impact radius, this kind of interactions can produce a thickening of the disk.

One of the first galaxy evolution scenarios involving mergers is the "collisional

starburst scenario" (CSS), proposed by [Somerville *et al.* \(2001\)](#), where the galaxies evolve principally through minor merger interactions. These are supposed to happen more frequently than major mergers. This scenario explains very well the observed properties of LBGs (Lyman Break Galaxies): color, velocity dispersion, luminosity functions between redshift 3 and 4, for example. However, when looking at lower redshifts, the CSS gets in trouble. It underestimates the number of EROs (Extremely Red Objects) at $z=1$, as well as the number of objects in the near-IR ($K<22$) by a factor of 3 at $z>1.7$, and a factor 10 at $z>2$. Minor mergers can not explain the strong morphological and kinematic evolution of galaxies at $z<1$ either, as mentioned above. This is because minor mergers should have a much lower efficiency to distort galaxy morphologies and kinematics ([Hopkins *et al.*, 2009a](#)). Additionally, minor mergers present moderate (and even negligible) star formation rates ([Cox *et al.*, 2008](#)), which are not consistent with the observed high values of the cosmic star formation rate density ([Le Flocc'h *et al.*, 2005](#); [Flores *et al.*, 1999](#)). Another major difficulty that can be found as well is the prediction of disks with too low angular momentum compared to present-day spirals.

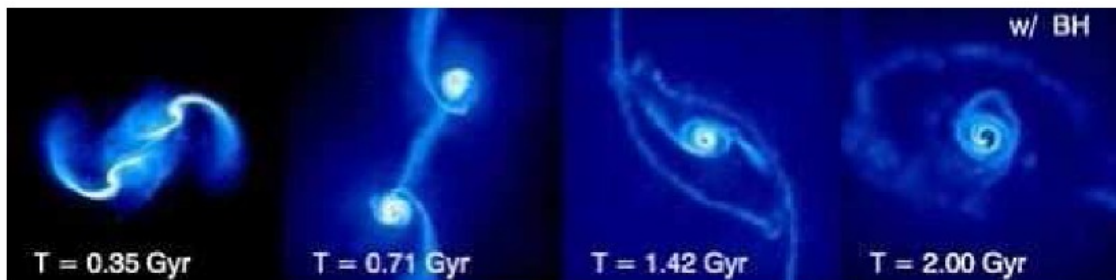


Figure 2.5: Major merger simulation from [Robertson *et al.* \(2006\)](#).

2.3 Violent encounters: major mergers

Contrary to minor mergers, major mergers can destroy the progenitor disks and may induce high SFRs ([Cox *et al.*, 2008, 2006](#); [Haas *et al.*, 2005](#)). Furthermore, they could potentially solve the angular momentum catastrophe² ([Maller *et al.*, 2002](#)). Up to now, the majority of the major merger simulations that have been carried out lead to the formation of elliptical galaxies. While mergers of stellar disks with mass ratios between 3:1 and 4:1 produce elliptical-discy galaxies with rapid rotation, mergers between 1:1 and 1:2 lead to the formation of elliptical-boxy galaxies with a very low rotation ([Naab & Burkert, 2003](#)). Later studies have

²if one accounts for the additional effect of the orbital angular momentum provided by major mergers.

also shown that the final elliptical galaxy type (discy or boxy) depends on the progenitors morphology, which allows the reproduction of the different populations of elliptical galaxies that have been observed in the local Universe (Khochfar & Burkert, 2005). What about the large percentage of late-type galaxies in the local Universe? It could be just a matter of gas fraction (Hopkins *et al.*, 2009a,b; Springel & Hernquist, 2005; Robertson *et al.*, 2006; Springel *et al.*, 2005a; Di Matteo *et al.*, 2005; Jonsson *et al.*, 2006). These authors are challenging the conventional origin of disk galaxies and show that many spirals could be indeed formed after major merger events. Due to the feedback by supernova and AGN, a significant fraction of gas could be expelled towards the galaxy outskirts, allowing a gas reservoir for the creation of a new disk (see figure 2.5). These simulations also suggest a solution to the angular momentum problem. Robertson *et al.* (2006) demonstrates that if large feedback was occurring, this may lead to rejuvenated disks with high angular momenta. Then, because of feedback, it is likely that the whole merger process can be observed during more than 1 or 2 Gyr (Hammer *et al.*, 2009a, see also figure 2.5).

Important progress is needed to disentangle the impact of the different physical mechanisms in the formation of bulges and disks. It seems that the numerical simulations may not be good enough to cover the whole problem. However, if the above hypothesis turns out to be true, the origin of the majority of the present Hubble sequence galaxies could thus be explain by a scenario in which the galaxy evolution is mainly driven by a violent process (major mergers).

2.3.1 An observational scenario: "The Spiral Rebuilding"

This scenario has been proposed by Hammer *et al.* (2005a), and is further detailed by Hammer *et al.* (2009a) (see section 7.1). It can be summarized by 3 major steps (see below for more details): a "pre-merger phase" during which two distant spirals merge, the "LCG phase" where all material from the progenitors falls into the mass barycenter of the system and forms a bulge, and the "disk growing phase" where subsequently accreted material forms a rotating disk. The rebuilding disk scenario suggests a merger origin of the whole Hubble sequence (from ellipticals to late type spirals). It was initially proposed to explain a number of observational pieces of evidence (see table 4 in Hammer *et al.*, 2005a), such as the evolution of the star formation density in the UV and IR, the evolution of the central color and morphology (Zheng *et al.*, 2004), as well as the estimated merger rate (Le Fèvre *et al.*, 2000). Moreover, this scenario is in agreement with further observations at $z < 1$ (e.g., the mass and metal evolution of galaxies (Liang *et al.*, 2006), see also chapters 5 and 6).

Hammer *et al.* (2005a) used multiwavelength observations of 195, $z > 0.4$ intermediate mass galaxies ($M_B < -20$), and found that 15% of them are LIRGs

(Luminous Infra-Red Galaxies). These galaxies are characterized by a high star formation rate, which could explain by themselves most of the stellar mass formed since $z=1$. Hammer *et al.* also showed that in such LIRGs the star formation must be produced in consecutive episodes, because if it is not the case they would evolve into local massive galaxies. This would lead to an over-population of massive elliptical galaxies. Nevertheless, observations show that the number fraction of elliptical galaxies is quite constant since $z \sim 1$. Taking these main results as a basis, Hammer *et al.* then describe all the above evolution trends as due to a recent merger origin of 50-75 % of spirals. Therefore, a majority of intermediate mass spirals could have experienced their last major merger event (leading to the disruption of the disk) within the last 8 Gyr.

The merger scenario is also supported by the merger rate found to be about 10 times more at $z \sim 1$ than it is today (Le Fèvre *et al.*, 2000). In this theory, the disk angular momentum mostly results from the orbital angular momentum of the last major collision (Puech *et al.*, 2007; Hammer *et al.*, 2007), and, as mentioned in the previous subsection, an increasing number of authors (e.g., Hopkins *et al.*, 2009a; Robertson *et al.*, 2006) have successfully tested disk survival after a merger. If the gas fraction is sufficient (about 50%), they predict that the re-formed disk can be the dominant component in the reshaped galaxy.

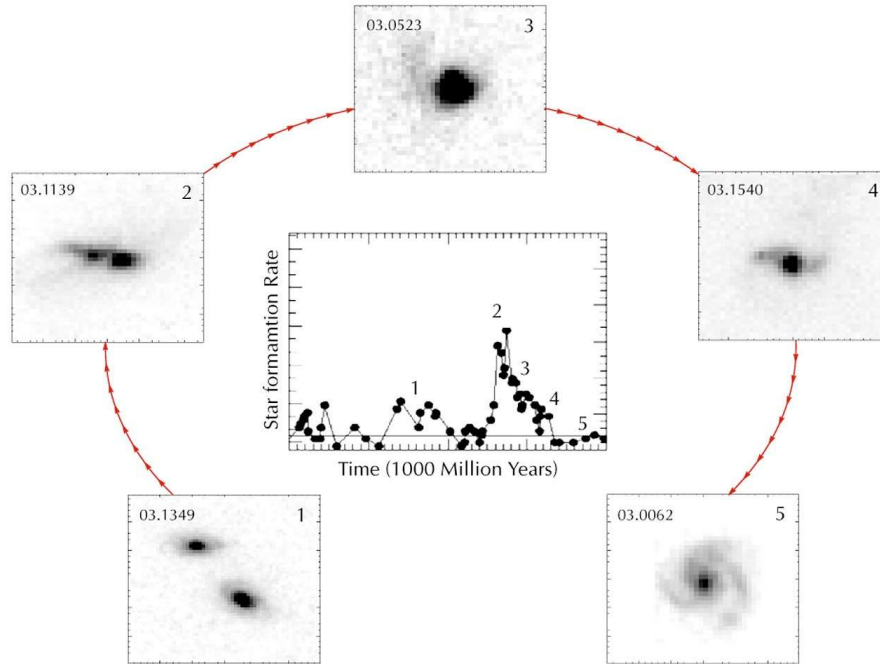


Figure 2.6: Illustration of the spiral rebuilding scenario.

More recently, Hammer *et al.* (2009a) have made a detailed study of the conditions and different phases a major merger can go through to form spiral disks,

including also the formation of the bulge, arms, bars and rings, which may mainly be originated from instabilities created during the last major merger of the system. As a result, we can distinguish five phases (see figure 2.6):

- Phase 1: or approaching phase, which corresponds to the time until the first passage,
- Phase 2: or interaction phase. It corresponds to the time elapsed between the first and the second passage. During this phase the dynamical changes in both progenitors are so intense that a lot of matter is ejected into the inter-galactic medium.
- Phase 3: this is the fusion phase, where the disk of the progenitors are totally destroyed. It corresponds to the time after the second passage and before the elaboration of the rebuilt disk. During phase 3 much of the matter falls toward the center of mass of the new system, and the galaxy may take the appearance of a chaotic morphology (see Fig. 3, top) or a central starburst (see Fig. 3, bottom) with an important peak of star formation quite short in time, always accompanied with chaotic velocity field and dispersion peaks clearly offset from the mass center.
- Phase 4: or disk rebuilding phase. While part of the matter is being compacted to form a bulge, the star formation rate decreases smoothly. At the same time the disk begins to be placed and can be detected. The galaxy would have a blue center associated to the bulge formation, and could be detected as a LCG. The rest of the gas ejected during the first phases (whose density could be too small to be detected) keeps falling into the new system, forming and extending the new disk. At this stage, the star formation through the disk would show a moderate rate. The galaxy rotation is evidenced in a velocity field, but could be offset from the main optical axis, and the dispersion peak(s) is (are) closer to the mass center (see appendix C).
- Phase 5: The last phase corresponds to rotating spirals with regular velocity fields and dispersion peak centred on the centre of mass (e.g., Flores *et al.*, 2006). Notice that, in such a phase, disks are not "a priori" cold, as Puech *et al.* (2007) have shown that most of them have small V/σ (thick disks). However, the high dispersion value begins to relax.

This scenario is supported by the following numerical simulations based on morphological and kinematic observations of distant galaxies:

- a.) Peirani *et al.* (2009) simulated a giant and star-bursting bar induced by a 3:1 merger, and reproduced both the morphology and kinematics of the observed galaxy.
- b.) Yang *et al.* (2009) showed that a giant disk with two embedded cores results

from a 4:1 collision.

c.) [Hammer *et al.* \(2009b\)](#) identified a compact and IR-luminous galaxy that is dominated by a dust-enshrouded compact disk³, itself surrounding a blue, centred "helix" (i.e., a "two arms-plus-bar" structure). This structure and the complex velocity field are predicted in post-merger phases.

d.) [Puech *et al.* \(2009\)](#) demonstrated that the presence of ionised gas without stars close to a highly asymmetric disk could be understood only as a merger remnant.

e.) [Fuentes-Carrera *et al.* \(2010\)](#) reproduced another giant blue bar with a flat velocity field which cannot be reproduced by any other mechanism than a merger with a face-on progenitor. By evolving these five models by 6 Gyr in time, they predict the formation of three spirals, one lenticular, and one massive disk that has survived an exceptional centred and polar collision.

A final important issue of assuming that major mergers are indeed the dominant process through galaxy evolution is that the number density of dwarf galaxies can also be accounted for if they result from material tidally ejected during such violent interactions ([Okazaki & Taniguchi, 2000](#)).

The main weakness of the disk rebuilding scenario focus on the undetermined amount of gas in distant galaxies and the large uncertainty on the major merger rate. Indeed, on the one hand, this scenario is extremely dependent on the gas availability, which was likely much higher in the past than today. Disk rebuilding is plausible only if the merger progenitors has enough available gas. Recent Kennicutt-Schmidt estimations ([Puech *et al.*, 2010](#), see chapter 7) are in agreement with the high amount of gas present in distant galaxies. On the other hand, [Hammer *et al.* \(2005a\)](#) predict that 75%(±25%) of galaxies must had been involved in a major merger since $z \sim 1$. Nevertheless, the estimation of the merger rate is still debated, and this scenario could underestimate the minor mergers importance.

2.4 Discussion

The improvement and difference between scenarios will be established by the three major issues in modern cosmology, which are the formation of large and thin disks, the acquisition of the disk angular momentum, and the relative importance of each physical process in galaxy formation.

As mentioned before, the secular evolution scenario started as the tidal torque theory ([Peebles, 1976](#); [White, 1984](#)), assuming that the angular momentum of

³It is one example of first stage (phase 4) of disk rebuilding.

disk galaxies had been acquired by early interactions. It was mainly supported by observations of the Milky Way (MW). Indeed, the past history of the MW appears to be devoid of significant mergers over the past 10 or 11 Gyr. However, compared to other spirals, the MW turns out to be exceptional, with a nearly pristine halo and a particularly small disk scale length and stellar mass (Hammer *et al.*, 2007). Then, could this scenario be applied to trace the history of the rest $\sim 70\%$ of local spiral galaxies, even if they present quite different properties values from the MW?

There are many observations that could favor the secular evolution of galaxies (see subsection 2.2). However, this process predicts a slow evolution of galaxies, so that galaxies could take more than 6 Gyr to form (Kormendy & Kennicutt, 2004). Then, being a non-violent process, during their evolution, galaxies change very slowly without showing drastic or chaotic changes. Therefore, if this were the mechanism that governs the bulk of galaxy formation (since $z \sim 2$), galaxies were expected to remain in a passive evolution during the past 8 Gyr. Recent studies show that it is not the case (van den Bergh, 2002; Flores *et al.*, 2006; Yang *et al.*, 2008; Le Floc'h *et al.*, 2005). These authors show that galaxies, in their majority, have complex morphologies and kinematics, and a high star formation rate, ~ 6 Gyr ago (see also chapter 6 for a complete and representative comparison of distant and local galaxies).

In addition, the secular scenario has to be accommodated with an episodic origin of gas accretions, to explain the observed SFR values in the distant Universe. Nonetheless, in such a case, the difficulty would then be to explain how the gas coming from the intergalactic medium, which ("a priori") does not have a "common" history with the already formed galaxy, and which is coming from different directions (following the filaments, see chapter 1), could have the right angular momentum to form the abundant local thin disks (with the observed galactic angular momentum values).

It seems that the disk rebuilding scenario does not present those problems. It is in good agreement with the formation of the high fraction of local young thin disks, and with their angular momentum values. Indeed, Yoachim & Dalcanton (2006) suggest that the properties of thick and thin disks are consistent with gas-rich mergers playing a significant role in their formation where stars formed in these mergers lead to the thick disk, while the settling gas formed much of the thin disk. There is more and more evidence supporting this scenario. Its success comes from the fact that it has been constructed principally from observations.

Part II

Shape and evolution of galaxies as a
witness of the Hubble sequence

Observables in galaxy morphology

Contents

4.1	Morphological studies in the distant universe	53
4.1.1	Local universe	53
4.1.2	Distant Universe ($z \gtrsim 0.3$)	55
4.2	Need of representativeness	56
4.2.1	Sample representativeness and luminosity function	57
4.2.2	What are the galaxies responsible for the evolution?	58

Following the morphological method exposed previously in section 2.1.1, a lot of work has been done during the last two decades. We must remember that such classifications were developed principally before the 1990s, when astronomers only had access to photometric plates. Even if some of them also take advantage of the galaxy spectroscopy and photometry, they are based mainly on the eye inspection of the galaxy images. Nevertheless, with the arrival of the new CCD technology during the 1990s, new tools and techniques have been developed to improve the morphological classifications. I will try to summarize them in this chapter.

In general we can distinguish between the standard method, and the automatic methods. The classification by eye allows us to examine each galaxy carefully and individually. However, it is affected by a low reproducibility and a strong subjectivity. In the case of the automatic morphological classifications, a few photometric parameters are measured using computing techniques. They can thus be easily applicable to very large galaxy samples, saving a lot of time. Nevertheless, they dare to classify galaxies morphologically by using only a few photometric parameters. Therefore, even if they may be reproducible and subjective, they are "blind".

3.1 The standard morphological classification method

The first method used to classify the galaxies according to their morphology consists in observing their optical band images and classifying them following the observer's

assessment (see section 1.2). The astronomer disposes of some criteria and images, as a basis, to compare and make his own judgment. The well known criteria for the visual Hubble classification are the size and importance of the bulge in comparison to the disk, the distribution of the spiral arms, and the degree of their resolution. An example of a sample of optical images that was used as a basis for comparison, leading to the morphological classification of other galaxies, is shown in figure 3.1. It is easily imaginable that this methodology can be seriously affected by the resolution of the galaxy images. Furthermore, concerning the distant galaxies, there are some other factors that can affect their visual classification:

- The farther a galaxy is, the less resolved it appears in the images. Not only because they are intrinsically smaller, but also because the inclination (projection) effect makes them less and less discernible.
- The dimming effect affects the galaxy surface brightness by a factor of $(1+z)^4$. Then, for a given exposition time, the faint structures of distant galaxies are easily lost.
- Finally, we have the spectral shift known as the K-correction. This latter makes galaxies to be observed at longer wavelengths than that in which the light was originally emitted. Thus, for example, if we could observe the same galaxy at different redshifts with the same filter, the galaxy aspect would change because we would be observing different aspects (stellar populations, regions, etc.) of the same galaxy (see subsection 1.2.1).

As a consequence of the above effects, it thus becomes more difficult, in function of redshift, to distinguish visually the differences between the different objects and the classification errors happen more easily. "Perhaps the most serious problem with galaxy classification is that it is still largely a subjective visual exercise. The human eye is very good at pattern recognition, and is capable of integrating the information in an image quite quickly. However, a morphological type is not a measured quantity even if it is coded on a numerical scale" Buta (1992b)¹.

During the past two decades, new methodologies have been developed to morphologically classify the galaxies, in order to take into account the previous effects. The principal common characteristics of these methods is that they take advantage of the modern computer and observational technologies, e.g., the CCD cameras (for a short introduction to the modern photometric observational techniques, see appendix B).

¹with "numerical scale" Buta refers to de Vaucouleurs numerical scale (see figure 1.11).

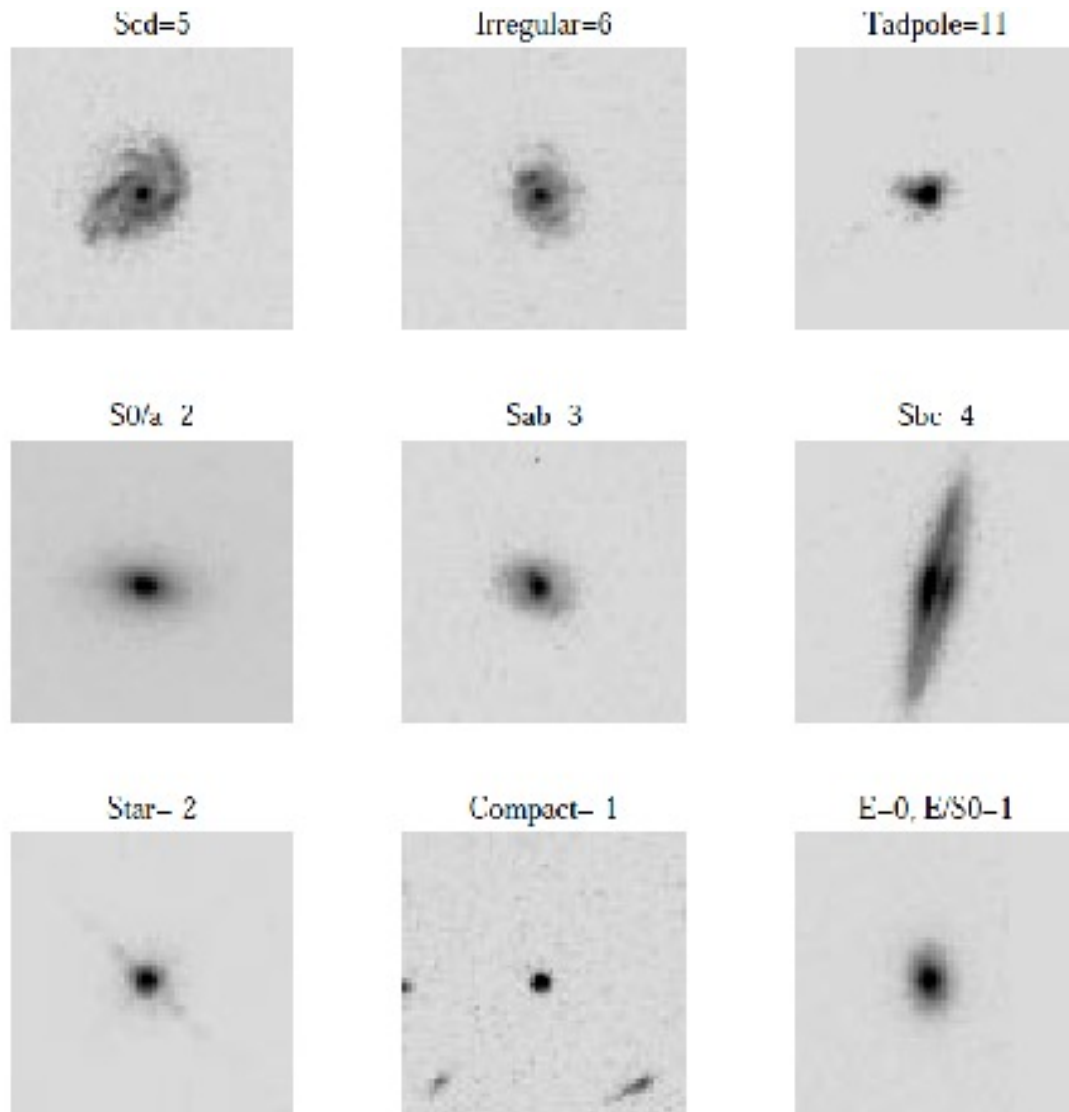


Figure 3.1: Example of images for the morphological classification ([Brinchmann *et al.*, 1998](#)). They use HST images in V band.

3.2 Modern methods for the morphological analysis

These methods are based on quantities linked with the galaxy light distribution. Therefore, by analyzing the light distribution of the objects, they derive such quantities in order to recover the morphological type of each galaxy. In any case, the classification assumes a strong correlation between the derived parameters and the morphological types. We can distinguish between the methods that do not have an "a priori" assumption on the light distribution of the galaxies, called non-parametric methods, and those which use a prior assumption about the light

distribution, called parametric methods.

3.2.1 The non-parametric methods

Even if the non-parametric methods do not use a prior assumption about the light distribution of the object, they need a "calibration" of their parameters by using galaxies that are already morphologically classified by other methods. After this calibration, the non-parametric methods extrapolate to recover the morphological type of new galaxies.

Amongst the different parameters, we can first mention the mean surface brightness, the radius containing half of the total luminosity, and the light concentration. This last is defined as the ratio between two radii, each one containing a fraction of the total light. This could be also interpreted as the ratio of two fluxes inside two different isophotes. In any case, the internal radius must be large enough to enclose a quite large number of pixels, and the external radius must not be too large in order to avoid any significant contamination from the sky. The definition of the Concentration (C) parameter the most often used is that of [Kent \(1985\)](#) and [Abraham *et al.* \(1994\)](#):

$$C = \frac{\sum \sum_{i,j \in E(\alpha)} I_{i,j}}{\sum \sum_{i,j \in E(1)} I_{i,j}} \quad (3.1)$$

where $I_{i,j}$ is the signal at the pixel coordinate (i, j) , and $E(x)$ represents a defined area described by isophotal ellipses. However, a more recent definition of the concentration parameter is that of [Conselice *et al.* \(2000\)](#):

$$C = 5 \cdot \log\left(\frac{R_{0.8}}{R_{0.2}}\right) \quad (3.2)$$

with R_f representing a radius containing a fraction f of the total luminosity of the galaxy.

Another parameter has been introduced by [Abraham *et al.* \(1996b\)](#): the asymmetric parameter A (see also [Schade *et al.*, 1995](#)). This parameter measures the degree of galaxy symmetry, and is calculated by obtaining the absolute value of the difference between the galaxy intensity and the intensity of the same galaxy rotated by 180° at each pixel (i, j) , and normalized by the total intensity of the galaxy. More precisely, it can be expressed as (following [Conselice *et al.*, 2000](#)):

$$A = \min\left(\frac{\sum |I_0(i, j) - I_{180}(i, j)|}{\sum I_0(i, j)}\right) - \min\left(\frac{\sum |B_0(i, j) - B_{180}(i, j)|}{\sum B_0(i, j)}\right) \quad (3.3)$$

where I is the intensity of the galaxy, and B the intensity of the image noise. This last is measured within an image area without any object, and equal in size to the

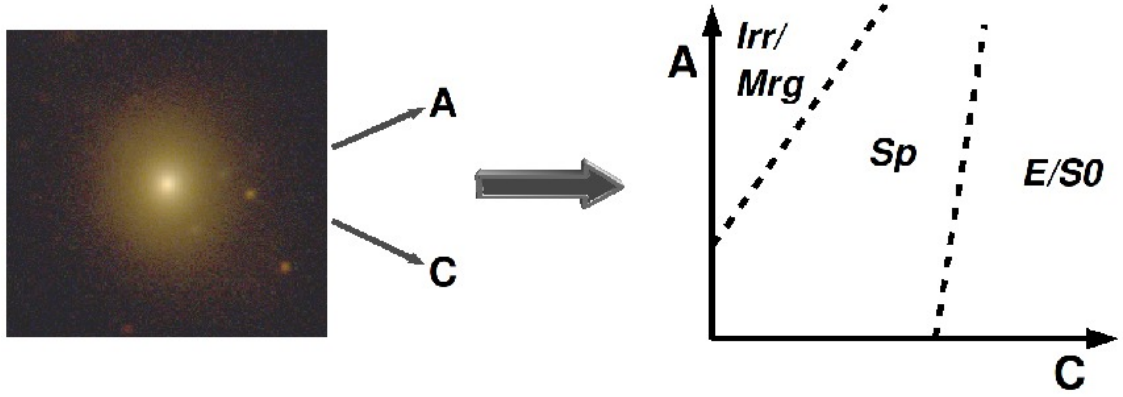


Figure 3.2: Expected distribution of the different morphologies within the Asymmetry (A) vs central Concentration (C) plane.

galaxy area, in order to take into account the effects of the sky background. It is very important for recovering the asymmetry A to precisely establish the center of the galaxy. [Abraham *et al.* \(1996b\)](#) take the brightest pixel from a smoothed version of the galaxy, and [Conselice *et al.* \(2000\)](#) take the position that minimized the asymmetry.

On the one hand, the C parameter is essentially a measure of the light concentration of the galaxy, and is correlated to the bulge size. It could then be correlated with the morphological type because elliptical galaxies are generally more concentrated than disk galaxies. On the other hand, the A parameter is a measure of the symmetry of the galaxy, which could be related to the morphological type too. Spiral galaxies, due to their spiral arms (for example), are more asymmetric than elliptical or lenticular galaxies. [Abraham *et al.* \(1996b\)](#) proposed to use the A - C plane to morphologically classify the galaxies, assuming that in such a plane the principal morphological types (E/S0, Sp, and Irr/Mrg) are separated in different regions, because of the above reasons (see figure 3.2). Nevertheless, as is shown in figure 3.3, such a method does not seem to be efficient. The separation of the morphological types presents a contamination higher than 15% from one type to the others ([Menanteau *et al.*, 2006](#)). Nonetheless, ignoring this significant consideration, this method is still used to morphologically classify local and distant ($z \sim 0.6$) galaxies (see next chapter)(e.g., [Abraham *et al.*, 1996a](#); [Smail *et al.*, 1997](#); [Brinchmann *et al.*, 1998](#); [Conselice *et al.*, 2004](#); [Papovich *et al.*, 2005](#); [Lauger *et al.*, 2005b](#); [Menanteau *et al.*, 2006](#); [Ilbert *et al.*, 2006](#), etc.).

More recently, other new parameters have been also introduced: the smoothness (S)([Conselice, 2003](#)), the Gini (G) coefficient ([Abraham *et al.*, 2003](#)), the M_{20} coefficient ([Lotz *et al.*, 2004](#)), and the coarseness parameter ([Yamauchi *et al.*,](#)

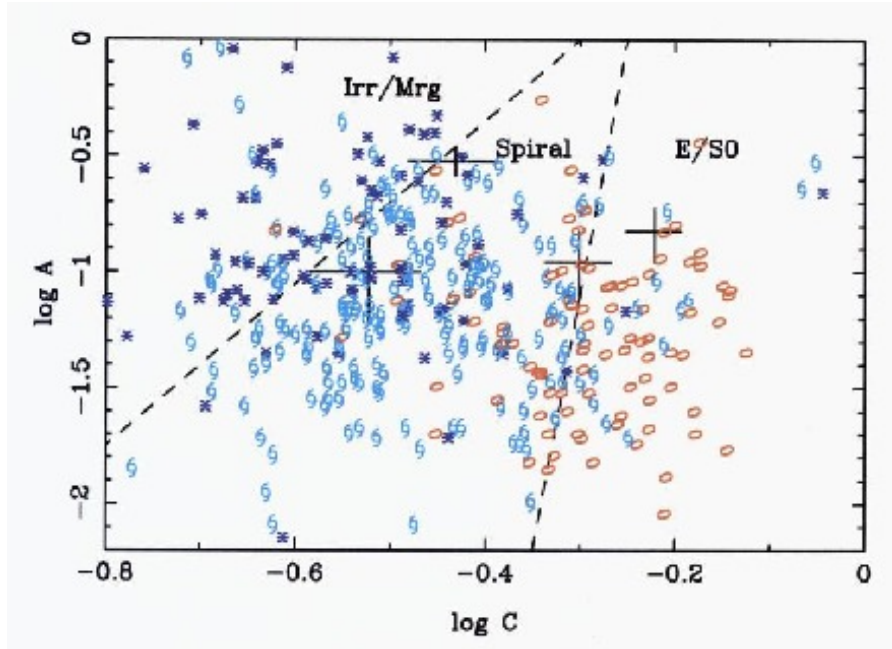


Figure 3.3: Distribution of a galaxy sample in the A-C plane from [Abraham *et al.* \(1996b\)](#). Their plot symbols and colors correspond to the visual classification by an expert (Sidney van den Bergh). Symbols are as follows: compact, S0 and elliptical galaxies are shown as red ellipses; spiral galaxies are shown using blue spiral symbols; and galaxies classified as irregular, peculiar, or mergers are shown as blue asterisks.

[2005](#)). Similar to the C-A plane, it has been also attempted to propose a G- M_{20} plane to separate the different morphological types. Nonetheless, it is not yet convincing either (see figure 3.4).

Due to the above uncertainties, further steps have been taken. The concentration, the asymmetry, and the smoothness parameters have been combined to form the CAS system. It seems more robust, though it is effective only in separating the early and late type galaxies ([Cassata *et al.*, 2005](#)). Then, larger quantities of coefficients (radius, C, A, G, and M_{20} , for example) have been combined ([Scarlata *et al.*, 2007](#)). Nonetheless, a significant contamination seems to be always present.

As a conclusion, the non-parametric methods or "automatic methods", are easily applied to a large number of galaxies, without human intervention, just by adapting them to a computer code. Nevertheless, even if they could be very promising for the future, at the present day they are not accurate enough to be applied in order to measure precisely and exactly the morphology of galaxies, and quantify accurately the morphological evolution of galaxies. Moreover, [Lisker \(2008\)](#) and [Chen *et al.* \(2010\)](#) show that the coefficients used in such methods present a strong dependence on S/N ratio.

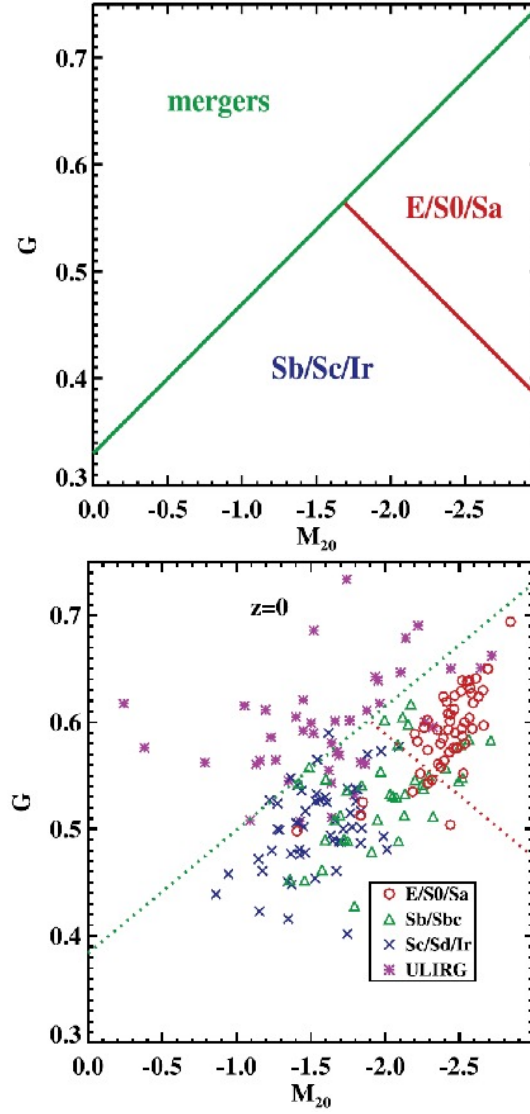


Figure 3.4: *Top*: Expected distribution of the different morphologies within the Gini (G) vs M_{20} plane. *Bottom*: Distribution of a local galaxy sample in the G - M_{20} plane from Lotz *et al.* (2008). Their symbols and colors correspond to the visual classification from the Carnegie Atlas (Sandage & Bedke, 1994). Symbols are as follows: elliptical, S0 and Sa galaxies are shown as red circles; Sb and Sbc galaxies are shown using green triangles; Sc, Sd and irregular galaxies are shown as blue crosses. The purple asterisks represent the merger candidates (ULIRGS).

3.2.2 The parametric methods

The main goal of the parametric methods consists in fitting one or different analytical models to the observed light distribution of the galaxy. They can include, e.g., radial multi-Gaussian deconvolution (Bendinelli, 1991; Fasano *et al.*, 1998), or

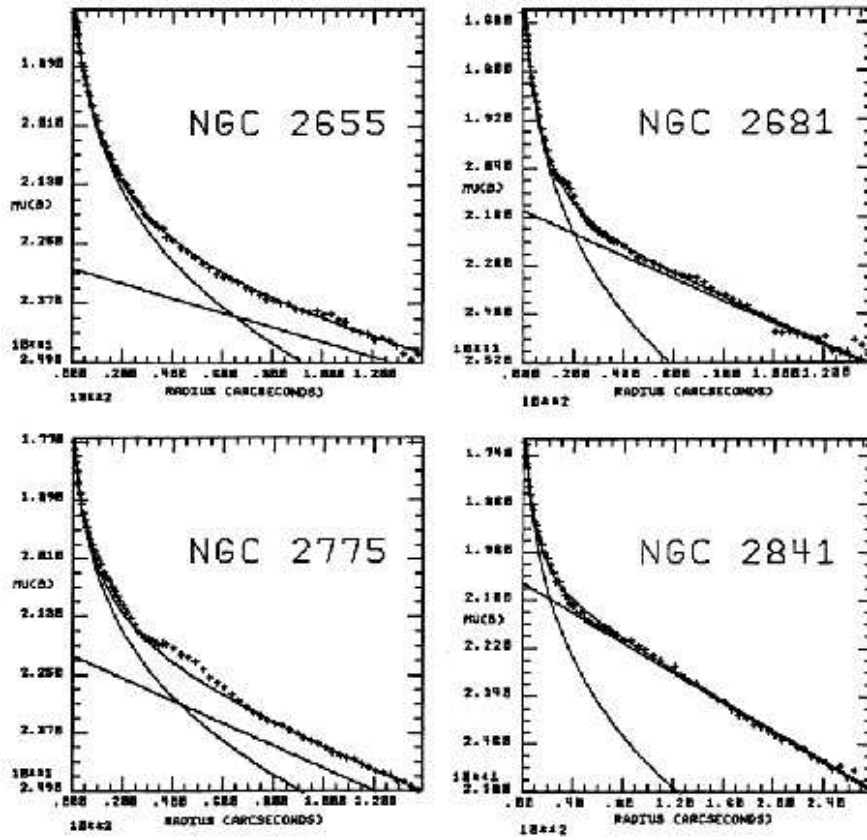


Figure 3.5: Example of bulge+disk decomposition from [Borison \(1981\)](#).

bulge+disk decomposition ([Schade *et al.*, 1995, 1996](#); [Ratnatunga *et al.*, 1999](#)) (see figure 3.5). The bulge+disk decomposition has become popular because, as noticed by [Simard *et al.* \(2002\)](#), (a) it is rooted in the very first studies of the functional form of galaxy radial surface brightness profiles ([de Vaucouleurs, 1948, 1959](#)); (b) it provides a comfortable mental picture of the overall structure of a distant galaxy, i.e., it is conceptually simple to relate a quantitative measurement of galaxy type such as bulge-to-total light ratio to the familiar Hubble types; and (c) photometric entities such as bulges and disks have distinct dynamical counterparts.

The bulge can be modeled with a de Vaucouleurs law ([de Vaucouleurs, 1948](#)), with $f(r) = f_e e^{(-r/r_e)^{1/4}}$, where r_e is the effective radius, and f_e the flux within the effective radius. The disk can be modeled with an exponential law: $f(r) = f_0 e^{-(r/r_d)}$, where f_0 is the flux in the center of the galaxy, and r_d is the disk radius. More recent studies show that it is more advisable to model the bulge, and the disk, with a Sersic law ([Sersic, 1968](#)). In such a case, the power 1/4 of the bulge profile is replaced by a power 1/n (n is the Sersic index), and the exponential profile describing the disk is similar to the Sersic law when $n=1$ (see more details in section 6.2.1).

Taking the best fit² to the above models, one can retrieve different physical parameters, such as flux, size, orientation, etc. These methods thus also allow us to measure the flux ratio between the different structures and the total galaxy flux. One example is the bulge to total light ratio (B/T), which is correlated to the morphological types (Simien & de Vaucouleurs, 1986; Kent, 1985).

The first parametric methods were based on 1D fits, which means that the light distribution of the galaxies was considered to be fixed within a unique value of inclination, position angle (P.A.), and ellipticity along the optical major axis. The first works focused on local galaxies (e.g., Kormendy, 1977; Burstein, 1979; Boroson, 1981; Kent, 1985, see figure 3.5)(or more recently Pignatelli *et al.*, 2006), even though, with the arrival of new technologies and the Hubble Space Telescope (HST), deeper images with good signal-to-noise ratios (S/N) have allowed them to be applied to galaxies in the distant Universe. However, their principal limitation is the fact that they assume a 1D light distribution. Many real galaxies exhibit more than two structural components such as nuclear sources, bars, spiral arms, etc., or even in the presence of only a bulge and a disk, the ellipticity and/or the P.A. of these components might be functions of galactocentric distance (Simard *et al.*, 2002). Another limitation is that they fix a unique center for the whole galaxy structures, which is not necessarily the case.

To improve upon these approximations, new techniques, such as isophotal ellipse fitting in which it is customary to let ellipticity, position angle, and centroid vary from one ellipse to another, were developed (e.g., Peng *et al.*, 2002, 2010). Thus, the whole galaxy light distribution is now taken into account in a 2D fitting model. Another improvement of such 2D models is that different structures can be modeled at the same time (for example, bulge+disk+bar). These 2D models present a higher number of parameters to be fitted than the 1D models. It is thus necessary to have images where objects are well resolved, and the S/N ratio is high enough to avoid degeneracies (see Simard *et al.*, 2002; Häussler *et al.*, 2007, for a more detailed discussion on the S/N effects). Another solution to reduce the possible degeneracies is to limit the number of free parameters during the fitting process.

From the retrieval of the physical parameters of the different components, several morphological classifications have been proposed. Ravindranath *et al.* (2004) and Barden *et al.* (2005), for example, proposed a classification based only on the Sersic index n . In such a case, they distinguish between spheroidal types ($n > 2.5$), and late type galaxies ($n < 2.5$). Cassata *et al.* (2005) and Sargent *et al.* (2007) showed later that a classification based only on n is not as robust as a classification based on the B/T index. Nevertheless, we show

²generally the best fit is determined by using a χ^2 minimisation. More details about the χ^2 procedure can be found in subsection 6.2.1.

in Neichel *et al.* (2008) (see also chapter 5 and 6 for more details) that even the B/T value alone is not sufficient to robustly classify morphologically all galaxies.

3.2.3 The color information

The color can be defined as the difference between two magnitudes (obtained using two different broad-band filters). By convention, the magnitude derived from the filter having the largest central wavelength is subtracted from the magnitude obtained from the filter having the smallest central wavelength (see subsections 6.2.3 and 6.2.5). A negative value will then means that we observe more light through the filter with smaller wavelength, and it is represented with a blue color. The contrary is represented with a red color.

We can then derive a color for the whole galaxy (integrated color), a color for the different components of the galaxy (e.g., disk, bulge, etc.; Ellis *et al.*, 2001), or even pixel by pixel color analysis (Abraham *et al.*, 1999; Menanteau *et al.*, 2001, 2004; Zheng *et al.*, 2004, 2005; Papovich *et al.*, 2005; Lanyon-Foster *et al.*, 2007)(see figure 3.6, and subsections 6.2.3 and 6.2.5). These last are only possible if the objects are well resolved. An important precaution when working with samples of galaxies at different redshifts is to use different filters which correspond to the same rest-frame band, in order to limit the k-correction effects (more details about the color analysis are shown in chapter 6).

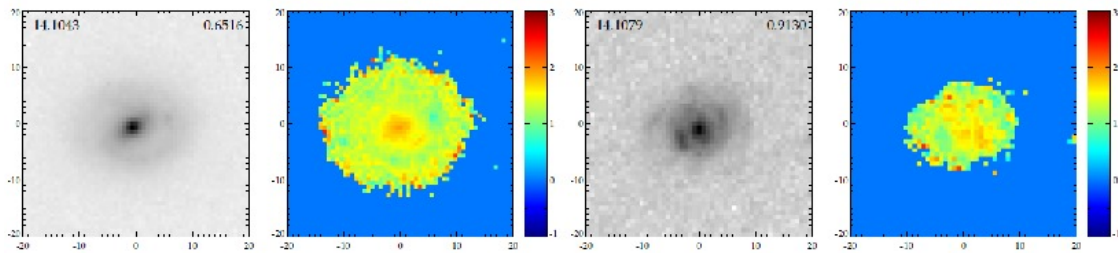


Figure 3.6: Example of color maps from Zheng *et al.* (2005).

In subsection 1.2.1, I show that each filter gives different information about the galaxy³. Thus, by comparing the magnitudes from two different bands one can have an idea, e.g., of the stellar population which dominate the whole galaxy or a part of it (old stars are red, and young stars are blue, even though it could be affected by dust). This can also give an idea of the history of the galaxy, or the history of the section of the galaxy we are interested in, by comparing its color

³revealing the different constituents of the galaxy.

with stellar population models (e.g., [Menanteau *et al.*, 2001](#); [Zheng *et al.*, 2004, 2005](#); [Rawat *et al.*, 2007](#)).

The integrated color is also related to the galaxy morphology ([Roberts & Haynes, 1994b](#)). Elliptical and lenticular galaxies are composed mainly by old stars, which are red. On the contrary, spiral and irregular galaxies are mainly composed of young stars, which are bluer. However, such a correspondence between integrated colors and morphological types must not be taken too seriously (for a detailed discussion see subsections [2.1](#), [6.2.5](#), and [6.4.3](#)). In any case, this correlation has also been adapted to the non-parametric coefficients (see subsection [3.2.1](#)). [Conselice *et al.* \(2000\)](#) proposed a sequence connecting the A and S parameters to the integrated color of galaxies, going from the red and symmetric galaxies (ellipticals) to blue and asymmetric Sc-d. [Lauger *et al.* \(2005a\)](#) also proposed to use the color information to make a kind of spectro-morphological classification. It is done by constructing A-C planes with the coefficients measured in different wavelength bands (i.e., k-morphological correction)(see also [Kuchinski *et al.*, 2000](#); [Burgarella *et al.*, 2001](#)).

Studying the morphological evolution

Contents

5.1	Introduction	63
5.2	The survey	70
5.3	Sample selection and representativeness	73
5.4	Results of the IMAGES survey	75
5.4.1	Kinematic evolution of galaxies since $z=1$	76
5.4.2	The morpho-kinematic correlation 6 Gyr ago	76
5.4.3	Chemical evolution of intermediate-mass galaxies since $z\sim 0.7$	77
5.5	Beyond the IMAGES survey	77

4.1 Morphological studies in the distant universe

4.1.1 Local universe

The local Universe has been studied over the past two centuries (see chapter 1), and it is better known than the distant one (at least in what concerns the fraction of the different galaxy populations). The most recent atlas of local galaxies are, amongst others, [Sandage & Bedke \(1994\)](#), and the Sloan Digital Sky Survey, including almost one million galaxies (see figure 4.1).

Nowadays, all studies confirm that in the local Universe $\sim 81\%$ of galaxies are spirals, $\sim 14\%$ are early-type, and $\sim 5\%$ are irregulars ([Nakamura *et al.*, 2004](#); [Fukugita *et al.*, 2007](#), see also chapter 1). This confirms the composition of the local Hubble sequence discussed in chapter 1.

However, no sequence has been derived for the distant Universe. The epoch from $z=1$ to $z=0.4$ is crucial for the assembly of galaxies. It still remains to understand how their morphological structures were formed and what physical processes fundamentally drove their assembly. While disks can be built by accreting cooling

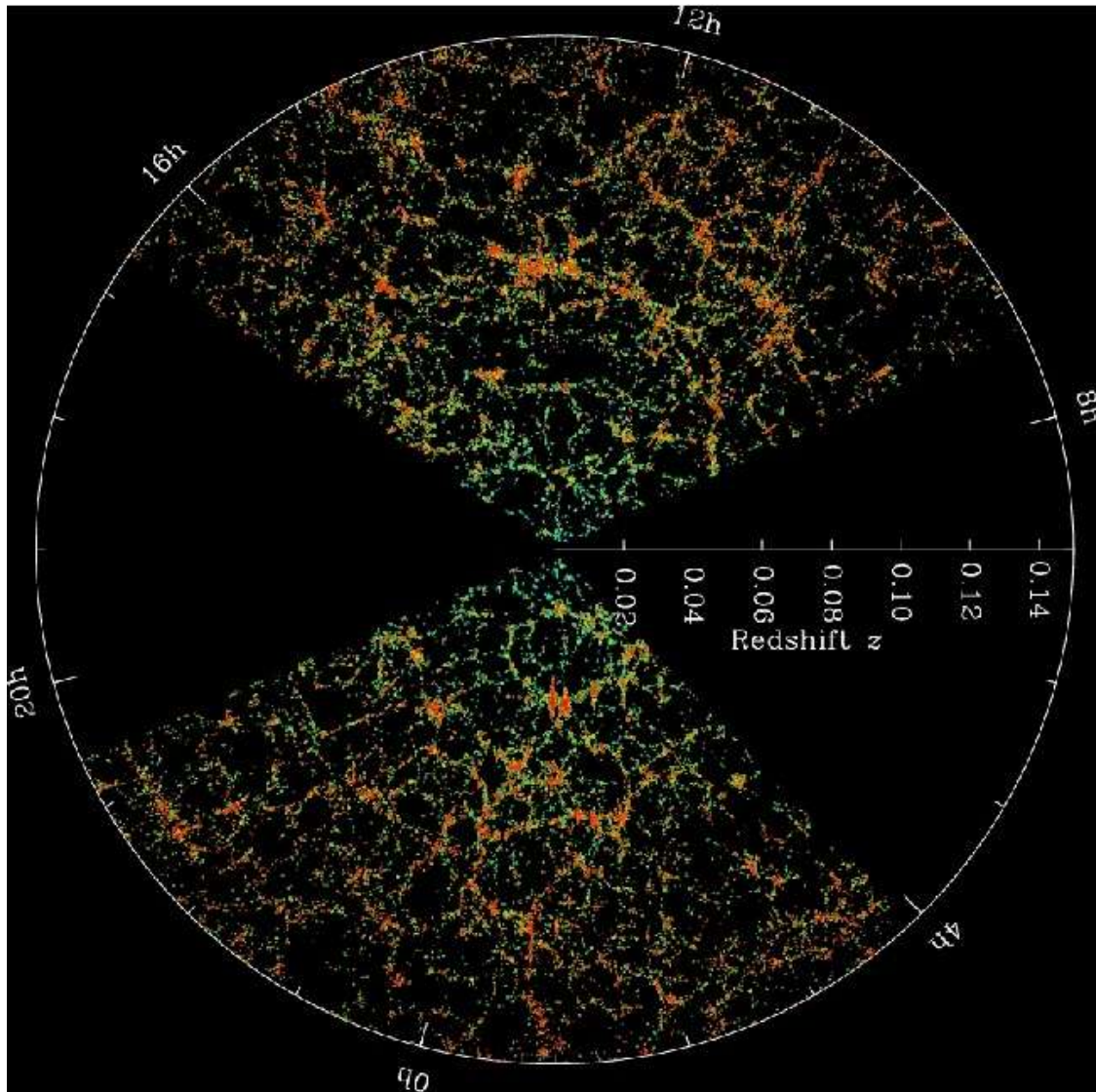


Figure 4.1: SDSS 3-dimensional map of the galaxy redshift distribution. Each point represents a galaxy, and colors are according to the ages of the galaxy stars (with the redder points showing galaxies that are made of older stars.). Both slices contain all galaxies within -1.25 and 1.25 degrees declination. (Credit: M. Blanton and the Sloan Digital Sky Survey.)

gas in a dark halo (e.g., [Fall & Efstathiou, 1980](#)), the formation of bulges may be regulated by either external or internal processes (see [Combes, 2000](#), for a review). The bulges can be formed via either primordial collapses at an early time (e.g., [Eggen *et al.*, 1962](#)) or hierarchical mergers (e.g., [Kauffmann, 1996](#)). In the later case, violent star formation is expected (ULIRGs are mostly associated with merging systems, [Sanders & Mirabel, 1996](#)). Comparison of morphological properties between distant and local galaxy populations is essential to, e.g., unveil whether

the merging process regulate bulge formation. In the secular processes, bars are mostly suggested to be efficient at driving gas into the galactic center and changing star orbits to form a central bulge-like structure (Combes *et al.*, 1990; Debattista *et al.*, 2004).

4.1.2 Distant Universe ($z \gtrsim 0.3$)

Undoubtedly, with the arrival of the HST, over the past two decades a lot of work has been carried out to uncover the morphology of distant galaxies.

One of the main contribution of such works has been to address the morphological evolution of field galaxies. Lilly *et al.* (1998) found that massive disk galaxies show a constant number density from $z \sim 1$. Elliptical galaxies also exhibit little evolution up to $z \sim 1$ in their number density (Schade *et al.*, 1999), although non-negligible star formation at $z < 1$ was detected in a substantial sub-population (Menanteau *et al.*, 2001; Treu *et al.*, 2002). Additionally, morphological investigations based on large galaxy samples revealed that the number density of irregular galaxies increases with redshift (Brinchmann *et al.*, 1998; van den Bergh *et al.*, 2000, see figure 4.2). Such a significant evolution of irregular galaxies was suggested to be associated with a transformation into regular galaxies (Brinchmann & Ellis, 2000).

Indeed, van den Bergh *et al.* (1996, 2000) and Brinchmann *et al.* (1998) found that disk galaxies at redshifts $z \gg 0.3$ have morphologies that appear to differ systematically from those of nearby galaxies. Furthermore, while accumulated evidence suggests that most massive elliptical galaxies in the field are in place prior to $z = 1$ (e.g., Daddi *et al.*, 2000; Cimatti *et al.*, 2002) (see also van Dokkum & Ellis, 2003; Bell *et al.*, 2004b; Drory *et al.*, 2004), the formation of spiral galaxies is still debated (Hammer *et al.*, 2005b).

However, such conclusions must still be taken carefully because they result from different studies, which have been done using different samples with different selection criteria, and not necessarily with equivalent observational data for distant and local galaxies. Moreover, some of these studies have been carried out using different morphological classification methods. It has been noted in the previous chapter that some methods are still not good enough to separate the different morphological types correctly. Therefore, compared with the galaxy distribution along the Hubble sequence in the local universe, a complete morphological census of field galaxies at $0.4 < z < 1$ will provide clues to understand their global morphological transformation and evolution. In such a case, a very careful analysis of the observational data available must be done, in order to guarantee the possible comparison between local and distant morphologies.

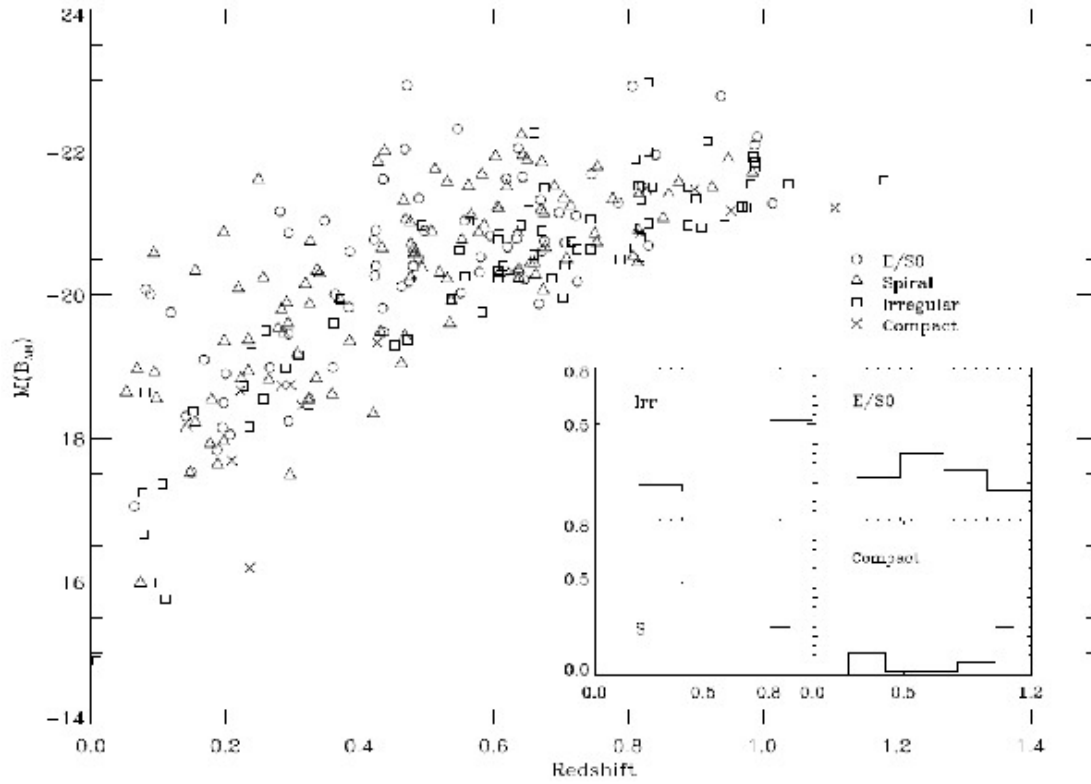


Figure 4.2: Distribution of galaxies in the $M(B_{AB}) - z$ plan from Brinchmann *et al.* (1998). As it can be noticed in the histograms at the right-bottom, the fraction of irregular galaxies increases with redshift.

Concerning objects at $z \gg 1$, nowadays we do not dispose of morphologically exploitable images for galaxies at more than 8 Gyr in the past. Nonetheless, the futures ELTs will give us a better morphological view of such epochs.

4.2 Need of representativeness

In subsection 1.2.1, I made a description of the principal considerations to be taken into account when classifying a sample of galaxies, assuming that the number of galaxies in the sample being studied is high enough to avoid any morphological type population to be missed (see below). However, beyond the selection criteria (see subsection 1.2.1), the representativeness of a sample is another fundamental consideration to be taken into account. How could we make conclusions, concerning the evolution of a specific galaxy characteristic, by studying a sample that does not statistically represent the whole galaxy populations? It is a difficult task. Indeed, my experience during my thesis showed me that representativeness and

selection criteria must be treated carefully. In [Neichel *et al.* \(2008\)](#) (see chapter 5), we studied a representative sample of distant galaxies (see also [Delgado-Serrano *et al.*, 2010](#), in chapter 6), proving such a representativeness by comparing them to the luminosity function at the respective redshift. Nonetheless, the selection criteria adopted in Neichel *et al.* limited the morphological types to some specific populations (see subsection 1.2.1).

4.2.1 Sample representativeness and luminosity function

Galaxy surveys are gathering large samples of galaxies. Their aims are to minimise statistical uncertainties (for 10000 galaxies, \sqrt{N}/N is 1%), and often to overcome the important problem of cosmic variance. One example of the consequence of such statistical uncertainties is evoked in subsection 1.2.1: concerning the different morphological type populations, the smaller is a sample, the larger is the probability to miss one of them (e.g., the less abundant population). However, the study of such large quantities of galaxies poses some time consuming problems, as well as some instrumental availability problems (e.g., if we study the morphology of 1000 galaxies, it will be quite difficult to dispose of kinematic observations for all of them, because the observational techniques are more complicated and time consuming).

As a result, a high fraction of works are based on small samples of galaxies to study carefully the different properties of all the galaxies in the sample. Nonetheless, they are facing the small statistics issue (for 100 galaxies, \sqrt{N}/N is 10%). Because of this, they have to be very efficient in controlling the selection effects related to the target selection. Having said this, they are quite unique to probe, at the same time, dynamics, stellar populations, gas abundances, extinction and star formation rate. Why is this so important? Because $z \sim 1$ is already probing the universe at less than half its present age, where changes in galaxy properties are expected. Indeed, we know that the morphological appearances of distant galaxies are far more complex than those illustrated in the Hubble sequence (see previous subsection).

To measure the representativeness of a small sample, it is therefore judicious to use the galaxy luminosity functions derived from larger samples (e.g., [Pozzetti *et al.*, 2003](#); [Cirasuolo *et al.*, 2007](#)). The luminosity function gives the space density of galaxies per luminosity bin. It is hence a representation of the galaxy number distribution with respect to their mass. Since the gravitational force is the principal responsible for the formation of structures (see appendix A), the mass can be consider as the most important parameter that characterized the whole galaxy population.

4.2.2 What are the galaxies responsible for the evolution?

The origin of the star formation density decline over the past 8 Gyr is still a matter of debate. Studies based on spectral energy distributions (SEDs) of galaxies predict that 30% to 50% of the mass locked into stars in present-day galaxies actually condensed into stars at $z < 1$ (Dickinson *et al.*, 2003; Pozzetti *et al.*, 2003; Drory *et al.*, 2004). This result is supported by the integration of the star formation density when it accounts for infrared light (Flores *et al.*, 1999). Indeed the rapid density evolution of luminous infrared galaxies (LIRGs, forming more than $20 \text{ M}_{\odot} \text{ yr}^{-1}$) suffices in itself to report for the formation of a high fraction of the total stellar mass found in intermediate mass galaxies (from 3×10^{10} to $3 \times 10^{11} \text{ M}_{\odot}$) (Hammer *et al.*, 2005a). As opposed to the idea of galaxy "downsizing" (Cowie *et al.*, 1996) - strong evolution only in the faint blue dwarf population - there is a growing consensus that most of the decline of the star formation density is indeed related to intermediate-mass galaxies (Hammer *et al.*, 2005a; Bell *et al.*, 2005) (see more details in section 5.1).

It is more and more convincing that massive E/S0s and dwarves¹ could not be responsible of the star formation density decline, because the first ones were mostly in place at $z=1$ (see previous subsection), and the second ones contribute marginally to the global stellar mass or metal content. It is therefore interesting to carry out a detailed study of the morphological and kinematic properties of the population of intermediate mass galaxies, in which at least 2/3 of the present-day stellar mass is locked (Brinchmann & Ellis, 2000; Heavens *et al.*, 2004).

¹Hammer (2005) shows how unclear are the words "massive" or "dwarves". Indeed, let's define massive galaxies as those having $M_{\text{star}} > 3 \times 10^{11} \text{ M}_{\odot}$ (i.e. bigger than the Milky Way), and dwarves as those having $M_{\text{star}} < 3 \times 10^{10} \text{ M}_{\odot}$. This is somewhat arbitrary (as any definition), although with these criteria, E/S0 dominate the massive regime, spirals dominate the intermediate mass regime, and irregulars become a significant population in the dwarf regime (see figure 4.3).

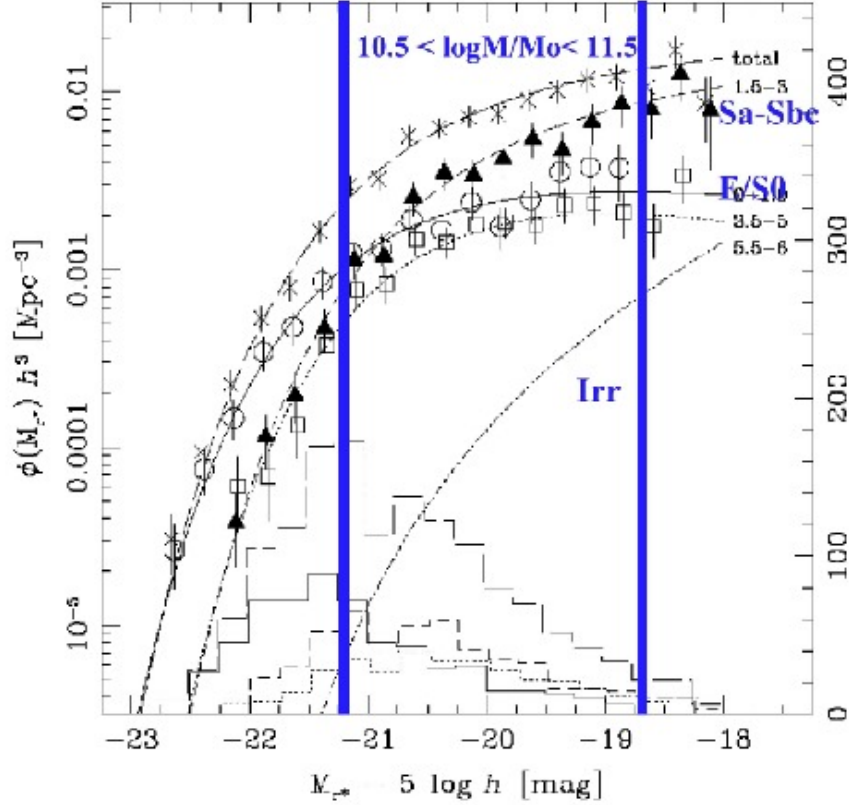


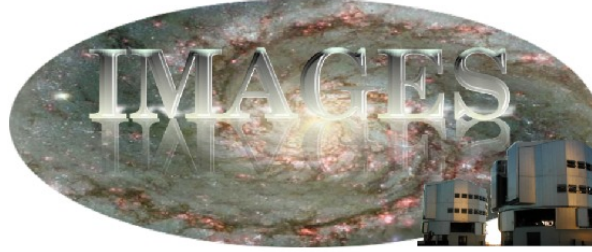
Figure 4.3: Intermediate mass galaxies (Hammer, 2005). This is an adaptation of figure 3 of Nakamura *et al.* (2004), which presents the morphological-dependent luminosity functions (MDLFs) from the SDSS. The two vertical blue lines distinguish the area of intermediate mass galaxies. For this purpose Hammer (2005) have assumed a ratio $M/L_{r*}=5$, by averaging results from Glazebrook *et al.* (2003) fits of the spectral energy distribution of SDSS galaxies.

Part III

Our approach: Looking for the
evolution at $z < 1$

CHAPTER 5

IMAGES



Intermediate
Mass
Galaxy
Evolution
Sequence

Contents

6.1	Our galaxy sample	82
6.2	The parameters retrieval: analysis of the observables . . .	82
6.2.1	The light profile analysis	83
6.2.2	Structural parameters	89
6.2.3	The color information	91
6.2.4	Bar inspection	94
6.2.5	Color determination	95
6.3	The morphological classification method	97
6.4	Results	98
6.4.1	Galaxy number density	98
6.4.2	Bar fractions	99
6.4.3	Color distribution	100

5.1 Introduction

Over the years before our survey IMAGES (Intermediate MAss Galaxies Evolution Sequence), a lot of efforts had been made to study the properties of galaxies in the distant universe (at $z \sim 1$), showing growing evidence of a significant evolution with cosmic time. Examples of such evidence are the rapid time decrease of the cosmic SFR (star formation rate) density, the role of merging in the evolution of galaxies, the importance of studying in details the morphology of high-redshift

galaxies, and the possible evolution of the TFR.

Concerning the SFR history, it had been found a decline of the cosmic SFR by a high factor ~ 10 from $z \sim 1$ to the present (see figure 5.1; *Le Floc'h et al.*, 2005; *Haarsma et al.*, 2000; *Wilson et al.*, 2002; *Cowie et al.*, 1999; *Flores et al.*, 1999; *Hammer et al.*, 1997; *Lilly et al.*, 1996; *Madau et al.*, 1996). Although the conclusions are reached from different data, they are consistent within a factor of 3 (*Hopkins*, 2004). Furthermore, recent results from Herschel observations, which give a more precise measurement of the SFR¹, consolidate such a strong evolution of the cosmic SFR (*Rodighiero et al.*, 2010). *Heavens et al.* (2004), using the SDSS survey, suggest that the co-mobile star formation density may have reached its peak as late as $z \sim 0.6$, and this bulk of star formation was mostly dominated by star formation in galaxies in the range $3\text{--}30 \times 10^{10} M_{\odot}$ (see also *Hammer et al.*, 2005a). Even if such a peak could be at $z \sim 2$ due to dust effects and the larger measure uncertainties at $z \geq 1$ (*Pérez-González et al.*, 2005, 2008), the high SFR values at $z < 1$ led argue that about half of the local stellar mass density has been formed since $z = 1$, mostly in luminous infrared galaxies (*Bell et al.*, 2005; *Hammer et al.*, 2005a; *Dickinson et al.*, 2003).

As a consequence of these facts, galaxy interactions and merging are mechanisms that could play a significantly larger role for star-formation and mass assembly in the distant universe than today (*Hammer et al.*, 2009a; *Hopkins et al.*, 2010). *Le Fèvre et al.* (2000) found that the merger rate in the distant universe ($z \sim 1$) was about 10 times higher than at low redshift (see also *Rawat et al.*, 2008; *Bell et al.*, 2006b; *Lotz et al.*, 2006; *Conselice et al.*, 2003). The high merger rate detected in the distant universe raises a challenge to the standard scenario of disk formation², since till today most of the simulations predict that major

¹The SFRs are calculated by assuming that they are proportional to the integrated infrared luminosity (LIR, typically $8\text{--}1000 \mu\text{m}$, Kennicutt 1998). Then, the flux through an IR broadband range is converted into LIR by fitting the flux using a SED library (e.g., *Chary & Elbaz*, 2001), in which for a given redshift and band flux, a unique solution to LIR exists. The previous works had only available observations in the $12\text{--}18 \mu\text{m}$ (e.g., *Flores et al.*, 1999) and $24 \mu\text{m}$ (Spitzer observations). These wavelengths are relatively far from the IR-SED peak (produced principally by the emission of the dust heated by young stars), which makes them sensitive to extrapolation errors. In addition, at these wavelengths, polycyclic aromatic hydrocarbon (PAH) emissions, as well as the AGN-heated dust emissions, are present and the ratio of their fluxes to LIR may create significant scatter. With Herschel observations at $160 \mu\text{m}$ (PACS), fluxes probe the emission much closer to the SED peak and are unaffected by the above issues (more details in *Nordon et al.*, 2010). It allows Herschel observations to provide the most reliable and least biased SFR measurements to date, avoiding large SED extrapolation errors.

²Early studies of the MilkyWay (MW) have led to a general description of the formation of a disk galaxy embedded in a halo (*Eggen et al.*, 1962). *Fall & Efstathiou* (1980) set out a model of galaxy formation assuming that disks form from gas cooling condensing in dark halos. Protogalactic disks are assumed to be made of gas containing a substantial amount of angular

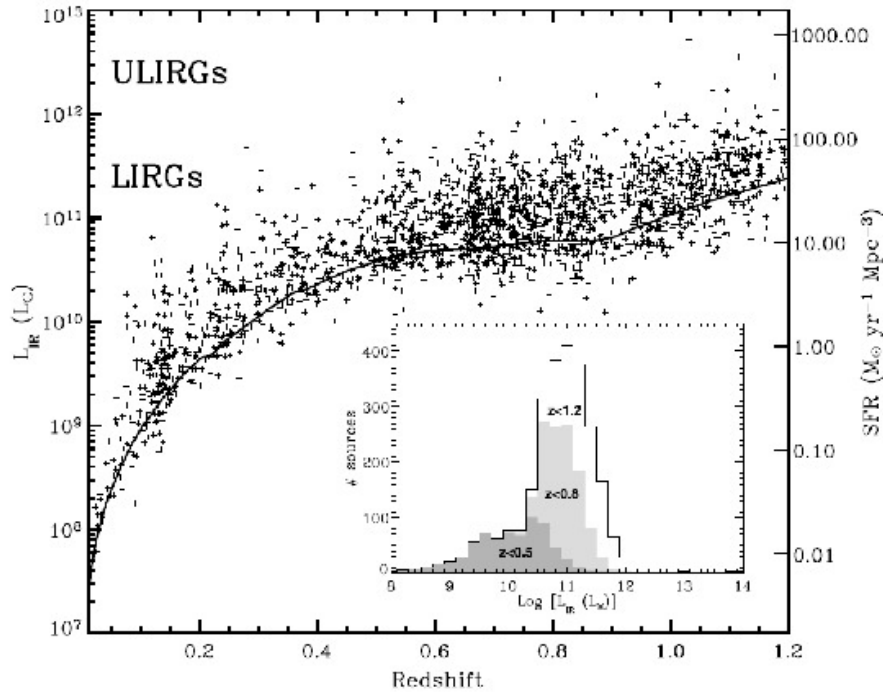


Figure 5.1: SFR evolution with redshift showed by [Le Flocc'h *et al.* \(2005\)](#) [Le Flocc'h *et al.* \(2005\)](#).

mergers form essentially elliptical galaxies (see subsection 2.2). Given the number of pairs detected in the past, if major mergers always generate elliptical galaxies inevitably, we would find a large fraction of elliptical galaxies in the local Universe rather than the $\sim 70\%$ of observed spiral galaxies. Similar problems appear with the observed fraction of luminous compact blue galaxies (LCBGs), which increases with redshift by about an order of magnitude out to $z \sim 1$ ([Rawat *et al.*, 2007](#); [Werk *et al.*, 2004](#)). First, LCBGs were associated to progenitors of local spheroidal or irregular galaxies at low redshift (e.g., [Koo *et al.*, 1995](#); [Guzmán, 1999](#)). Later, [Hammer *et al.* \(2001\)](#) proposed that these galaxies were the progenitors of the bulges of intermediate-mass spirals (admitted later by [Noeske *et al.*, 2006](#)). The last authors, using deep (HST/UDF) images, detect disk around distant LCBGs. Further 3D spectroscopic studies of the internal kinematics of LCBGs suggest that they are likely merger remnants (see [Puech *et al.*, 2006b](#), for a distant Universe sample)(see [Östlin *et al.*, 2001](#), for a local example). Interestingly, just a quick look of the ACS/HST images of most of the galaxies showed in [Puech *et al.* \(2006b\)](#) reveals quite peculiar morphologies.

momentum, which condenses into stars to form thin disks ([Larson, 1976](#)). These disks then evolve only through secular processes. This so-called standard model successfully reproduces the flat rotation curves and the size of spiral galaxies (e.g., [Mo *et al.*, 1998](#), and references therein), even though it does not reproduce the observed local angular momentum values (see subsection 2.2).

Indeed, in the past, morphological investigations have brought observational evidence that a large fraction of galaxies at intermediate redshift have peculiar morphologies that do not fit into the standard Hubble sequence (e.g., [Abraham *et al.*, 1996b](#); [Brinchmann *et al.*, 1998](#); [van den Bergh *et al.*, 2001](#); [Zheng *et al.*, 2005](#)). This could be related to the merger rate and SFR evolution cited above ([Hammer *et al.*, 2005a](#)). Furthermore, different observations suggest that most of the massive elliptical galaxies were in place prior to $z = 1$ ([Jimenez *et al.*, 2007](#); [Bernardi *et al.*, 2006](#)). While the formation and evolution of spiral galaxies still pose some problems and different physical processes can modify the galaxy properties over cosmic time (mergers have always been associated to the destruction of the disk), a robust morphological analysis of distant galaxies is crucial to understand their component structures and the eventual relation between morphology and kinematics in the distant Universe.

In addition to the study of properties of individual galaxies with the IMAGES survey, we have also studied fundamental relations such as the Tully-Fisher relationship (TFR, [Tully & Fisher, 1977](#)) (see [Giovanelli *et al.*, 1997](#), for a cosmological view), which relates the luminosity and the rotation velocity of disk galaxies (see figure 5.2). Pioneering studies ([Vogt *et al.*, 1996, 1997](#)), using slit spectroscopy, have claimed a strong evolution of the TFR as a function of cosmic time. Out to $z \sim 1$, the B-band TFR has been found to evolve by ~ 0.2 -2 mag (e.g., [Portinari & Sommer-Larsen, 2007](#), and references therein). This brightening of the B-band TFR can be explained by the enhanced star-formation rates at higher redshifts ([Ferreras & Silk, 2001](#); [Ferreras *et al.*, 2004](#)), but it is still a matter of debate. [Conselice *et al.* \(2005b\)](#), instead of B-band, used the K-band to retrieve the TF relationship. The importance of the K-band is that it is less affected by the dust and is a better tracer of the stellar mass than the B-band. Conselice *et al.* do not find significant evolution in either the stellar mass or K-band TFR's slope or zero point. However, the most striking evolution of the TFR is provided by its large scatter at high redshifts ([Conselice *et al.*, 2005b](#), see figure 5.2), which may be related to disturbed kinematics in distant galaxies that can be infer by extrapolating the observed kinematics of local galaxies (e.g., [Kannappan & Barton, 2004](#), see figure 5.3). Another possible cause of this scatter at high z is the sample selection (see subsection 1.2.1). In any case, it is crucial to find an explanation to the discrepancy between the previous studies, in order to understand whether the TF relationship is preserved at higher redshift, or if it is only a property of local galaxies, as well as better understand the morpho-kinematic evolution of galaxies.

As the above kinematic investigations at intermediate redshift were based on long (or multi) slit spectroscopy, the large dispersion (e.g., in the TFR) may thus be related to instrumental effects. Indeed, measuring the kinematics of distant galaxies precisely and robustly is necessary to study galaxy evolution. However,

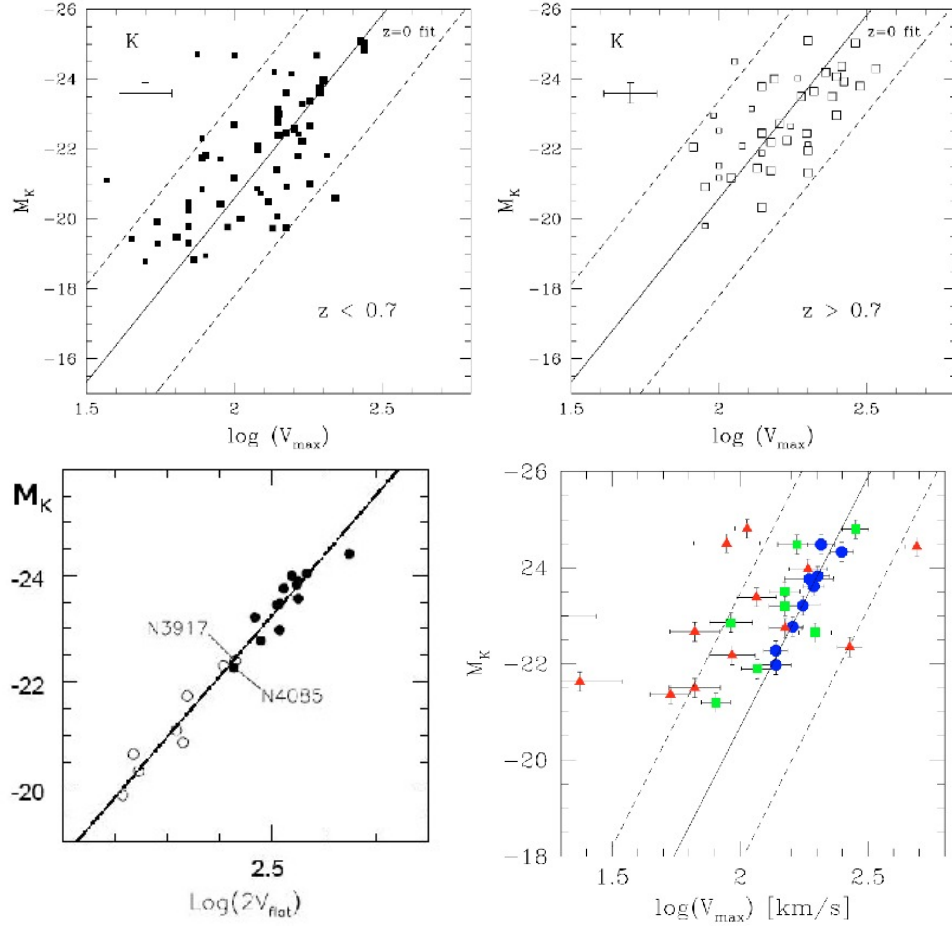


Figure 5.2: *Top:* TFR scatter at high redshift from [Conselice et al. \(2005b\)](#). *Bottom* (from left to right): 1.) TFR scatter in the local Universe from [Verheijen \(1997b,a\)](#) (see also [Bell & de Jong, 2001](#)). 2.) TFR scatter in the distant Universe using integral field spectroscopy from [Flores et al. \(2006\)](#). Here, the blue circles are the galaxies classified as rotating disk, red triangles are galaxies with complex kinematics, and green squares are galaxies presenting a perturbed rotation. If we take into account only the rotating disk galaxies the significant scatter observed in the distant TFR (bottom-left) disappears.

this is often beyond what can be achieved with classical long-slit spectroscopy (see figure 5.4). The morphologies and kinematics of distant galaxies are often complex, and their small sizes make it very difficult to precisely position and align the slit. Both limitations can be overcome with integral-field spectroscopy. 3D spectroscopy appears to be a pre-requisite to sample the whole velocity field of individual galaxies in order to limit the uncertainties related to the major axis determination and those related to galaxy interactions. Such effects have been already tested for nearby spirals by comparing Fabry-Perot to slit measurements which show that slit measurements can easily provide under or over estimates of the maximum velocity by factors reaching 50% ([Amram et al., 1995](#)). Worse yet is that many of

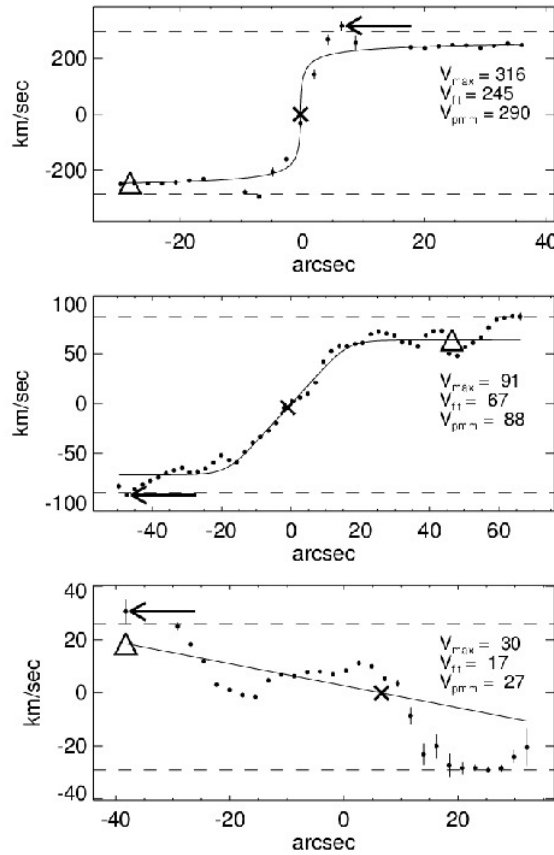


Figure 5.3: Detection of anomalous rotating curves in local galaxies by [Kannappan *et al.* \(2002\)](#). We can see the waves in the part corresponding to the "plateau" of the rotating curves.

the high redshift studies do not even place the slits along the major axis in order to preserve the multiplex advantage of slitlet MOS. Physically speaking, much larger uncertainties are expected for distant galaxies which are actively forming stars (up to rates larger than $100M_{\odot}/\text{yr}$) and for which the frequency of interactions is very common. Only velocity fields from 3D spectroscopy can disentangle the pure circular rotation from chaotic/non circular motions ([Flores *et al.*, 2006](#)). Even if rotation curve anomalies, such as those detected by [Kannappan *et al.* \(2002\)](#) (see figure 5.3) using long slit spectroscopy on nearby galaxies, can be explained by velocity field distortions due to minor or major mergers taking place during the history of each galaxy, it is unclear whether such details can be identified on distant galaxies by using long slit spectroscopy. These last years, it has then become urgent to investigate the full 3D kinematics of distant emission line galaxies.

3D spectroscopic observations can provide us with detailed kinematics, including accurate measurements of velocities in order to study physical relations such as the Tully-Fisher one ([Tully & Fisher, 1977](#)) (see also [Flores *et al.*, 2006](#)).

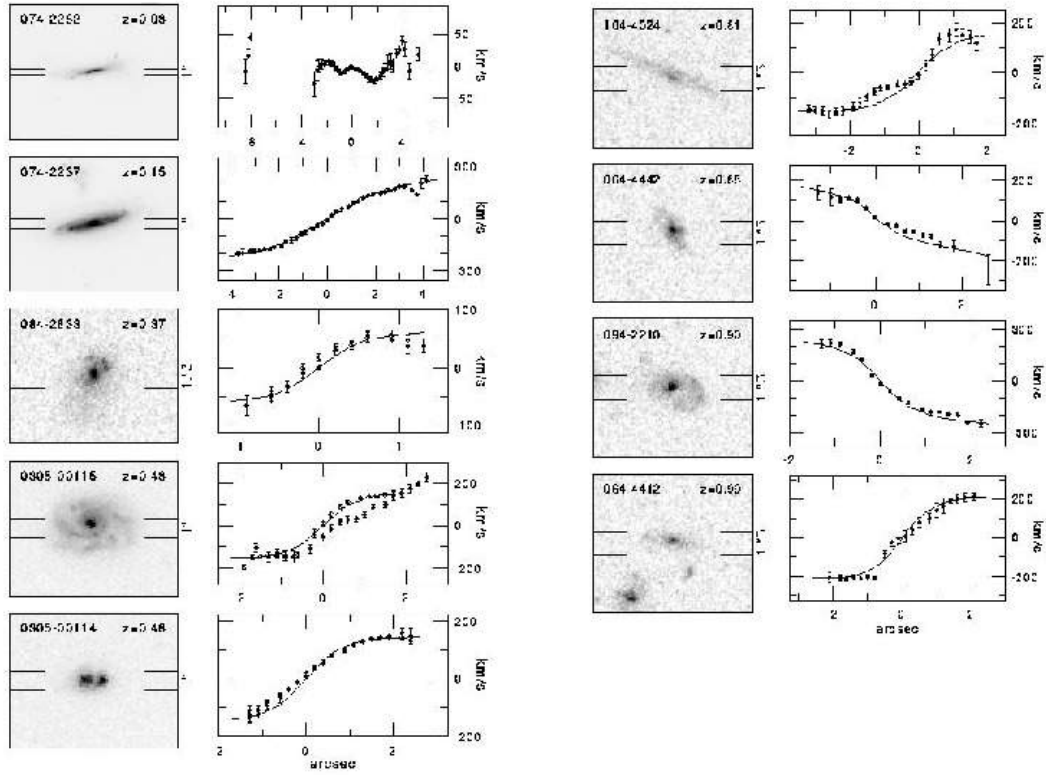


Figure 5.4: Rotating curves obtained by *Vogt et al. (1996)*. One column shows the spectroscopic long-slit arrangement overplotted on the galaxy image, while the other column shows the respective rotating curves.

VLT/GIRAFFE is one of the instrument which provides us with such an IFU mode. This special mode, thanks to the high spectral resolution ($R \sim 9\,000$) of GIRAFFE, allows us to disentangle the [OII] $\lambda\lambda 3726, 3729$ doublet (see figure 5.5). For these reasons, the kinematics observations of galaxies by IMAGES are made with the integral field spectrograph FLAMES/GIRAFFE. This spectrograph is installed on the UT2 at VLT, and has a wavelength range from 370 nm to 950 nm. The Integral Field Unit (IFU) mode of this instrument is composed of 15 IFUs with $R=9\,000$. Each IFU is made of 6×4 micro-lens (0.52 arcsec/lens) that can be displayed in the telescope focal plan. This makes it the only instrument in the world able to get the integral field spectroscopy of 15 objects at the same time (see figure 5.6).

Therefore, given the above tantalizing hints for galaxy evolution, the obvious complexity of the problem, and the contradictory results, the IMAGES survey has applied a different approach, using the state of the art in instrumentation, in order to study the kinematic of distant galaxies. We then consider that the most significant way forward is to conduct a dynamical study of a large

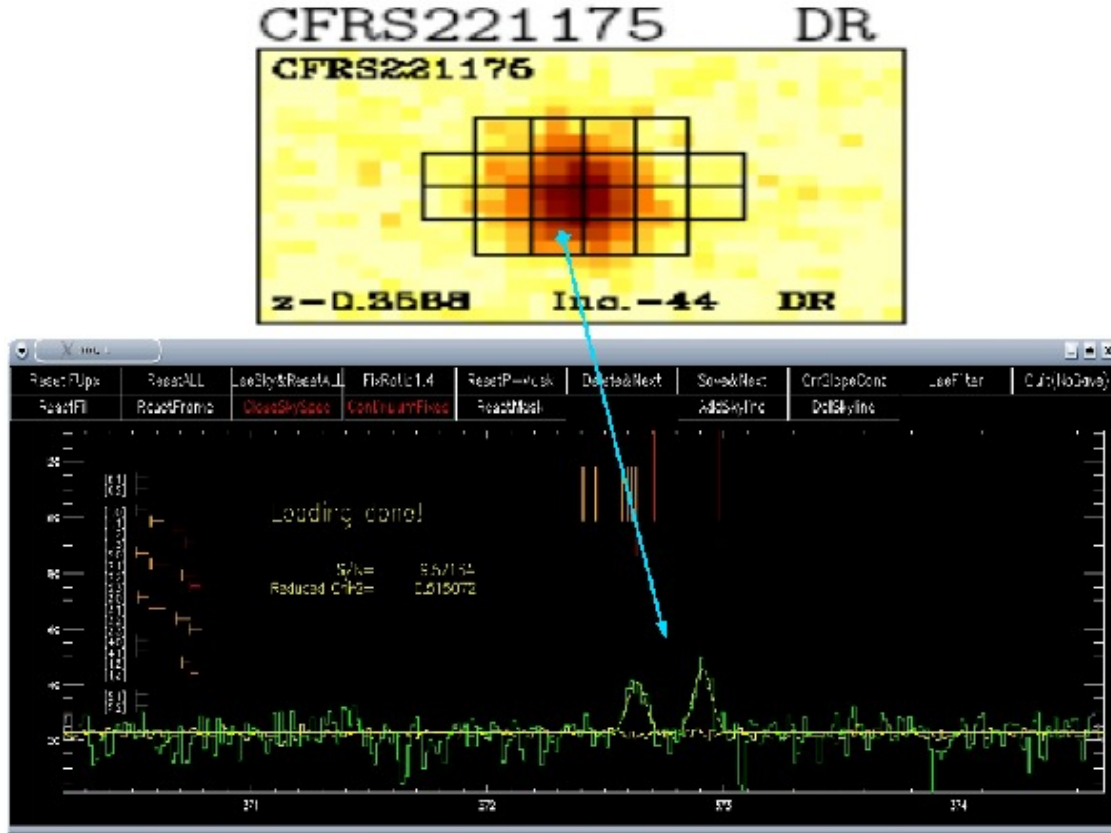


Figure 5.5: Measurement of the line wavelength and its full width at half maximum (FWHM) using the GIRAFFE line analysis interface.

sample of galaxies with excellent integral spectrophotometry (VLT/FORS2 observations) and photometric data (in terms of depth and angular resolution). The combination of the integral field spectrograph FLAMES/GIRAFFE with high resolution images from HST/ACS allow us to take advantage of estimating the evolution in both the morphological properties and kinematics of galaxies of a large sample of galaxies. As a result, with IMAGES, we will be in a position to evaluate the relative importance of the different physical processes (merging, dynamical friction between sub-components, monolithic collapse) driving the evolution of the ensemble of galaxies spanning a wide range of morphologies.

5.2 The survey

The Intermediate MAss Galaxies Evolution Sequence (IMAGES) survey has been constructed to get a maximum of information in a representative sample of distant galaxies (see below, and figure 5.7). Through the ESO large programme IMAGES, it has been intended to (1) establish the kinematic and morphological evolution

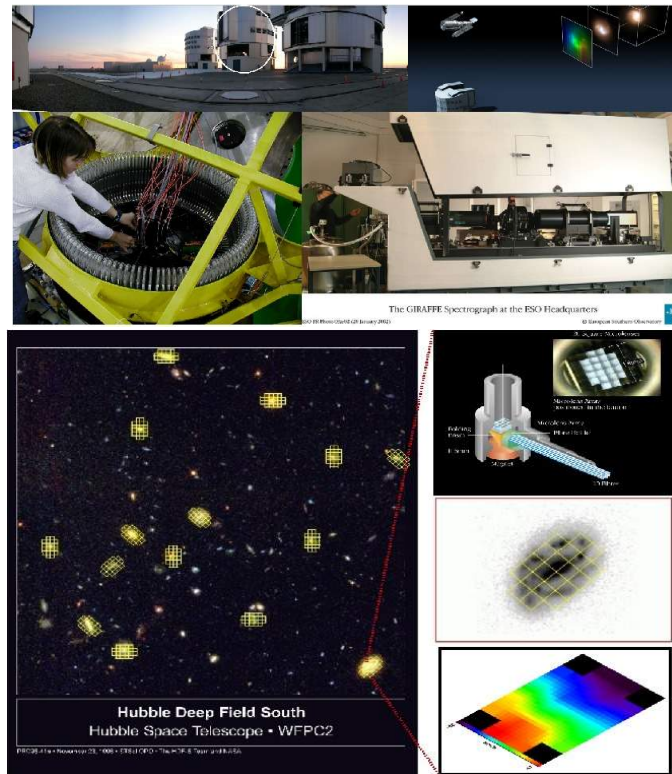


Figure 5.6: FLAMES/GIRAFFE, installed on the UT2 at VLT, can get the integral field spectroscopy of 15 objects at the same time. For this, in its IFU mode, it is equipped with 15 IFUs. Each one composed of 6x4 micro-lens (0.52 arsec/lens) which spatially cut the light of the galaxy, allowing to obtain 20 spectrum of different parts of the galaxy. Like this, the internal kinematics of distant galaxies can be decrypted.

of galaxies; (2) test the different physical processes leading to the present day Hubble sequence; (3) explain the star formation history of individual galaxy; and (4) test the evolution of mass-metallicity relation, angular momentum, size, and mass. The analysis involves combining multi-instrumental (principally GIRAFFE, FORS2 and HST) observations being carried out of a sample of intermediate mass galaxies, selected mainly by their rest-frame J_{AB} magnitude, derived from the multi-wavelength photometric data available.

The galaxies in the IMAGES survey are situated in the Chandra Deep Field South (see figure 5.8). The principal reason to chose this field is that it has been observed with a large number of instrument telescopes (WFI/MPI-2.2, EMMI/NTT, MIPS/Spitzer, RGS and EPIC/XMM-Newton, et.). Thus, photometry and morphology of galaxies in the visible comes from deep HST observations with the ACS camera (0.03"/pix). The coverage in the mid-IR at 3.6 μm , 8 μm , 12 μm and 24 μm is provided by the deep survey of the satellite Spitzer (with its instruments IRAC and MIPS). Observations in the radio range (3 mm, 12 mm, 3



Figure 5.7: Instruments used by IMAGES and the related observed quantities. These observations allow us to study the kinematics, the morphology, emission/absorption line properties, and the integral chemical properties of galaxies.

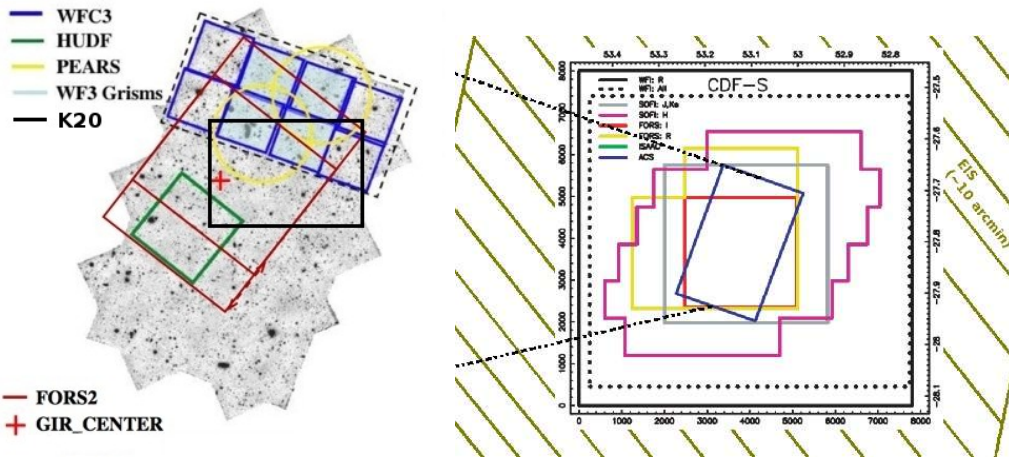


Figure 5.8: *Right*: schematic view of the CDF-S (Chandra Deep Field - South) amongst other surveys. *Left*: a zoom of the HST/ACS observation.

cm, 6 cm, 13 cm and 20 cm) from the Australian Telescope Compact Array and the Very Large Array (VLA), and X observations (0.1 to 15 keV, which correspond to ~ 0.1 nm - 12.4 nm) from the Chandra X Ray Observatory and XMM-Newton telescope are also public. Finally, many spectroscopic observations from ground telescopes provide the redshift of objects (e.g. VVDS, FORS2, K20, and our survey IMAGES). This field is then one of the largest deep field of sky observed by such a multitude of instruments.

5.3 Sample selection and representativeness

The IMAGES sample has been selected with the aim of containing a representative sample of galaxies having an absolute magnitude in J band brighter than -20.3 . This corresponds to galaxies with a mass roughly $> 1.5 \times 10^{10} M_{\odot}$. Galaxies with stellar masses from 3×10^{10} to $3 \times 10^{11} M_{\odot}$ are also known as intermediate mass galaxies, and at intermediate redshift ($0.4 \leq z \leq 1$), where the cosmic SFR density reaches its peak (Heavens *et al.*, 2004), they host most of the star formation (Hammer *et al.*, 2005a). Furthermore, these galaxies include most (from 65 to 85%) of the present-day stellar mass, which implies that about half of the stellar mass in intermediate-mass galaxies was formed since $z = 1$ (Dickinson *et al.*, 2003). Therefore, in the frame of the IMAGES survey, and complementary to the existing data from low resolution spectroscopic follow up (VVDS, K20, GOODS/FORS2/VIMOS), Ravikumar *et al.* (2007) observed a sample of galaxies with VIMOS/VLT to define the full IMAGES sample. This includes galaxies with $0.4 \leq z \leq 0.9$, and $M_J \leq -20.3$.

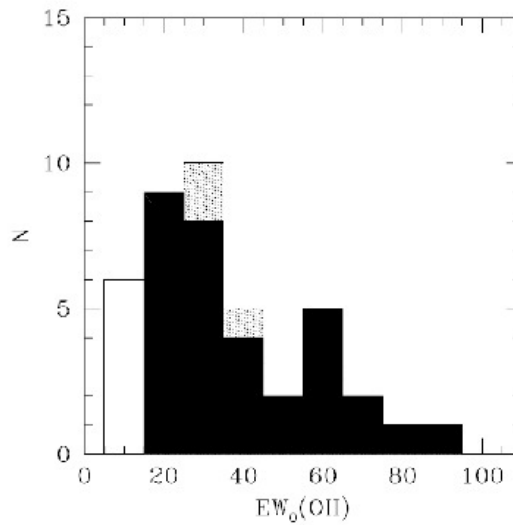


Figure 5.9: EW[OII] histogram for GTO sample galaxies (Flores *et al.*, 2006). For galaxies with $EW([OII]) \geq 15 \text{ \AA}$, GIRAFFE can retrieve their kinematics after 8 h of integration time (black region). The major difficulty studying the detected galaxies is then related to the flux strength. The three galaxies with $EW[OII] \geq 15 \text{ \AA}$, but with too spatially concentrated emission are displayed in grey. The open histogram includes objects with $EW_0([OII]) < 15 \text{ \AA}$.

Concerning the kinematics, galaxies have been also selected by having enough [OII] $\lambda 3727$ line emission, to be detected by GIRAFFE in a reasonable integration time. This line is inside the spectral range of GIRAFFE observations for galaxies at intermediate redshifts ($0.4 \leq z \leq 0.9$). Based on the GIRAFFE GTO by Flores

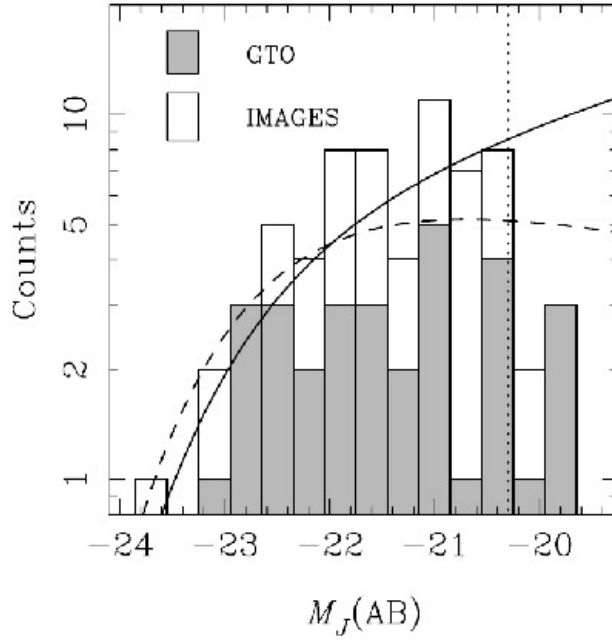


Figure 5.10: Number counts (in logarithmic scale) of selected galaxies versus AB absolute magnitude in J-band. In this figure, the GTO sample refers to [Flores *et al.* \(2006\)](#); the IMAGES sample refers to this paper. The vertical dotted line indicates the limit of the IMAGES program. Two luminosity functions derived from [Pozzetti *et al.* \(2003\)](#) are shown (full line: $z = 0.5$; dashed line: $z = 1$). The galaxies of IMAGES sample have redshifts ranging from $z = 0.4$ to $z = 0.75$. This implies that the combined sample of 63 galaxies with $M_J(\text{AB}) \leq -20.3$ is representative of galaxies with stellar masses larger than $1.5 \times 10^{10} M_\odot$ at $z \sim 0.6$.

[et al. \(2006\)](#), intermediate redshift galaxies with an $\text{EW}[\text{OII}]\lambda 3727 > 15 \text{ \AA}$ can be detected by GIRAFFE (see figure 5.9). These galaxies having a significant line emission flux represent 60% of intermediate mass galaxies at intermediate redshifts ([Hammer *et al.*, 1997](#)). Then, the kinematic observations of the IMAGES sample are based on the analysis of emission lines, mainly the $[\text{OII}]\lambda 3727$ emission line ([Yang *et al.*, 2008](#), and appendix C).

In order to test the representativeness of the sample we have compared the distribution of the J-band absolute magnitudes of the IMAGES sample, combined with the GTO sample of 35 galaxies ([Flores *et al.*, 2006](#)), with the luminosity function (LF) from ([Pozzetti *et al.*, 2003](#)). Both samples (GTO+IMAGES) can be merged because the selection of Flores *et al.* is equivalent to that of IMAGES and because both studies use the same instrumental set-ups and integration times ([Yang *et al.*, 2008](#)). Applying our criteria of $M_J(\text{AB}) \leq -20.3$, $0.4 \leq z \leq 0.9$, and $\text{EW}([\text{OII}]) \geq 15$, the IMAGES+GTO sample is left with 63 galaxies with high quality data to carry out our analysis. The luminosity distribution of the combined sample and the luminosity function at redshift of 0.5 and 1 are compared

in figure 5.10. Kolmogorov-Smirnov tests support that the complete sample follows the luminosity function in the $z = 0.4 - 0.75$ range at $>99.9\%$ confidence level (Yang *et al.*, 2008). Furthermore, the combined two samples include galaxies from 4 different fields, namely the CDFS, HDFS, CFRS03h and CFRS22h. It is then unlikely that our conclusions are affected by cosmological variance due to field-to-field fluctuations, and related to large scale structures (see Ravikumar *et al.*, 2007; Somerville *et al.*, 2004). Our sample is thus representative of $\text{MJ(AB)} \leq -20.3$ emission line galaxies at $z = 0.4 - 0.75$. At this redshift range, it is the only representative sample of distant galaxies with measured 3D kinematics that exist nowadays.

5.4 Results of the IMAGES survey

IMAGES broad results are described within a series of four papers. The first one (Yang *et al.*, 2008, see subsection 5.4.1) presents the kinematic study of distant galaxies, the second (Neichel *et al.*, 2008) makes the morpho-kinematic comparison in galaxies 6 Gyr ago, the third (Puech *et al.*, 2008) studies the Tully-Fisher relation and its evolution since $z \sim 0.6$, and the last one (Rodrigues *et al.*, 2008) investigates the chemical abundance evolution and the mass/metallicity relation of galaxies over the past 8 Gyr. I participated in two of them (IMAGES II and IMAGES IV, see sections 5.4.2 and 5.4.3). In these studies, my contribution is related to the morphological analysis of galaxies and its relation with their kinematics, the measure of $R_{1/2}$, inclinations, disk radius, EW[OII] , among others. Disk radius and inclinations are also important to establish the rotation velocities of galaxies. More details about the morphological analysis can be found in chapter 6. I have also studied the morphology of distant and local galaxies (Delgado-Serrano *et al.*, 2010), using this survey and the SDSS (Sloan Digital Sky Survey). This last study is detailed in chapter 6.

To better understand our results in subsections 5.4.2 and 5.4.3, I must introduce the kinematic studies of the IMAGES survey and its conclusions. The first study of intermediate redshift galaxy kinematics using FLAMES/GIRAFFE was carried out by Flores *et al.* (2006). They presented the first study of a statistically meaningful sample of 35 intermediate-mass galaxies at $z = 0.4-0.7$, using the integral-field multi-object spectrograph GIRAFFE at the ESO-VLT (see figure 5.6). They defined a classification scheme to distinguish between rotation and kinematic perturbations, which may stem from interactions and mergers, based on the 3D kinematics and high-resolution HST imaging (see appendix C). Yang *et al.* (2008) enlarges this first sample to finally count 63 distant galaxies kinematically studied with FLAMES/GIRAFFE. As mentioned in the previous section, this final sample is representative of intermediate redshift galaxies with $\text{MJ(AB)} \leq -20.3$. In addition, I have been analyzing new galaxies

(see appendix C). The methodology we use to retrieve the galaxy kinematic through FLAMES/GIRAFFE is well described in Flores *et al.* (2006) and Yang *et al.* (2008) (see also appendix C for more details about the 3D kinematic analysis).

5.4.1 Kinematic evolution of galaxies since $z=1$

Applying the same kinematic analysis than Flores *et al.* (2006) to a larger and representative sample of 63 distant galaxies from the IMAGES survey, Yang *et al.* (2008) find 32% of rotating disk, 25% of perturbed rotation galaxies, and 43% of galaxies with complex kinematics (see figure 5.11).

	HDFS	CFRS22h	CFRS03h	CDFS	Total (fraction)
RD	4	2	5	9	20 (32% \pm 12%)
PR	2	2	2	10	16 (25% \pm 12%)
CK	3	2	6	16	27 (43% \pm 12%)
UC	3 in total			3	6 (9%)

Figure 5.11: Results from Yang *et al.* (2008) showing the large percentage of galaxies with perturbed or complex kinematics 6 Gyr ago.

Considering that galaxies with significant emission line flux ($EW([OII]\lambda 3727) > 15 \text{ \AA}$) represent 60% of intermediate mass galaxies at $0.4 < z < 1.0$ (Hammer *et al.*, 1997), and assuming the rest 40% of galaxies to be dynamically relax, they conclude that at this redshift range at least $41 \pm 7\%$ of galaxies has perturbed or complex kinematics. This kinematic state of galaxies at $z \sim 0.6$ is very different from that observed 6 Gyr later (in the local Universe). Indeed, in the local Universe, roughly 70% of intermediate mass galaxies are dynamically relax spiral galaxies, while a few percents correspond to irregular, compact, or merger galaxies (Fukugita *et al.*, 2007, and references therein). Therefore, galaxy kinematics are among the most rapidly evolving properties between $z \sim 0.6$ and today. Which is the physical process driving to such fast evolution?, Is this kinematic evolution corroborated by a morphological evolution?

5.4.2 The morpho-kinematic correlation 6 Gyr ago

First, we have studied the correlation between morphology and kinematics at $z \sim 0.6$, as well as compared different morphological classification methods (Concentration-Asymmetry, Gini-M20, our own).

This was the principal objective in the second IMAGES paper (Neichel *et al.*, 2008), in which we defined a robust morphological classification methodology.

By applying this new classification to a kinematically studied sample of distant galaxies (see previous subsection), we show that the retrieved morphologies are well correlated to their kinematic classification. We find that, at $z \sim 0.6$, 4/5 spiral galaxies are rotating disk, and more than 4/5 peculiar galaxies are not in a dynamical equilibrium. Therefore, using this new method to morphologically classify a galaxy guarantees, in a high percentage (see figures 5 and 7 in the paper), that the morphology is representative of the dynamical state of that galaxy. This correlation represents a new important tool to understand the galaxy formation and evolution. However, such a correlation is only guaranteed when our classification methodology is applied. Indeed, we further show that automatic morphological classifications over-estimate the number of spiral rotating disks by a large fraction (see also [Conselice *et al.*, 2003, 2005a](#)).

See: *Neichel et al. 2008, A&A, 484, 159N*

5.4.3 Chemical evolution of intermediate-mass galaxies since $z \sim 0.7$

Since the previous studies reveal the agitated history of galaxies over the past 6 Gyr, one could expect a chemical abundance evolution of galaxies since that epoch. This is the principal goal of our IMAGES IV paper, where we find that galaxies at $z \sim 0.6$ are, on average, two times less metal-rich than local galaxies at a given stellar mass, confirming the earlier results of [Liang *et al.* \(2006\)](#). Combining our results with other studies, we also find that the metal abundance of the gaseous phase of galaxies is evolving linearly with time since $z \sim 3$ until now. Such result implies that $\sim 30\%$ of the stellar mass of local galaxies have been formed through a gas supply. It could be interesting to compare this result to the evolution of the baryonic TFR (see section 7.1).

See: *Rodrigues et al. 2008, A&A, 492, 371R*

5.5 Beyond the IMAGES survey

The IMAGES survey has then allowed us to develop new techniques and methodologies in order to preserve a well correlation between kinematics and morphology of distant galaxies, as well as unravel the evolution of some of their physical properties.

At this stage, it becomes naturally necessary to undertake a more complete study of the galaxy morphology, from the distant Universe to the local one, in order to estimate its evolution. Different reasons support it. First, morphology is the result of the different physical process that form a galaxy. Second, we dispose now of a classification method that guarantee the correlation between

kinematics and morphology. Third, this method must be extended to include all the morphological types amongst the Hubble sequence. Fourth, there is still no work to date that has studied representative samples of local and distant galaxies at the same time, applying the same methodology to equivalent local and distant observation data. Fifth, there is still no work to date able to determine the past Hubble sequence.

Reconstructing the distant Hubble sequence

"El mundo era tan reciente que muchas cosas carecían de nombre, y para mencionarlas había que señalarlas con el dedo."
Gabriel García Márquez, Cien años de soledad.

Contents

7.1	Merger events and the baryonic Tully-Fisher relation . . .	107
7.2	Prospectives	108

This chapter represents the heart of my work during my thesis. Here, I present a complete description of the morphological analysis and methodology we have developed during the past three years, as well as our results concerning the morphological evolution of galaxies since the past 6 Gyr. Further results of my work are also described. Then, I finish by a discussion about the different morphological classification methods, and I argue why our method is more reliable than the standard ones to retrieve the morphological properties of galaxies (see also chapters 3 and 4.).

As mentioned in chapter 2, the Hubble sequence was created in 1936, and has been used during the last century by different authors to classify the Schmidt plates and the first CCD images of local galaxies. In the 1990s, with the arrival of the HST, astronomers began to obtain good resolution images of distant galaxies. Only high resolution images allow us to quantify the structural parameters such as, e.g., B/T (Lilly *et al.*, 1998, see subsection 6.2.2)¹, because only a high spatial resolution allow us to deblend the information coming from different regions of

¹Other kind of parameters have also been created (see chapter 3 for more information and details). Briefly, we can mention the Concentration (C) parameter (Abraham *et al.*, 1994) which roughly correlates with the bulge over disk ratio (B/D), and the Asymmetry (A) parameter (Abraham *et al.*, 1996b) which divides the sample between irregulars and more symmetric objects. More recently two other parameters have been introduced: the Gini coefficient (Abraham *et al.*, 2003) which is a measure of the relative distribution of galaxy pixel flux values, and the M20 parameter (Lotz *et al.*, 2004), which is the relative second-order moment of the brightest 20% of a galaxy's pixels.

the galaxy, in particular the bulge and the disk. In the case of WFPC images, it was considered that only in galaxies with an $R_{1/2}$ (see below) larger than 3 kpc (known as the compactness limit; [Melbourne *et al.*, 2005](#)), it could be possible to differentiate such structures. It is interesting to note that one of the best ground images at that time were those from the CFRS, having a 0.8" FWHM with a pixel size of 0.207" ([Hammer *et al.*, 2001](#)). Such FWHM (and pixel size) represents 5.5 kpc (and 1.43 kpc) at $z=0.65$, implying that the classification (compactness) limit of 3 kpc would be strictly and largely smaller than the smallest spatial resolution element imposed by the PSF ($\text{limit}_{R_{1/2}} \sim \text{FWHM}/2$), and thus the structural deblending would not take into account the scatter induced by the measurement process. Here, the importance of HST images. Astronomers then started to classify samples of such galaxies using the traditional methods. Nevertheless, authors also started to create new methodologies to recover the structural parameters of distant and local galaxies, and study their evolution ([Brinchmann *et al.*, 1998](#); [Frei *et al.*, 1996](#), and reference therein). In this context, during the past decade, the structural parameters are usually recovered using "deconvolution"² softwares, such as GIM2D and Galfit ([Simard *et al.*, 2002](#); [Peng *et al.*, 2010](#), respectively).

Our methodology to classify galaxies according to their morphology began to be developed in 2004 by [Zheng *et al.* \(2004\)](#), introducing, for the first time, the color information (color maps) to classify galaxies (see subsection 6.2.3). It was later improved by [Neichel *et al.* \(2008\)](#), where we introduce a decision tree to schematise our morphological classification process. Finally, I have extended this methodology in order to account for all the morphological types amongst the Hubble sequence, to include the analysis of bulge and disk center positions during the determination of the morphology, and to allow the study of galaxies with smaller sizes. This last, thanks to the spatial resolution of the images at which we have access. Indeed, with the arrival of the HST/ACS images we have been able to push the compactness limit to 1 kpc (see subsection 6.2.2), thanks to their 0.108" FWHM and their pixel size of 0.03". Such FWHM (and pixel size) represents 0.75 kpc (and 0.2 kpc) at $z=0.65$. Our classification (compactness) limit is thus larger than the smallest spatial resolution element ($\text{limit}_{R_{1/2}} \sim 1.33 \times \text{FWHM}$), with a well sampling of the PSF, and consequently takes also into account the scatter due to the measurement process. For a further comparison with observations of the local Universe, the SDSS images present a 1.4" FWHM (and a pixel size of 0.396). In the local Universe, e.g. at $z=0.025$, such value corresponds to 0.74 kpc (and 0.2 kpc), which matches perfectly with HST/ACS observations of distant galaxies (see above).

As mentioned in section 1.2.6, the morphological classification by eye, which

²what is really done is a convolution of the model with the PSF. This convolution focus on reproducing the different effects caused by the telescope optics and/or the atmosphere.

has been used till recently (e.g., Brinchmann *et al.*, 1998, see chapter 3), can generate an important scatter when different astronomers do it (Naim *et al.*, 1995). It will depend a lot on "*the experience or pleasure of who is doing it*". Then, a less subjective method must be constructed to guide the classifier, and let the morphological classification process be reproducible with a very little scatter³. On the other hand, the method must not let the process be totally automatic ("blind") because it could affect its accuracy, and introduces systematic errors, given the different shapes and independent physical properties a galaxy can have (especially, those that can be found in distant galaxies, see figure 6.1). As we cannot, e.g., describe the appearance of a person by only measuring the size of his nose, it is similarly difficult to determine the morphology of a galaxy only using one automatic measurement. Even if this last could be an easier and faster method, we lose the goal in the study of distant galaxies which can be cited as: "understanding the evolution and state of each galaxy".



Figure 6.1: Distant galaxies. They present a huge variety of shapes and physical properties.

³This is related to the precision of the method.

During my thesis, I worked in order to improve the method on how galaxies are morphologically classified. In the next sections I will describe the sample used in our study (local and distant), the different parameters used to classify the galaxies, and the methodology to recover them.

6.1 Our galaxy sample

We have worked with two samples of galaxies. One made up with local galaxies ($0.0207 \leq z \leq 0.030$) observed by the SDSS, and the other one composed of distant galaxies ($0.4 \leq z \leq 0.8$) located in the CDFS field and observed by the HST/ACS (see [Delgado-Serrano *et al.*, 2010](#), at the end of this chapter for more details). Both samples have been set up following one simple selection criterion: the absolute magnitude in J band brighter than -20.3. Furthermore, during the construction of our samples we have ensured that each galaxy have the information necessary for our analysis: good quality spectrum which includes the [OII] λ 3727, and high resolution images in at least three optical bands. The first would allow us to distinguish between starburst and quiescent galaxies. The second, to construct color maps and three color images. In this way, we got a local sample of 116 galaxies, and a distant sample of 143 galaxies.

Finally, we show that both samples are representative of the galaxies at each respective epoch. To do so, we compare our samples with the luminosity functions obtained for local and distant galaxies. Kolmogorov-Smirnov tests indicate probabilities larger than 94% that our samples and the corresponding luminosity functions are drawn from the same distribution.

6.2 The parameters retrieval: analysis of the observables

As discussed in section 1.2.6, one of the basis of any morphological classification method is the definition of the observables to be taken into account (images bands, color images, etc.), as well as fixing the importance of the different morphological details (bulge, disk, bar, ring, etc.). This is important in order to extract the underlying physical processes (kinematics, composition, physical events, etc.). In this context, we have developed a method that allows us to correlate morphology and kinematics of distant galaxies (see section 5.4.2), and with other physical properties and events (e.g., mergers). This method is summarized by a decision tree illustrated later in section 6.3. In our methodology we use different tools and all the available information to morphologically classify each galaxy:

- GALFIT parameters: these include the bulge and disk centers, magnitudes, radius, inclinations, P.A.s, and sersic index (see figure 6.2).
- GALFIT model and residual images: to gauge the fitting process, and carefully examine the different structures.
- Error image: to weight the different structures detection.
- disk-bulge-galaxy profile: to analysis the light profiles of different components.
- bulge-to-total light ratio (B/T): to distinguish the different morphological types.
- half light radius ($R_{1/2}$): to study the light concentration and define the compactness.
- color-map: to measure the color of individual features. It is constructed using two images in different filter bands.
- color image: to examine the small-scale structures. It is constructed using three images in different filter bands.
- Original images in three different bands: together with the color map and the color image, to identified dusty or star forming regions, as well as examine the different structures.

In the next sections I describe in more details the extraction of the parameters, the construction of the different images (or maps), and their utility inside our decision tree.

6.2.1 The light profile analysis

This step in our methodology is essential to determine the majority of all the parameters we use to classify each galaxy (the five first items above). Therefore, special attention must be given to it for a good understanding of what we are retrieving.

We use the software *galfit* (Peng *et al.*, 2010) to carry out two-dimensional modeling of each galaxy in order to obtain their structural parameters. For this we use optical high resolution images: HST/ACS z band images in the case of distant galaxies, and SDSS r band for the local galaxies. These two bands are equivalent due to the K-correction: $r \text{ band} \sim (z \text{ band}) / (1 + (z - 0.65))$. *Galfit* models the galaxy image as a linear combination of a bulge and a disk, using a well established analytic model for each of the two components (see below), and

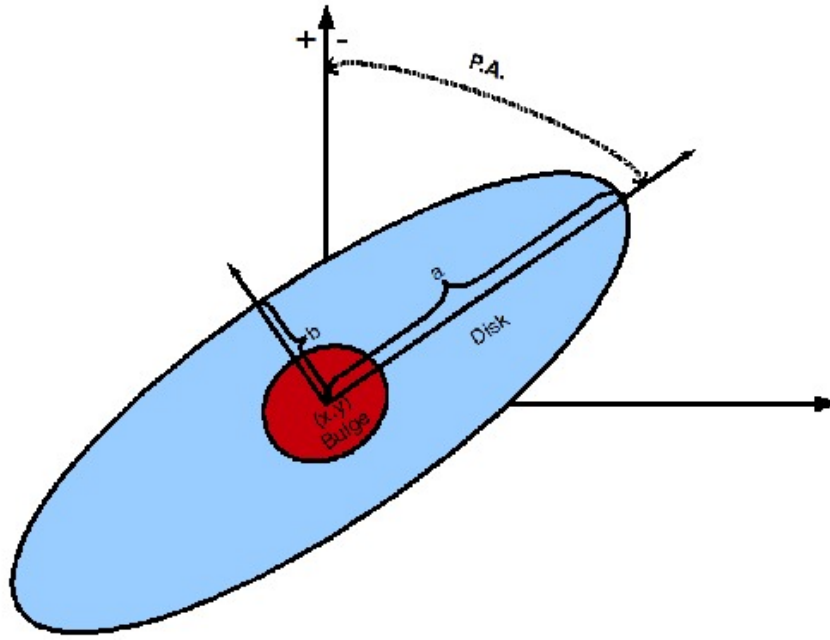


Figure 6.2: Galaxy parameters. They are define as follow: a = semi-major axis, b = semi-minor axis, (x,y) = center coordinates, P.A. = position angle (which goes from 0 to 90 degrees. Positive within the left of the grand y axis, and negative in the other direction), ellipticity = $1-(b/a)$, inclination = $\arccos(b/a)$.

convolves them with a PSF in order to extract the parameters free of instrumental effects. An important caveat in this approach is the underlying assumption that a galaxy can be represented as a linear combination of simple, smooth analytic functions (Rawat *et al.*, 2007). Real galaxies are known to be much more complex, with the presence of spiral arms, bars and central point sources, etc. Despite these reservations, galaxy fitting algorithms have been demonstrated to be successful in the past for the purpose of quantifying the galaxy morphological parameters (Peng *et al.*, 2002; Simard *et al.*, 2002).

To model the galaxy bulge+disk intensity profile we use the combination of two Sersic laws (Sersic, 1968)⁴,

$$\Sigma(r) = \Sigma_e \exp[-\kappa[(\frac{r}{r_e})^{\frac{1}{n}} - 1]] \quad (6.1)$$

with r_e being the half light radius, Σ_e the surface brightness at r_e , κ a constant⁵,

⁴The elegance of the Sersic profile is that it forms a continuous sequence from a Gaussian ($n = 0.5$) to an exponential ($n = 1$) and a de Vaucouleurs ($n = 4$) profiles simply by varying the exponent. It is then very useful for modeling bulge, pseudo-bulges, ovals, bars and flat disks; the smaller the index n is, the faster the core flattens within $r < r_e$, and the steeper the intensity drop beyond $r > r_e$.

⁵ κ is coupled to n such that half of the total flux is always within r_e . Then, for $n \gtrsim 2$, $\kappa \approx 2n$

and n being the sersic index. The difference between the bulge and the disk lies then in the sersic index. For the bulge the sersic index is let free⁶, while for the disk the sersic index is fixed to 1. This last case is equivalent to the exponential function (Freeman, 1970)⁷,

$$\Sigma(r) = \Sigma_0 \exp\left[-\frac{r}{r_d}\right] \quad (6.2)$$

with Σ_0 being the central surface brightness and r_d the e-folding scale length.

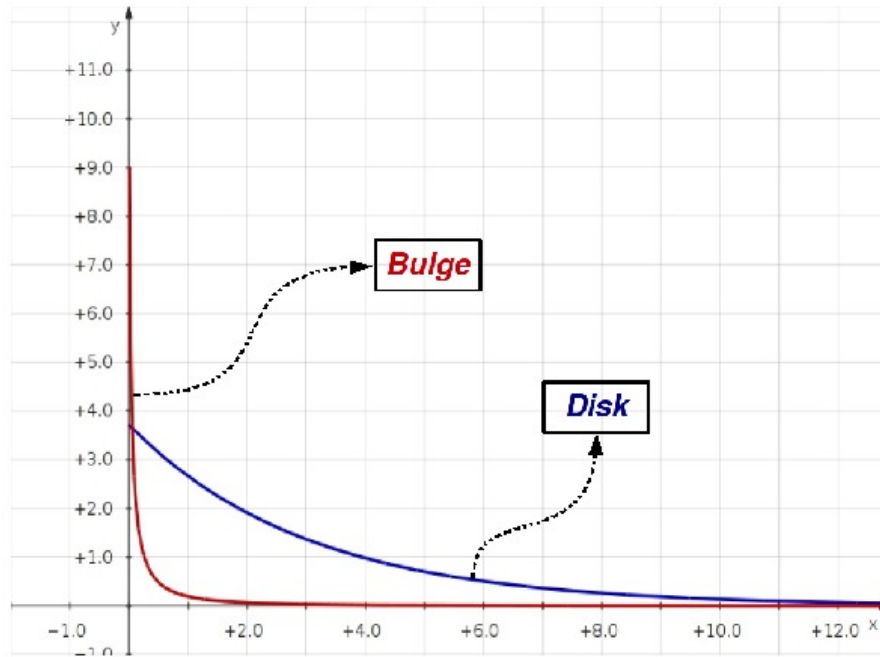


Figure 6.3: Examples of Sersic profiles. In red a Sersic profile with $n=4$, which correspond to a bulge. In blue a Sersic profile with $n=1$, modeling a disk.

The galaxy model is then constructed as a linear combination of these two components which includes some free⁸ parameters such as:

- 0.331. At low n , κ flattens out toward 0 and is obtained by interpolation (Peng *et al.*, 2010).

⁶the classic de Vaucouleurs profile (de Vaucouleurs, 1948) that describes a number of galaxy bulges is a special case of the Sersic profile when $n = 4$ ($\kappa = 7.67$). Nevertheless, some bulges may be better represented by other Sersic profiles (Kormendy *et al.*, 2009; Kormendy & Fisher, 2008; Laurikainen *et al.*, 2007; Kormendy & Kennicutt, 2004; Andredakis & Sanders, 1994; Kent *et al.*, 1991; Shaw & Gilmore, 1989; Kormendy & Bruzual A., 1978).

⁷Freeman showed that dynamically "hot" stars in galaxies make up spheroidal bulges having a roughly de Vaucouleurs light profile, whereas "cold" stellar components make up the more flattened, rotationally supported, exponential disk region (see also de Jong, 1996a,b, and the references cited in the previous footnote).

⁸All parameters like r_e , r_d , n , position angle etc., with the exception of the sky background, are allowed to be free in the fitting process, so that galfit can explore the full range of parameter

- the sky background value bg , which is assumed to be constant across the galaxy image. This is a good approximation because the images we use are $15 \times 15 \text{ arcsec}^2$ large for distant galaxies ($\sim 103 \times 103 \text{ kpc}^2$ at $z=0.65$), and $198 \times 198 \text{ arcsec}^2$ large for local galaxies ($\sim 100 \times 100 \text{ kpc}^2$ at $z=0.025$).
- the ellipticities ε_{bulge} and ε_{disk} of the bulge and the disk isophotes respectively,
- and their position angles θ_{bulge} and θ_{disk} .

Galfit needs a first guess of such parameters, as well as the magnitude, radii and position angle (PA) of each component, to run the fitting. The SExtractor software (Bertin & Arnouts, 1996) applied to our galaxies allows us to recover these initial guesses⁹. Then, galfit iterates the best analytic model of the galaxy using the PSF of the observation (see below) and comparing systematically with the observed galaxy image. The values of the free parameters are determined iteratively by minimizing the reduced χ^2_{red} defined as usual (see Peng *et al.*, 2010, for more details),

$$\chi^2_{red} = \frac{1}{N_{d.o.f}} \sum_{x=1}^{nx} \sum_{y=1}^{ny} \frac{(galaxy_{x,y} - model_{x,y})^2}{\sigma_{x,y}^2} \quad (6.3)$$

where $N_{d.o.f.}$ is the number of degrees of freedom, $galaxy_{x,y}$ and $model_{x,y}$ are the counts in the pixel (x, y) of the galaxy and the model image respectively, $\sigma_{x,y}$ is the noise in the pixel (x, y) and nx, ny are the number of pixels in the galaxy image in the x and y direction respectively.

The point-spread-function (PSF)

The PSF is a mathematical function describing the response of an imaging system to a point source.

Therefore, a special attention is paid when determining the PSF to be used during the fitting of each galaxy because it is fundamental to well simulate the original galaxy image. As it has been mentioned before, the convolution with a PSF is necessary to reproduce the blurring caused by the telescope optics and/or the atmosphere. In our work, the star closest to a given galaxy is used to determine the PSF for the purpose of bulge+disk decomposition. Stars are the most pristine characterization of the PSF in any given astronomical observation, as they have gone through the same optics as well as the reduction pipeline as

space to find the global minimum. In such a case, we avoid galfit to pull into a local minimum due to constraints put in by hand.

⁹We use SExtractor software for this task because it performs source detection and photometry, and it is able to deblend sources using flux multithresholding, as well as estimate a sky value using the complete image and not just an specific area.

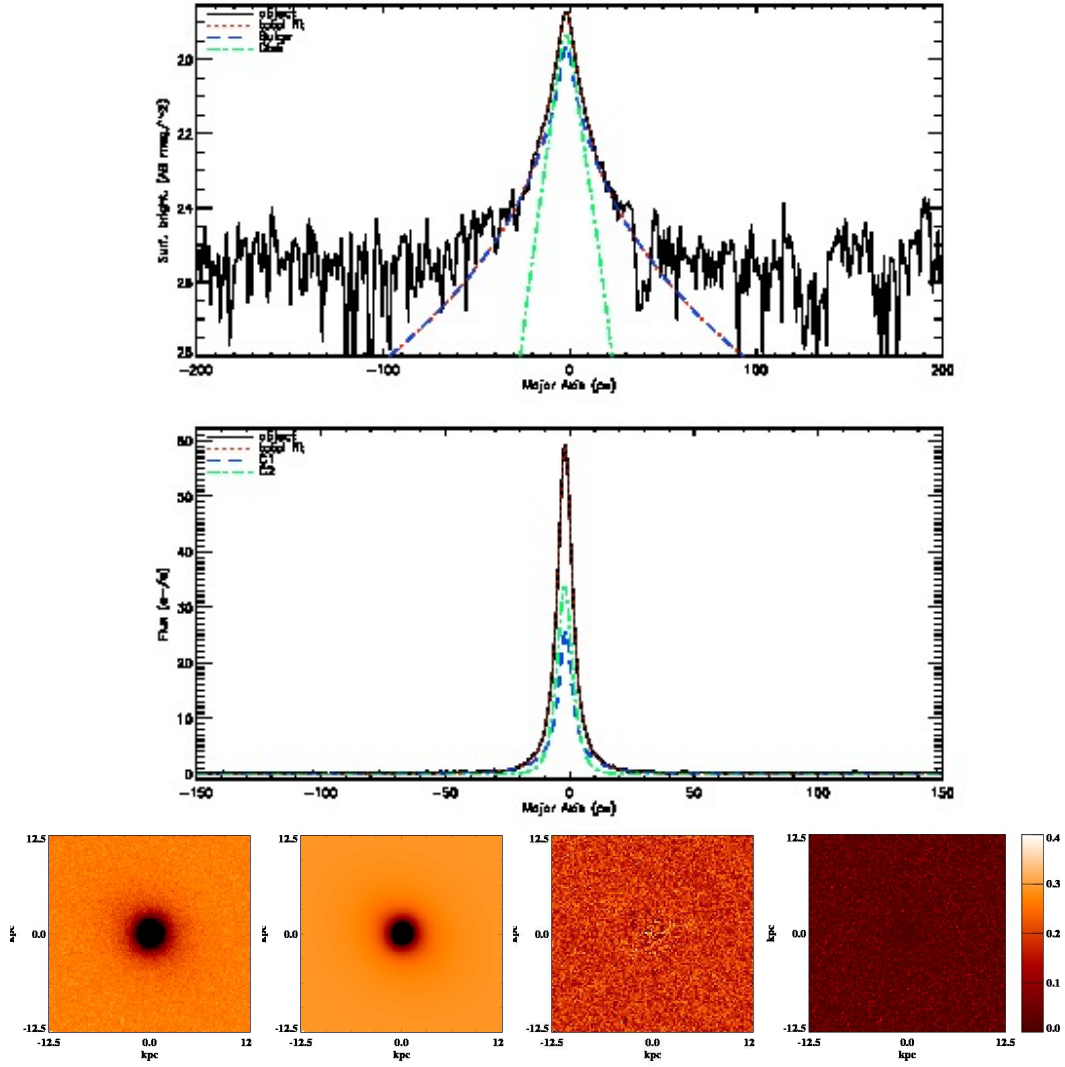


Figure 6.4: Example of a galfit simulation for one galaxy in our sample. *Top*: display of the components profiles over-plotted to the original galaxy profile in magnitude units. *Middle*: same as before, but the profile are in flux units. *Bottom*: from left to right we have (a) the observed galaxy image; (b) the best model; (c) the residual image, constructed by taking the difference between the real and the modeled light distribution; (d) the "error" image.

the studied galaxies. In this purpose, especially in the case of HST/ACS drizzled images, real stars are better than simulated ones in order to take into account all the optics and reduction effects. It must be remembered that during the drizzling process a linear reconstruction of the individual astronomical images is done before their combination. This implies that, even if the algorithm preserves photometry and resolution, each input images is weighted according to the statistical significance of each pixel. The effects of geometric distortion on both image shape and photometry are also removed. In addition, individual images

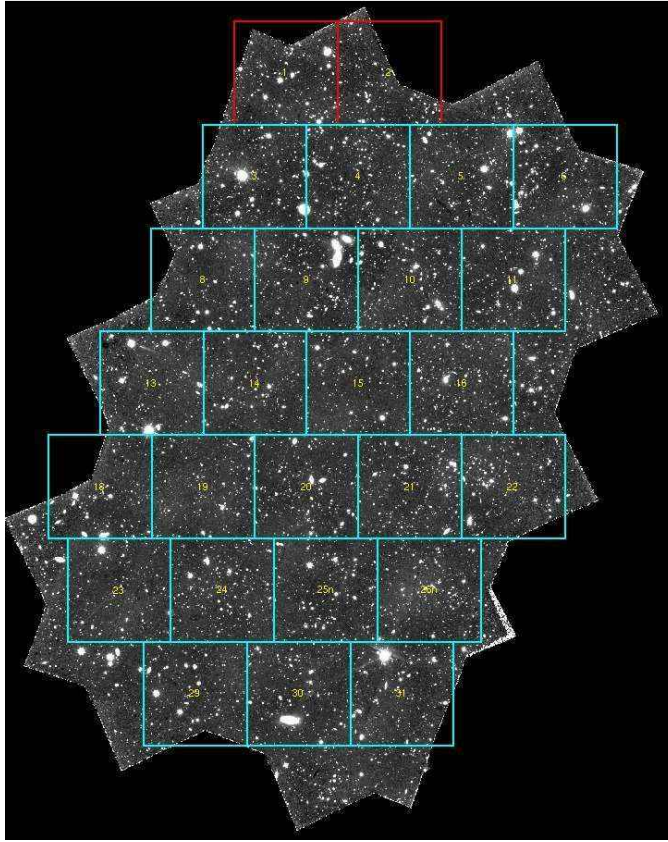


Figure 6.5: HST/ACS GOODS image from the ESO/GOODS project (Retzlaff *et al.*, 2010) (Credit: <http://archive.eso.org/cms/>).

must be rotated according to their orientation, and it is possible that, in the presence of cosmic rays, the images are combined by a dithering procedure. As a consequence, the simulated PSFs may not be able to reproduce all these steps, which could become complicated enough. Only bright (non saturated) and well behaved stars, free of neighbours and other contamination were used as candidate PSF stars in our work following the study carried out by Rawat *et al.* (2007).

The σ -image and the χ_{red}^2 role to retrieve the best model

In the above scheme, an accurate estimation of the noise model $\sigma_{x,y}$ to be used in Eq. 6.3 is also crucial for a robust determination of the derived structural parameters of a galaxy. As the χ_{red}^2 "measures" how far the modeled image is compared to the original light distribution, it is generally used to estimate the quality of the fit. Then, the role of the σ -image is to give relative weights to the pixels during the fit, because, even with the absence of other eventualities (cosmic ray hits, dead/hot pixels, flatfielding problems) in the galaxy image, all pixels are not equal due to the counting uncertainties of the photon (Poisson) statistics. In an image, pixels with high signal have smaller uncertainties (fractionally speaking)

than pixels with fewer counts. Therefore, the fit can not be weighted by the uncertain data at the same degree as the more certain ones. Thus, in Eq. 6.3 each point is normalized by the uncertainty at each pixel (the σ -image), following the Poisson weighting as it is the natural scheme for number counting.

Due to the fact that Poisson statistics applies to electrons, when constructing the σ -image, pixel values must be in electrons. Thus, we use the GAIN, NCOMBINE, and EXP_TIME parameters of the image, to convert all the pixel values into electrons. Then, following the Galfit manual¹⁰ and Peng *et al.* (2002, 2010), we do the noise calculation by making the sum of the Poisson uncertainty at each pixel with the other noise sources in quadrature (e.g. detector readnoise). Finally, we convert everything back to the same units as the input data (counts/second).

Statistically, if the model would be a perfect fit of the data, the difference ($\text{galaxy}_{x,y} - \text{model}_{x,y}$) in Eq. 6.3 would be roughly the size of $\sigma_{x,y}^2$, on average, over infinite number of observations at each pixel. Therefore, when the sum is computed over all the pixels, and then divided by the number of pixels χ_{red}^2 will be roughly equal to 1. In galaxy fitting, you almost never get χ_{red}^2 equal to 1 because galaxies are not perfect ellipsoids with the profiles we try to force on them. Nevertheless, it is still important to get the right sigma image because if not it might be hard to interpret the profile parameters such as the Sersic index (n).¹¹

As a result, we found that the χ_{red}^2 parameter alone is not sufficient for deciding whether a fit is reliable or not (see figure 6.6). In fact, the main limitation of parametric methods is that they use an "a priori" assumption on the light distribution, making them unsuitable for treating patchy light distribution often found in spiral galaxies, for example, spiral arms. A spiral galaxy with prominent arms unavoidably produces a $\chi_{red}^2 > 1$ because the spiral pattern is taken as if it was noise during the fitting. However, we can gauge the appropriateness of the fit by carefully examining the residual map, the "error" map, and the flux and magnitude profiles shown in figure 6.4. Then, the combination of the χ_{red}^2 value and the careful examination of the aboves allows us to adequately recognise the successful fits.

6.2.2 Structural parameters

Figure 6.7 shows an example of the structural parameters values resulting from the fitting procedure detailed in the previous subsection. Furthermore, a series of images and plots, also resulting from the galfit fitting procedure, are shown in

¹⁰<http://users.obs.carnegiescience.edu/peng/work/galfit/galfit.html>

¹¹<http://users.obs.carnegiescience.edu/peng/work/galfit/CHI2.html>

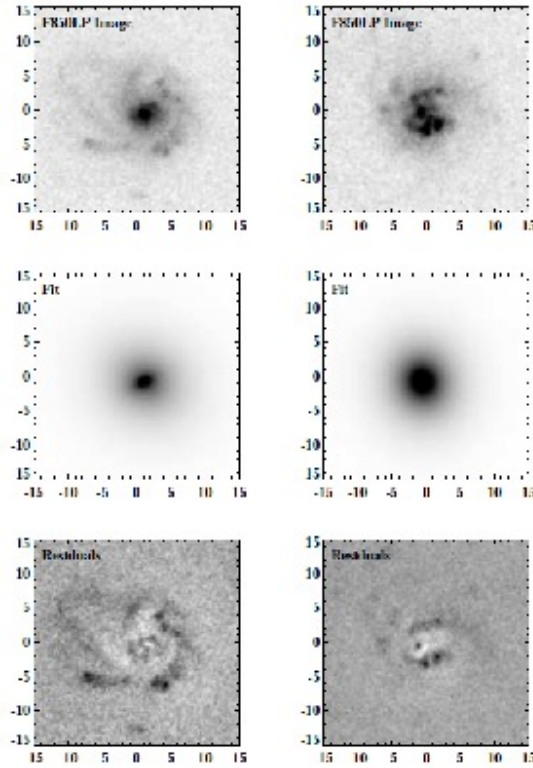


Figure 6.6: χ^2_{red} parameter of two different galaxies (Neichel *et al.*, 2008). From top to bottom: original image, Galfit model image, and residual image. For these two objects the software gives a similar confidence level in the fitting process ($\chi^2_{red} \approx 1.4$). For the galaxy on the left, the χ^2_{red} is high due to spiral arms, whereas it is due to the two clumps located at the southeast of the center for the galaxy on the right.

Galfit results										
Band	Co	[x,y]	Magnitude	Radius	Sersic	F_i	b/a	Inc.	P.A.	Chi2/tot
z	C1	1252.00 251.98	22.22 \pm 0.02	3.75 \pm 0.11	5.42 \pm 0.25	0.88 \pm 0.03	0.58	54.55	-35.21	1.24
	C2	1252.00 251.80	23.00 \pm 0.04	8.42 \pm 0.15	1.00 \pm 0.00	0.31 \pm 0.01	0.23	78.70	40.92	

Figure 6.7: Example of Galfit result parameters from our morphological analysis. C1 represents the bulge and C2 the disk. $[x, y]$ indicates the center position in pixel values, *Sersic* is the sersic index value (n in equation 6.1), F_i is the component flux to the total flux ratio (B/T and D/T respectively), b/a is the semi-minor axis to the semi-major axis ratio, and *Inc.* is the inclination in degrees.

figure 6.4.

Bulge-to-total light ratio (B/T)

Once the best fit galaxy model has been obtained, we calculate the bulge fraction B/T, defined as:

$$\frac{B}{T} = \frac{flux_{bulge}}{flux_{bulge} + flux_{disk}} \quad (6.4)$$

where the $flux_{bulge}$ and $flux_{disk}$ are calculated by integrating the bulge and the disk profiles respectively over the major axis using the best fit parameters obtained by galfit (see figures 6.7 and 6.2). This bulge fraction B/T is found to be broadly correlated with the traditional Hubble type of a galaxy in the sense that an early type galaxy has a high B/T ratio and a late type spiral has a low value (Kent, 1985; Simien & de Vaucouleurs, 1986; Laurikainen *et al.*, 2007). It is this ratio that we use for characterizing the morphology of our galaxy sample (see section 6.3).

Another parameter not included in figure 6.7, because it does not result from the galfit fitting, is the half light radius. Nonetheless, our morphological classification method also takes advantage of this parameter (see decision tree in figure 6.13).

Half light radius ($R_{1/2}$)

This is the radius within which half the light (luminosity or flux) of the galaxy is contained.

To measure the half-light radius, we have developed our own IDL procedure, which allows us to visually analyze different profiles of the galaxy at the same time: (1) the flux and magnitude profiles; and (2) the flux content within ellipses of different radii with a step of one pixel (the PA used here is the one retrieve by galfit). The first profiles let us determine a reasonable sky value and the last one gives us the half light-radius when a real "plateau" is visualized (see figure 6.8).

6.2.3 The color information

The galaxy color is information of great significance, as it is the comparison of the light in different wavelengths coming from the galaxy. It can be obtained by comparing its magnitude in two or three different bands. It is even possible to get a color of each galaxy features (similar, for example, to a picture of someone taken by a modern photographic camera), if the images have a high spatial resolution and their alignment is better than 0.16 pixels (Zheng *et al.*, 2004). We made use of the available multi-band high-resolution images to construct two sets of color maps, used in our morphological classification methodology.

Color maps

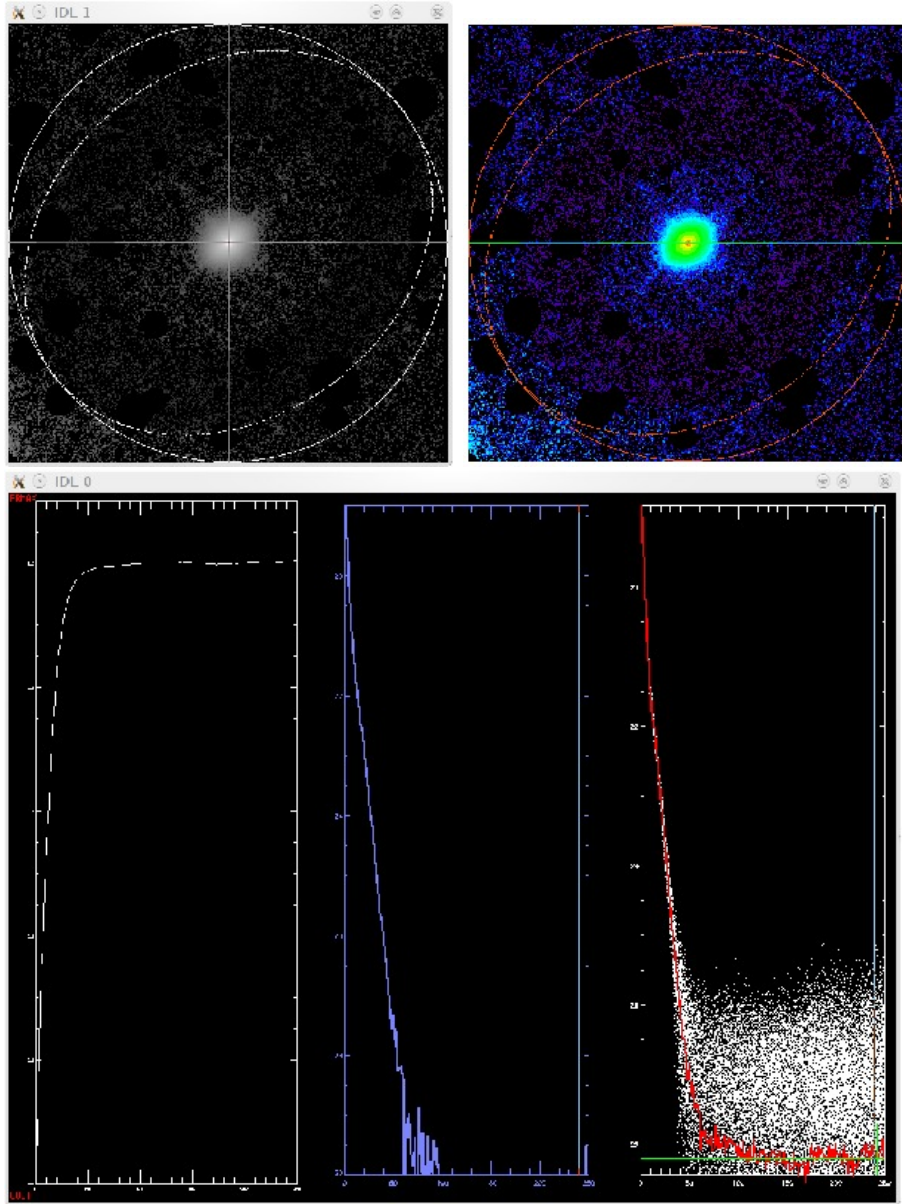


Figure 6.8: Measuring $R_{1/2}$. *Top*: display of the progression of the ellipses with different radii overplotted on the galaxy image. These animations are used to better visualize, in real time, the ellipses regions being measured, as well as the selected region to derive the sky background value. *Bottom*: from left to right we have (a) the plot of the flux content within ellipses of different radii with a step of one pixel, (b) the magnitude profile, (c) the flux profile.

We subtract, pixel by pixel, the magnitude in two observed bands using our own algorithm that allows us to estimate colors and their uncertainties (Zheng *et al.*, 2004).

A color map is a difference of two images in a logarithm scale. Here, we can

ignore the possible scaling constant which will not affect the final results. Given one image in the blue rest-frame band with flux F_B and another one in the red rest-frame band with flux F_R , the color image is defined as

$$Y = \log F_B - \log F_R \quad (6.5)$$

In this relation, the flux is a function of the position in an image, including signals of background and object. Then, applying SExtractor to the red rest-frame image and taking only the detected pixels through a $3\text{-}\sigma$ threshold, we obtain a color map similar to figure 6.9.

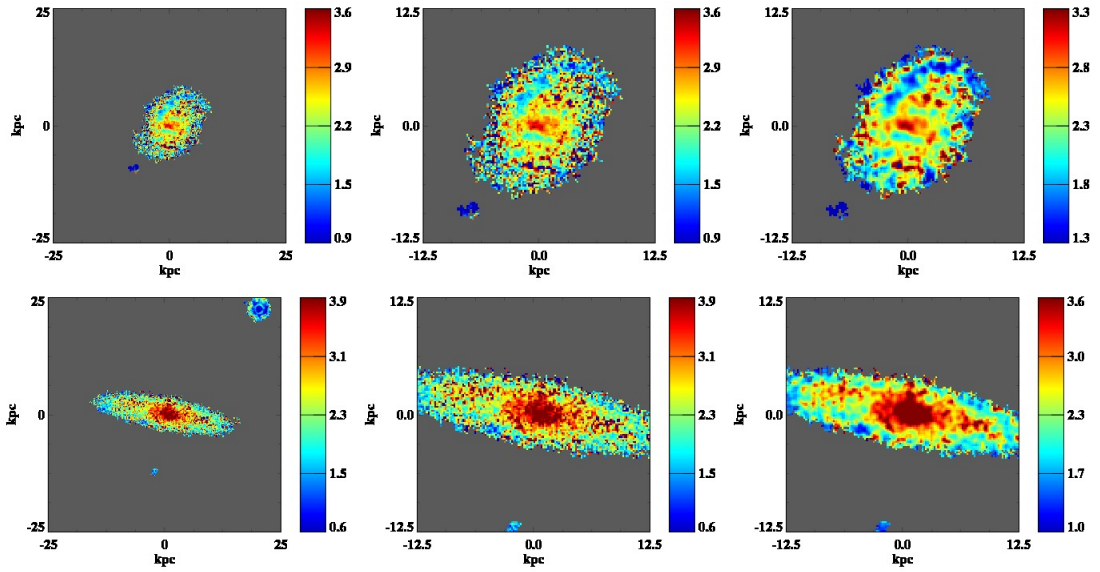


Figure 6.9: Example of color maps for two different galaxies in our morphological analysis methodology. *Left*: 50x50 kpc color map. *Middle*: 25x25 kpc color map. *Right*: Smoothed color map. This last is created from the 25x25 kpc color map, applying a 2x2 boxcar average. The scales are adjusted to have a nice view of the whole galaxy.

It is important to note that the color information in the color map is normalized, pixel by pixel, by the S/N ratio. It allows to create a real and homogeneous color information of the galaxy. If the color map does not take into account the S/N ratio, it could give incorrect information. One example is the extreme case where one structure, within a resolution element, is detected with the B band, but it is not detected with the R band. In such a case, without a S/N normalization, equation 6.5 will be equal to infinity ($-\infty$, if we do not ignore the scaling constant).

Color images

With "color image" I refer to the combination of images in three different bands. For a better visualisation of the difference scale structures of each galaxy, we create three color images with different intensity and spatial scales. In the intensity space, linear and logarithm scales are used. For the spatial case, we compute 25x25 kpc and 50x50 kpc images, as shown in figure 6.10.

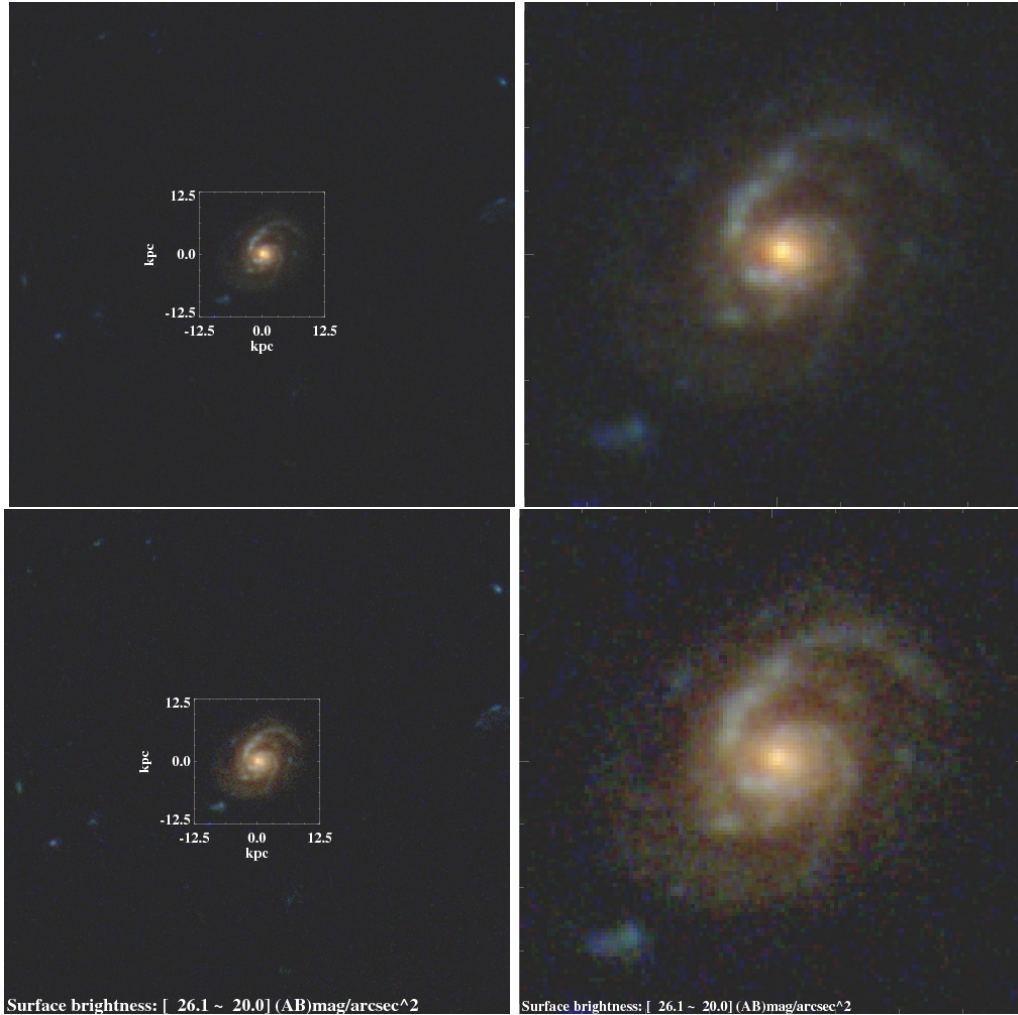


Figure 6.10: Examples of color images we use in our morphological analysis methodology. *Top*: linear intensity scale. *Bottom*: Logarithm intensity scale. *Left*: image with a spatial scale of 50x50 kpc. *Right*: image with a spatial scale of 25x25 kpc.

6.2.4 Bar inspection

Bars are primarily stellar structures in the center of galaxies and it has been shown that they play an important role in the dynamic and structure formation of galaxies. Models show that the nonaxisymmetric bar potential induces large-scale streaming motions in the stars and gas (Sellwood & Wilkinson, 1993; Athanassoula, 1992b,a, and references therein). They are mostly suggested to be

efficient at driving gas into the galactic center and changing star orbits to form a central bulge-like structure (Combes *et al.*, 1990; Debattista *et al.*, 2004), as well as inducing the formation of spiral arms.

A bar structure can be recognized by a characteristic change of ellipticity (ε) and position angle (P.A.) from an analysis of isophotes over the entire image of the galaxy. The existence of a bar will cause a monotonically increase of the isophote ellipticity, while the P.A. remains relatively constant. At the end of the bar, the ellipticity drops sharply, and the P.A. changes as the isophotes belonging to the underlying disk are fitted (Zheng *et al.*, 2005; Sheth *et al.*, 2003; Regan & Elmegreen, 1997).

We use the tool IRAF/ELLIPSE to perform the analysis of the surface brightness distribution via fitting the isophotes with ellipses as shown in figure 6.11.

Plotting the ellipticity and P.A. of the isophotal ellipses can thus allow us to detect a bar as in figure 6.11. A bar detection is validated when the increase of ellipticity exceeds 0.2, and then drops by at least $\delta\varepsilon > 0.1$ (Sheth *et al.*, 2008, and references therein). Moreover, the position angle profile, after keeping a relatively constant value over the bar region, must change by at least 10° as the isophotes enter the disk.

It is easy to suspect that this technique is quite ineffective in detecting bars in highly inclined spiral galaxies, as well as in detecting bars having a similar P.A. than the galactic disk, and/or if the underlying galactic disk is too faint to be adequately imaged, and/or if the data have inadequate resolution to resolve bars.

For these reasons, a further confirmation of the bar existence is carry out by carefully examining the color maps and color images of the galaxy (see subsection 6.2.3), the galfit simulations maps, and the flux and magnitude profiles (see subsection 6.2.1). In any case, we can infer that the ellipse fitting technique is unlikely to overestimate the fraction of barred galaxies.

6.2.5 Color determination

I argued in subsection 1.2.6 that even if large number of physical properties/parameters are well correlated with the galaxy morphological types through the Hubble sequence, some of them, as it is the case for the integrated color (see end of subsection 2.1; see also section 6 in Cirasuolo *et al.*, 2007), present considerable scatter. Is this particular scatter due to the applied morphological

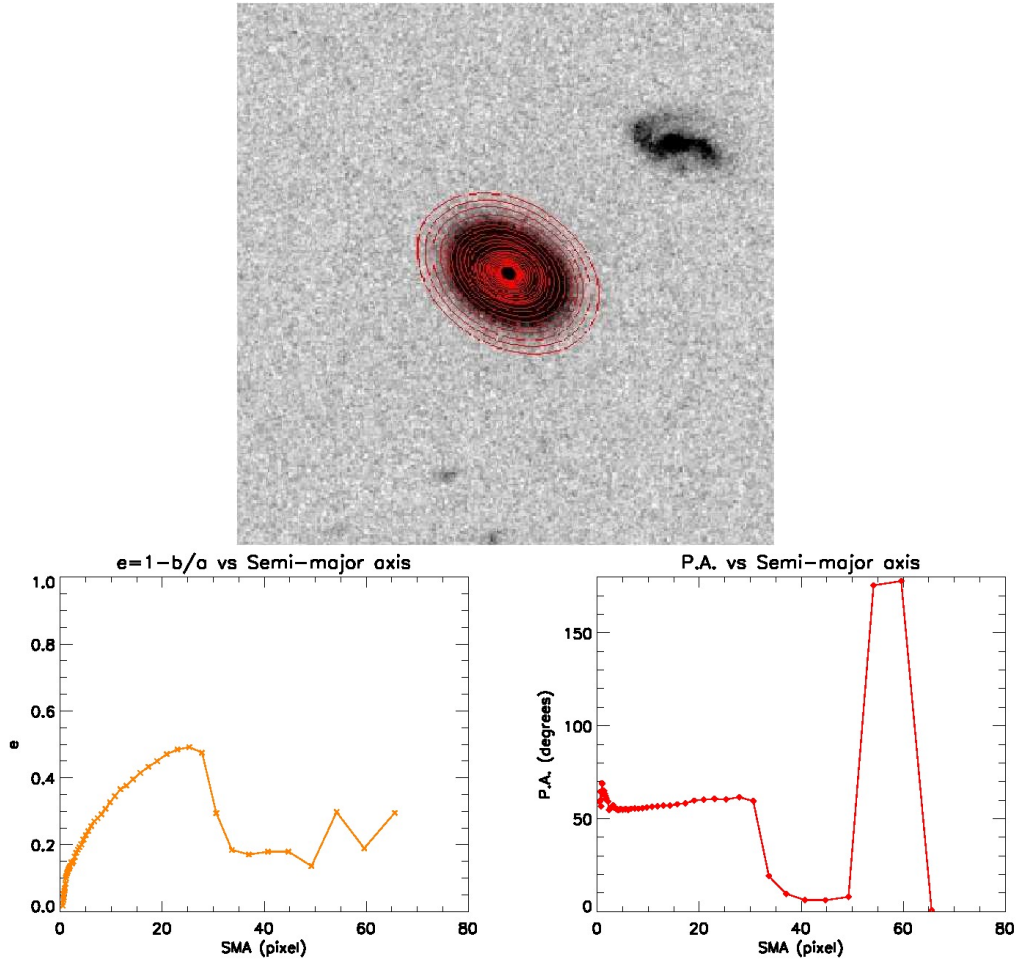


Figure 6.11: Example of the isophotal fitting using the tool IRAF/ELLIPSE, and the respective ellipticity and P.A. analysis showing a bar detection.

classification method, and/or is it caused by real intrinsic physical properties? Having representative samples of distant and local galaxies, I have tried to get new insights on this issue.

As remarked at the end of subsection 2.1, some recent studies show quite high contaminations of late-type galaxies in the so called "red-sequence" ($\sim 20\%$ in the local Universe, and $\sim 35\%$ in the distant one), which is expected to be composed of just early-type galaxies. This is a controversial topic, which needs to be clarified to better understand the evolution of galaxies and the color-luminosity functions. In this context, I have thus compared the integrated color vs the morphological type of Delgado-Serrano *et al.* (2010) representative samples.

To extract the integrated color of the galaxies, I have subtracted the rest-frame U and B absolute magnitudes. The rest-frame (U-B) color of each galaxy allowed me then to separate blue from red galaxies by applying a separa-

tion limit. I used the limit define by [Cirasuolo *et al.* \(2007\)](#). Following [Bell *et al.* \(2004b\)](#), "it is defensible and perhaps more natural to define early types in terms of colors". This seems not to be the case. Results are shown in section 6.4.

6.3 The morphological classification method

We thus adopt a methodology that systematically compares morphologies of distant galaxies to those of local galaxies. Identification of peculiarities is directly assessed by the discrepancy between a given galaxy and the galaxies that populate the local Hubble sequence (see figure 6.12). Such a technique is based on a simple and reproducible decision tree (see figure 6.13).

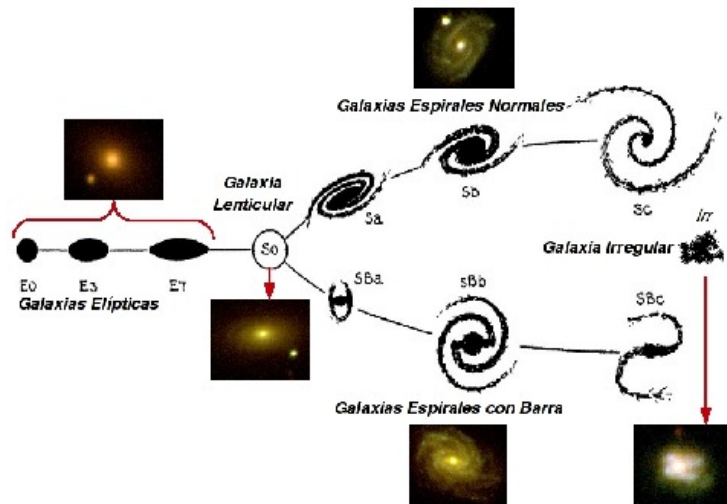


Figure 6.12: Scheme of the local Hubble sequence.

First, we identify those galaxies that are compact, and can thus not be decomposed in a bulge and a disk due to their small size. Second, we model the galaxy as detailed in subsection 6.2.1. If the fit does not succeed, the galaxy is classified as peculiar according to its color map and image. If the fit succeeds, we derive a B/T value to distinguish between spiral, lenticular and elliptical galaxies. Even though, to be classified as spiral, lenticular or elliptical, the color map must show a center redder than the disk, the centers of the bulge and the disk must be in agreement, and all the images (color images, galfit residual images, etc.) must show compatible features (see section 3.4 in [Delgado-Serrano *et al.*, 2010](#)).

I have then created a data base, as shown in figure 6.14, in order to have a fast and easy access to all the information concerning each galaxy (absolute magnitudes, SFR, redshift, galfit parameters, B/T, $R_{1/2}$, bulge-disk-galaxy

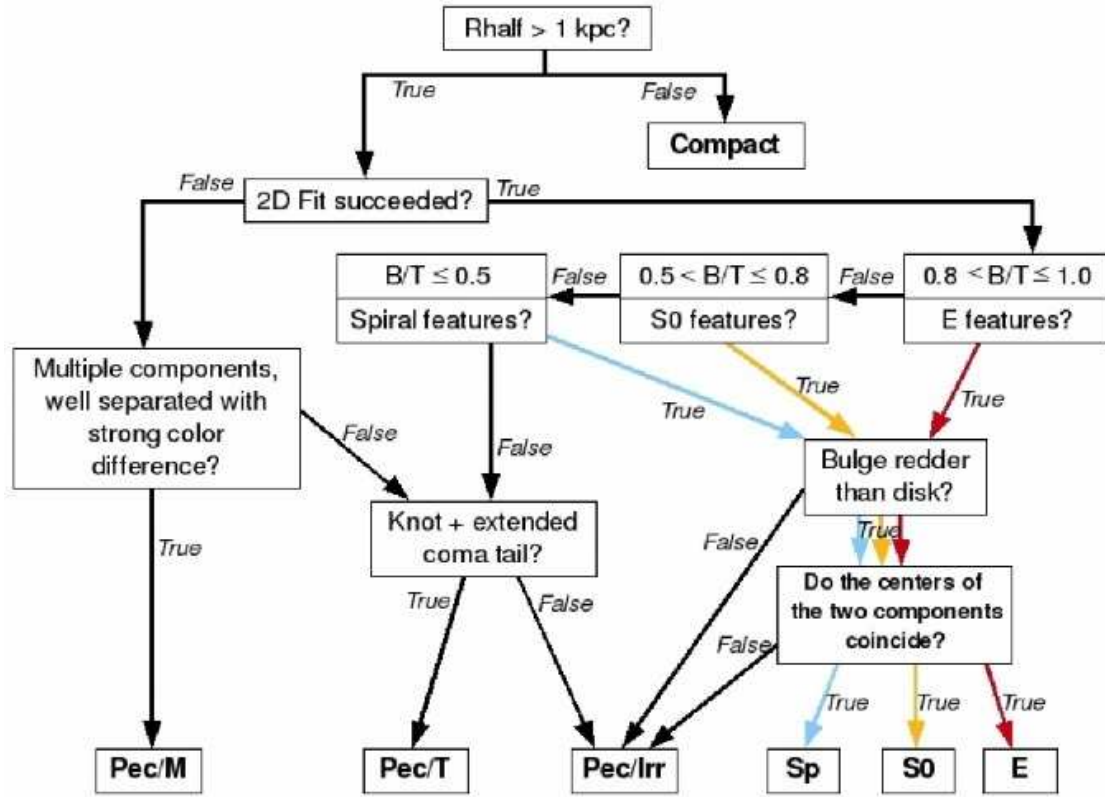


Figure 6.13: Our morphological classification decision tree.

profiles, galfit images, color maps, color images, etc.). Finally, the morphological classification was made individually by three of us (RD, FH, YY) and compared. The agreement between the individual classification was excellent (only 2 galaxies of 143 led to a discussion, arguing between peculiar or spiral galaxy. It was due to their relatively low surface brightness).

6.4 Results

6.4.1 Galaxy number density

In short, for our morphological study we have gathered a distant representative sample of galaxies observed by the HST/ACS in the GOODS survey area. We have further selected a representative sample of nearby galaxies from the SDSS. In applying the same morphological classification method, we have been able to derive a past and a present Hubble sequence. We also estimated the uncertainties of our reliable methodology, finding unprecedented results. Moreover, we showed that the observational conditions of the distant and local galaxies in our samples, needed to retrieve their morphology, are similar in an unbiased way. This has allowed us

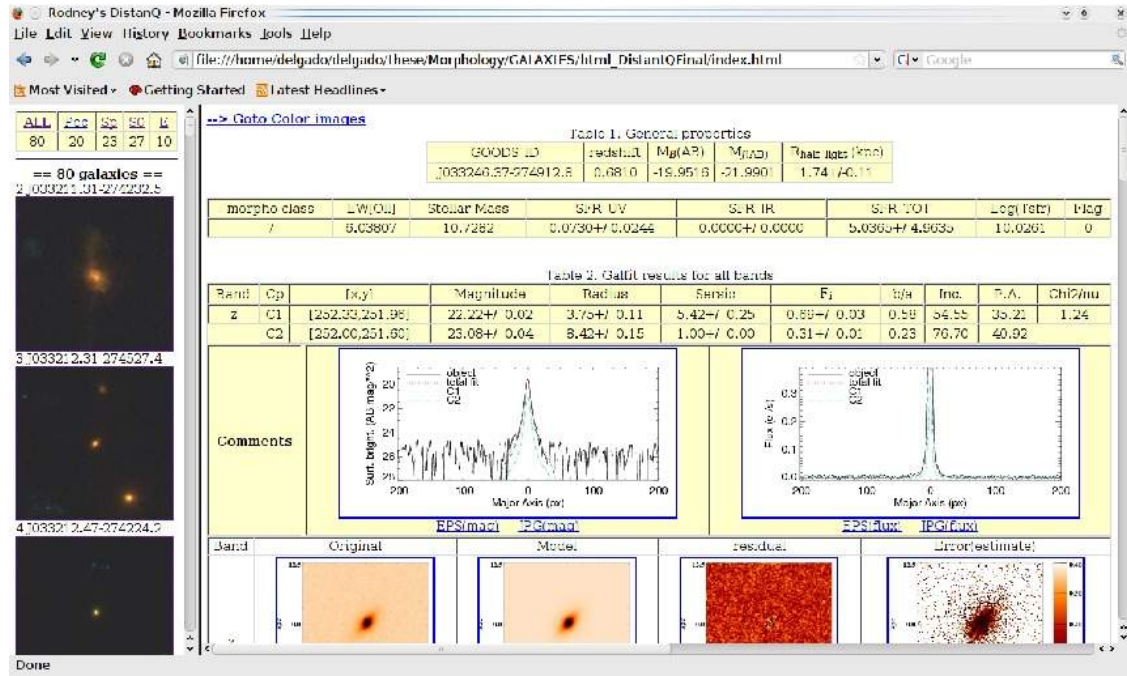


Figure 6.14: Galaxies database (webpage format) created to gather all the galaxies information used during our classification methodology. It makes the application of the decision tree by any astronomer a lot much easier.

to link the past Hubble sequence to the present-day one. We do find that spiral galaxies were 2.3 times less abundant in the past, which is compensated exactly by the strong decrease by a factor 5 of peculiar galaxies, while the fraction number of elliptical and lenticular galaxies remains constant. It shows that more than half of the present-day spirals had peculiar morphologies, 6 Gyr ago (see figure 6.17).

6.4.2 Bar fractions

Taking into account only bar detection in Sp and S0 galaxies¹², I find $\sim 6\% \pm 3\%$ of galaxies with bars in the distant sample, and $\sim 21\% \pm 4\%$ in the local sample (see green circles in figure 6.15). In the distant sample there are less than 10% of Sp or S0 galaxies having an inclination (i) higher than 65° , while in the local sample $\sim 24\%$ of Sp or S0 galaxies have the same property. In the literature it has been argued that galactic structures such as bars are difficult to identify and quantify in galaxies with $i > 65^\circ$ (Sheth *et al.*, 2008). Thus these results give a lower limit to the fraction density of barred galaxies at each epoch.

To compare my results to (Sheth *et al.*, 2008), I quantified the fraction of

¹²It means I do not take into account those detections in galaxies that have been classified as Peculiar.

barred galaxies only within those galaxies classified as spirals, as Sheth et al. eliminated all elliptical, lenticular, and peculiar galaxies when constructing their sample. In such a case, I find $18\% \pm 10\%$ and $25\% \pm 5\%$ of barred galaxies within the distant and local spirals, respectively (see red circles in figure 6.15). These results are in good agreement with Sheth et al. (see also Athanassoula, 2008).

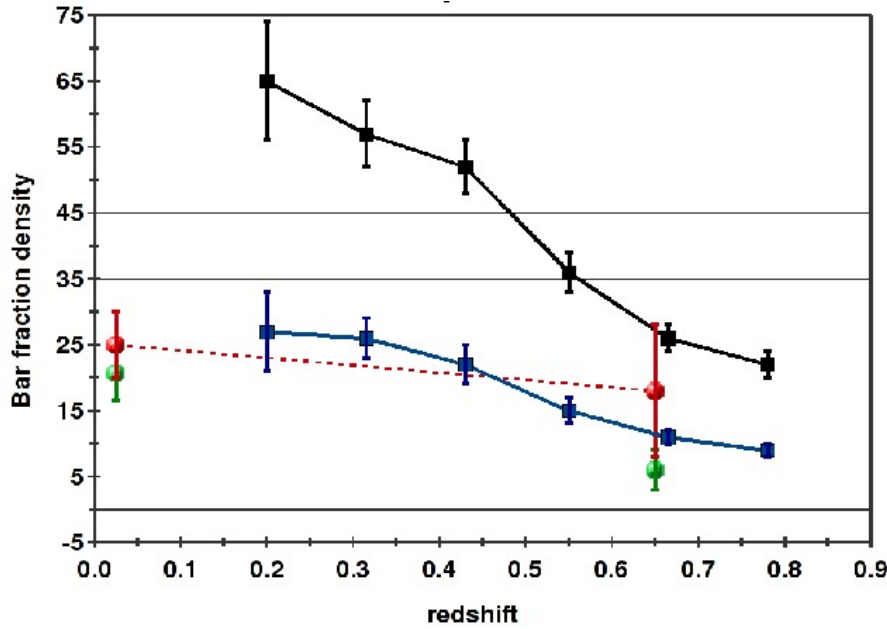


Figure 6.15: Sheth *et al.* (2008) results are presented by straight lines. The blue straight line takes only into account galaxies with strong bars. Such bars are defined arbitrarily as having an ellipticity higher than 0.4. The black straight line includes all bar detections (weak + strong bars). Results from our representative local and distant samples are shown as red and green circles. The red circles can be compared to Sheth et al. as they are calculated using a similar criteria (bar detections within spiral galaxies). The green circles represent the fraction of barred Sp and S0 galaxies within the whole population. Error bars are calculated using a Poisson statistics.

Finally, I want to remark that the morphological classification used by Sheth et al. is very different from the accurate methodology I have presented in this chapter. Moreover, even if the present results are limited by the Poisson statistic, I have showed that our samples are representative of local and distant galaxies. Being also limited by the fraction of galaxies with $i > 65^\circ$ cited above, my result may be consider as a lower limit.

6.4.3 Color distribution

Figure 6.16 shows the color distribution of our local and distant samples. Yellow and red symbols represents the S0 and elliptical galaxies, respectively. Thus

the well known "red sequence"¹³ is not only composed by such galaxy types. I find that in our local sample the red sequence is composed by: $33\% \pm 8\%$ of E/S0, $61\% \pm 11\%$ of Sp, and $6\% \pm 3\%$ of peculiar galaxies. In the case of the distant sample the red sequence includes $49\% \pm 8\%$ of E/S0, $25\% \pm 6\%$ of Sp, and $26\% \pm 6\%$ of peculiar galaxies.

These results imply that more than 50% of galaxies in the local and distant red sequence are not elliptical or lenticular galaxies. This is a lot more than what has been published previously (e.g., *Cirasuolo et al., 2007*, and references therein; see also subsection 6.2.5). It may be due to our morphological classification methodology, which we have shown to be more reliable than other methods. Indeed, the use of colors to estimate morphological evolution of galaxies has been done erroneously, as galaxy color alone is not a good indicative of the galaxy morphology. Different reasons can explain this. One of them is that U-B color are very sensitive to extinction, which is more important in spiral and peculiar galaxies because of their large amount of gas.

In short, colors are well used to classify stars. Nevertheless, galaxies are much more complex systems, composed of gas and millions of stars. It is therefore expected that extinction and geometric effects (edge-on galaxies) affect their color with a significant deviation.

¹³all galaxies above the black straight line.

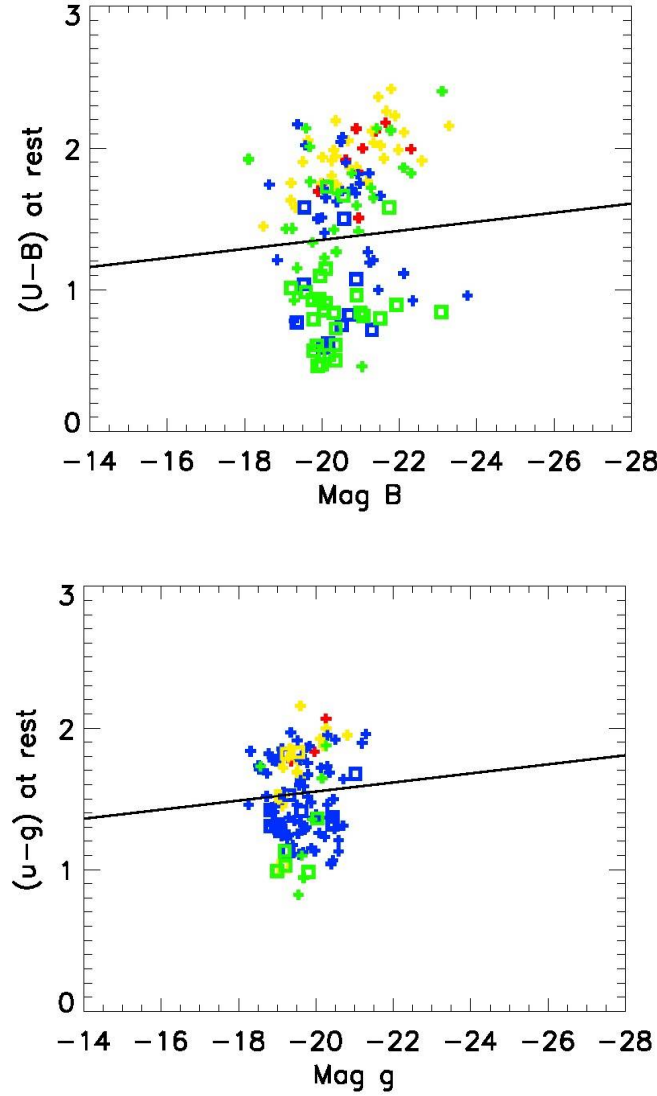


Figure 6.16: Morphological contamination in the so called "red sequence" shown by a 3D plot of the color distribution of our representative distant (at *top*) and local (at *bottom*) samples. Red/yellow crosses represent E/S0 galaxies, blue symbols represent spiral galaxies, and green symbols represent peculiar galaxies. Crosses show galaxies classified as quiescent ($\text{EW}[\text{OII}]\lambda 3727 < 15\text{\AA}$), and squares galaxies classified as starburst. The straight line gives the limit between red and blue galaxies from Cirasuolo *et al.* (2007) (in the local plot, I made a correction for the straight line of +0.2 mag to roughly fall in the "separation" between "red" and "blue" galaxies). All E/S0 galaxies of our representative samples are well in the red region. However, the "contamination" of the red region by other morphologies (Sp and Pec) is quite large. Noteworthy, I have found that using a starburst-quiescent limit smaller than 11\AA there is a better correlation between starburst-quiescent galaxies and blue-red galaxies, respectively.

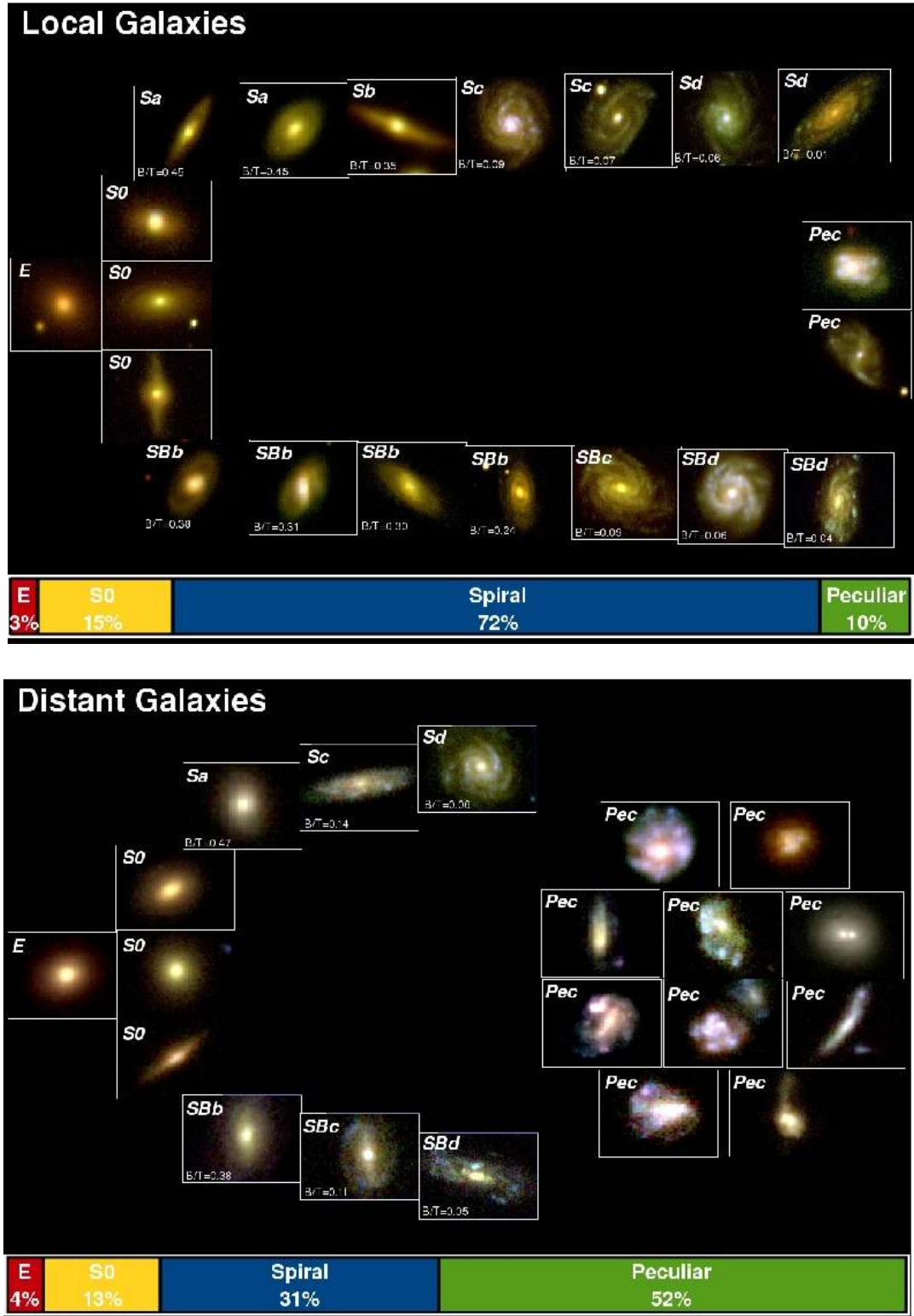


Figure 6.17: Local and Distant Hubble sequences. Each galaxy image represents $\sim 5\%$ of the whole galaxy population at each respective epoch.

See: *Delgado-Serrano et al. 2010, A&A, 509A, 78D*

Conclusion and Discussion

During my PhD thesis I have confronted serious problems of methodology concerning the morphological and kinematic classification of distant galaxies. This has forced us to create a new simple and effective morphological classification methodology in order to guarantee a morpho-kinematic correlation, make the reproducibility easier and restrict its subjectivity. This is not the case for the rest of morphological classification proposed in the past decades. Such classification methodologies¹ suppose that the high number of galaxies they can classify in a relative short time compensate for the errors they make in the morphological classification of a quite important fraction of galaxies. It is impudent to believe that methodology has a second role when classifying galaxies. How could a limited methodology not affect the results?

Giving the characteristic of our morphological classification, we have thus been able to apply the same methodology, using equivalent observations, to local and distant galaxies. It has allowed us to determine a morphological evolution of galaxies over the last 6 Gyr. Our results present just a small statistical error bar, which could be improved by adding more galaxies to the studied samples.

Indeed, the IMAGES survey and subsequents studies, in which I participated, provide us with a complete description of galaxy properties 6 Gyr ago (see figure 7.1). In short, this thesis has thus allowed me to work on the morphology and kinematics of galaxies. By making a careful analysis of each galaxy, we have been able to determine the evolution of their morphology and kinematics. The conclusions are the following:

- The morphological classification method presented here represents a very promising tool, as (1) it provides a strong correlation with the kinematic stage of the galaxies, (2) it is easily reproducible, and (3) it has a considerably limited subjectivity. It could be easily extended to higher redshifts when deeper and better resolution images will be available (e.g., from the ELT).
- We find that E/S0 galaxy populations show no evidence of number density evolution during the past 6 Gyr, while slightly more than half of the distant

¹concerning the automated ones.

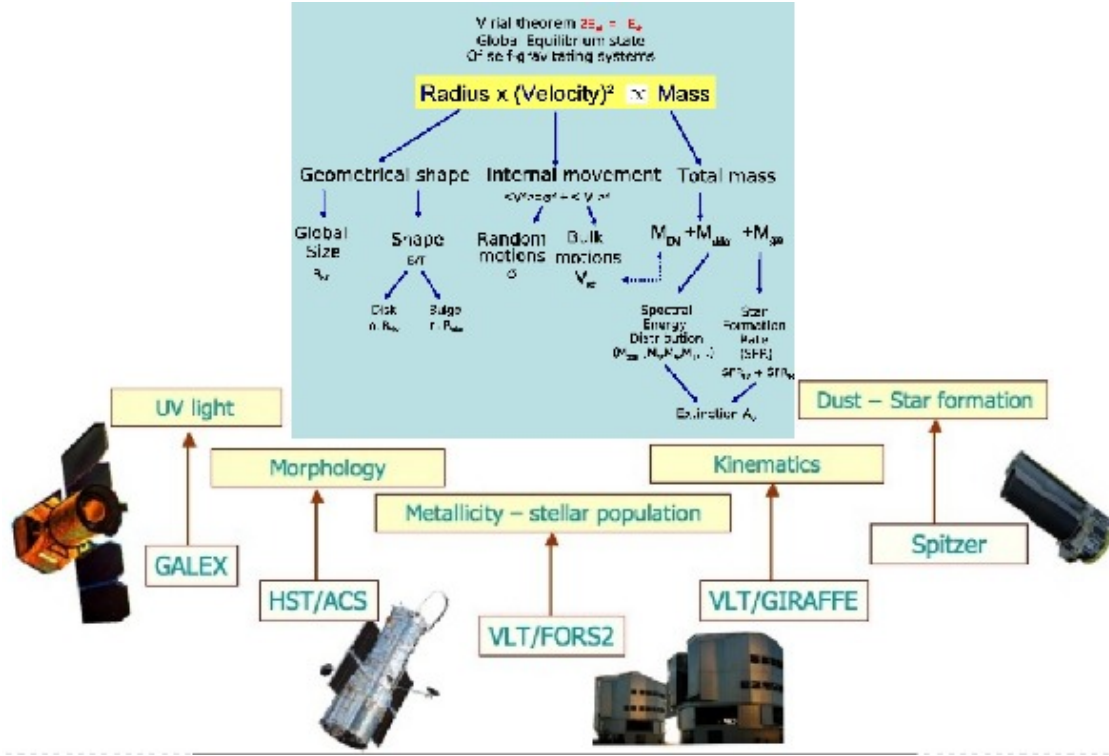


Figure 7.1: IMAGES results diagram from different instrument observations (Courtesy of M. Puech).

galaxies had peculiar morphologies. These last are associated to anomalous kinematics.

- The fraction of regular spirals was 2.3 times lower 6 Gyr ago than in the present epoch. This shows that more than half of the present-day spirals had peculiar morphologies, 6 Gyr ago. Thus almost all the evolution is caused by the transformation of galaxies with peculiar morphologies into regular spiral galaxies at present epoch.
- The number fraction of barred galaxies in the local Universe is higher than at $z \sim 0.65$.
- Integrated color determination to separate early and late type galaxies is not an adequate tool. A similar result has been found for the parametric methods (A-C plane, Gini and M_{20} coefficients, etc.)
- Further results, concerning the kinematics of $M_{B_{Vegamagnitude}} < -16.4$ galaxies at $z \sim 0.25$ (see appendix C), allow us to state that galaxies with complex kinematics present the same signature in emission lines of the same ionization (e.g., [OIII] $\lambda 4959$ and [OIII] $\lambda 5007$), while emission lines of different species

(e.g., $H\beta$ and [OIII]) show different complex kinematics. In contrast, rotating disks have the same kinematic signature using any emission line. This indicates that our methodology is effective at separating spiral rotating disks from galaxies having complex kinematics and peculiar morphology. While spiral rotating disks are dynamically stable, peculiar galaxies with complex kinematics undergo chaotic internal motion.

7.1 Merger events and the baryonic Tully-Fisher relation

The previous results seem to favor a "spiral rebuilding" scenario (Hammer *et al.*, 2005a; Hammer *et al.*, 2009a). In this context, we can add the following conclusions to Hammer *et al.* (2009a), and Puech *et al.* (2010):

- Analysis of the Tully-Fisher relation at $z = 0.65$ (Flores *et al.*, 2006; Puech *et al.*, 2008, 2010) are more consistent with merger processes happening at that time (see also Covington *et al.*, 2010); Hammer *et al.* (2009a) reproduced the morphology and the kinematics of anomalous galaxies at $z=0.65$ assuming major merger processes, including instabilities in the remnant phase;
- The merger rate required to explain that half of the $z=0.65$ galaxies are in a merger process is in agreement with the most recent models of halo occupation (see Hopkins *et al.*, 2009b). This is because the whole duration of the merger process is long, and can reach up to 2, 3 or even more Gyr;
- The comparison between the distant and the local Hubble sequences implies that most peculiar galaxies should be the progenitors of present-day spirals. This is because the fraction of early-type galaxies (E/S0) does not evolve. Hammer *et al.* (2009a), and Puech *et al.* (2010) have shown that the progenitors $z \sim 0.6$ galaxies had large enough gas fractions ($>50\%$), implying that the progenitors of the assumed mergers were very gas-rich, thereby allowing a significant rebuilding of the disk of the merger remnant (see Hopkins *et al.*, 2009a; Stewart *et al.*, 2009);
- Other mechanisms such as minor mergers or outflows are unlikely to be dominant because they have a considerable lower efficiency (see Hopkins *et al.*, 2008), and because their observational signatures are not detected in the galaxy spectra (Hammer *et al.*, 2009a).
- The non evolution of the baryonic TF relation, and the previous conclusion concerning the higher content of gas in distant galaxies, implies that such gas is gravitationally bound to the system, which suggest that galaxies evolve on average as in a close box model since $z \sim 0.65$. This could explain the evolution

of the stellar mass-metallicity relation reported by [Rodrigues *et al.* \(2008\)](#) (see subsection 5.4.3). This is in agreement with a "spiral rebuilding scenario" (see subsection 2.3.1). This last explains that gas-rich major mergers can expel gas, which can be later re-accreted to re-build a new disk.

- The fact that the gas is exhausted with time would unavoidably limit star formation during the post-merger phase at lower redshift. The lack of available gas with which to form a new disk would naturally lead to no new disks forming with strong star formation at low redshift, as reported by [Melbourne *et al.* \(2005\)](#).
- The relative abundance of E/S0 has not changed in the past 6 Gyr, which does not imply that E/S0 galaxies did not undergo mergers since then (possible dry mergers; [Bell *et al.*, 2006a](#)). Nonetheless, it makes clear that the process of mergers favors the formation of spirals since $z \sim 0.65$.

See: [Hammer *et al.* 2009, A&A, 507, 1313H](#)

See: [Puech *et al.* 2010, A&A, 510A, 68P](#)

7.2 Prospectives

The previous results open several interesting prospectives:

- 1.) *Searching for dynamic substructures in the core of galaxies in fusion.* The morphological analysis developed in this thesis, and observations from the HST/UDF, will allow us to trace the different morphological signatures of the abundant merger events at $z \sim 0.65$. Such morphological properties may allow us to understand how the system move (and evolve), as for example the detection of inner spiral structures. I have already created a data base concerning such galaxies, similar to that created for the galaxies I studied during my PhD, making galfit fitting in four different bands to analyze the fit and residual image of each galaxy. A new type of error map is also in perspective, which could allow us to make a real measure of the galfit pixel detections. Thus, the work is in progress.
- 2.) *Stellar tidal streams in nearby galaxies.* The detection of such streams ((e.g., [Ibata *et al.*, 2001](#); [Martínez-Delgado *et al.*, 2008, 2009](#)) will contribute to constrain the hydrodynamical simulations, and will give us a better idea of the past merger history of the local Universe. I participated in three night observations at the ESO-NTT searching for such streams in six local MW like galaxies. This data is being exploited. Furthermore, one of the project that

will be developed in the Panama observatory (see appendix D) concerns the study of tidal stream in local galaxies. It has been already shown (Martínez-Delgado *et al.*, 2008, 2009) that, with enough exposition time, it is possible to detect such structures with small diameter telescopes. However, it is necessary to develop a project which allow to do the photometry of such faint structures with small telescopes.

- 3.) *Morpho-kinematic Study of higher redshift galaxies.* There might be a transition epoch where the main driver for star formation shifts from cold gas streams to major mergers, around $z \sim 0.8-1.4$, since preliminary results at $z \sim 1.5$ suggest that cold flows were still important at this epoch (Bournaud *et al.*, 2008; Epinat *et al.*, 2009, and references therein). Indeed, numerical simulations, at $z \geq 1.5$, suggest that cold-gas streams from inter-galactic filaments can feed galaxies in fresh gas (e.g., Agertz *et al.*, 2009; Ceverino *et al.*, 2010), which could explain their observed very high star formation rate and clumpiness (e.g., Genzel *et al.*, 2008; Law *et al.*, 2009; Bournaud & Elmegreen, 2009). In this scenario, major mergers have a much lower duty cycle and therefore are not expected to be the main driver for star formation in $z \sim 2$ galaxies (Dekel *et al.*, 2009), as the study of individual galaxies apparently show no signs of major merging events (Förster Schreiber *et al.*, 2006; Wright *et al.*, 2007, 2009; Law *et al.*, 2007, 2009; Genzel *et al.*, 2006, 2008). However, what we currently know at high redshift is simply too fragmentary to tell us exactly what is going on. Thus, alternatively, there may not be such cold flows, as the number of kinematic studied galaxies at these redshift is still very small to have precised conclusions. Moreover, the morphology of very high redshift galaxies has been very difficult to exploit, because of the need of very deep data. Noteworthy, it is precisely at these epochs that the co-mobile star formation density reaches its peak, which makes this range particularly valuable for further 3D-kinematic and deep morphological studies. This is the reason why we are applying to ESO with a large program to observe a representative sample of 120 $z=0.6-1.4$ galaxies with GIRRAFFE CDD and FORS2 in the HUDF and WFC3-ERS (Early Release Science) fields (R. Delgado-Serrano: CoI). The available deep NIR imaging (i.e., rest-frame V-band) in these fields is essential to correctly image the distribution of stellar mass, an information which is currently lacking in all 3D surveys at $z \geq 1$.
- 4.) *Kinematic studies of quiescent intermediate redshift galaxies.* Since kinematic studies in our sample are based on star-forming galaxies (arbitrary defined as galaxies having an $\text{EW}[\text{OII}]\lambda 3727 \geq 15\text{\AA}$), a complementary study of our quiescent galaxies ($\text{EW}[\text{OII}]\lambda 3727 < 15\text{\AA}$) is needed. Yang *et al.* (2009) has shown it is possible, as the $z \sim 0.4$ galaxy they kinetically studied with Flames/Giraffe has an $\text{EW}[\text{OII}]\lambda 3727 = 2\text{\AA}$. We may take advantage of the much larger sensitivity of X-SHOOTER to observe a set of emission lines

in these objects. Indeed, using the exceptionally large spectral bandwidth of X-SHOOTER, it is now possible to obtain spatially resolved line maps of distant galaxies, using 5 prominent emissions lines (i.e., [OII] λ 3726,3729, H β , [OIII] λ 5007, H α). These lines are the most important tracers of the gaseous phase, which fuels star formation and disk growth in distant galaxies. As an example we have that for $z \sim 0.6$ galaxies, under good seeing conditions (≤ 0.8 arcsec), FLAMES can spatially resolve the [OII] emission line in 8 hours of integration time in $z \sim 0.6$ intermediate-mass galaxies. X-SHOOTER will roughly provide a five to six times better throughput compared with GIRAFFE at a smaller spectral resolution, which means that the same signal-to-noise ratio will be reachable in only ~ 1 hours (on-source). As a result, within the team GTO, there is an on-going proposal to ESO (R. Delgado-Serrano: CoI).

- 5.) *Hydrodynamical simulations.* The comparison of the observations with such simulations will allow us to constrain the different dynamical process that play an important role during the merger phases, as well as the progenitors stage. For each distant galaxy, we have at our disposal a complete description of its physical properties, including morphology, kinematics, and mass. As has been demonstrated in five explicit examples (see subsection 2.3.1), this allows us to model distant galaxies in a way similar to what is currently done for nearby galaxies. Restricting the simulations with all the information we dispose for each galaxy through the IMAGES survey (especially the morphological and kinematic information) is a promising way to model, with high accuracy, the formation of structures and substructures within discs.

A longer term prospective is the application of the morphological classification method developed here to observations with the future ELTs. Such next generation of telescopes are a very promising tool for the astronomical community, as they will improve the observation deepness in some order of magnitude compared with the present instruments.

Publication list

Publications

1. Neichel B., Hammer F., Puech M., Flores H., Lehnert M., Rawat A., Yang Y., **Delgado-Serrano R.**, Amram P., Balkowski C., Cesarsky C., Dannerbauer H., Fuentes-Carrera I., Guiderdoni B., Kembhavi A., Liang Y. C., Nesvadba N., Östlin G., Pozzetti L., Ravikumar C. D., di Serego Alighieri S., Vergani D., Vernet J. and Wozniak H., *IMAGES. II. A surprisingly low fraction of undisturbed rotating spiral disks at $z \sim 0.6$ The morpho-kinematical relation 6 Gyr ago*, A&A, vol. 484, pages 159-172, June 2008, 484, 159
2. Rodrigues M., Hammer F., Flores H., Puech M., Liang Y. C., Fuentes-Carrera I., Nesvadba N., Lehnert M., Yang Y., Amram P., Balkowski C., Cesarsky C., Dannerbauer H., **Delgado-Serrano R.**, Guiderdoni B., Kembhavi A., Neichel B., Östlin G., Pozzetti L., Ravikumar C. D., Rawat A., di Serego Alighieri S., Vergani D., Vernet J. and Wozniak H., *IMAGES IV: strong evolution of the oxygen abundance in gaseous phases of intermediate mass galaxies from $z \sim 0.8$* , A&A, vol. 492, pages 371-388, December 2008, 73, 105
3. Hammer F., Flores H., Puech M., Yang Y. B., Athanassoula E., Rodrigues M. and **Delgado-Serrano R.**, *The Hubble sequence: just a vestige of merger events?*, A&A, vol. 507, pages 1313-1326, December 2009, 507, 1313
4. **Delgado-Serrano R.**, Hammer F., Yang Y. B., Puech M., Flores H. and Rodrigues M., *How was the Hubble sequence 6 Gyr ago?*, A&A, vol. 509, pages A78+, January 2010, 509, A78
5. Puech M., Hammer F., Flores H., **Delgado-Serrano R.**, Rodrigues M., & Yang Y., *The baryonic content and Tully-Fisher relation at $z \sim 0.6$* , A&A, 2010, 510, 68

Press release

1. ESA/NASA/HST: *Forming the present-day spiral galaxies*, February 2010,
2. CNRS/INSU/Observatoire de Paris: *L'origine des galaxies spirales actuelles*, February 2010,

Appendix

Cosmology: The history of the Universe and the formation of structures

"...You need a lot of smart peoples, and faith that with enough smart people, thinking about difficult problems in enough different ways, someone can transform our view about how the world works. It's happened many times before, and it will surely happen again."
 Liddle and Loveday, The Oxford Companion to Cosmology.

Contents

B.1	Filters and photometric calibration	132
B.2	The magnitude systems	134

In the observable Universe, the gravitational force is the principal responsible for the formation of structures. One little mass overdensity can result in an accretion process. It is the beginning of the formation of structures. Then, other forces show up, while the accretion process is in action, and they could finally drive the system to equilibrium. The final spatial scale of the object will depend on the amount of mass accreted or that could be accreted. Two examples of forces that could counteract gravity, in the case of small scales, are the thermal radiation and the nuclear forces. For large scales, the conservation of angular momentum is crucial in the way to the equilibrium.

In any case, the new structure can be considered as an isolated *set of components* which do not follow the general Universe expansion, but its own evolution. However, the first thought, before studying those sets as isolated, is how the Universe has evolved to form all the different objects or structures at different scales as we can see today through the best telescopes in the world. This is not so well known until now. Nevertheless, two theories confront each other to try to explain the Universe evolution, and find an answer to how the different structures at different scales have been formed. Both of them are based on observational and theoretical results, but they present two different ways of the Universe evolution.

A.1 The primordial collapse model

The primordial collapse model, also known as the adiabatic scenario, proposes the formation of smaller structures after the formation of the largest ones. This is the reason why it is known as the *top-down* model (see figure A.1). As a consequence, this model predicts the formation of massive galaxies very soon after the big-bang ($z \geq 3$) when a primordial collapse of matter is produced.

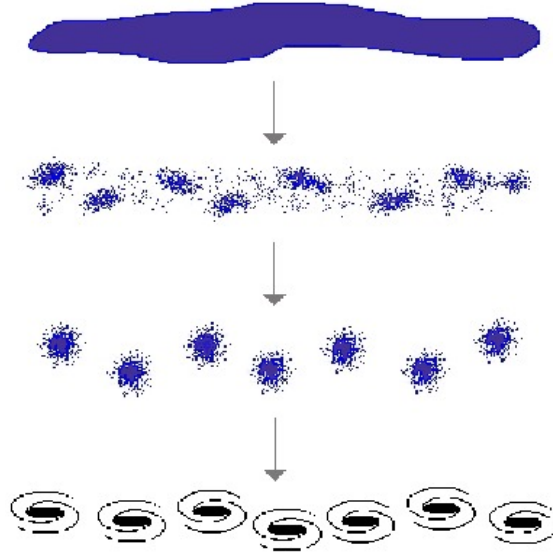


Figure A.1: Illustration of the Top-Down model.

Sunyaev & Zeldovich (1970) give the principle (see also Zel'dovich, 1967; Zel'Dovich, 1970; Doroshkevich *et al.*, 1967; Peebles, 1970; Peebles & Yu, 1970; Shandarin & Zeldovich, 1989). First, little adiabatic perturbations take place in the beginning of the Universe. Then, only the most important perturbations survive the Recombination¹ because those smaller than a limit mass were smoothed by the photon diffusion. Finally, large structures are formed with ellipsoid shape ($z \sim 5$), to be then flattened following the minor axis and forming what Zeldovich called "pancakes". These pancakes segment and form the galaxies. One of the principal results of this theory is that it is consistent, as a natural consequence, with the scale of the large structures.

So far, the model takes care only of the baryonic matter assuming that the baryons dominate the Universe, and thus predicts that the perturbations during the Recombination are of the order of 3×10^{-3} . Nevertheless, with satellite COBE it has been found that those perturbations could not be larger than 2×10^{-5} (see

¹It is the moment when the decoupling of photons and matter take place (see more details in section A.2).

figure A.2; Smoot *et al.*, 1992)(see also Scott & Smoot, 2006, for a review). Here there was then a problem to solve. Moreover, astronomers had been finding evidence about a disagreement between the mass of galaxies derived from their luminosity and that from their dynamics (e.g., Zwicky, 1937; Gottesman *et al.*, 1983b; Dressler *et al.*, 1986; Ninkovic *et al.*, 1990; Rohlfs & Kreitschmann, 1988; Lupton *et al.*, 1987)(see also Lynden-Bell, 1983; Freese, 2009; Roberts, 2008; Primack, 2009, for a review)². The mass calculated after their dynamics was much bigger than the mass estimated after the total luminosity we receive from them. Consequently, a logical hypothesis to emerge was the idea of the presence of a certain kind of mass we can not see, and which differ in some characteristics from the "normal" baryonic mass³. The non-baryonic "dark matter" was thus born.

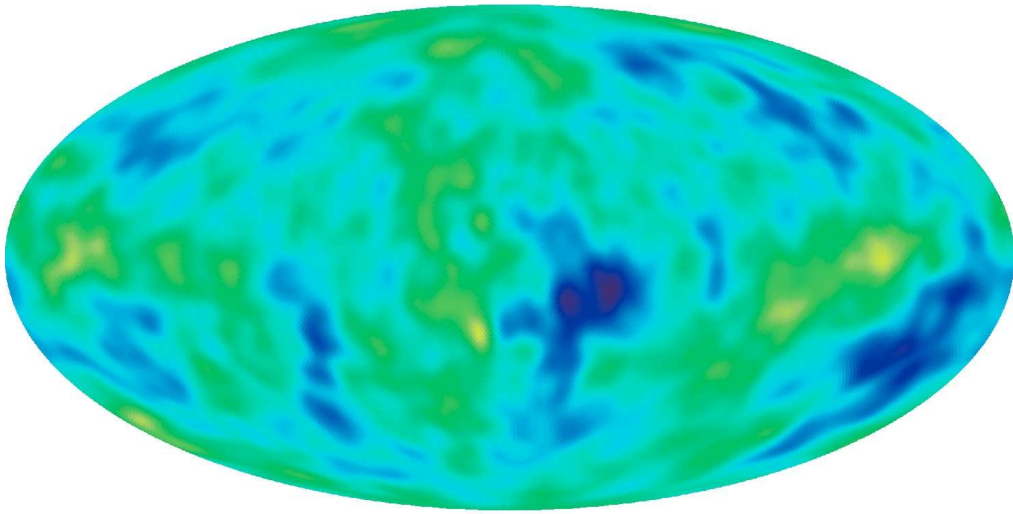


Figure A.2: Cosmic Microwave Background (CMB) map observed by COBE (Credit: NASA/WMAP Science Team; see also Bennett *et al.*, 1996). The spectrum of the CMB is well described by a blackbody function with $T = 2.725\text{K}$.

With the idea of the existence of dark matter, the adiabatic model became the Hot Dark Matter (HDM) model. Within a few years, this renewed model was developed to be in agreement with the results mentioned above. The HDM model predicts, similar to the original adiabatic model, the formation of large structures at the beginning which break up in smaller structures through time. The principal candidates for the hot dark matter are the super-massive neutrinos (e.g., Scherrer, 1988; Chungpei, 1996; Nieuwenhuizen, 2010; Gershtein & Zel'Dovich, 1966; Cowsik & McClelland, 1972). Neutrinos travel with ultrarelativistic velocities, and are very difficult to detect because of their way to interact with baryonic matter.

²Very few studies were against this idea (e.g., Gottesman & Hunter, 1982; Gottesman *et al.*, 1983a).

³For example, it does not interact with electromagnetic radiation, neither with the ordinary matter via electromagnetic forces.

Neutrinos only interact with baryonic mass by the weak interaction and gravity, which are well known not to be strong forces. One of the most famous projects to detect neutrinos is the Super-Kamiokande neutrino observatory in Gifu-Japan (see figure A.3).

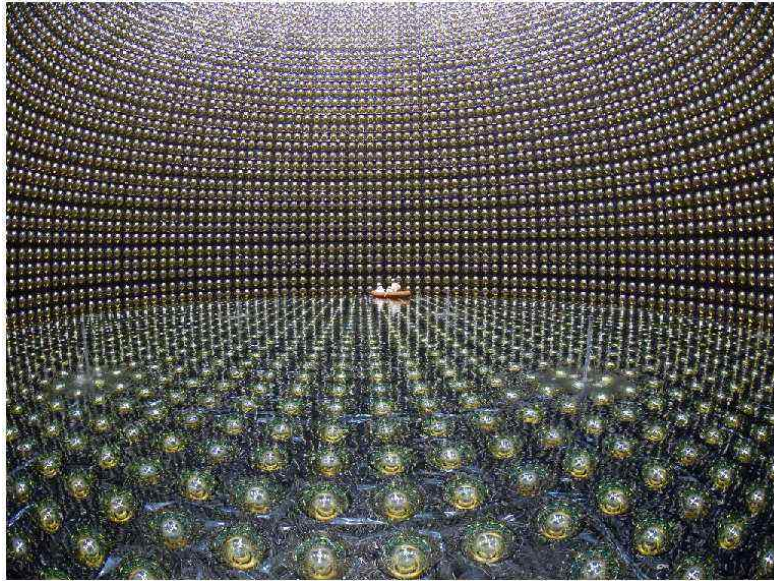


Figure A.3: Photo of one part of the Super-Kamiokande. For scale, in the center one can distinguish a rowboat with two scientists inside. The Super-Kamiokande is surrounded by 50 000 tons of pure water, and is composed of 11 200 photomultiplier detectors. Its dimensions are: 41.4 m high, and 39.3 m across (Credit: Kamioka Observatory, ICRR-Institute for Cosmic Ray Research, The University of Tokyo).

During the first three minutes of the Bing Bang, while the Universe goes from its spectacular 10^{32} kelvin to roughly 10^9 Kelvin, takes place the production of neutrinos among the reactions which produce photons. The theory also predicts a decoupling of neutrinos from matter, similar to the photon-matter decoupling which creates the today well known CMB (Cosmic Microwave Background). However, the neutrino-matter decoupling happens before the Recombination. Therefore, a cosmic neutrino background as dense as the photons of the CMB is also predicted.

One of the problems of the HDM model is the inability to account for the galaxy distribution observed in the Universe (e.g., [White *et al.*, 1983](#)). The neutrino density was very high in the early Universe, and added to their greatly relativistic velocities, they could then smooth out any fluctuation in matter density and make the formation of any overdense region impossible. This implies that those overdense regions could be formed only later when neutrinos notably slow down (called neutrino "cooling") as a consequence of the decreasing temperature of the expanding Universe. Then, combining this result with those observed by the

satellite COBE on large scales, scientists have found that a Universe dominated by neutrinos would not contain enough power on small scales to fit the observed Universe properties.

As a result, any purely HDM model of the Universe is excluded. For this reason, when scientists talk about HDM model today, they mostly refer to a "Mixed Dark Matter" model, which combines "Cold" and "Hot" dark matter (CHDM, for Cold+Hot Dark Matter; see for example Primack & Gross, 1998; Choi & Ryu, 1998)⁴. A huge fraction of the dark matter is cold, while the hot fraction is tiny. Experiments predict that the amount of hot dark matter in the Universe would be a few percent⁵, while the cold dark matter component represents roughly 85% of the total mass ($\sim 33\%$ of the total energy) in the Universe.

A.2 The hierarchical model

This model, also known as the isothermal model, proposes the formation of small structures at the beginning and then, by accretion of these ones, the largest structures develop. Therefore, it is an hierarchical model with a *bottom-up* evolution.

It was developed almost paralely to the primordial collapse model (Peebles & Dicke, 1968; Peebles, 1969b)(see also Zel'dovich, 1967; Doroshkevich *et al.*, 1967), and could be seen as the opponent of it if we consider their scale evolution. Its principal idea states that almost each fluctuation before the Recombination could give birth to one structure. In this context, the formation of structures has begun just after the Recombination. At such an epoch, the Universe was smaller, and thus its density was a lot much higher. This implies that the probability of objects to collide was much more important. Hence the first little objects interact and begin to form larger and larger structures until the formation of galaxies, galaxy clusters and so on.

Two important results of this model are the following. The first one is that it predicts that between the first baryonic objects to be formed some of them have sizes roughly similar to the known globular clusters. Curiously enough, these last are also known to be amongst the oldest objects in the Universe. The second result is that this model can explain very well the fast metal increase of the Universe by the action of the first massive stars, or more exactly by the explosion of these ones

⁴There are also other combinations giving for example a Λ CHDM model (e.g., Popa *et al.*, 2001), which includes a cosmological constant different from 0, or even we could also have a Warm DM model (e.g., Acedo, 2009; Tikhonov *et al.*, 2009)(see Primack & Gross, 2001, for a review).

⁵some experiments even predict an amount of HDM which could be unmeasurable.

in supernovae.

Similar to the adiabatic model, the hierarchical model needed to be adapted to the new results coming from COBE and those about the dynamic of galaxies, among others. It then became the Cold Dark Matter (CDM) model ([Primack & Blumenthal, 1984](#)). The dark (non baryonic) matter, in this case, travels relatively slow, and this is the reason why it has been called "cold". In the CDM model, very early in the Universe history (before the Recombination), the dark matter follows the little fluctuations and began to form structures of very small mass, then by coalescence the bigger structures form.

One weakness of the cold dark matter theory is that it does not make any predictions about exactly what the cold dark matter particles are. Nevertheless, there are some candidates to constitute the "cold dark matter". They have very curious names: (1) WIMPs, for Weakly Interacting Massive Particles; (2) MACHOs, for Massive Astronomical Compact Halo Objects; and (3) Axions, coming from the quantum chromodynamics (QCD) theory⁶. The first ones (WIMPs) are supposed to be a kind of massive particles. There is no known particle within the standard model of particle physics with the required properties (similar to HDM particles, but with higher masses and much slower velocities)⁷. Researches continue in the particle accelerators. The second ones (MACHOs) would be composed of very compact objects like black holes, neutron stars, white dwarfs, very faint stars, or even objects such as planets. However, until now, the studies, using gravitational microlensings, show that such objects do not represent a significant percentage of the required amount of mass. Finally, particles called axions are still hypotheticals and are being searched.

In any case, according to the different (assumed) nature of the dark matter, a family of CDM models has been developed during the past three decades: SCDM (Standard-CDM), OCDM (Open-CDM), τ CDM, ν CDM, HCDM, WCDM, and the Λ CDM (see [Dodelson et al., 1996](#), for a quick review about the CDM models)(see figures [A.4](#) and [A.5](#))⁸. Nonetheless, nowadays, looking for the combination of

⁶Just for curiosity, the name "Axion" was adopted from a brand of detergent, making allusion to the fact that one of the QCD problems had been "cleaned" with their assumption.

⁷Nonetheless, in supersymmetry theories, the neutralino is a possible WIMP (e.g., [Braun et al., 2009](#), and references therein)(see also [Bertone et al., 2004](#), for a review).

⁸Concerning the topology of the Universe, there are also a subclass of big bang models that are Friedmann-Lemaître solutions in which the space topology is multiply-connected instead of being simply-connected. One example is the Wraparound Universe theory ([Luminet, 2001, 2008b](#)), which proposes a positive spatial curvature within a Poincaré Dodecahedral Space (PDS) topology ([Luminet et al., 2003; Luminet, 2008a](#)). In this theory, the Universe has a finite spatial extension without edge. The Wraparound Models have only implications on space geometry, and not on time evolution. They share exactly the same dynamics (time evolution starting from a big bang,

the parameters that lead to the better agreement with the existing data on both large and small length scales, the more accepted, adopted by a large part of the scientific community, is the Λ CDM model (see figure A.6, and also see figure A.7 for a 3D visualization). It is described below.

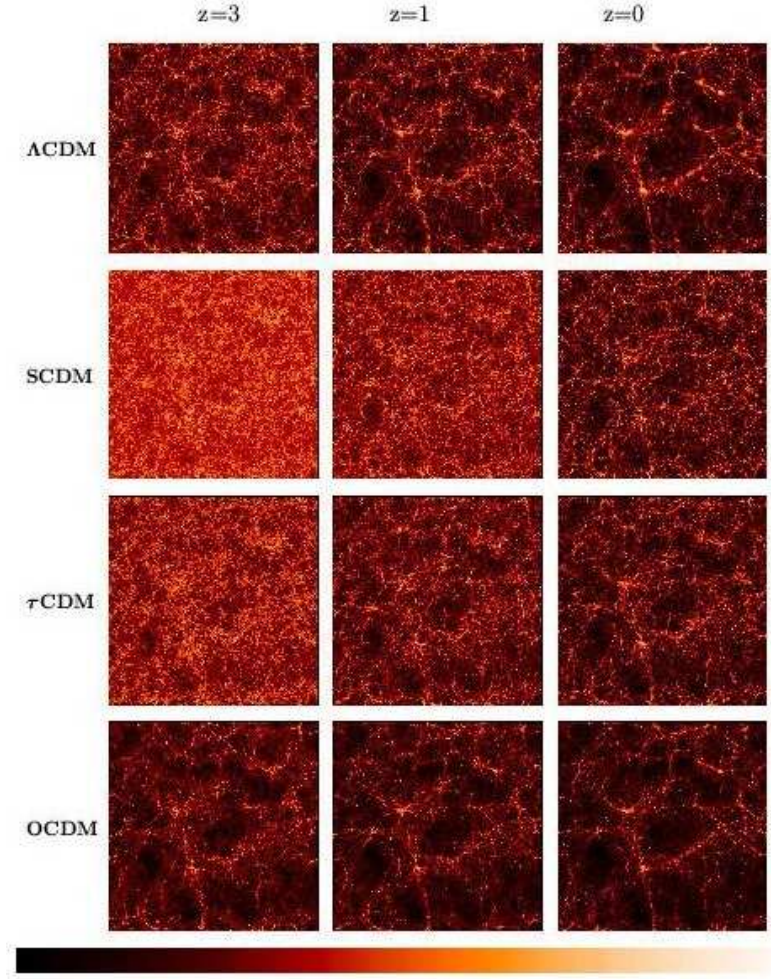


Figure A.4: CDM model simulations (Jenkins *et al.*, 1998; Thomas *et al.*, 1998, for the Virgo Collaboration).

The Lambda-Cold Dark Matter (Λ CDM) model

The Λ CDM could be seen as an extension of the previous CDM models as it has been developed by changing, adding or suppressing some parameter values to be in agreement with the new observations (see Larson *et al.*, 2010, for the more recent parameter values, as their constraints come from seven years data-observations of the CMB anisotropies by the WMAP satellite). Then, the Λ CDM model supposes

and in perpetual accelerated expansion if dominated by dark energy) as the standard model.

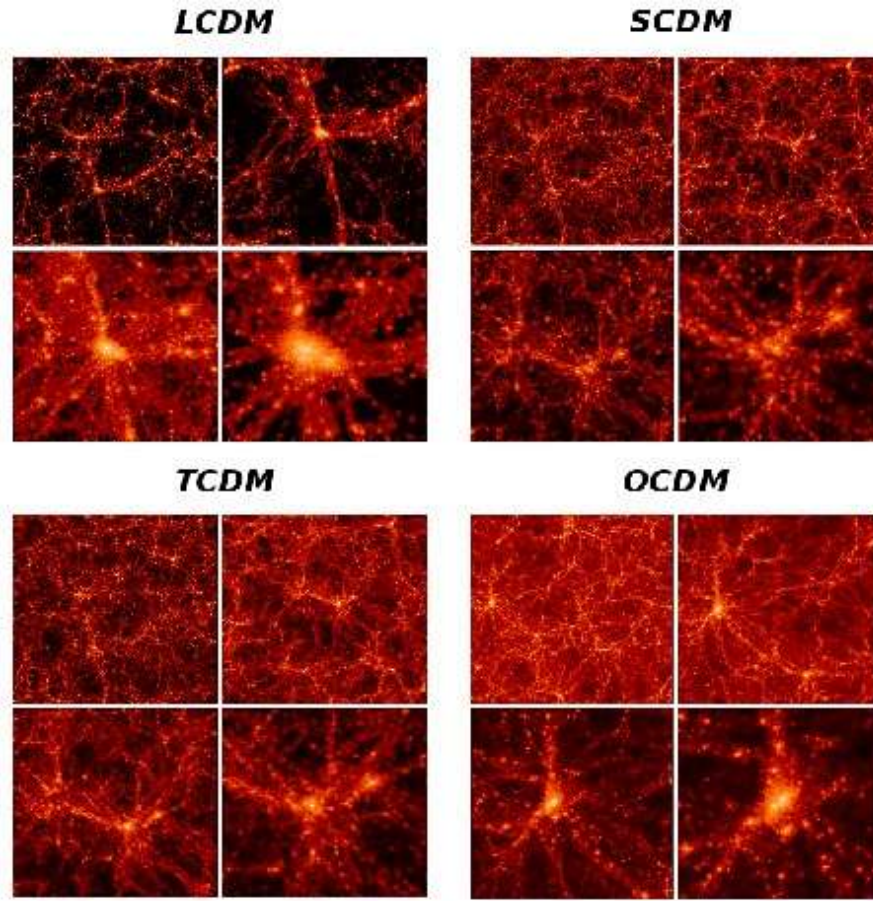


Figure A.5: LCDM, SCDM, TCDM and OCDM model simulations showing different scales at $z=0$. (Jenkins *et al.*, 1998; Thomas *et al.*, 1998, for the Virgo Collaboration).

an expanding Universe composed of baryonic and cold dark matter. This cold dark matter, as it has been said before, is dissipationless and collisionless, which means, respectively, that it can not be cooled by photons and that CDM particles can interact between them and with other particles only through gravitation. The real innovation of the Λ CDM model is the assumption of a non-zero cosmological constant (Λ) (Peebles, 1984). This last is associated with a vacuum energy or dark energy, which would explain the current accelerating expansion of space against the attractive effects of gravity. In the Λ CDM model the Universe is described by a hot big bang cosmology, where the Einstein's general relativity describes how gravity works, while the standard model of particle physics, with the addition of dark matter and dark energy, explains the material content and the way particles interact.

In this context, the numerical simulations of the Λ CDM model show the more recent view of the evolution history of our Universe. It is known as the concordance

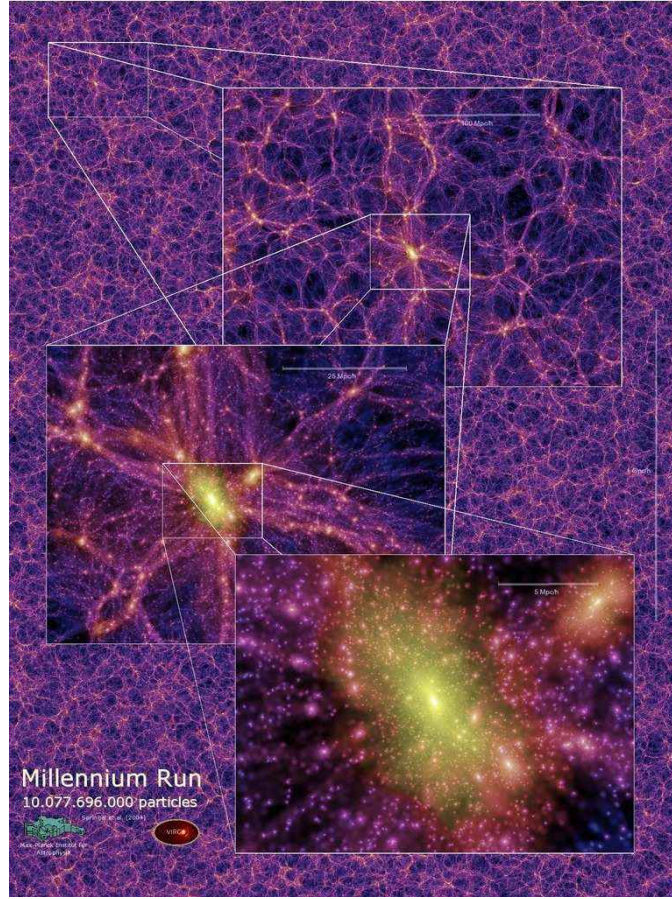


Figure A.6: Illustration of the Millennium simulation (Springel *et al.*, 2005b). It shows the dark matter density field on various scales at redshift $z=0$ with a thickness slice of 15 Mpc/h. The zoom sequence displays consecutive enlargements by factors of four, centred on one of the many galaxy cluster halos present in the simulation. Colors are coded by density and local dark matter velocity dispersion (Credit: Virgo Consortium).

model. In some cases, this model is also called the standard cosmological model, which should not be confused with the standard CDM model mentioned above. Therefore, the evolution history of our Universe through the Λ CDM model could be summarized as follows.

After the Big-Bang, we have, in principle, four main epochs. First, the inflationary epoch (Guth, 1981; Linde, 1982; Albrecht *et al.*, 1982; Guth, 1986), where the seed density perturbations, which are responsible for the formation of the cosmic structures and all the properties of the Universe we see today, take place. Second, the radiation dominated era, during which the formation of the atomic nuclei ("nucleosynthesis", see below) take place. Third, the matter dominated era, where the recombination, the decoupling, and, the formation of larger structures, in that order, take place. Finally, we would be, eventually,

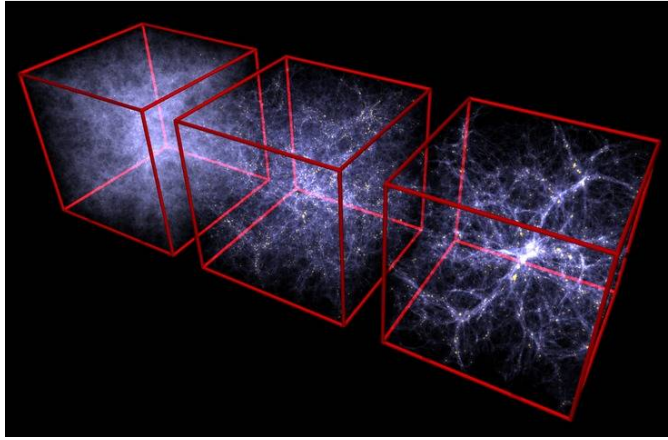


Figure A.7: Structure formation in the gaseous component of the universe (within the dark matter density field), in a simulation box 100 Mpc/h on a side. From left to right: $z=6$, $z=2$, and $z=0$. Formed stellar material is shown in yellow (Credit: Volker Springel).

in the dark energy dominated epoch which main characteristic is the Universe accelerating expansion. It is not known what happened before the inflation, if we could say so, and it is neither known what will happen after the dark energy dominated era, if there is such an after.

The seed density fluctuations during inflation are scale-invariant according to the Harrison-Zeldovich spectrum (see figure A.8; Harrison, 1970; Zeldovich, 1972). More precisely, if one would have access to a map of the perturbations, one would not be able to distinguish whether the map is one kiloparsec across, one megaparsec across, the size of the whole observable Universe, or even zillion times larger than the whole observable Universe. The Harrison-Zeldovich perturbations are adiabatic, which corresponds to a perturbation in the total density shared amongst the different components (they have the same profile, e.g., where the DM density has a maximum, the densities of all other materials have also a maximum). These adiabatic perturbations are density perturbations (point-to-point variations in density) coming from earlier quantum fluctuations in the original scalar field that dominated the Universe during inflation. This scalar field is known as "the inflaton" and could thus be considered as the original material that later decays to create the material filling the present Universe. In such a case, the Universe, in its origin, presents a thermal equilibrium during which energy is exchanged between the different "materials" until the adiabatic conditions are satisfied. Such a thermal state is important as it forces the perturbations in any kind of material participating in the thermal equilibrium to become adiabatic perturbations. Two properties characterize these perturbations, their length scale (e.g., peak to peak distance) and their amplitude. Then, when the quantum fluctuations begin, they

lead to large-scale density energy perturbations. As the inflation continues, smaller density energy perturbations are generated, with the smallest ones near the end. Hence, when the Universe finishes its inflation, the density energy perturbations coexist in a very wide range of length scales, and the quantum nature of the first fluctuations are no longer important as perturbations can be considered to follow classical physics laws. The transition from quantum to classical nature is called "decoherence".

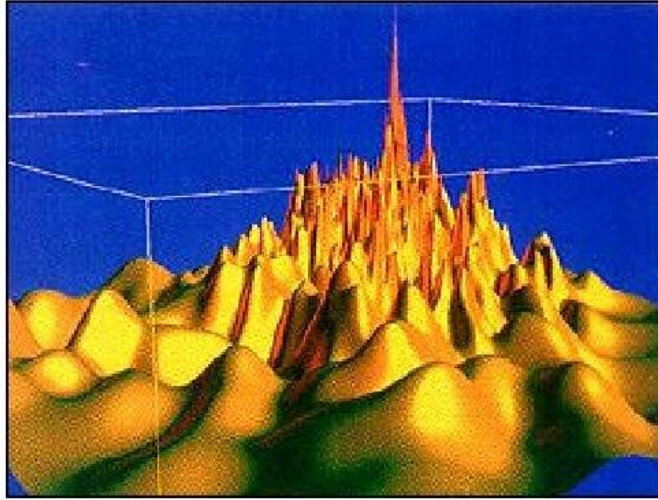


Figure A.8: Illustration of the primordial scalar field fluctuations (Credit: Linde, A.) (see also [Linde, 2008](#)).

This is how the radiation dominated era begins. Given the fact that Einstein energy-matter relation ($E=mc^2$) allows us to go from matter to energy, and vice versa, the name of "radiation-dominated" only refers to the idea of a relativistic matter domination. During this epoch, the constituent particles (e.g., photons of light or neutrinos) travel at or near to the speed of light. However, it does not mean there is no other constituent. The Friedmann equation shows that the principal quantity that governs the expansion rate of the Universe is the density of the different material which dominate it in a specific epoch. In such a case, the total energy density of relativistic particles dominate, in a large range, over the baryon, dark matter, and dark energy densities. Nevertheless, as the Universe expands, this tendency changes. In any case, even though by the end of the radiation-dominated era only photons and neutrinos were relativistic, in the earlier moments the Universe was hotter and its ambient energy was thus higher, which could allow other particles to be also relativistic. It is during this epoch where the atomic nuclei of hydrogen and helium-4 are formed⁹ in a process called nucleosynthesis ([Gamow, 1946](#); [Alpher *et al.*, 1948](#), see also figure A.9).

⁹in less amount, atomic nuclei of deuterium, helium-3, and lithium-7 are also formed.

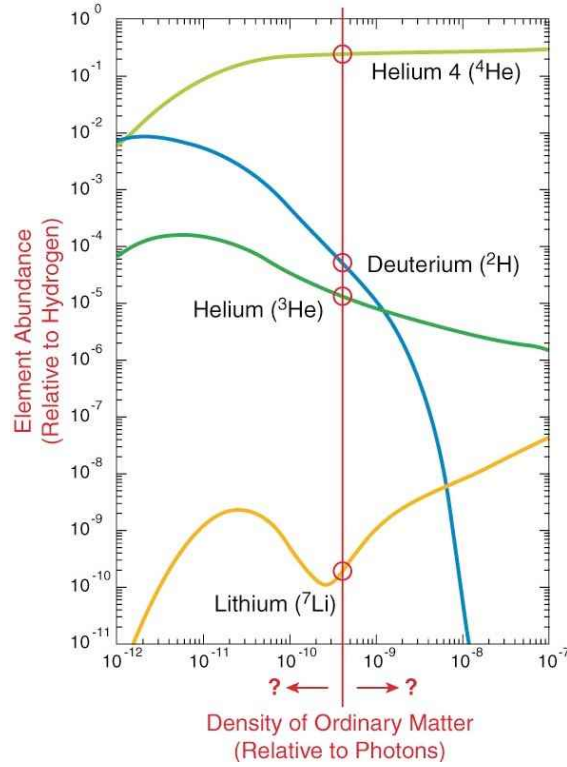


Figure A.9: The abundance of the main four light elements vs. baryon density in the Universe, as predicted by the theory. The baryon density is given in $\mu\text{g}/\text{km}^3$. The vertical red line indicates a strong interpretation of the observational data (for more details see Schramm & Turner, 1998; Copi *et al.*, 1995).

As the Universe continues its expansion, it becomes cooler and bigger, with the density of relativistic particles dropping faster than non-relativistic particles density. When the non-relativistic particles (principally, cold dark matter) took over, a long matter-dominated era began, and extending roughly until half of the present age of the Universe. Recombination, decoupling and reionization are key events of this era. The first makes reference to the process when electrons bind to the atomic nuclei formed during nucleosynthesis. Hence, the Universe become gradually populated by atoms, more and more neutral. This phenomena combined to the expansion¹⁰ makes the interaction between photons and matter particles negligible, and thus the Universe becomes transparent to radiation. This is the so called decoupling. Before these two process (recombination and decoupling), the competition between gravity, expansion and radiation pressure induces acoustic fluctuations in the primordial plasma that stop matter over-densities to grow. However, after these two processes, matter over-densities are amplified by gravity

¹⁰the expansion of the Universe decreases the photon energies and the particle densities. The first reduces the probability of photons to interact, and the second reduces the probability of two particles to meet.

because the radiation pressure of photons can not stop it any more. As we can imagine, recombination and decoupling take place in a range of redshift (~ 200) that is named, abusively, *surface of last diffusion*. During this period, the radiation is still not totally decoupled from matter, interacting with the first over-densities in formation. What we see on the CMB map (see figure A.10) are those fluctuations. Finally, the other key event during the matter-dominated era that has been mentioned above is the reionization. This one refers to the formation of the first massive stars and their supernova explosions, by which considerable amounts of energy are release into the intergalactic medium causing the dissociation of electrons from their atomic nuclei and ionizing the Universe again. Quasars and active galactic nuclei also contribute to this process, which take place at a redshift value of approximatly ten. After this, the formation of structures continues by the influence of gravity, and the Universe arrives to a period where the dark energy dominates, causing the acceleration of the Universe expansion (Riess *et al.*, 1998; Perlmutter *et al.*, 1999; Schrabback *et al.*, 2010, see figure A.12 for an artistic view of the Universe history).¹¹

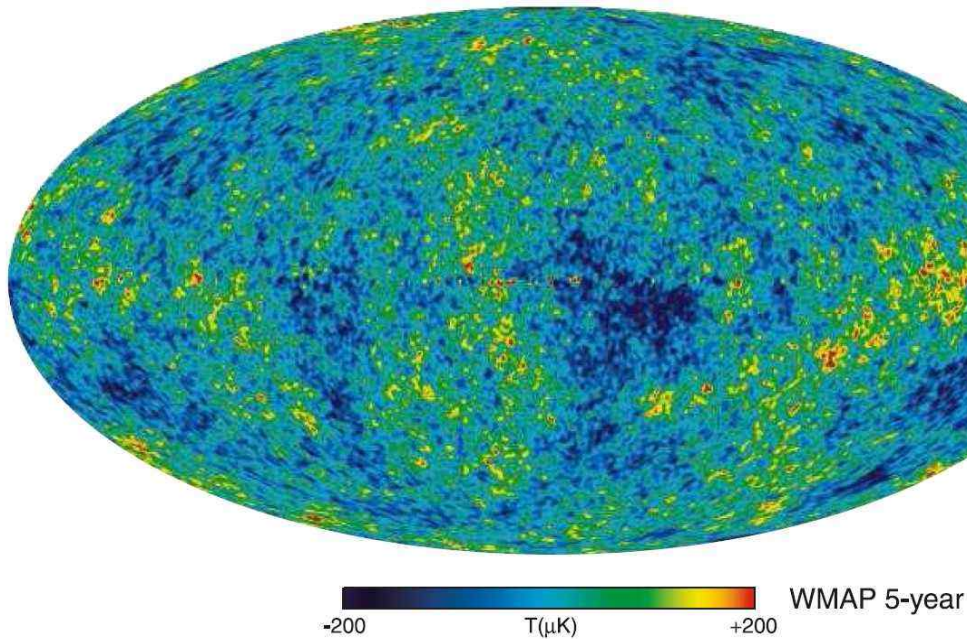


Figure A.10: Cosmic Microwave Background (CMB) see by WMAP. The fluctuations in temperature, as determined from five years of WMAP data, are of the order of 10^{-5} , and the temperature has an average value of 2.725 K (Hinshaw *et al.*, 2009)(see also Challinor & Peiris, 2009, for a general explanation).

¹¹(For more details about the history of the Universe, with a good pedagogical aim, see Liddle & Loveday, 2008).

In short, we have that the Λ CDM model is called hierarchical because structures grow by successive fusion of dark matter halos, which are followed by their baryonic content. When the cold dark matter is decoupled from the primordial plasma, it becomes insensitive to the interactions that bind the other components of that primordial plasma. Hence, it begins to condense, by the action of gravity, to form the dark matter halos. Later, as baryons become free, they are gravitationally caught by these halos, which make the growth of baryonic over-densities easier. At the moment these over-densities exceed the Jeans' mass, their gravitational and kinetic energies can then compensate each other, reaching the equilibrium and fixing their macroscopic properties (e.g., size, temperature), to finally condense by different cooling processes (Miralda-Escudé, 2003). The first baryonic structures to be formed like this have then a typical size of the present globular clusters (10^5 - $10^6 M_\odot$) (Abel *et al.*, 2002; Bromm & Larson, 2004). Inside these halos will form the first stars, which are metal-free and very massive ($> 100 M_\odot$), at redshift 20-30. These are named population III stars, and will live for a very short time, exploding in extremely energetic supernovae which may destroy the halos and, at the same time, disperse their metals throughout the universe. The next star generations (populations I and II) are thus metal rich, less massive and have a longer life. Their supernovae being less strong do not destroy the dark matter halos, making the formation of larger gravitational structures possible (galaxies and clusters, for example; see figure A.11).

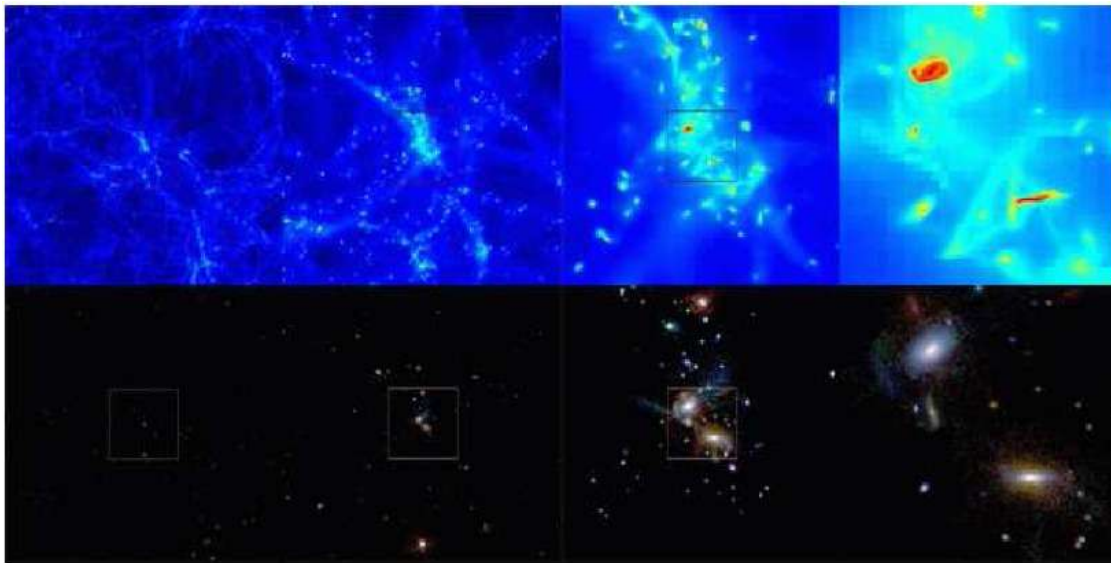


Figure A.11: Simulated galaxies in the Λ CDM model (Rasera & Teyssier, 2006).

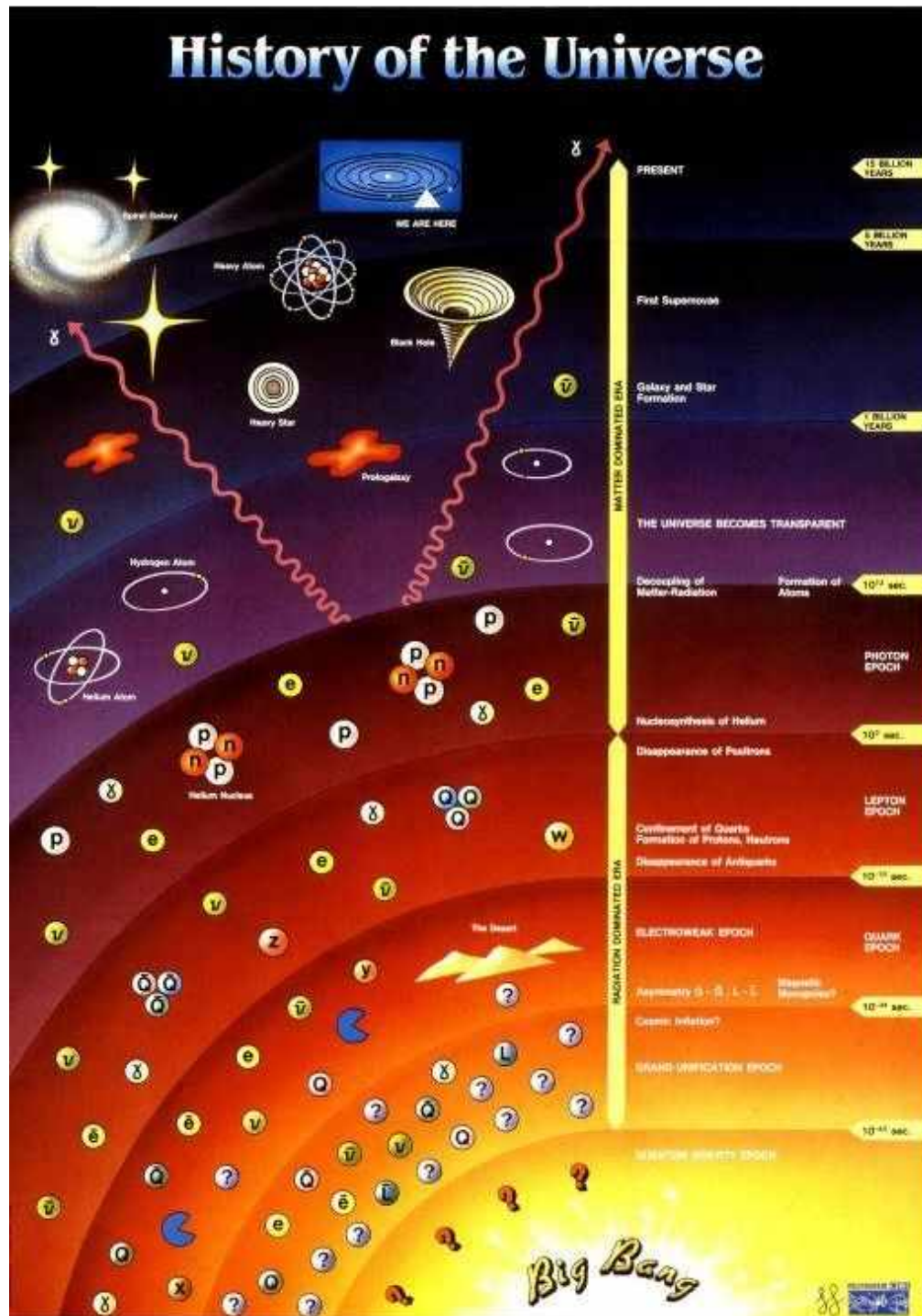


Figure A.12: Artistic view of the Universe history (Credit: Microscop-CERN).

Basic and short introduction to modern imagery and photometry

Contents

C.1	Toward a kinematic classification of distant galaxies . . .	137
C.2	The kinematic analysis using GIRAFFE	138
C.3	Some preliminary results	141

¹In the present, the photometry and the imagery are made thanks to the CCD (Charge Coupled Device). The CCD is composed of a photosensitive cells matrix (see figure B.1). Each time a photon hit one of this cells, it produces electrons that are counted later. These cells are called pixels, and they are the basic elements of a digital image. Like this, when the exposition time finishes, the system begins the signal reading by transferring the electric charges collected in each pixel to an electronic circuit where they are counted. The whole reading proceeding can be summarize by two step:

- 1.) The lecture begins by the bottom line, transferring at each time the electric charges from left to right,
- 2.) the charges in each line are transferred downwards to the next line, and the cycle return to step 1 (until there is no more line to read).

It is noted that the reading time can represent a substantial constraint for the observers, and may be greater than the exposure time. In any case, some corrections must be applied to the CCD images before use them, in order to rectify some instrument imperfections. The most important are described below:

The bias: this is the residual background noise, which is a constant noise received by the instrument. An image of the bias can be obtained making an instantaneous exposure with the shutter closed (i.e., in the dark).

The dark: this corresponds to the bias plus an intrinsic thermal background noise produced by the instrument. It is proportional to the exposure time, and can also be imaged with the shutter closed.

¹This appendix B has been written thanks to the more detailed description presented in Lamareille (2006).

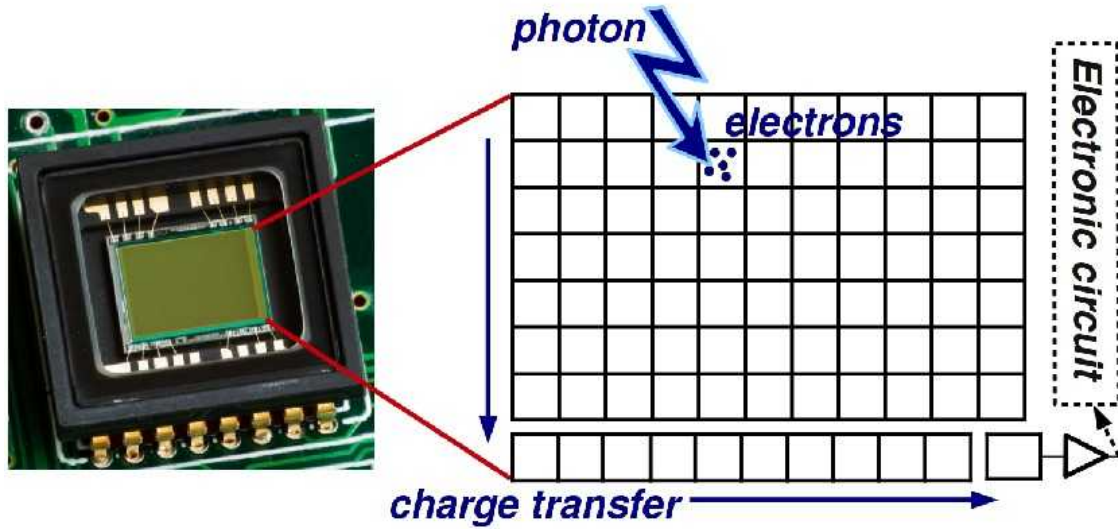


Figure B.1: CCD diagram to illustrate how it works.

The flatfield: it allows to normalize the different responses that could have the matrix from one pixel to the other, taking into account that each pixel could react differently compared to the others to a photon arrival, as well as some of them could be dead (with no response at all). The flatfield image can be obtained making an exposure of a diffuse light source, which is considered to be perfectly uniform.

Then, if, for a pixel i , the bias is noted B_i , the thermal background noise T_i within an exposure time t_T , the dark D_i is defined as,

$$D = \frac{B_i + T_i}{t_T} \quad (\text{B.1})$$

Finally, noting I_0 the original image taken by the CCD sensor with an exposure time t_o , F the flatfield image taken with an exposure time t_F , and m_F the mean value of the $(F - D \times t_F)$ image, the final corrected image (I) for each pixel i would be:

$$I_i = \frac{(I_{0i} - D_i \times t_o) \cdot m_F}{F_i - D_i \times t_F} \quad (\text{B.2})$$

B.1 Filters and photometric calibration

The principal role of a filter is to allow a precise vision of the observed object in a specific wavelength. Then, by combining the images obtained using different (wavelength) filters, we could have a better understanding of the object. However,

all the filters do not have the same response, and this must be taken into account when comparing different observations. Fortunately, each filter is carefully studied, and finally characterized by a response curve (see figure B.2) with a bandwidth $\Delta\lambda$ and a central waveleght λ_0 .

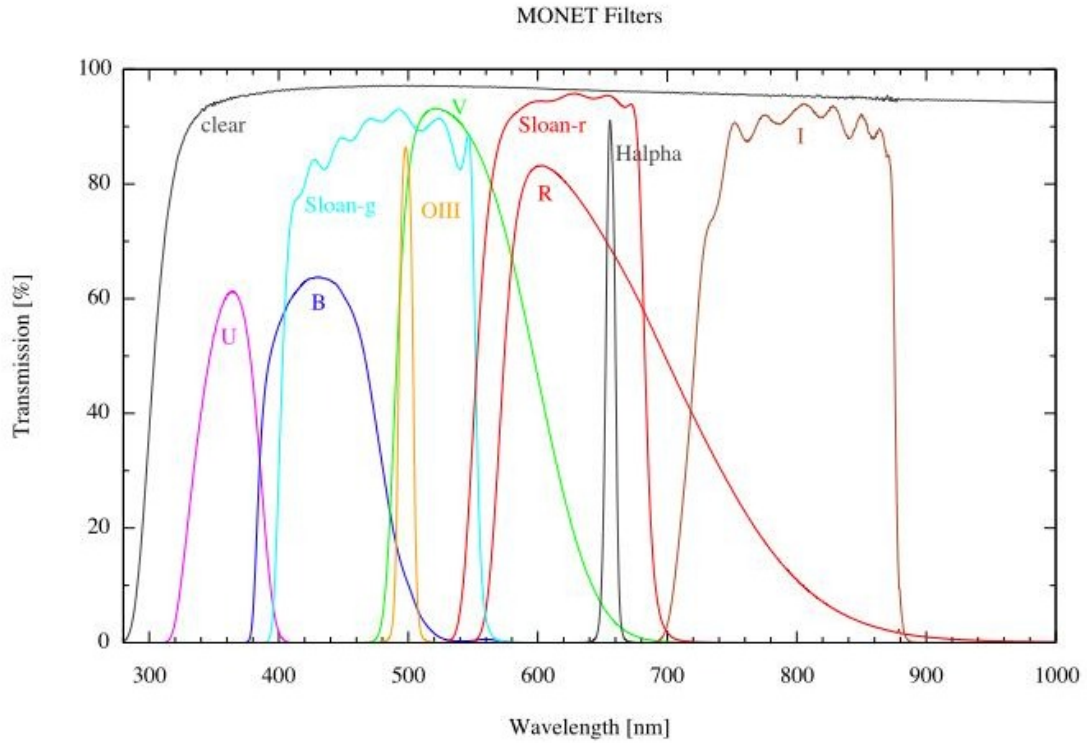


Figure B.2: Example of response curves. These correspond to the available filters for the Monet telescope at McDonald Observatory (Credit: Monet telescope webpage).

The photometric calibration lies in finding the relationship between the number of electrons detected at each sensor cell, and the luminosity corresponding to each pixel of the image. In astrophysics, it is common to express the luminosity of an object in magnitude, which is a logarithmic unit that allows to work with a wide range of scales. Moreover, the total luminosity of an astrophysical object can be calculated only if one knows its distance², which poses some observational problems. Thus, the magnitudes are not calculated from the luminosity, but from the observed flux, which corresponds to the luminosity received per unit area of the detector.

²Luminosity refers to the amount of electromagnetic energy a body radiates per unit of time, and can be calculated as $L = 4\pi r^2 F$. Where, r is the object distant and F the flux measured at the distant r .

Being ADU (Analog-to-Digital Unit) the number of electrons detected per pixel for a given object, and t_e the used exposure time, the observed magnitude or "apparent magnitude" m of such object is calculated as follow:

$$m = -2,5 \cdot \log\left(\frac{ADU}{t_e}\right) + ZP \quad (\text{B.3})$$

The constant ZP is called the image "zero-point". It contains various information including the area of each pixel, the atmospheric absorption, the physical units used to represent the observed fluxes, or even the normalization constant of the magnitude system (see below). Rather than calculating theoretically the zero point value, it is more reasonable to take images of reference stars which one already knows the apparent magnitude. It must be stressed that the image of the reference star must be achieved through the same filter as the image we want to calibrate. In addition, we must take into account the atmospheric absorption difference between the image to be calibrated and the reference image. Indeed, the atmospheric absorption is directly proportional to the height (called "airmass") of the observed objects, so to the length of atmosphere that has been crossed (by projection, it is smaller at the zenith than at the horizon). It is unusual that the image to be calibrated and the reference image are taken at the same height.

Then, let ADU_\star be the number of electrons detected per pixel for the reference star, m_\star its apparent magnitude, t_\star the exposure time of the reference image (in the same unit as t_e), a the airmass of the image to be calibrated, a_\star the airmass of the reference image, and c_a the coefficient of atmospheric absorption which depends on the telescope and the instruments used for the observation. Like this, the zero-point can be calculated by

$$ZP = m_\star + 2,5 \cdot \log\left(\frac{ADU_\star}{t_\star}\right) + c_a \times (a_\star - a) \quad (\text{B.4})$$

B.2 The magnitude systems

Now, as mentioned before, it is important to ensure that all magnitudes across the different filters are expressed in the same system. There are several systems of magnitude, each one characterized by a different normalization method. The magnitudes normalization, which is nothing more than the division of the observed flux by a reference flux, is performed for two main reasons: to overcome the physical units used to express the observed flux, and to overcome the response curve of the used filter (see above). This last point is absolutely necessary if one wants to really compare the luminous properties of the object in different range of

wavelengths, rather than comparing the response curves of the filters.

As a result, an object magnitude through a given filter is defined as

$$m = -2,5 \cdot \log\left(\frac{\int_0^\infty T(\lambda) \cdot f_\lambda(\lambda) d\lambda}{\int_0^\infty T(\lambda) \cdot f_\lambda^n d\lambda}\right) = -2,5 \cdot \log\left(\frac{\int_0^\infty T(\nu) \cdot f_\nu(\nu) d\nu}{\int_0^\infty T(\nu) \cdot f_\nu^n d\nu}\right) \quad (\text{B.5})$$

where λ is the wavelength of the received light, ν its frequency, $f_\lambda(\lambda)$ or $f_\nu(\nu)$ the monochromatic flux³, $T(\lambda)$ or $T(\nu)$ the response curve of the used filter, and f_λ^n or f_ν^n the monochromatic flux of reference.

In here, the observed monochromatic flux must be expressed in the same units than the reference one, and it is this last which defines the magnitude system. Even if equation B.5 comes from a different technique (i.e., the spectroscopy) to measure the monochromatic flux, rather than the photometry, in both cases there are two different systems to express the magnitude of an object. These are the Vega system and the AB system.

The Vega system is the more ancient, and it is based on the measure of the magnitude of the star Vega (α Lyrae)⁴ which is consider as equal to 0. The Vega system thus uses this definition for any employed filter, taking the respective Vega star magnitude (or the monochromatic flux in equation B.5) as the reference.

Differently to the Vega system, the AB system (Oke, 1974) does not depend on the observation of a particular object. The AB system is defined by having a constant monochromatic flux as reference expressed per frequency unit as follow⁵:

$$f_\nu(AB)(\nu) = 3631 \text{ Jy} \quad (\text{B.6})$$

It is the most popular system nowadays. Then, equation B.5 becomes

$$m_{AB} = -2,5 \cdot \log\left(\frac{\int_0^\infty T(\nu) \cdot f_\nu(\nu) d\nu}{\int_0^\infty T(\nu) d\nu}\right) - 48,6 \quad (\text{B.7})$$

with $f_\nu(\nu)$ in $\text{erg} \cdot \text{s}^{-1} \cdot \text{cm}^{-2} \cdot \text{Hz}^{-1}$. Curiously, the value of the monochromatic flux has been chosen in order to have a zero magnitude value for the star Vega through the V filter.

Finally, we can hence go from one system to the other by

$$m_{AB} = m_{Vega} + m_{AB}(Vega) \quad (\text{B.8})$$

for which the values of $m_{AB}(Vega)$ for different filters are shown in table B.1.

³this is the flux in a precise wavelength or frequency, per wavelength or frequency unit respectively.

⁴It is one of the brightest stars in the sky, situated in the Lyra constellation.

⁵1 jansky (Jy) = $10^{-23} \text{ erg} \cdot \text{s}^{-1} \cdot \text{cm}^{-2} \cdot \text{Hz}^{-1} = 10^{-28} \text{ J} \cdot \text{m}^{-2}$

Filter	U	B	V	R	I	J	H	K
$m_{AB}(Vega)$	1,0	-0,09	0,0	0,18	0,46	0,9	1,37	1,88
Filter	u	g	r	i	z			
$m_{AB}(Vega)$	0,96	-0,09	0,16	0,39	0,54			

Table B.1: Magnitude AB of the star Vega through different common filters from [Lamareille \(2006\)](#).

Kinematic studies of distant galaxies using integral field spectroscopy

Contents

D.1	A very short history	149
D.2	Location	150
D.3	General description	150
D.4	The Instruments	151
D.5	The Projects	151

The first 3D kinematic studies of a representative sample of intermediate redshift galaxies, using FLAMES/GIRAFFE (see figure 5.6 and section 5.1), were carried out by Flores *et al.* (2006) and Yang *et al.* (2008). Here I present a short description of the kinematic analysis, as well as some preliminary results of a small sample I studied during my PhD.

C.1 Toward a kinematic classification of distant galaxies

Flores *et al.* (2006) developed a simple kinematic classification scheme for distant galaxies based on their 3D kinematics and their HST optical images. It relies on the fact that at low spatial resolution, a rotating disk should show a well defined peak in the center of the σ -map, which corresponds to the convolution of the large scale motion (i.e., the rotation) with the (relatively small) dispersion of the gas in the disk or in the bulge. Indeed, the central parts of the galaxy, where the rotation curve rises most quickly, are not spatially resolved with ground-based optical spectroscopy and our classification fully accounts for its convolution with the actual PSF (point spread function). To summarize, we distinguish between the following classes:

- Rotating disks (RD): the VF shows an ordered gradient, and the dynamical major axis is aligned with the morphological major axis. The σ -map indicates a single peak close to the dynamical center;

- Perturbed rotations (PR): the kinematics shows all the features of a rotating disk (see above), but the peak in the σ -map is either absent or clearly shifted away from the dynamical center;
- Complex kinematics (CK): neither the VF nor the σ -map are compatible with regular disk rotation, including VFs that are misaligned with the morphological major axis.

Examples of each class are shown in figure C.1. Interestingly, Flores *et al.* (2006) find that the large scatter of distant TFR shown in previous studies is due to non-relaxed systems while the pure rotational disks exhibit a TFR that is similarly tight as that of local spirals.

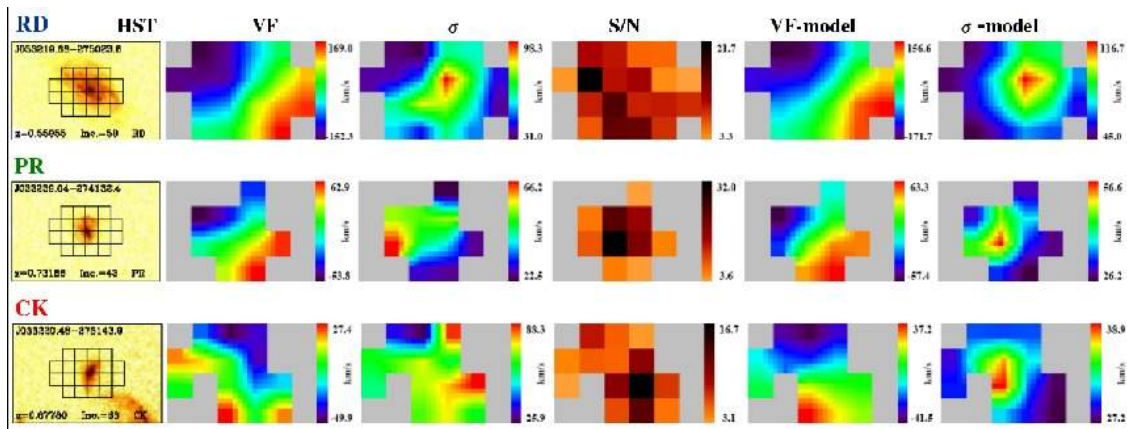


Figure C.1: From *top* to *bottom*: Rotating disk, perturbed rotation, and complex kinematics. From *left* to *right*: HST/ACS image, measured velocity field, measured FWHM map, S/N map, simulated velocity field, simulated FWHM map.

C.2 The kinematic analysis using GIRAFFE

This is a topic well developed by Puech (2006), and Neichel (2008). However, during my thesis I also had the opportunity to make the kinematic analysis of 15 galaxies using all the observed lines in each galaxy spectrum, and not just the O[II] λ 3727 line. The procedure is the following.

First, we must accentuate that the special size of the pixel in the GIRAFFE IFU makes the width of the detected lines to be the result not only of the random movements of gas particles, but the product of the convolution between them and the tidy movements at larger scales (for example, the rotation in the case of spiral galaxies; Puech *et al.*, 2008). Thanks to the resolution of FLAME/GIRAFFE ($R \sim 9\,000$), we can deblend the O[II] doublet (see figure 5.5) for galaxies having

a uniform movement (RD; see Puech *et al.*, 2008; Yang *et al.*, 2008; Flores *et al.*, 2006). If the convolution of large and small scale motions become more important, even with the high resolution of FLAMES/GIRAFFE, the lines are blended. Such cases are related to the signature of perturbed movements inside the galaxy (Puech, 2006), and makes impossible to calculate a barycenter for each line of the doublet. In kinematic studies of local galaxies, only those spatial pixels with S/N (signal to noise ratio) > 3.0 are taken into account (Flores *et al.*, 2006). In those studies the S/N is defined as the ratio between the barycenter flux and the pseudo-continuum noise. As a result of the facts cited in the above phrases of this paragraph, a such S/N definition would severely under-estimate the signal to noise ratio in our case because of the trough separating the two lines of the [OII] doublet. We have hence chosen to define the signal to noise ratio as the total flux in the doublet normalized by the root mean square deviation of the pseudo-continuum (noise) surrounding the doublet. We then normalized again this S/N by the number of spectral resolution elements (N), over which the doublet [OII] emission line is spread, to obtain the mean S/N ratio: $\langle S/N \rangle = \frac{\sum_i^N S_i}{\sqrt{N} \times \sigma}$, where S_i is the signal in the pixel i and σ is the dispersion of the noise in the continuum of the spectra. For simplicity, we call this " $\langle S/N \rangle$ " simply "spectral S/N" or even "S/N".

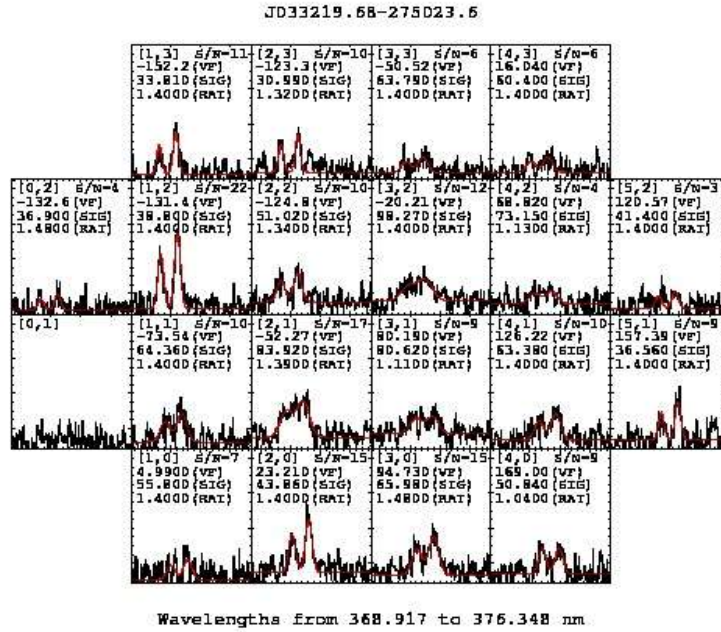


Figure C.2: [OII] GIRAFFE data-cube detections.

We fit the O[II] doublet with a double Gaussian function satisfying the following constraints: distance between the lines = 2.783 ($\lambda_1 - \lambda_2 = 2.783$ at rest), same FWHM for both lines ($\sigma_1 = \sigma_2$), and ratio between the two lines of the

doublet free (see figures 5.5 and C.2). Therefore, the result from the fitting gives us the doublet position, the common FWHM, and the line ratio. In the case the fitting fails, we set the line ratio equal to 1.4, which is the median value observed in the integrated spectra (Puech *et al.*, 2006b; Weiner *et al.*, 2006) ($R(3729/3727) = 1.4$ is also a good approximation for the maximum line ratio in gas regions, as estimated from Osterbrock & Ferland (2006); see more details in Puech *et al.* (2006a) and references therein)¹. This fitting failure is caused either by the low S/N, or by the difficulty to de-blend the [OII] doublet in some complex systems. It affects only ~ 10 -15% of the measured pixels and thus cannot significantly alter our conclusions (Flores *et al.*, 2006; Yang *et al.*, 2008). In each case, we have checked by eye if the derived fit was acceptable. In some cases, we found blended [OII] spectra, in spite of the relatively high spectral resolution ($R \sim 10\,000$). This effect is independant of the S/N and is thus not an instrumental/observational artefact (Puech, 2006). This could be due to high local velocity gradients, multiple structures in the velocity field and/or high local extinction. Blended doublets are present in most of the complex kinematic systems, rather than in the more regular ones (rotating disks and perturbed rotation) (Flores *et al.*, 2006; Yang *et al.*, 2008). Then, after interactively fitting the spectrum coming from each IFU pixel (see figure 5.5), we get a 3 dimension data-cube as shown in figure C.3 (I show here an example of low redshift galaxy, using the $O[III]\lambda 5007$ emission line). Finally, we can thus construct the respective velocity field (see figure C.4), and, in the same way, the FWHM map and the S/N map. A 5x5 linear interpolation is also applied to the velocity field and the FWHM map. However, this linear interpolation only has a visual impact, as its only utilization is limited to the visual interpretation of the internal kinematics of the galaxy. (Puech *et al.*, 2008) shows that the rotation velocities retrieved through the IFU pixels of GIRAFFE have a systematic uncertainty within ~ 0.02 dex (see also the independet study of Epinat *et al.*, 2010).

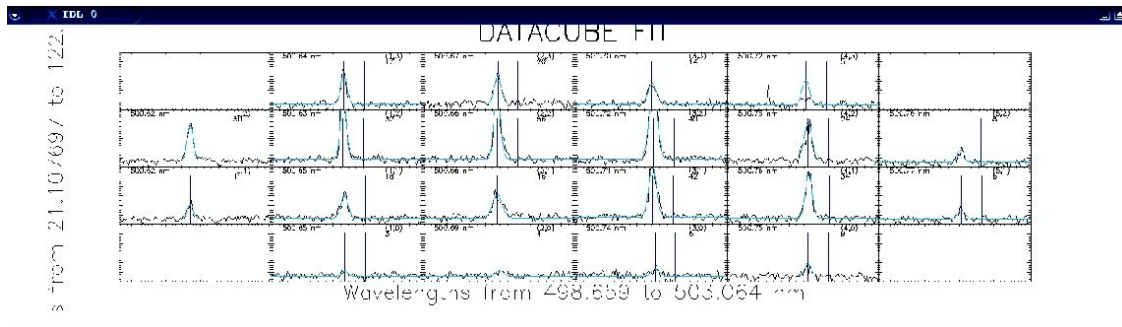


Figure C.3: Spatial data-cube for a low redshift galaxy ($z=0.14$).

¹Other works concerning the [OII] line ratio are presented by Kingsburgh & Barlow (1992) and Barlow (1987).

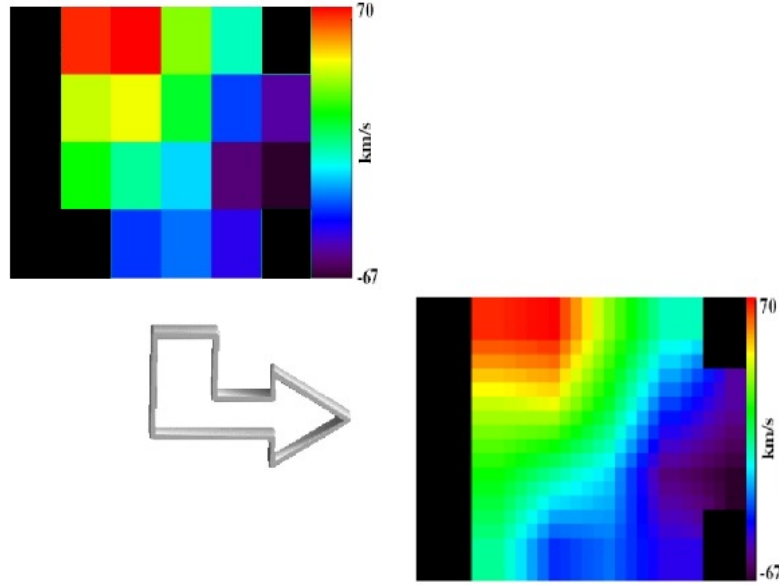


Figure C.4: *Left*: Example of a velocity field we can get with FLAMES/GIRAFFE. *Right*: Linear interpolation, for a better view of the velocity field. In the same way, we can also get the FWHM map (sigma map) and S/N map.

Concerning other emission lines (e.g., $H\gamma$, $H\beta$, $[\text{OIII}]\lambda 4959$, $[\text{OIII}]\lambda 5007$), the fitting is done by a simple Gaussian function. In this case, we keep the same S/N definition because it allows us to better exploit the detection of emission lines in the distant galaxies. For each line presents in each galaxy we keep only those IFU pixels with $\langle S/N \rangle \geq 3$ during the confection of different maps (velocity field, sigma-map, S/N map, see figure C.5). Nevertheless, for a map to be considered as significantly representative of the internal kinematic of a given galaxy, it must contain at least four GIRAFFE spatial pixels with $S/N \geq 4$.

In short, following the above procedure, I constructed 3 dimension data-cubes (see figure C.3) using all the observed emission lines in each galaxy spectrum with and without background subtraction. For this, an IDL procedure has been implemented. Subsequently, from these data-cubes, the *velocity fields*, *sigma-maps* and *S/N maps* have been build also using IDL procedures that follow the definitions and explanations detailed before.

C.3 Some preliminary results

From the sample of 15 galaxies, 12 of them are kinematically exploitable. They are in the redshift bin $0.11 < z < 0.40$, and they have absolute B magnitude between $-19.65 < M_{B_{Vegamagnitude}} < -16.40$. Their velocity fields, sigma maps, and S/N maps are shown in figure C.7 at the end of this appendix. These

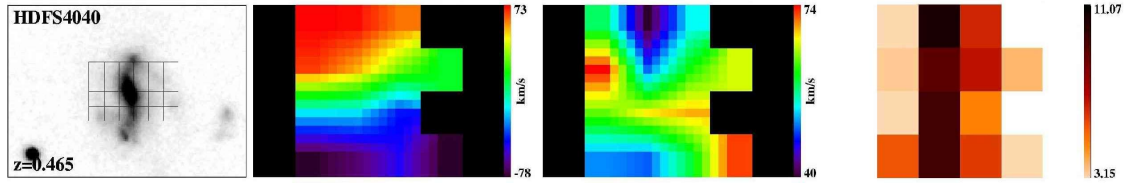


Figure C.5: From *left to right*: HST/ACS image of the galaxy, velocity field, FWHM map (sigma-map), and S/N map.

results interestingly show that galaxies with complex kinematics (called DC in the figure) present the same complex signature through the same ionised emission lines (e.g., [OIII] λ 4959 and [OIII] λ 5007), while different emission lines (e.g., H β and [OIII]) show different complex kinematics. In contrast, rotating disks (called DR in the figure) have the same kinematic signature using any emission line.

Another preliminary result is shown in figure C.6. Similar to precedent results these plots show that all the scatter of the TF relation is caused by interloper galaxies with kinematics classified as complex. Considering only rotating disks, the TF relationship at $0.11 < z < 0.40$ is similar to that in the local universe.

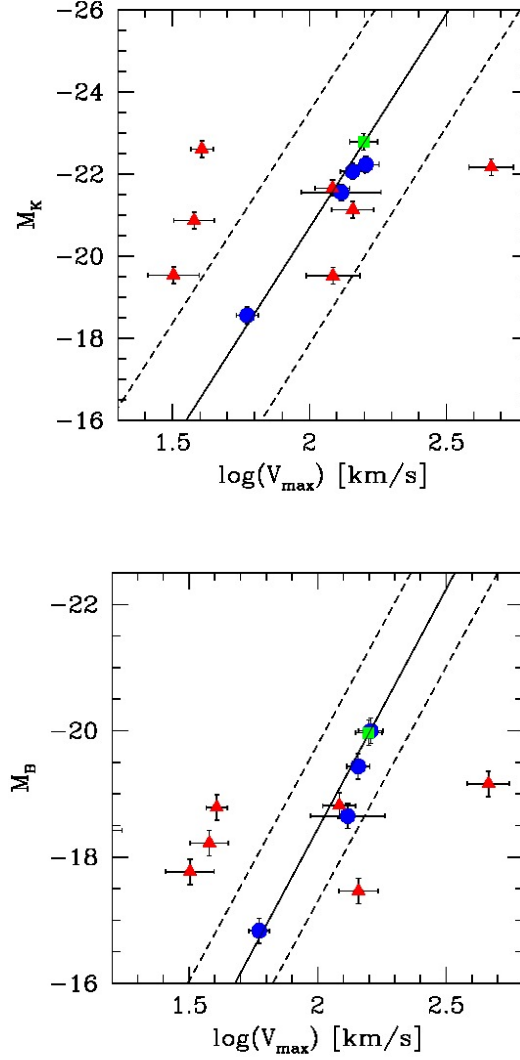
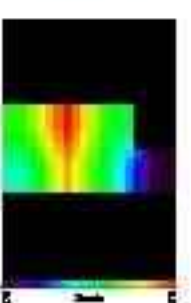
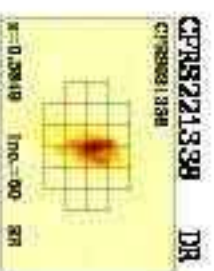
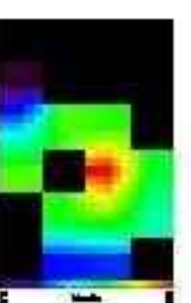
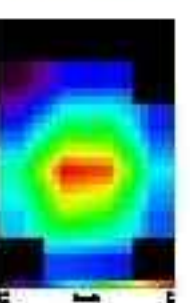
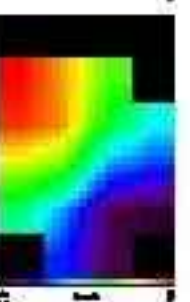
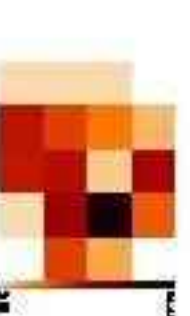
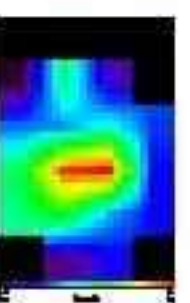
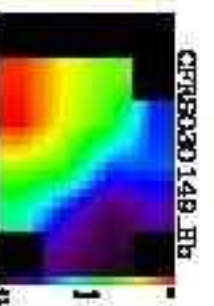
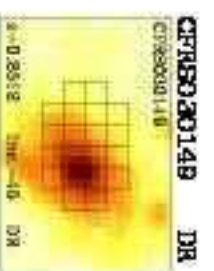
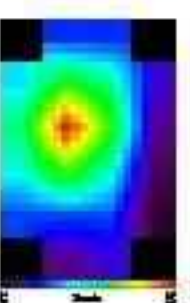
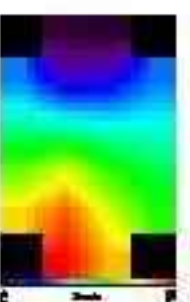
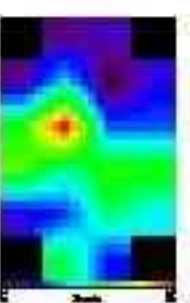
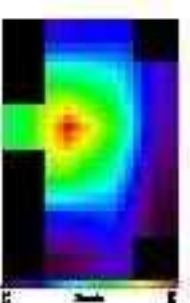
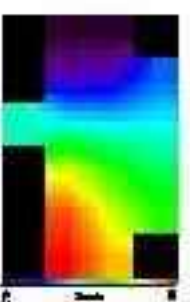
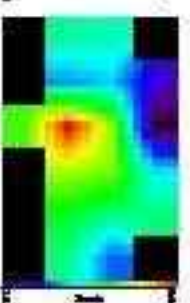
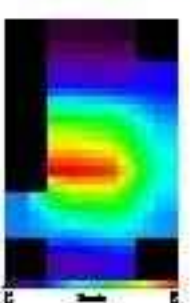
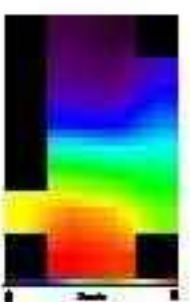
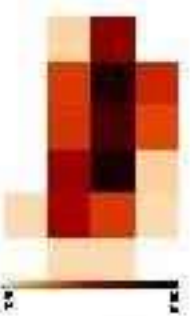
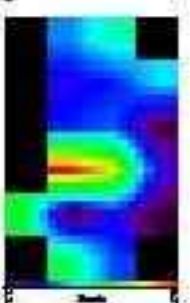
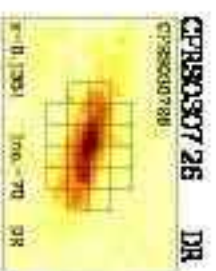
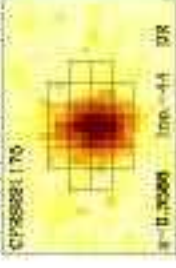


Figure C.6: Tully-Fisher relation, for the sample of 12 galaxies, in K band (Vega magnitudes) and in B band (Vega magnitude, corrected for extinction), as in Flores *et al.* (2006). Red triangles, green squares and blue dots represent complex kinematics, perturbed rotations and rotating disks, respectively. Full and dotted lines represent the local TF and its 3 sigma scatter amplitude (following Conselice *et al.*, 2005b)(see also Verheijen, 2001).

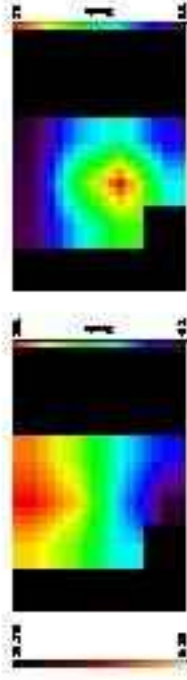
Figure C.7: For each galaxy in the sample I present here their HST/ACS image, measured velocity field, measured FWHM map, S/N map, simulated velocity field, simulated FWHM map (in that order), corresponding to each emission line that could be analyze.



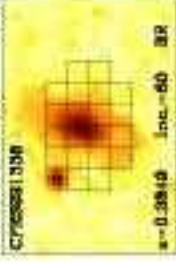
CFRS221176 DR



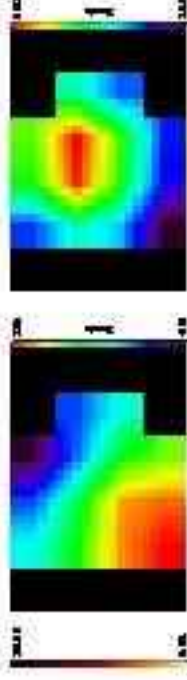
CFRS221176.D11



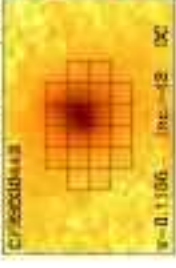
CFRS031338 RP



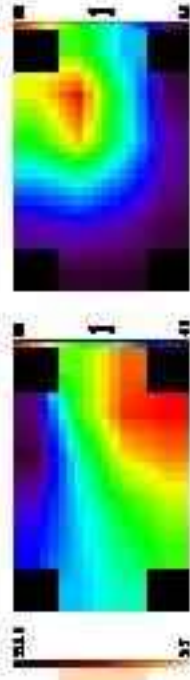
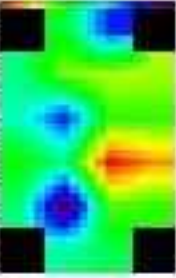
CFRS031338.D11



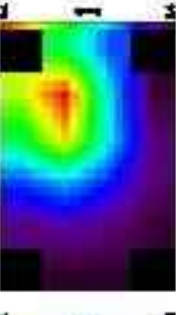
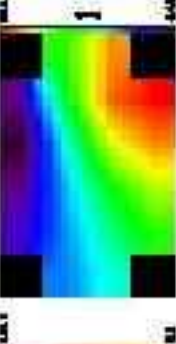
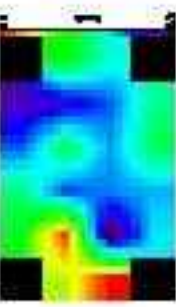
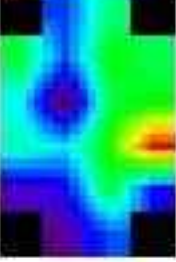
CFRS030443 DC



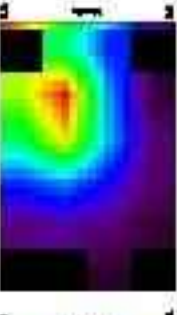
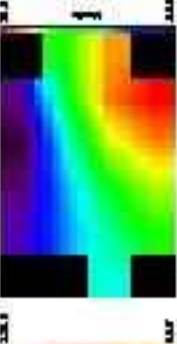
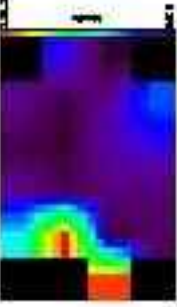
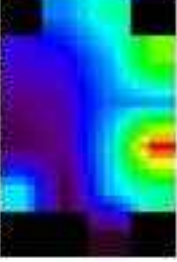
CFRS030443.Hb



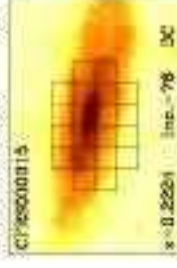
CFRS030443.D111



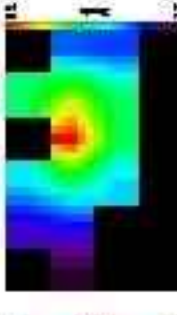
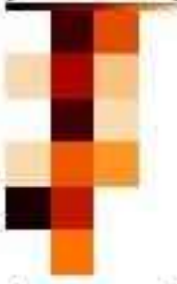
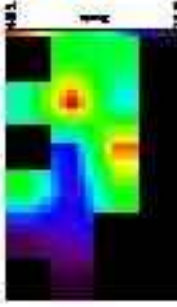
CFRS030443.D111

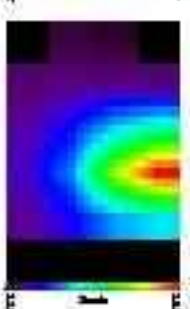
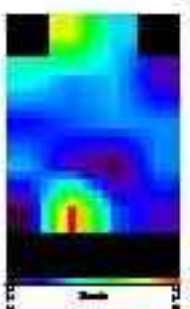
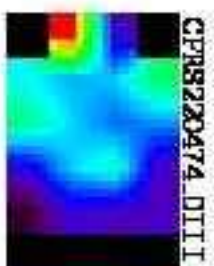
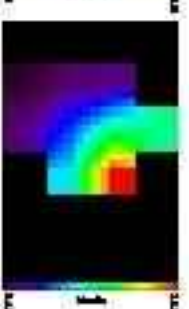
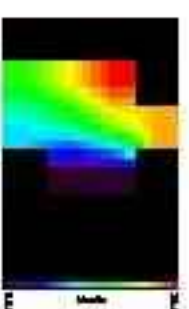
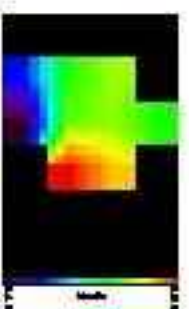
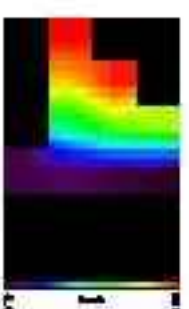
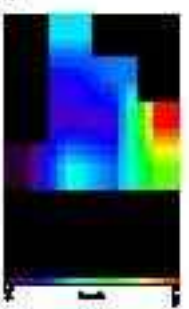
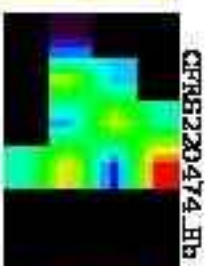
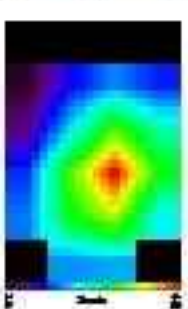
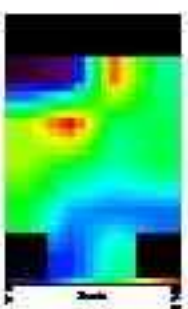
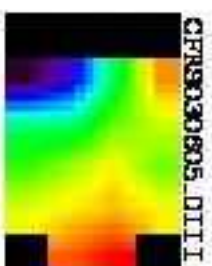
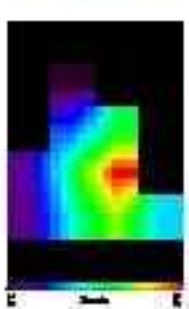
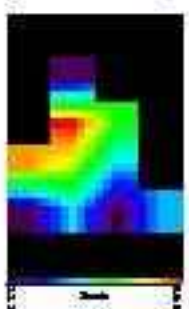
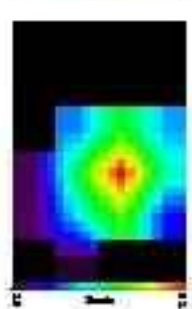
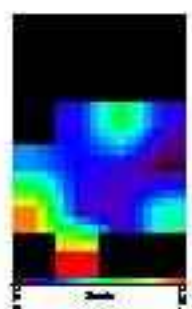
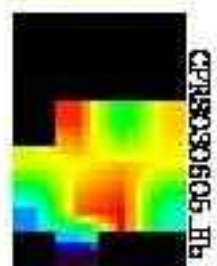
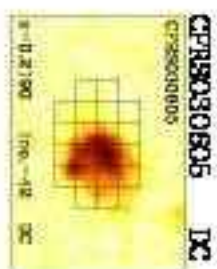


CFRS030315 DC

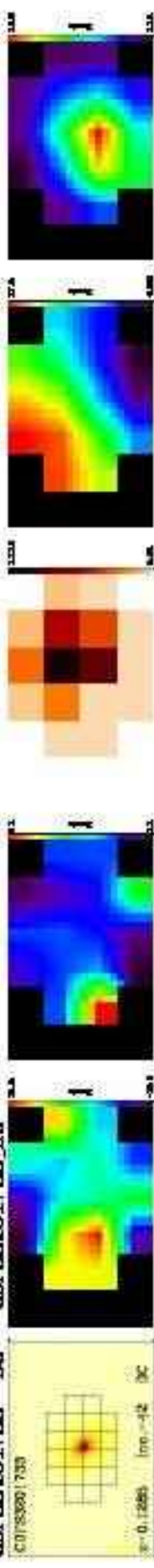


CFRS030315.Hg





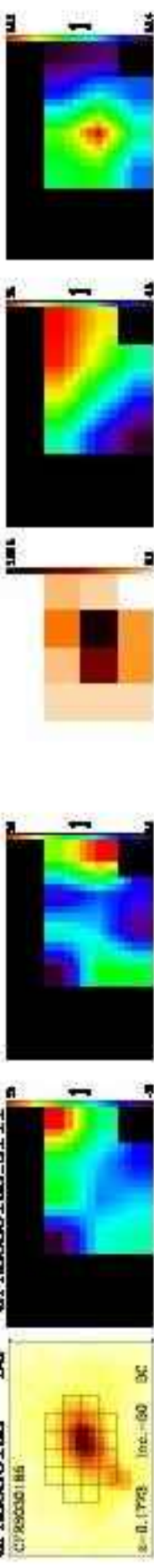
CFRS0301733 DC CFRS0301733_Hb



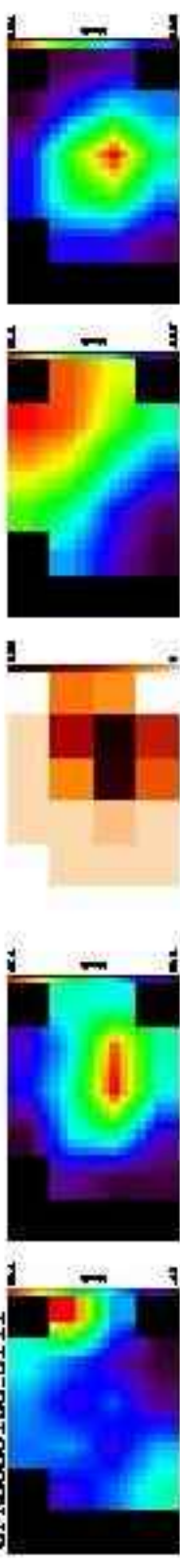
CFRS0301733_DIII



CFRS030165 DC CFRS030165_DIII



CFRS030165_DIII



CFRS030786 DC CFRS030786_DII



Building an Observatory in Panama

D.1 A very short history

If I must give a starting date of the project, I would say "solar eclipse of February 1998". Thanks to the opportunity we were going to have in Panama to observe such total solar eclipse, a delegation of the "Uranoscope de France" traveled to Panama. Once they were in place, and after having a nice time watching the eclipse, they made contact with some government authorities and with the APAA ("Asociación Panameña de Aficionados a la Astronomía"¹). The Uranoscope then let them know about the Uranoscope idea to help the interested people in Panama to construct an astronomical observatory there. With this in mind, the Uranoscope proposed to offer a telescope to Panama. However, Panama should take the responsibility to build the appropriate structure.

It was until 2000 when I arrived at the School of Physics at the University of Panama. Since then I was interested in studying Astrophysics, and with other classmates I formed a group with the aim of organizing talks and other activities. At the end of that year, professor Bernardo Fernandez told me about the possibility to make an agreement of mutual collaboration between the University of Panama and the Uranoscope de France. Immediately, professor Fernandez and I began to work on that, and the following year (2001), it was done and signed.

Between 2001 and 2005, a lot of activities were developed. Amongst them, the biggest one took place once a year, and was called "The French scientific fortnight in Panama". In its organization participated the "Alliance Francaise au Panama", the French Embassy, the University of Panama, and the Technological University of Panama.

Finally, on April 2005 a hybrid solar eclipse was visible in Panama². The Uranoscope visited again Panama, and made, through the French Embassy, the official donation of a telescope to the Technological University of Panama. It was now our turn to continue with the project. As a result, since then, we have been

¹Panamanian Association of Amateur Astronomy.

²Yes, another one, so I have seen 3 solar eclipses in my life without the need to leave my country (11 July 1991, 26 February 1998, and 08 April 2005).

working on it, and the observatory is almost finished (see figures D.4 and D.5). Moreover, a new agreement of mutual collaboration between the Technological University of Panama and the Uranoscope de France was signed in 2008.

D.2 Location

The new astronomical observatory of Panama has been built inside a regional center of the Technological University of Panama, located at Llano Marín at ~ 5 km from Penonome city (latitude: $08^{\circ}30'00''\text{N}$, longitude: $80^{\circ}19'48''\text{W}$; see figure D.1).

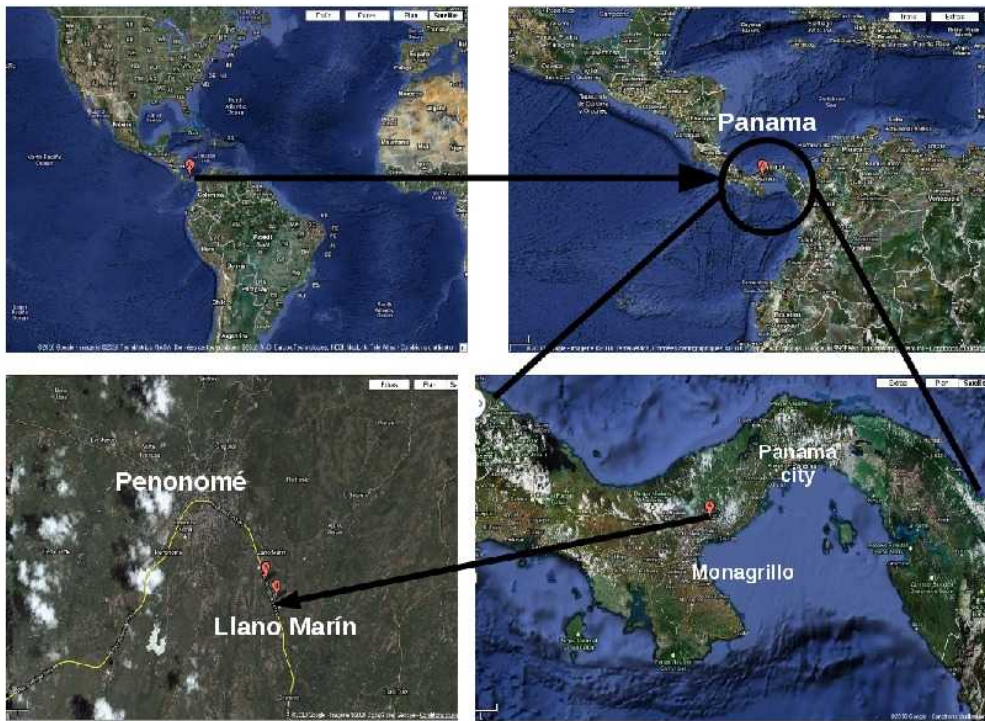


Figure D.1: How to arrive to the Panama observatory.

D.3 General description

The building has three floors including the dome, and measures 5.52 m from the ground to the base of the dome (see figure D.2). The dome dimensions are the following: 3.69 m high, and a diameter of 4.57 m at the base.

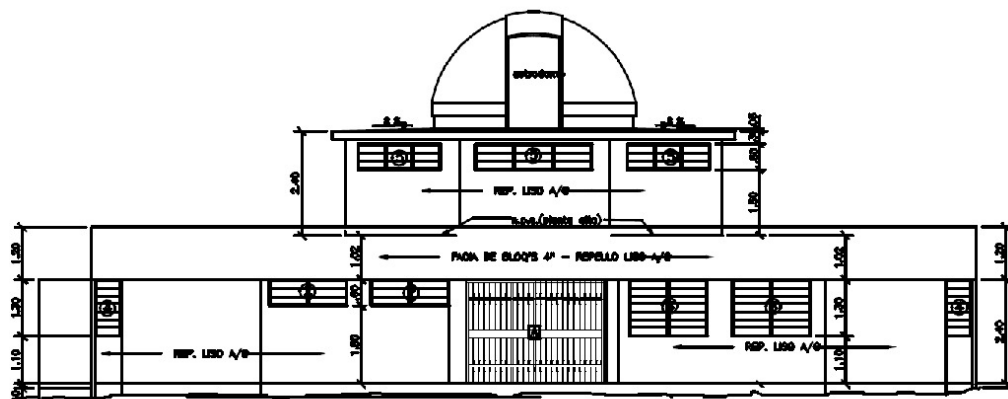


Figure D.2: Architectural scheme of the Panama observatory building.

D.4 The Instruments

Nowadays, the observatory owns a Meade LX200GPS telescope. It has an aperture diameter of 35.56 cm. The telescope will be mounted on a Astro-Physics 1200 mount, which is already in Panama.

The rest of the instruments are still being purchased. Indeed, we plan to have them in Panama before the end of the year. Amongst such instruments we have a CCD SXVF-H16 Starlight Xpress, a LHIRES III spectrograph with three gratin modules (1200, 600, and 500 line/mm), a Lodestar Stand-Alone autoguider, and an active optics system. We will also have other essential accessories as a set of Sloan photometric filters, field corrector, focal reducer, polarizing filters, bandpass CCD imaging filters, light pollution suppression filters, barlows, a last generation eyepiece set, as well as a Zenithstar APO telescope for a better follow-up control, and a Coronado telescope. A series of other amateur telescope are also included to be used in educational activities.

D.5 The Projects

The first projects to be developed with our first generation of instruments are the following:

- 1. Imagery and photometry of tidal stream in nearby galaxies (see prospective 2 in chapter 7).
- 2. Follow-up of lunar events: to the hunt of lunar flashes. It is an inter-

national project integrated by different observatories (see figure D.3) to track meteoroid impacts on the moon. Its principal scientific issues are, for example, to derive the amount of kinetic energy being radiated and the fraction being transmitted through seismic energy at each impact, as well as measuring the crater dimensions in function of the produced flash. This data will be very important in order to be compared with the information that has been and will be obtained by different missions on the moon (measurements "in situ" with spectrometers, magnetometers, seismic detectors, gravimeters, etc.).

- 3. NEOs (Near-Earth Objects) detection and tracking (in collaboration with the IMCCE of Paris Observatory).



Figure D.3: Observatories international network to study the lunar flash.

Other projects will be focused on the education (in collaboration with Paris Observatory, Planète Science Institute, Uranoscope de France, and with the Palais de la Decouverte-Minister de la Culture de France).

Another idea is also to test automatisation systems, such as Tarot (Télescope à Action Rapide pour les Objets Transitoires) system, and Hatnet, for example. Undoubtedly, any other project and/or collaboration is happily welcome.

A long (but not so long) term project is the installation of an observatory, hosting a bigger (at least 1 m diameter) telescope, at an altitude higher than 1300 m in Panama, and having an automatic control system.



Figure D.4: Images of the observatory during March 2010.



Figure D.5: Images of the observatory during July 2010.

Bibliography

- Abadi M. G., Navarro J. F., Steinmetz M. and Eke V. R. *Simulations of Galaxy Formation in a Λ Cold Dark Matter Universe. II. The Fine Structure of Simulated Galactic Disks*. ApJ, vol. 597, pages 21–34, November 2003. [32](#)
- Abel T., Bryan G. L. and Norman M. L. *The Formation of the First Star in the Universe*. Science, vol. 295, pages 93–98, January 2002. [128](#)
- Abraham R. G., Valdes F., Yee H. K. C. and van den Bergh S. *The morphologies of distant galaxies. 1: an automated classification system*. ApJ, vol. 432, pages 75–90, September 1994. [44](#), [79](#)
- Abraham R. G., Tanvir N. R., Santiago B. X., Ellis R. S., Glazebrook K. and van den Bergh S. *Galaxy morphology to $I=25$ mag in the Hubble Deep Field*. MNRAS, vol. 279, pages L47–L52, April 1996. [45](#)
- Abraham R. G., van den Bergh S., Glazebrook K., Ellis R. S., Santiago B. X., Surma P. and Griffiths R. E. *The Morphologies of Distant Galaxies. II. Classifications from the Hubble Space Telescope Medium Deep Survey*. ApJS, vol. 107, pages 1–+, November 1996. [44](#), [45](#), [46](#), [66](#), [79](#)
- Abraham R. G., Ellis R. S., Fabian A. C., Tanvir N. R. and Glazebrook K. *The star formation history of the Hubble sequence: spatially resolved colour distributions of intermediate-redshift galaxies in the Hubble Deep Field*. MNRAS, vol. 303, pages 641–658, March 1999. [50](#)
- Abraham R. G., van den Bergh S. and Nair P. *A New Approach to Galaxy Morphology. I. Analysis of the Sloan Digital Sky Survey Early Data Release*. ApJ, vol. 588, pages 218–229, May 2003. [45](#), [79](#)
- Acedo L. *A WDM model for the evolution of galactic halos*. JCAP, vol. 7, pages 37–+, July 2009. [119](#)
- Agertz O., Teyssier R. and Moore B. *Disc formation and the origin of clumpy galaxies at high redshift*. MNRAS, vol. 397, pages L64–L68, July 2009. [109](#)
- Albrecht A., Steinhardt P. J., Turner M. S. and Wilczek F. *Reheating an inflationary universe*. Physical Review Letters, vol. 48, pages 1437–1440, May 1982. [123](#)
- Alpher R. A., Bethe H. and Gamow G. *The Origin of Chemical Elements*. Phys. Rev., vol. 73, no. 7, pages 803–804, Apr 1948. [125](#)

- Amram P., Boulesteix J., Marcelin M., Balkowski C., Cayatte V. and Sullivan III W. T. *H α velocity fields and rotation curves of galaxies in clusters. III. Nine galaxies in DC 1842-63*. A&AS, vol. 113, pages 35–+, October 1995. [67](#)
- Andredakis Y. C. and Sanders R. H. *Exponential bulges in late-type spirals: an improved description of the light distribution*. MNRAS, vol. 267, pages 283–296, March 1994. [85](#)
- Athanassoula E., Lambert J. C. and Dehnen W. *Can bars be destroyed by a central mass concentration? - I. Simulations*. MNRAS, vol. 363, pages 496–508, October 2005. [31](#)
- Athanassoula E. *Morphology of bar orbits*. MNRAS, vol. 259, pages 328–344, November 1992. [94](#)
- Athanassoula E. *The existence and shapes of dust lanes in galactic bars*. MNRAS, vol. 259, pages 345–364, November 1992. [29](#), [94](#)
- Athanassoula E. *On the nature of bulges in general and of box/peanut bulges in particular: input from N-body simulations*. MNRAS, vol. 358, pages 1477–1488, April 2005. [29](#)
- Athanassoula E. *Topics on Bar and Bulge Formation and Evolution*. In J. G. Funes & E. M. Corsini, editeur, Astronomical Society of the Pacific Conference Series, volume 396 of *Astronomical Society of the Pacific Conference Series*, pages 333–+, October 2008. [31](#), [100](#)
- Barden M., Rix H.-W., Somerville R. S., Bell E. F., Häußler B., Peng C. Y., Borch A., Beckwith S. V. W., Caldwell J. A. R., Heymans C., Jahnke K., Jogee S., McIntosh D. H., Meisenheimer K., Sánchez S. F., Wisotzki L. and Wolf C. *GEMS: The Surface Brightness and Surface Mass Density Evolution of Disk Galaxies*. ApJ, vol. 635, pages 959–981, December 2005. [49](#)
- Barlow M. J. *The determination of the masses of Magellanic Cloud planetary nebulae using forbidden O II doublet ratio electron densities*. MNRAS, vol. 227, pages 161–183, July 1987. [140](#)
- Bell E. F. and de Jong R. S. *Stellar Mass-to-Light Ratios and the Tully-Fisher Relation*. ApJ, vol. 550, pages 212–229, March 2001. [67](#)
- Bell E. F., McIntosh D. H., Barden M., Wolf C., Caldwell J. A. R., Rix H.-W., Beckwith S. V. W., Borch A., Häußler B., Jahnke K., Jogee S., Meisenheimer K., Peng C., Sanchez S. F., Somerville R. S. and Wisotzki L. *GEMS Imaging of Red-Sequence Galaxies at $z \sim 0.7$: Dusty or Old?* ApJ, vol. 600, pages L11–L14, January 2004. [28](#), [29](#)

- Bell E. F., Wolf C., Meisenheimer K., Rix H.-W., Borch A., Dye S., Kleinheinrich M., Wisotzki L. and McIntosh D. H. *Nearly 5000 Distant Early-Type Galaxies in COMBO-17: A Red Sequence and Its Evolution since $z \sim 1$* . ApJ, vol. 608, pages 752–767, June 2004. [27](#), [28](#), [55](#), [97](#)
- Bell E. F., Papovich C., Wolf C., Le Floch E., Caldwell J. A. R., Barden M., Egami E., McIntosh D. H., Meisenheimer K., Pérez-González P. G., Rieke G. H., Rieke M. J., Rigby J. R. and Rix H.-W. *Toward an Understanding of the Rapid Decline of the Cosmic Star Formation Rate*. ApJ, vol. 625, pages 23–36, May 2005. [29](#), [58](#), [64](#)
- Bell E. F., Naab T., McIntosh D. H., Somerville R. S., Caldwell J. A. R., Barden M., Wolf C., Rix H.-W., Beckwith S. V., Borch A., Häussler B., Heymans C., Jahnke K., Jogee S., Koposov S., Meisenheimer K., Peng C. Y., Sanchez S. F. and Wisotzki L. *Dry Mergers in GEMS: The Dynamical Evolution of Massive Early-Type Galaxies*. ApJ, vol. 640, pages 241–251, March 2006. [108](#)
- Bell E. F., Phleps S., Somerville R. S., Wolf C., Borch A. and Meisenheimer K. *The Merger Rate of Massive Galaxies*. ApJ, vol. 652, pages 270–276, November 2006. [64](#)
- Bendinelli O. *Abel integral equation inversion and deconvolution by multi-Gaussian approximation*. ApJ, vol. 366, pages 599–604, January 1991. [47](#)
- Bennett C. L., Banday A. J., Gorski K. M., Hinshaw G., Jackson P., Keegstra P., Kogut A., Smoot G. F., Wilkinson D. T. and Wright E. L. *Four-Year COBE DMR Cosmic Microwave Background Observations: Maps and Basic Results*. ApJ, vol. 464, pages L1+, June 1996. [117](#)
- Berentzen I., Athanassoula E., Heller C. H. and Fricke K. J. *Numerical simulations of interacting gas-rich barred galaxies: vertical impact of small companions*. MNRAS, vol. 341, pages 343–360, May 2003. [32](#)
- Bernardi M., Nichol R. C., Sheth R. K., Miller C. J. and Brinkmann J. *Evolution and Environment of Early-Type Galaxies*. AJ, vol. 131, pages 1288–1317, March 2006. [66](#)
- Bertin E. and Arnouts S. *SExtractor: Software for source extraction*. A&AS, vol. 117, pages 393–404, June 1996. [86](#)
- Bertola F., Buson L. M. and Zeilinger W. W. *The external origin of the gas in S0 galaxies*. ApJ, vol. 401, pages L79–L81, December 1992. [32](#)
- Bertone G., Hooper D. and Silk J. *Particle dark matter: evidence, candidates and constraints*. Phys. Rep., vol. 405, pages 279–390, 2004. [120](#)

- Block D. L., Bournaud F., Combes F., Puerari I. and Buta R. *Gravitational torques in spiral galaxies: Gas accretion as a driving mechanism of galactic evolution*. A&A, vol. 394, pages L35–L38, November 2002. [31](#)
- Boroson T. *The distribution of luminosity in spiral galaxies*. ApJS, vol. 46, pages 177–209, June 1981. [48](#), [49](#)
- Bournaud F. and Combes F. *Gas accretion on spiral galaxies: Bar formation and renewal*. A&A, vol. 392, pages 83–102, September 2002. [30](#)
- Bournaud F. and Elmegreen B. G. *Unstable Disks at High Redshift: Evidence for Smooth Accretion in Galaxy Formation*. ApJ, vol. 694, pages L158–L161, April 2009. [109](#)
- Bournaud F., Combes F. and Semelin B. *The lifetime of galactic bars: central mass concentrations and gravity torques*. MNRAS, vol. 364, pages L18–L22, November 2005. [30](#)
- Bournaud F., Daddi E., Elmegreen B. G., Elmegreen D. M., Nesvadba N., Vanzella E., Di Matteo P., Le Tiran L., Lehnert M. and Elbaz D. *Observations and modeling of a clumpy galaxy at $z = 1.6$. Spectroscopic clues to the origin and evolution of chain galaxies*. A&A, vol. 486, pages 741–753, August 2008. [109](#)
- Braun J., Hubert D. and for the IceCube Collaboration . *Searches for WIMP Dark Matter from the Sun with AMANDA*. ArXiv e-prints, June 2009. [120](#)
- Brinchmann J. and Ellis R. S. *The Mass Assembly and Star Formation Characteristics of Field Galaxies of Known Morphology*. ApJ, vol. 536, pages L77–L80, June 2000. [27](#), [28](#), [55](#), [58](#)
- Brinchmann J., Abraham R., Schade D., Tresse L., Ellis R. S., Lilly S., Le Fevre O., Glazebrook K., Hammer F., Colless M., Crampton D. and Broadhurst T. *Hubble Space Telescope Imaging of the CFRS and LDSS Redshift Surveys. I. Morphological Properties*. ApJ, vol. 499, pages 112–+, May 1998. [43](#), [45](#), [55](#), [56](#), [66](#), [80](#), [81](#)
- Bromm V. and Larson R. B. *The First Stars*. ARA&A, vol. 42, pages 79–118, September 2004. [128](#)
- Bundy K., Fukugita M., Ellis R. S., Kodama T. and Conselice C. J. *A Slow Merger History of Field Galaxies since $z \sim 1$* . ApJ, vol. 601, pages L123–L126, February 2004. [29](#)
- Bundy K., Ellis R. S. and Conselice C. J. *The Mass Assembly Histories of Galaxies of Various Morphologies in the GOODS Fields*. ApJ, vol. 625, pages 621–632, June 2005. [27](#)

- Bundy K., Ellis R. S., Conselice C. J., Taylor J. E., Cooper M. C., Willmer C. N. A., Weiner B. J., Coil A. L., Noeske K. G. and Eisenhardt P. R. M. *The Mass Assembly History of Field Galaxies: Detection of an Evolving Mass Limit for Star-Forming Galaxies*. ApJ, vol. 651, pages 120–141, November 2006. [28](#)
- Burgarella D., Buat V., Donas J., Milliard B. and Chapelon S. *The ultraviolet visibility and quantitative morphology of galactic disks at low and high redshift*. A&A, vol. 369, pages 421–431, April 2001. [51](#)
- Burstein D. *Structure and origin of S0 galaxies. III - The luminosity distribution perpendicular to the plane of the disks in S0's*. ApJ, vol. 234, pages 829–836, December 1979. [49](#)
- Buta R. *Morphology of Galaxies: an Overview*. In G. Longo, M. Capaccioli, & G. Busarello , editeur, Morphological and Physical Classification of Galaxies, volume 178 of *Astrophysics and Space Science Library*, pages 1–+, 1992. [23](#)
- Buta R. *The morphological classification of galaxies*. In T. X. Thuan, C. Balkowski, & J. Tran Thanh Van , editeur, Physics of Nearby Galaxies: Nature or Nurture?, pages 3–+, 1992. [42](#)
- Cassata P., Cimatti A., Franceschini A., Daddi E., Pignatelli E., Fasano G., Rodighiero G., Pozzetti L., Mignoli M. and Renzini A. *The evolution of the galaxy B-band rest-frame morphology to $z \sim 2$: new clues from the K20/GOODS sample*. MNRAS, vol. 357, pages 903–917, March 2005. [46](#), [49](#)
- Ceverino D., Dekel A. and Bournaud F. *High-redshift clumpy discs and bulges in cosmological simulations*. MNRAS, vol. 404, pages 2151–2169, June 2010. [109](#)
- Challinor A. and Peiris H. *Lecture notes on the physics of cosmic microwave background anisotropies*. In M. Novello & S. Perez , editeur, American Institute of Physics Conference Series, volume 1132 of *American Institute of Physics Conference Series*, pages 86–140, May 2009. [8](#), [127](#)
- Chary R. and Elbaz D. *Interpreting the Cosmic Infrared Background: Constraints on the Evolution of the Dust-enshrouded Star Formation Rate*. ApJ, vol. 556, pages 562–581, August 2001. [64](#)
- Chen Y., Lowenthal J. D. and Yun M. S. *Color-Magnitude Relation and Morphology of Low-Redshift ULIRGs in Sloan Digital Sky Survey*. ApJ, vol. 712, pages 1385–1402, April 2010. [46](#)
- Choi E. and Ryu D. *Baryonic fraction in the cold plus hot dark matter universe*. MNRAS, vol. 296, pages 109–118, May 1998. [119](#)
- Chungpei M. *Constraints on massive neutrinos as hot dark matter*. Nuclear Physics B Proceedings Supplements, Vol. 51, vol. 51, pages 254–258, November 1996. [117](#)

- Cimatti A., Daddi E., Mignoli M., Pozzetti L., Renzini A., Zamorani G., Broadhurst T., Fontana A., Saracco P., Poli F., Cristiani S., D’Odorico S., Giallongo E., Gilmozzi R. and Menci N. *The K20 survey. I. Disentangling old and dusty star-forming galaxies in the ERO population*. A&A, vol. 381, pages L68–L72, January 2002. [55](#)
- Cimatti A., Daddi E., Renzini A., Cassata P., Vanzella E., Pozzetti L., Cristiani S., Fontana A., Rodighiero G., Mignoli M. and Zamorani G. *Old galaxies in the young Universe*. Nature, vol. 430, pages 184–187, July 2004. [26](#)
- Cimatti A., Cassata P., Pozzetti L., Kurk J., Mignoli M., Renzini A., Daddi E., Bolzonella M., Brusa M., Rodighiero G., Dickinson M., Franceschini A., Zamorani G., Berta S., Rosati P. and Halliday C. *GMASS ultradeep spectroscopy of galaxies at $z \sim 2$. II. Superdense passive galaxies: how did they form and evolve?* A&A, vol. 482, pages 21–42, April 2008. [26](#)
- Cirasuolo M., McLure R. J., Dunlop J. S., Almaini O., Foucaud S., Smail I., Sekiguchi K., Simpson C., Eales S., Dye S., Watson M. G., Page M. J. and Hirst P. *The evolution of the near-infrared galaxy luminosity function and colour bimodality up to $z \sim 2$ from the UKIDSS Ultra Deep Survey Early Data Release*. MNRAS, vol. 380, pages 585–595, September 2007. [22](#), [28](#), [57](#), [95](#), [97](#), [101](#), [102](#)
- Colless M., Dalton G., Maddox S., Sutherland W., Norberg P., Cole S., Bland-Hawthorn J., Bridges T., Cannon R., Collins C., Couch W., Cross N., Deeley K., De Propriis R., Driver S. P., Efstathiou G., Ellis R. S., Frenk C. S., Glazebrook K., Jackson C., Lahav O., Lewis I., Lumsden S., Madgwick D., Peacock J. A., Peterson B. A., Price I., Seaborne M. and Taylor K. *The 2dF Galaxy Redshift Survey: spectra and redshifts*. MNRAS, vol. 328, pages 1039–1063, December 2001. [6](#)
- Combes F., Debbasch F., Friedli D. and Pfenniger D. *Box and peanut shapes generated by stellar bars*. A&A, vol. 233, pages 82–95, July 1990. [29](#), [55](#), [95](#)
- Combes F. *Bulge formation*. In F. Hammer, T. X. Thuan, V. Cayatte, B. Guiderdoni, & J. T. Thanh Van , editeur, Building Galaxies; from the Primordial Universe to the Present, pages 413–+, 2000. [54](#)
- Combes F. *Secular Evolution of Galaxies*. ArXiv Astrophysics e-prints, June 2005. [30](#), [31](#)
- Conselice C. J., Bershadsky M. A. and Jangren A. *The Asymmetry of Galaxies: Physical Morphology for Nearby and High-Redshift Galaxies*. ApJ, vol. 529, pages 886–910, February 2000. [44](#), [45](#), [51](#)

- Conselice C. J., Bershadsky M. A., Dickinson M. and Papovich C. *A Direct Measurement of Major Galaxy Mergers at $z \sim 3$* . AJ, vol. 126, pages 1183–1207, September 2003. [29](#), [64](#), [77](#)
- Conselice C. J., Grogin N. A., Jogee S., Lucas R. A., Dahlen T., de Mello D., Gardner J. P., Mobasher B. and Ravindranath S. *Observing the Formation of the Hubble Sequence in the Great Observatories Origins Deep Survey*. ApJ, vol. 600, pages L139–L142, January 2004. [45](#)
- Conselice C. J., Blackburne J. A. and Papovich C. *The Luminosity, Stellar Mass, and Number Density Evolution of Field Galaxies of Known Morphology from $z = 0.5$ to 3*. ApJ, vol. 620, pages 564–583, February 2005. [77](#)
- Conselice C. J., Bundy K., Ellis R. S., Brichmann J., Vogt N. P. and Phillips A. C. *Evolution of the Near-Infrared Tully-Fisher Relation: Constraints on the Relationship between the Stellar and Total Masses of Disk Galaxies since $z \sim 1$* . ApJ, vol. 628, pages 160–168, July 2005. [66](#), [67](#), [143](#)
- Conselice C. J. *The Relationship between Stellar Light Distributions of Galaxies and Their Formation Histories*. ApJS, vol. 147, pages 1–28, July 2003. [45](#)
- Conselice C. J. *The fundamental properties of galaxies and a new galaxy classification system*. MNRAS, vol. 373, pages 1389–1408, December 2006. [21](#), [22](#)
- Copi C. J., Schramm D. N. and Turner M. S. *Big-Bang Nucleosynthesis and the Baryon Density of the Universe*. Science, vol. 267, pages 192–199, January 1995. [126](#)
- Covington M. D., Kassin S. A., Dutton A. A., Weiner B. J., Cox T. J., Jonsson P., Primack J. R., Faber S. M. and Koo D. C. *Evolution of the Stellar Mass Tully-Fisher Relation in Disk Galaxy Merger Simulations*. ApJ, vol. 710, pages 279–288, February 2010. [107](#)
- Cowie L. L., Songaila A., Hu E. M. and Cohen J. G. *New Insight on Galaxy Formation and Evolution From Keck Spectroscopy of the Hawaii Deep Fields*. AJ, vol. 112, pages 839–+, September 1996. [26](#), [58](#)
- Cowie L. L., Songaila A. and Barger A. J. *Evidence for a Gradual Decline in the Universal Rest-Frame Ultraviolet Luminosity Density for $Z < 1$* . AJ, vol. 118, pages 603–612, August 1999. [64](#)
- Cowsik R. and McClelland J. *An Upper Limit on the Neutrino Rest Mass*. Physical Review Letters, vol. 29, pages 669–670, September 1972. [117](#)
- Cox T. J., Jonsson P., Primack J. R. and Somerville R. S. *Feedback in simulations of disc-galaxy major mergers*. MNRAS, vol. 373, pages 1013–1038, December 2006. [33](#)

- Cox T. J., Jonsson P., Somerville R. S., Primack J. R. and Dekel A. *The effect of galaxy mass ratio on merger-driven starbursts*. MNRAS, vol. 384, pages 386–409, February 2008. [33](#)
- Daddi E., Cimatti A. and Renzini A. *EROs and the formation epoch of field ellipticals*. A&A, vol. 362, pages L45–L48, October 2000. [55](#)
- Daddi E., Renzini A., Pirzkal N., Cimatti A., Malhotra S., Stiavelli M., Xu C., Pasquali A., Rhoads J. E., Brusa M., di Serego Alighieri S., Ferguson H. C., Koekemoer A. M., Moustakas L. A., Panagia N. and Windhorst R. A. *Passively Evolving Early-Type Galaxies at $1.4 < z < 2.5$ in the Hubble Ultra Deep Field*. ApJ, vol. 626, pages 680–697, June 2005. [26](#)
- Darwin C. R. On the origin of species by means of natural selection, or the preservation of favoured races in the struggle for life. W. Clowes and Sons, Stamford Street, and Charing Cross, London, 1859. [21](#)
- de Jong R. S. *Near-infrared and optical broadband surface photometry of 86 face-on disk dominated galaxies. II. A two-dimensional method to determine bulge and disk parameters*. A&AS, vol. 118, pages 557–573, September 1996. [85](#)
- de Jong R. S. *Near-infrared and optical broadband surface photometry of 86 face-on disk dominated galaxies. III. The statistics of the disk and bulge parameters*. A&A, vol. 313, pages 45–64, September 1996. [85](#)
- de Vaucouleurs G., de Vaucouleurs A., Corwin Jr. H. G., Buta R. J., Paturel G. and Fouque P. Third Reference Catalogue of Bright Galaxies. 1991. [9](#)
- de Vaucouleurs G. *Recherches sur les Nebuleuses Extragalactiques*. Annales d’Astrophysique, vol. 11, pages 247–+, January 1948. [48](#), [85](#)
- de Vaucouleurs G. *Classification and Morphology of External Galaxies*. Handbuch der Physik, vol. 53, pages 275–+, 1959. [10](#), [15](#), [48](#)
- de Vaucouleurs G. *Revised Classification of 1500 Bright Galaxies*. ApJS, vol. 8, pages 31–+, April 1963. [23](#)
- de Vaucouleurs G. *Global Physical Parameters of Galaxies*. In Quantifying Galaxy Morphology at High Redshift Workshop, Space Telescope Science Institute, Baltimore MD, 1994. [21](#), [23](#)
- Debattista V. P., Carollo C. M., Mayer L. and Moore B. *Bulges or Bars from Secular Evolution?* ApJ, vol. 604, pages L93–L96, April 2004. [55](#), [95](#)
- Dekel A., Birnboim Y., Engel G., Freundlich J., Goerdt T., Mumcuoglu M., Neistein E., Pichon C., Teyssier R. and Zinger E. *Cold streams in early massive hot haloes as the main mode of galaxy formation*. Nature, vol. 457, pages 451–454, January 2009. [109](#)

- Delgado-Serrano R., Hammer F., Yang Y. B., Puech M., Flores H. and Rodrigues M. *How was the Hubble sequence 6 Gyr ago?* A&A, vol. 509, pages A78+, January 2010. [10](#), [57](#), [75](#), [82](#), [96](#), [97](#)
- Dey A., Graham J. R., Ivison R. J., Smail I., Wright G. S. and Liu M. C. *Observations of a $Z = 1.44$ Dusty, Ultraluminous Galaxy and Implications for Deep Submillimeter Surveys*. ApJ, vol. 519, pages 610–621, July 1999. [26](#)
- Di Matteo T., Springel V. and Hernquist L. *Energy input from quasars regulates the growth and activity of black holes and their host galaxies*. Nature, vol. 433, pages 604–607, February 2005. [34](#)
- Dickinson M., Hanley C., Elston R., Eisenhardt P. R., Stanford S. A., Adelberger K. L., Shapley A., Steidel C. C., Papovich C., Szalay A. S., Bershadsky M. A., Conselice C. J., Ferguson H. C. and Fruchter A. S. *The Unusual Infrared Object HDF-N J123656.3+621322*. ApJ, vol. 531, pages 624–634, March 2000. [26](#)
- Dickinson M., Papovich C., Ferguson H. C. and Budavári T. *The Evolution of the Global Stellar Mass Density at $0 < z < 3$* . ApJ, vol. 587, pages 25–40, April 2003. [28](#), [58](#), [64](#), [73](#)
- Dodelson S., Gates E. I. and Turner M. S. *Cold Dark Matter*. Science, vol. 274, pages 69–75, October 1996. [120](#)
- Doroshkevich A. G., Zel'Dovich Y. B. and Novikov I. D. *The Origin of Galaxies in an Expanding Universe*. Soviet Ast., vol. 11, pages 233–+, October 1967. [116](#), [119](#)
- Dressler A., Schechter P. L. and Rose J. A. *The mass of the isolated elliptical NGC 720 as determined from the dynamics of its companions*. AJ, vol. 91, pages 1058–1061, May 1986. [117](#)
- Drory N., Bender R., Feulner G., Hopp U., Maraston C., Snigula J. and Hill G. J. *The Munich Near-Infrared Cluster Survey (MUNICS). VI. The Stellar Masses of K-Band-selected Field Galaxies to $z \sim 1.2$* . ApJ, vol. 608, pages 742–751, June 2004. [55](#), [58](#)
- Eggen O. J., Lynden-Bell D. and Sandage A. R. *Evidence from the motions of old stars that the Galaxy collapsed*. ApJ, vol. 136, pages 748–+, November 1962. [54](#), [64](#)
- Ellis R. S., Abraham R. G. and Dickinson M. *The Relative Star Formation Histories of Spiral Bulges and Elliptical Galaxies in the Hubble Deep Fields*. ApJ, vol. 551, pages 111–130, April 2001. [50](#)

- Elmegreen D. M. and Elmegreen B. G. *Flocculent and grand design spiral structure in field, binary and group galaxies*. MNRAS, vol. 201, pages 1021–1034, December 1982. [21](#)
- Elmegreen D. M. and Elmegreen B. G. *Arm classifications for spiral galaxies*. ApJ, vol. 314, pages 3–9, March 1987. [21](#)
- Elston R., Rieke G. H. and Rieke M. J. *Deep 2 micron imaging of the sky - Evidence for a new extragalactic population*. ApJ, vol. 331, pages L77–L80, August 1988. [26](#)
- Epinat B., Contini T., Le Fèvre O., Vergani D., Garilli B., Amram P., Queyrel J., Tasca L. and Tresse L. *Integral field spectroscopy with SINFONI of VVDS galaxies. I. Galaxy dynamics and mass assembly at $1.2 < z < 1.6$* . A&A, vol. 504, pages 789–805, September 2009. [109](#)
- Epinat B., Amram P., Balkowski C. and Marcelin M. *Evidence for strong dynamical evolution in disc galaxies through the last 11 Gyr. GHASP VIII - a local reference sample of rotating disc galaxies for high-redshift studies*. MNRAS, vol. 401, pages 2113–2147, February 2010. [140](#)
- Fall S. M. and Efstathiou G. *Formation and rotation of disc galaxies with haloes*. MNRAS, vol. 193, pages 189–206, October 1980. [54](#), [64](#)
- Fasano G., Cristiani S., Arnouts S. and Filippi M. *Early-Type Galaxies in the Hubble Deep Field: The $\langle \mu_e \rangle - r_e$ Relation and the Lack of Large Galaxies at High Redshift*. AJ, vol. 115, pages 1400–1411, April 1998. [47](#)
- Ferreras I. and Silk J. *A Backwards Approach to the Formation of Disk Galaxies. I. Stellar and Gas Content*. ApJ, vol. 557, pages 165–179, August 2001. [66](#)
- Ferreras I., Silk J., Böhm A. and Ziegler B. *The star formation history of intermediate-redshift late-type galaxies*. MNRAS, vol. 355, pages 64–72, November 2004. [66](#)
- Flores H., Hammer F., Thuan T. X., Césarsky C., Desert F. X., Omont A., Lilly S. J., Eales S., Crampton D. and Le Fèvre O. *15 Micron Infrared Space Observatory Observations of the 1415+52 Canada-France Redshift Survey Field: The Cosmic Star Formation Rate as Derived from Deep Ultraviolet, Optical, Mid-Infrared, and Radio Photometry*. ApJ, vol. 517, pages 148–167, May 1999. [33](#), [58](#), [64](#)
- Flores H., Hammer F., Puech M., Amram P. and Balkowski C. *3D spectroscopy with VLT/GIRAFFE. I. The true Tully Fisher relationship at $z \sim 0.6$* . A&A, vol. 455, pages 107–118, August 2006. [31](#), [36](#), [38](#), [67](#), [68](#), [73](#), [74](#), [75](#), [76](#), [107](#), [137](#), [138](#), [139](#), [140](#), [143](#)

- Förster Schreiber N. M., Genzel R., Lehnert M. D., Bouché N., Verma A., Erb D. K., Shapley A. E., Steidel C. C., Davies R., Lutz D., Nesvadba N., Tacconi L. J., Eisenhauer F., Abuter R., Gilbert A., Gillessen S. and Sternberg A. *SINFONI Integral Field Spectroscopy of $z \sim 2$ UV-selected Galaxies: Rotation Curves and Dynamical Evolution*. ApJ, vol. 645, pages 1062–1075, July 2006. 109
- Franzetti P., Scodeggio M., Garilli B., Vergani D., Maccagni D., Guzzo L., Tresse L., Ilbert O., Lamareille F., Contini T., Le Fèvre O., Zamorani G., Brinchmann J., Charlot S., Bottini D., Le Brun V., Picat J. P., Scaramella R., Vettolani G., Zanichelli A., Adami C., Arnouts S., Bardelli S., Bolzonella M., Cappi A., Ciliegi P., Foucaud S., Gavignaud I., Iovino A., McCracken H. J., Marano B., Marinoni C., Mazure A., Meneux B., Merighi R., Paltani S., Pellò R., Pollo A., Pozzetti L., Radovich M., Zucca E., Cucciati O. and Walcher C. J. *The VIMOS-VLT deep survey. Color bimodality and the mix of galaxy populations up to $z \sim 2$* . A&A, vol. 465, pages 711–723, April 2007. 29
- Freeman K. C. *On the Disks of Spiral and so Galaxies*. ApJ, vol. 160, pages 811–+, June 1970. 85
- Freese K. *Review of Observational Evidence for Dark Matter in the Universe and in upcoming searches for Dark Stars*. In E. Pécontal, T. Buchert, P. di Stefano, & Y. Copin , editeur, EAS Publications Series, volume 36 of *EAS Publications Series*, pages 113–126, 2009. 117
- Frei Z., Guhathakurta P., Gunn J. E. and Tyson J. A. *A Catalog of Digital Images of 113 Nearby Galaxies*. AJ, vol. 111, pages 174–+, January 1996. 80
- Fuentes-Carrera I., Flores H., Yang Y., Peirani S., Hammer F., Rodrigues M. and Balkowski C. *Determining the morpho-kinematic properties of a face-on merger at $z \sim 0.7$* . A&A, vol. 513, pages A43+, April 2010. 37
- Fukugita M., Hogan C. J. and Peebles P. J. E. *The Cosmic Baryon Budget*. ApJ, vol. 503, pages 518–+, August 1998. 28
- Fukugita M., Nakamura O., Okamura S., Yasuda N., Barentine J. C., Brinkmann J., Gunn J. E., Harvanek M., Ichikawa T., Lupton R. H., Schneider D. P., Strauss M. A. and York D. G. *A Catalog of Morphologically Classified Galaxies from the Sloan Digital Sky Survey: North Equatorial Region*. AJ, vol. 134, pages 579–593, August 2007. 53, 76
- Gadotti D. A. and dos Anjos S. *Homogenization of the Stellar Population along Late-Type Spiral Galaxies*. AJ, vol. 122, pages 1298–1318, September 2001. 30
- Gamow G. *Expanding Universe and the Origin of Elements*. Phys. Rev., vol. 70, no. 7-8, pages 572–573, Oct 1946. 125

- Genzel R., Tacconi L. J., Eisenhauer F., Förster Schreiber N. M., Cimatti A., Daddi E., Bouché N., Davies R., Lehnert M. D., Lutz D., Nesvadba N., Verma A., Abuter R., Shapiro K., Sternberg A., Renzini A., Kong X., Arimoto N. and Mignoli M. *The rapid formation of a large rotating disk galaxy three billion years after the Big Bang*. *Nature*, vol. 442, pages 786–789, August 2006. 109
- Genzel R., Burkert A., Bouché N., Cresci G., Förster Schreiber N. M., Shapley A., Shapiro K., Tacconi L. J., Buschkamp P., Cimatti A., Daddi E., Davies R., Eisenhauer F., Erb D. K., Genel S., Gerhard O., Hicks E., Lutz D., Naab T., Ott T., Rabien S., Renzini A., Steidel C. C., Sternberg A. and Lilly S. J. *From Rings to Bulges: Evidence for Rapid Secular Galaxy Evolution at $z \sim 2$ from Integral Field Spectroscopy in the SINS Survey*. *ApJ*, vol. 687, pages 59–77, November 2008. 109
- Gershtein S. S. and Zel'Dovich Y. B. *Rest Mass of Muonic Neutrino and Cosmology*. *Soviet Journal of Experimental and Theoretical Physics Letters*, vol. 4, pages 120–+, September 1966. 117
- Giovanelli R., Haynes M. P., da Costa L. N., Freudling W., Salzer J. J. and Wegner G. *The Tully-Fisher Relation and H_0* . *ApJ*, vol. 477, pages L1+, March 1997. 66
- Glazebrook K., Baldry I. K., Blanton M. R., Brinkmann J., Connolly A., Csabai I., Fukugita M., Ivezić Ž., Loveday J., Meiksin A., Nichol R., Peng E., Schneider D. P., SubbaRao M., Tremonti C. and York D. G. *The Sloan Digital Sky Survey: The Cosmic Spectrum and Star Formation History*. *ApJ*, vol. 587, pages 55–70, April 2003. 59
- Gottesman S. T. and Hunter Jr. J. H. *The barred spiral galaxy NGC 3992 - Does it have a massive halo*. *ApJ*, vol. 260, pages 65–69, September 1982. 117
- Gottesman S. T., Hunter Jr. J. H. and Ball J. R. *NGC 3992 - A galaxy without a massive halo*. In E. Athanassoula, editeur, *Internal Kinematics and Dynamics of Galaxies*, volume 100 of *IAU Symposium*, pages 93–+, 1983. 117
- Gottesman S. T., Hunter Jr. J. H. and Shostak G. S. *The NGC 1961 group of galaxies*. *MNRAS*, vol. 202, pages 21P–24P, February 1983. 117
- Gunn J. E. and Gott III J. R. *On the Infall of Matter Into Clusters of Galaxies and Some Effects on Their Evolution*. *ApJ*, vol. 176, pages 1–+, August 1972. 25
- Gunn J. E. *The Friedmann models and optical observations in cosmology*. In A. Maeder, L. Martinet, & G. Tammann, editeurs, *Saas-Fee Advanced Course 8: Observational Cosmology Advanced Course*, pages 1–+, 1978. 7

- Guth A. H. *Inflationary universe: A possible solution to the horizon and flatness problems*. Phys. Rev. D, vol. 23, pages 347–356, January 1981. [123](#)
- Guth A. H. The new inflationary universe, 1984, pages 287–301. 1986. [123](#)
- Guzmán R. *Luminous Blue Compact Dwarf Galaxies: a Key Player in Galaxy Evolution*. In J. E. Beckman & T. J. Mahoney , editeur, The Evolution of Galaxies on Cosmological Timescales, volume 187 of *Astronomical Society of the Pacific Conference Series*, pages 271–280, 1999. [65](#)
- Haarsma D. B., Partridge R. B., Windhorst R. A. and Richards E. A. *Faint Radio Sources and Star Formation History*. ApJ, vol. 544, pages 641–658, December 2000. [64](#)
- Haas M., Chini R. and Klaas U. *Exceptional H_2 emission in the Antennae galaxies: Pre-starburst shocks from the galaxy collision*. A&A, vol. 433, pages L17–L20, April 2005. [33](#)
- Hammer F., Flores H., Lilly S. J., Crampton D., Le Fevre O., Rola C., Mallen-Ornelas G., Schade D. and Tresse L. *Canada-France Redshift Survey. XIV. Spectral Properties of Field Galaxies up to $z=1$* . ApJ, vol. 481, pages 49–+, May 1997. [64](#), [74](#), [76](#)
- Hammer F., Gruel N., Thuan T. X., Flores H. and Infante L. *Luminous Compact Galaxies at Intermediate Redshifts: Progenitors of Bulges of Massive Spirals?* ApJ, vol. 550, pages 570–584, April 2001. [65](#), [80](#)
- Hammer F., Flores H., Elbaz D., Zheng X. Z., Liang Y. C. and Cesarsky C. *Did most present-day spirals form during the last 8 Gyr?. A formation history with violent episodes revealed by panchromatic observations*. A&A, vol. 430, pages 115–128, January 2005. [29](#), [34](#), [37](#), [58](#), [64](#), [66](#), [73](#), [107](#)
- Hammer F., Flores H., Liang Y., Zheng X., Elbaz D. and Cesarsky C. *Galaxy Formation and Evolution since $z = 1$* . In A. Renzini & R. Bender , editeur, Multiwavelength Mapping of Galaxy Formation and Evolution, pages 263–+, 2005. [55](#)
- Hammer F., Puech M., Chemin L., Flores H. and Lehnert M. D. *The Milky Way, an Exceptionally Quiet Galaxy: Implications for the Formation of Spiral Galaxies*. ApJ, vol. 662, pages 322–334, June 2007. [35](#), [38](#)
- Hammer F., Flores H., Puech M., Yang Y. B., Athanassoula E., Rodrigues M. and Delgado-Serrano R. *The Hubble sequence: just a vestige of merger events?* A&A, vol. 507, pages 1313–1326, December 2009. [25](#), [34](#), [35](#), [64](#), [107](#)

- Hammer F., Flores H., Yang Y. B., Athanassoula E., Puech M., Rodrigues M. and Peirani S. *A forming, dust-enshrouded disk at $z = 0.43$: the first example of a massive, late-type spiral rebuilt after a major merger?* A&A, vol. 496, pages 381–387, March 2009. [37](#)
- Hammer F. *Growth of Spirals: Secular or Driven by Mergers ?* ArXiv Astrophysics e-prints, September 2005. [58](#), [59](#)
- Harrison E. R. *Fluctuations at the Threshold of Classical Cosmology*. Phys. Rev. D, vol. 1, pages 2726–2730, May 1970. [124](#)
- Häussler B., McIntosh D. H., Barden M., Bell E. F., Rix H.-W., Borch A., Beckwith S. V. W., Caldwell J. A. R., Heymans C., Jahnke K., Jogee S., Koposov S. E., Meisenheimer K., Sánchez S. F., Somerville R. S., Wisotzki L. and Wolf C. *GEMS: Galaxy Fitting Catalogs and Testing Parametric Galaxy Fitting Codes: GALFIT and GIM2D*. ApJS, vol. 172, pages 615–633, October 2007. [49](#)
- Heavens A., Panter B., Jimenez R. and Dunlop J. *The star-formation history of the Universe from the stellar populations of nearby galaxies*. Nature, vol. 428, pages 625–627, April 2004. [29](#), [58](#), [64](#), [73](#)
- Hinshaw G., Weiland J. L., Hill R. S., Odegard N., Larson D., Bennett C. L., Dunkley J., Gold B., Greason M. R., Jarosik N., Komatsu E., Nolte M. R., Page L., Spergel D. N., Wollack E., Halpern M., Kogut A., Limon M., Meyer S. S., Tucker G. S. and Wright E. L. *Five-Year Wilkinson Microwave Anisotropy Probe Observations: Data Processing, Sky Maps, and Basic Results*. ApJS, vol. 180, pages 225–245, February 2009. [127](#)
- Hopkins P. F., Hernquist L., Cox T. J., Younger J. D. and Besla G. *The Radical Consequences of Realistic Satellite Orbits for the Heating and Implied Merger Histories of Galactic Disks*. ApJ, vol. 688, pages 757–769, December 2008. [107](#)
- Hopkins P. F., Cox T. J., Younger J. D. and Hernquist L. *How do Disks Survive Mergers?* ApJ, vol. 691, pages 1168–1201, February 2009. [33](#), [34](#), [35](#), [107](#)
- Hopkins P. F., Somerville R. S., Cox T. J., Hernquist L., Jogee S., Kereš D., Ma C.-P., Robertson B. and Stewart K. *The effects of gas on morphological transformation in mergers: implications for bulge and disc demographics*. MNRAS, vol. 397, pages 802–814, August 2009. [34](#), [107](#)
- Hopkins P. F., Younger J. D., Hayward C. C., Narayanan D. and Hernquist L. *Mergers, active galactic nuclei and ‘normal’ galaxies: contributions to the distribution of star formation rates and infrared luminosity functions*. MNRAS, vol. 402, pages 1693–1713, March 2010. [64](#)

- Hopkins A. M. *On the Evolution of Star-forming Galaxies*. ApJ, vol. 615, pages 209–221, November 2004. [64](#)
- Hubble E. P. *Extragalactic nebulae*. ApJ, vol. 64, pages 321–369, December 1926. [8](#), [9](#), [12](#)
- Hubble E. P. *Realm of the Nebulae*. 1936. [10](#), [14](#), [15](#)
- Ibata R., Irwin M., Lewis G., Ferguson A. M. N. and Tanvir N. *A giant stream of metal-rich stars in the halo of the galaxy M31*. Nature, vol. 412, pages 49–52, July 2001. [108](#)
- Ilbert O., Lauger S., Tresse L., Buat V., Arnouts S., Le Fèvre O., Burgarella D., Zucca E., Bardelli S., Zamorani G., Bottini D., Garilli B., Le Brun V., Maccagni D., Picat J.-P., Scaramella R., Scodeggio M., Vettolani G., Zanichelli A., Adami C., Arnaboldi M., Bolzonella M., Cappi A., Charlot S., Contini T., Foucaud S., Franzetti P., Gavignaud I., Guzzo L., Iovino A., McCracken H. J., Marano B., Marinoni C., Mathez G., Mazure A., Meneux B., Merighi R., Paltani S., Pello R., Pollo A., Pozzetti L., Radovich M., Bondi M., Bongiorno A., Busarello G., Ciliegi P., Mellier Y., Merluzzi P., Ripepi V. and Rizzo D. *The VIMOS-VLT Deep Survey. Galaxy luminosity function per morphological type up to $z = 1.2$* . A&A, vol. 453, pages 809–815, July 2006. [45](#)
- Im M., Yamada T., Tanaka I. and Kajisawa M. *A Hyper Extremely Red Object in the Field near 53W002*. ApJ, vol. 578, pages L19–L22, October 2002. [26](#)
- Impey C. D., Sprayberry D., Irwin M. J. and Bothun G. D. *Low Surface Brightness Galaxies in the Local Universe. I. The Catalog*. ApJS, vol. 105, pages 209–+, August 1996. [9](#)
- Jenkins A., Frenk C. S., Pearce F. R., Thomas P. A., Colberg J. M., White S. D. M., Couchman H. M. P., Peacock J. A., Efstathiou G. and Nelson A. H. *Evolution of Structure in Cold Dark Matter Universes*. ApJ, vol. 499, pages 20–+, May 1998. [5](#), [121](#), [122](#)
- Jimenez R., Bernardi M., Haiman Z., Panter B. and Heavens A. F. *The Ages, Metallicities, and Star Formation Histories of Early-Type Galaxies in the SDSS*. ApJ, vol. 669, pages 947–951, November 2007. [66](#)
- Jogee S., Barazza F. D., Rix H.-W., Shlosman I., Barden M., Wolf C., Davies J., Heyer I., Beckwith S. V. W., Bell E. F., Borch A., Caldwell J. A. R., Conselice C. J., Dahlen T., Häussler B., Heymans C., Jahnke K., Knapen J. H., Laine S., Lubell G. M., Mobasher B., McIntosh D. H., Meisenheimer K., Peng C. Y., Ravindranath S., Sanchez S. F., Somerville R. S. and Wisotzki L. *Bar Evolution over the Last 8 Billion Years: A Constant Fraction of Strong Bars in the GEMS Survey*. ApJ, vol. 615, pages L105–L108, November 2004. [30](#)

- Jonsson P., Cox T. J., Primack J. R. and Somerville R. S. *Simulations of Dust in Interacting Galaxies. I. Dust Attenuation*. ApJ, vol. 637, pages 255–268, January 2006. [34](#)
- Kannappan S. J. and Barton E. J. *Tools for Identifying Spurious Luminosity Offsets in Tully-Fisher Studies: Application at Low Redshift and Implications for High Redshift*. AJ, vol. 127, pages 2694–2710, May 2004. [66](#)
- Kannappan S. J., Fabricant D. G. and Franx M. *Physical Sources of Scatter in the Tully-Fisher Relation*. AJ, vol. 123, pages 2358–2386, May 2002. [68](#)
- Kauffmann G., Heckman T. M., White S. D. M., Charlot S., Tremonti C., Brinchmann J., Bruzual G., Peng E. W., Seibert M., Bernardi M., Blanton M., Brinkmann J., Castander F., Csábai I., Fukugita M., Ivezić Z., Munn J. A., Nichol R. C., Padmanabhan N., Thakar A. R., Weinberg D. H. and York D. *Stellar masses and star formation histories for 10^5 galaxies from the Sloan Digital Sky Survey*. MNRAS, vol. 341, pages 33–53, May 2003. [22](#)
- Kauffmann G. *The age of elliptical galaxies and bulges in a merger model*. MNRAS, vol. 281, pages 487–492, July 1996. [54](#)
- Kennicutt Jr. R. C. *The integrated spectra of nearby galaxies - General properties and emission-line spectra*. ApJ, vol. 388, pages 310–327, April 1992. [22](#)
- Kent S. M., Dame T. M. and Fazio G. *Galactic structure from the Spacelab infrared telescope. II - Luminosity models of the Milky Way*. ApJ, vol. 378, pages 131–138, September 1991. [85](#)
- Kent S. M. *CCD surface photometry of field Galaxies. II - Bulge/disk decompositions*. ApJS, vol. 59, pages 115–159, October 1985. [22](#), [44](#), [49](#), [91](#)
- Khochfar S. and Burkert A. *On the origin of isophotal shapes in elliptical galaxies*. MNRAS, vol. 359, pages 1379–1385, June 2005. [34](#)
- Kingsburgh R. L. and Barlow M. J. *Distances for galactic planetary nebulae using mean forbidden O II doublet ratio electron densities*. MNRAS, vol. 257, pages 317–339, July 1992. [140](#)
- Koo D. C., Guzman R., Faber S. M., Illingworth G. D., Bershadsky M. A., Kron R. G. and Takamiya M. *High-resolution spectra of distant compact narrow emission line galaxies: Progenitors of spheroidal galaxies*. ApJ, vol. 440, pages L49–L52, February 1995. [65](#)
- Kormendy J. and Bender R. *A Proposed Revision of the Hubble Sequence for Elliptical Galaxies*. ApJ, vol. 464, pages L119+, June 1996. [21](#)

- Kormendy J. and Bruzual A. G. *The minor-axis brightness profile of the spiral galaxy NGC 4565 and the problem of massive halos*. ApJ, vol. 223, pages L63–L66, July 1978. [85](#)
- Kormendy J. and Fisher D. B. *Secular Evolution in Disk Galaxies: Pseudobulge Growth and the Formation of Spheroidal Galaxies*. In J. G. Funes & E. M. Corsini, editeur, Astronomical Society of the Pacific Conference Series, volume 396 of *Astronomical Society of the Pacific Conference Series*, pages 297–+, October 2008. [30](#), [85](#)
- Kormendy J. and Kennicutt Jr. R. C. *Secular Evolution and the Formation of Pseudobulges in Disk Galaxies*. ARA&A, vol. 42, pages 603–683, September 2004. [29](#), [30](#), [38](#), [85](#)
- Kormendy J., Fisher D. B., Cornell M. E. and Bender R. *Structure and Formation of Elliptical and Spheroidal Galaxies*. ApJS, vol. 182, pages 216–309, May 2009. [85](#)
- Kormendy J. *Brightness distributions in compact and normal galaxies. III - Decomposition of observed profiles into spheroid and disk components*. ApJ, vol. 217, pages 406–419, October 1977. [49](#)
- Kriek M., van Dokkum P. G., Franx M., Quadri R., Gawiser E., Herrera D., Illingworth G. D., Labbé I., Lira P., Marchesini D., Rix H.-W., Rudnick G., Taylor E. N., Toft S., Urry C. M. and Wuyts S. *Spectroscopic Identification of Massive Galaxies at $z \sim 2.3$ with Strongly Suppressed Star Formation*. ApJ, vol. 649, pages L71–L74, October 2006. [26](#)
- Kuchinski L. E., Freedman W. L., Madore B. F., Trewhella M., Bohlin R. C., Cornett R. H., Fanelli M. N., Marcum P. M., Neff S. G., O’Connell R. W., Roberts M. S., Smith A. M., Stecher T. P. and Waller W. H. *Comparing Galaxy Morphology at Ultraviolet and Optical Wavelengths*. ApJS, vol. 131, pages 441–463, December 2000. [51](#)
- Lamareille F. *Évolution cosmologique des propriétés physiques des galaxies*. PhD thesis, Université Toulouse III - Paul Sabatier, 2006. [131](#), [136](#)
- Lanyon-Foster M. M., Conselice C. J. and Merrifield M. R. *Structure through colour: a pixel approach towards understanding galaxies*. MNRAS, vol. 380, pages 571–584, September 2007. [50](#)
- Larson D., Dunkley J., Hinshaw G., Komatsu E., Nolte M. R., Bennett C. L., Gold B., Halpern M., Hill R. S., Jarosik N., Kogut A., Limon M., Meyer S. S., Odegard N., Page L., Smith K. M., Spergel D. N., Tucker G. S., Weiland J. L., Wollack E. and Wright E. L. *Seven-Year Wilkinson Microwave Anisotropy Probe (WMAP)*

- Observations: Power Spectra and WMAP-Derived Parameters.* ArXiv e-prints, January 2010. [8](#), [121](#)
- Larson R. B. *Models for the formation of disc galaxies.* MNRAS, vol. 176, pages 31–52, July 1976. [65](#)
- Lauger S., Burgarella D. and Buat V. *Spectro-morphology of galaxies: A multi-wavelength (UV-R) classification method.* A&A, vol. 434, pages 77–87, April 2005. [51](#)
- Lauger S., Ilbert O., Buat V., Tresse L., Burgarella D., Arnouts S., Le Fèvre O. and VVDS Collaboration . *Evolution of morphology in the Chandra Deep Field South.* In F. Casoli, T. Contini, J. M. Hameury, & L. Pagani , editeur, SF2A-2005: Semaine de l’Astrophysique Francaise, pages 667–+, December 2005. [45](#)
- Laurikainen E., Salo H., Buta R. and Knapen J. H. *Properties of bars and bulges in the Hubble sequence.* MNRAS, vol. 381, pages 401–417, October 2007. [85](#), [91](#)
- Law D. R., Steidel C. C., Erb D. K., Larkin J. E., Pettini M., Shapley A. E. and Wright S. A. *Integral Field Spectroscopy of High-Redshift Star-forming Galaxies with Laser-guided Adaptive Optics: Evidence for Dispersion-dominated Kinematics.* ApJ, vol. 669, pages 929–946, November 2007. [109](#)
- Law D. R., Steidel C. C., Erb D. K., Larkin J. E., Pettini M., Shapley A. E. and Wright S. A. *The Kiloparsec-scale Kinematics of High-redshift Star-forming Galaxies.* ApJ, vol. 697, pages 2057–2082, June 2009. [109](#)
- Le Fèvre O., Abraham R., Lilly S. J., Ellis R. S., Brinchmann J., Schade D., Tresse L., Colless M., Crampton D., Glazebrook K., Hammer F. and Broadhurst T. *Hubble Space Telescope imaging of the CFRS and LDSS redshift surveys - IV. Influence of mergers in the evolution of faint field galaxies from $z \sim 1$.* MNRAS, vol. 311, pages 565–575, January 2000. [29](#), [34](#), [35](#), [64](#)
- Le Flocc’h E., Papovich C., Dole H., Bell E. F., Lagache G., Rieke G. H., Egami E., Pérez-González P. G., Alonso-Herrero A., Rieke M. J., Blaylock M., Engelbracht C. W., Gordon K. D., Hines D. C., Misselt K. A., Morrison J. E. and Mould J. *Infrared Luminosity Functions from the Chandra Deep Field-South: The Spitzer View on the History of Dusty Star Formation at $0 < z < 1$.* ApJ, vol. 632, pages 169–190, October 2005. [33](#), [38](#), [64](#), [65](#)
- Liang Y. C., Hammer F. and Flores H. *Significant evolution of the stellar mass-metallicity relation since $z \sim 0.65$.* A&A, vol. 447, pages 113–119, February 2006. [29](#), [34](#), [77](#)
- Liddle A. and Loveday J. *The oxford companion to cosmology.* Oxford University Press Inc., 2008. [6](#), [127](#)

- Lilly S. J., Le Fevre O., Hammer F. and Crampton D. *The Canada-France Redshift Survey: The Luminosity Density and Star Formation History of the Universe to Z approximately 1*. ApJ, vol. 460, pages L1+, March 1996. [64](#)
- Lilly S., Schade D., Ellis R., Le Fevre O., Brinchmann J., Tresse L., Abraham R., Hammer F., Crampton D., Colless M., Glazebrook K., Mallen-Ornelas G. and Broadhurst T. *Hubble Space Telescope Imaging of the CFRS and LDSS Redshift Surveys. II. Structural Parameters and the Evolution of Disk Galaxies to Z approximately 1*. ApJ, vol. 500, pages 75–+, June 1998. [26](#), [55](#), [79](#)
- Linde A. D. *A new inflationary universe scenario: A possible solution of the horizon, flatness, homogeneity, isotropy and primordial monopole problems*. Physics Letters B, vol. 108, pages 389–393, February 1982. [123](#)
- Linde A. *Inflationary Cosmology*. In M. Lemoine, J. Martin, & P. Peter, editeurs, *Inflationary Cosmology*, volume 738 of *Lecture Notes in Physics*, Berlin Springer Verlag, pages 1–+, 2008. [125](#)
- Lisker T. *Is the Gini Coefficient a Stable Measure of Galaxy Structure?* ApJS, vol. 179, pages 319–325, December 2008. [46](#)
- Lotz J. M., Primack J. and Madau P. *A New Nonparametric Approach to Galaxy Morphological Classification*. AJ, vol. 128, pages 163–182, July 2004. [45](#), [79](#)
- Lotz J. M., Madau P., Giavalisco M., Primack J. and Ferguson H. C. *The Rest-Frame Far-Ultraviolet Morphologies of Star-forming Galaxies at $z \sim 1.5$ and 4*. ApJ, vol. 636, pages 592–609, January 2006. [29](#), [64](#)
- Lotz J. M., Davis M., Faber S. M., Guhathakurta P., Gwyn S., Huang J., Koo D. C., Le Floch E., Lin L., Newman J., Noeske K., Papovich C., Willmer C. N. A., Coil A., Conselice C. J., Cooper M., Hopkins A. M., Metevier A., Primack J., Rieke G. and Weiner B. J. *The Evolution of Galaxy Mergers and Morphology at $z < 1.2$ in the Extended Groth Strip*. ApJ, vol. 672, pages 177–197, January 2008. [47](#)
- Luminet J.-P., Weeks J. R., Riazuelo A., Lehoucq R. and Uzan J.-P. *Dodecahedral space topology as an explanation for weak wide-angle temperature correlations in the cosmic microwave background*. Nature, vol. 425, pages 593–595, October 2003. [120](#)
- Luminet J.-P. *L’univers chiffonne*. Fayard, 2001. [120](#)
- Luminet J.-P. *The Shape and Topology of the Universe*. ArXiv e-prints, February 2008. [120](#)
- Luminet J.-P. *The Wraparound Universe*. A, 2008. [120](#)

- Lupton R. H., Gunn J. E. and Griffin R. F. *Dynamical studies of globular clusters based on photoelectric radial velocities of individual stars and on the observed mass function. II - M13*. AJ, vol. 93, pages 1114–1136, May 1987. [117](#)
- Lynden-Bell D. *Mysterious mass in local group galaxies*. Mitteilungen der Astronomischen Gesellschaft Hamburg, vol. 60, pages 23–30, 1983. [117](#)
- Madau P., Ferguson H. C., Dickinson M. E., Giavalisco M., Steidel C. C. and Fruchter A. *High-redshift galaxies in the Hubble Deep Field: colour selection and star formation history to $z \sim 4$* . MNRAS, vol. 283, pages 1388–1404, December 1996. [64](#)
- Maller A. H., Dekel A. and Somerville R. *Modelling angular-momentum history in dark-matter haloes*. MNRAS, vol. 329, pages 423–430, January 2002. [33](#)
- Martínez-Delgado D., Peñarrubia J., Gabany R. J., Trujillo I., Majewski S. R. and Pohlen M. *The Ghost of a Dwarf Galaxy: Fossils of the Hierarchical Formation of the Nearby Spiral Galaxy NGC 5907*. ApJ, vol. 689, pages 184–193, December 2008. [108](#), [109](#)
- Martínez-Delgado D., Pohlen M., Gabany R. J., Majewski S. R., Peñarrubia J. and Palma C. *Discovery of a Giant Stellar Tidal Stream Around The Disk Galaxy NGC 4013*. ApJ, vol. 692, pages 955–963, February 2009. [108](#), [109](#)
- Melbourne J., Koo D. C. and Le Floch E. *Optical Morphology Evolution of Infrared Luminous Galaxies in GOODS-N*. ApJ, vol. 632, pages L65–L68, October 2005. [80](#), [108](#)
- Menanteau F., Abraham R. G. and Ellis R. S. *Evidence for evolving spheroidals in the Hubble Deep Fields North and South*. MNRAS, vol. 322, pages 1–12, March 2001. [50](#), [51](#), [55](#)
- Menanteau F., Ford H. C., Illingworth G. D., Sirianni M., Blakeslee J. P., Meurer G. R., Martel A. R., Benítez N., Postman M., Franx M., Ardila D. R., Bartko F., Bouwens R. J., Broadhurst T. J., Brown R. A., Burrows C. J., Cheng E. S., Clampin M., Cross N. J. G., Feldman P. D., Golimowski D. A., Gronwall C., Hartig G. F., Infante L., Kimble R. A., Krist J. E., Lesser M. P., Miley G. K., Rosati P., Sparks W. B., Tran H. D., Tsvetanov Z. I., White R. L. and Zheng W. *Internal Color Properties of Resolved Spheroids in the Deep Hubble Space Telescope Advanced Camera for Surveys Field of UGC 10214*. ApJ, vol. 612, pages 202–214, September 2004. [50](#)
- Menanteau F., Ford H. C., Motta V., Benítez N., Martel A. R., Blakeslee J. P. and Infante L. *The Morphological Demographics of Galaxies in the Advanced Camera for Surveys Hubble Ultra Deep Parallel Fields*. AJ, vol. 131, pages 208–215, January 2006. [45](#)

- Miralda-Escudé J. *The Dark Age of the Universe*. Science, vol. 300, pages 1904–1909, June 2003. [128](#)
- Mo H. J., Mao S. and White S. D. M. *The formation of galactic discs*. MNRAS, vol. 295, pages 319–336, April 1998. [65](#)
- Moore B., Katz N., Lake G., Dressler A. and Oemler A. *Galaxy harassment and the evolution of clusters of galaxies*. Nature, vol. 379, pages 613–616, February 1996. [25](#)
- Morgan W. W. and Keenan P. C. *Spectral Classification*. ARA&A, vol. 11, pages 29–+, 1973. [17](#)
- Morgan W. W. and Mayall N. U. *A Spectral Classification of Galaxies*. PASP, vol. 69, pages 291–+, August 1957. [17](#)
- Morgan W. W., Keenan P. C. and Kellman E. An atlas of stellar spectra, with an outline of spectral classification. 1943. [17](#)
- Morgan W. W. *A Preliminary Classification of the Forms of Galaxies According to Their Stellar Population*. PASP, vol. 70, pages 364–+, August 1958. [17](#), [18](#)
- Morgan W. W. *Preliminary Classification of the Forms of Galaxies According to Their Stellar Population. II*. PASP, vol. 71, pages 394–+, October 1959. [17](#)
- Mouri H. and Taniguchi Y. *Downsizing of star-forming galaxies by gravitational processes*. A&A, vol. 459, pages 371–374, November 2006. [26](#)
- Naab T. and Burkert A. *Statistical Properties of Collisionless Equal- and Unequal-Mass Merger Remnants of Disk Galaxies*. ApJ, vol. 597, pages 893–906, November 2003. [33](#)
- Naim A., Lahav O., Buta R. J., Corwin Jr. H. G., de Vaucouleurs G., Dressler A., Huchra J. P., van den Bergh S., Raychaudhury S., Sodre Jr. L. and Storrie-Lombardi M. C. *A comparative study of morphological classifications of APM galaxies*. MNRAS, vol. 274, pages 1107–1125, June 1995. [11](#), [81](#)
- Nakamura O., Fukugita M., Brinkmann J. and Schneider D. P. *The H α Luminosity Function of Morphologically Classified Galaxies in the Sloan Digital Sky Survey*. AJ, vol. 127, pages 2511–2521, May 2004. [22](#), [53](#), [59](#)
- Neichel B., Hammer F., Puech M., Flores H., Lehnert M., Rawat A., Yang Y., Delgado-Serrano R., Amram P., Balkowski C., Cesarsky C., Dannerbauer H., Fuentes-Carrera I., Guiderdoni B., Kembhavi A., Liang Y. C., Nesvadba N., Östlin G., Pozzetti L., Ravikumar C. D., di Serego Alighieri S., Vergani D., Vernet J. and Wozniak H. *IMAGES. II. A surprisingly low fraction of undisturbed rotating spiral disks at $z \sim 0.6$ The morpho-kinematical relation 6 Gyr ago*. A&A, vol. 484, pages 159–172, June 2008. [10](#), [50](#), [57](#), [75](#), [76](#), [80](#), [90](#)

- Neichel B. *Etude des galaxies lointaines et optiques adaptatives tomographiques pour les ELTs*. PhD thesis, Université Paris VII - Denis Diderot, 2008. [138](#)
- Neistein E., van den Bosch F. C. and Dekel A. *Natural downsizing in hierarchical galaxy formation*. MNRAS, vol. 372, pages 933–948, October 2006. [26](#)
- Nieuwenhuizen T. M. *The case of 1.5 eV neutrino hot dark matter*. ArXiv e-prints, March 2010. [117](#)
- Ninkovic S., Chernin A. and Shakenov M. *Missing Mass and the Dynamics of the Local Group*. Soviet Astronomy Letters, vol. 16, pages 454–+, November 1990. [117](#)
- Noeske K. G., Koo D. C., Phillips A. C., Willmer C. N. A., Melbourne J., Gil de Paz A. and Papaderos P. *Luminous Compact Blue Galaxies up to $z \sim 1$ in the Hubble Space Telescope Ultra Deep Field. I. Small Galaxies or Blue Centers of Massive Disks?* ApJ, vol. 640, pages L143–L146, April 2006. [65](#)
- Nordon R., Lutz D., Shao L., Magnelli B., Berta S., Altieri B., Andreani P., Aussel H., Bongiovanni A., Cava A., Cepa J., Cimatti A., Daddi E., Dominguez H., Elbaz D., Förster Schreiber N. M., Genzel R., Grazian A., Magdis G., Maiolino R., Pérez García A. M., Poglitsch A., Popesso P., Pozzi F., Riguccini L., Rodighiero G., Saintonge A., Sanchez-Portal M., Santini P., Sturm E., Tacconi L., Valtchanov I., Wetzstein M. and Wieprecht E. *The star-formation rates of $1.5 < z < 2.5$ massive galaxies*. A&A, vol. 518, pages L24+, July 2010. [64](#)
- Okazaki T. and Taniguchi Y. *Dwarf Galaxy Formation Induced by Galaxy Interactions*. ApJ, vol. 543, pages 149–152, November 2000. [37](#)
- Oke J. B. *Absolute Spectral Energy Distributions for White Dwarfs*. ApJS, vol. 27, pages 21–+, February 1974. [135](#)
- Osterbrock D. E. and Ferland G. J. *Astrophysics of gaseous nebulae and active galactic nuclei*. 2006. [140](#)
- Östlin G., Amram P., Bergvall N., Masegosa J., Boulesteix J. and Márquez I. *Dynamics of blue compact galaxies, as revealed by their $H\alpha$ velocity fields. II. Mass models and the starburst triggering mechanism*. A&A, vol. 374, pages 800–823, August 2001. [65](#)
- Papovich C., Dickinson M., Giavalisco M., Conselice C. J. and Ferguson H. C. *The Assembly of Diversity in the Morphologies and Stellar Populations of High-Redshift Galaxies*. ApJ, vol. 631, pages 101–120, September 2005. [45](#), [50](#)
- Peebles P. J. E. and Dicke R. H. *Origin of the Globular Star Clusters*. ApJ, vol. 154, pages 891–+, December 1968. [119](#)

- Peebles P. J. E. and Yu J. T. *Primeval Adiabatic Perturbation in an Expanding Universe*. ApJ, vol. 162, pages 815–+, December 1970. [116](#)
- Peebles P. J. E. *Origin of the Angular Momentum of Galaxies*. ApJ, vol. 155, pages 393–+, February 1969. [29](#)
- Peebles P. J. E. *Primeval Globular Clusters. II*. ApJ, vol. 157, pages 1075–+, September 1969. [119](#)
- Peebles P. J. *Nonlinear Limit on Primeval Adiabatic Perturbations*. Phys. Rev. D, vol. 1, pages 397–399, January 1970. [116](#)
- Peebles P. J. E. *A Cosmic Virial Theorem*. ApJ, vol. 205, pages L109+, May 1976. [37](#)
- Peebles P. J. E. *Tests of cosmological models constrained by inflation*. ApJ, vol. 284, pages 439–444, September 1984. [122](#)
- Peirani S., Hammer F., Flores H., Yang Y. and Athanassoula E. *A giant bar induced by a merger event at $z = 0.4$?* A&A, vol. 496, pages 51–56, March 2009. [36](#)
- Peng C. Y., Ho L. C., Impey C. D. and Rix H.-W. *Detailed Structural Decomposition of Galaxy Images*. AJ, vol. 124, pages 266–293, July 2002. [49](#), [84](#), [89](#)
- Peng C. Y., Ho L. C., Impey C. D. and Rix H.-W. *Detailed Decomposition of Galaxy Images. II. Beyond Axisymmetric Models*. AJ, vol. 139, pages 2097–2129, June 2010. [49](#), [80](#), [83](#), [85](#), [86](#), [89](#)
- Pérez-González P. G., Rieke G. H., Egami E., Alonso-Herrero A., Dole H., Papovich C., Blaylock M., Jones J., Rieke M., Rigby J., Barmby P., Fazio G. G., Huang J. and Martin C. *Spitzer View on the Evolution of Star-forming Galaxies from $z = 0$ to $z \sim 3$* . ApJ, vol. 630, pages 82–107, September 2005. [64](#)
- Pérez-González P. G., Rieke G. H., Villar V., Barro G., Blaylock M., Egami E., Gallego J., Gil de Paz A., Pascual S., Zamorano J. and Donley J. L. *The Stellar Mass Assembly of Galaxies from $z = 0$ to $z = 4$: Analysis of a Sample Selected in the Rest-Frame Near-Infrared with Spitzer*. ApJ, vol. 675, pages 234–261, March 2008. [64](#)
- Perlmutter S., Aldering G., Goldhaber G., Knop R. A., Nugent P., Castro P. G., Deustua S., Fabbro S., Goobar A., Groom D. E., Hook I. M., Kim A. G., Kim M. Y., Lee J. C., Nunes N. J., Pain R., Pennypacker C. R., Quimby R., Lidman C., Ellis R. S., Irwin M., McMahon R. G., Ruiz-Lapuente P., Walton N., Schaefer B., Boyle B. J., Filippenko A. V., Matheson T., Fruchter A. S., Panagia N., Newberg H. J. M., Couch W. J. and The Supernova Cosmology Project. *Measurements of Ω and Λ from 42 High-Redshift Supernovae*. ApJ, vol. 517, pages 565–586, June 1999. [127](#)

- Pignatelli E., Fasano G. and Cassata P. *GASPHOT: a tool for Galaxy Automatic Surface PHOTometry*. A&A, vol. 446, pages 373–388, January 2006. [49](#)
- Pizzella A., Corsini E. M., Vega Beltrán J. C. and Bertola F. *Ionized gas and stellar kinematics of seventeen nearby spiral galaxies*. A&A, vol. 424, pages 447–454, September 2004. [22](#)
- Popa L. A., Burigana C. and Mandolesi N. *Cosmological Parameter Determination from Planck and Sloan Digital Sky Survey Data in Λ Cold+Hot Dark Matter Cosmologies*. ApJ, vol. 558, pages 10–22, September 2001. [119](#)
- Portinari L. and Sommer-Larsen J. *The Tully-Fisher relation and its evolution with redshift in cosmological simulations of disc galaxy formation*. MNRAS, vol. 375, pages 913–924, March 2007. [66](#)
- Pozzetti L., Cimatti A., Zamorani G., Daddi E., Menci N., Fontana A., Renzini A., Mignoli M., Poli F., Saracco P., Broadhurst T., Cristiani S., D’Odorico S., Giallongo E. and Gilmozzi R. *The K20 survey. V. The evolution of the near-IR Luminosity Function*. A&A, vol. 402, pages 837–848, May 2003. [57](#), [58](#), [74](#)
- Primack J. R. and Blumenthal G. R. *What is the dark matter? - Implications for galaxy formation and particle physics*. In J. Audouze & J. Tran Thanh Van , editeur, NATO ASIC Proc. 117: Formation and Evolution of Galaxies and Large Structures in the Universe, pages 163–183, 1984. [4](#), [120](#)
- Primack J. R. and Gross M. A. K. *Cold + Hot Dark Matter After Super-Kamiokande*. ArXiv Astrophysics e-prints, October 1998. [119](#)
- Primack J. R. and Gross M. A. K. *Hot dark matter in cosmology*, pages 287–308. 2001. [119](#)
- Primack J. R. *Dark Matter and Galaxy Formation*. In F. Roig, D. Lopes, R. de La Reza, & V. Ortega , editeur, American Institute of Physics Conference Series, volume 1192 of *American Institute of Physics Conference Series*, pages 101–137, December 2009. [117](#)
- Puech M., Flores H., Hammer F. and Lehnert M. D. *3D spectroscopy with VLT/GIRAFFE. III. Mapping electron densities in distant galaxies*. A&A, vol. 455, pages 131–134, August 2006. [140](#)
- Puech M., Hammer F., Flores H., Östlin G. and Marquart T. *3D spectroscopy with VLT/GIRAFFE. II. Are luminous compact galaxies merger remnants?* A&A, vol. 455, pages 119–129, August 2006. [65](#), [140](#)
- Puech M., Hammer F., Lehnert M. D. and Flores H. *3D spectroscopy with VLT/GIRAFFE. IV. Angular momentum and dynamical support of intermediate redshift galaxies*. A&A, vol. 466, pages 83–92, April 2007. [35](#), [36](#)

- Puech M., Flores H., Hammer F., Yang Y., Neichel B., Lehnert M., Chemin L., Nesvadba N., Epinat B., Amram P., Balkowski C., Cesarsky C., Dannerbauer H., di Serego Alighieri S., Fuentes-Carrera I., Guiderdoni B., Kembhavi A., Liang Y. C., Östlin G., Pozzetti L., Ravikumar C. D., Rawat A., Vergani D., Vernet J. and Wozniak H. *IMAGES. III. The evolution of the near-infrared Tully-Fisher relation over the last 6 Gyr.* A&A, vol. 484, pages 173–187, June 2008. [75](#), [107](#), [138](#), [139](#), [140](#)
- Puech M., Hammer F., Flores H., Neichel B. and Yang Y. *A forming disk at $z \sim 0.6$: collapse of a gaseous disk or major merger remnant?* A&A, vol. 493, pages 899–906, January 2009. [37](#)
- Puech M., Hammer F., Flores H., Delgado-Serrano R., Rodrigues M. and Yang Y. *The baryonic content and Tully-Fisher relation at $z \sim 0.6$.* A&A, vol. 510, pages A68+, February 2010. [37](#), [107](#)
- Puech M. *Contraintes apportées par la spectroscopie intégrale de champ à la formation et à l'évolution des galaxies.* PhD thesis, Université Paris VII - Denis Diderot, 2006. [138](#), [139](#), [140](#)
- Rasera Y. and Teyssier R. *The history of the baryon budget. Cosmic logistics in a hierarchical universe.* A&A, vol. 445, pages 1–27, January 2006. [128](#)
- Ratnatunga K. U., Griffiths R. E. and Ostrander E. J. *Disk and Bulge Morphology of WFPC2 Galaxies: The HUBBLE SPACE TELESCOPE Medium Deep Survey.* AJ, vol. 118, pages 86–107, July 1999. [48](#)
- Ravikumar C. D., Puech M., Flores H., Proust D., Hammer F., Lehnert M., Rawat A., Amram P., Balkowski C., Burgarella D., Cassata P., Cesarsky C., Cimatti A., Combes F., Daddi E., Dannerbauer H., di Serego Alighieri S., Elbaz D., Guiderdoni B., Kembhavi A., Liang Y. C., Pozzetti L., Vergani D., Vernet J., Wozniak H. and Zheng X. Z. *New spectroscopic redshifts from the CDFS and a test of the cosmological relevance of the GOODS-South field.* A&A, vol. 465, pages 1099–1108, April 2007. [73](#), [75](#)
- Ravindranath S., Ferguson H. C., Conselice C., Giavalisco M., Dickinson M., Chatzichristou E., de Mello D., Fall S. M., Gardner J. P., Grogin N. A., Hornschemeier A., Jogee S., Koekemoer A., Kretchmer C., Livio M., Mobasher B. and Somerville R. *The Evolution of Disk Galaxies in the GOODS-South Field: Number Densities and Size Distribution.* ApJ, vol. 604, pages L9–L12, March 2004. [49](#)
- Rawat A., Kembhavi A. K., Hammer F., Flores H. and Barway S. *Unravelling the morphologies of luminous compact galaxies using the HST/ACS GOODS survey.* A&A, vol. 469, pages 483–501, July 2007. [51](#), [65](#), [84](#), [88](#)

- Rawat A., Hammer F., Kembhavi A. K. and Flores H. *Toward a Robust Estimate of the Merger Rate Evolution Using Near-IR Photometry*. ApJ, vol. 681, pages 1089–1098, July 2008. [29](#), [64](#)
- Regan M. W. and Elmegreen D. M. *K-Band observations of barred spiral galaxies*. AJ, vol. 114, pages 965–+, September 1997. [95](#)
- Reichardt C. L., Ade P. A. R., Bock J. J., Bond J. R., Brevik J. A., Contaldi C. R., Daub M. D., Dempsey J. T., Goldstein J. H., Holzapfel W. L., Kuo C. L., Lange A. E., Lueker M., Newcomb M., Peterson J. B., Ruhl J., Runyan M. C. and Staniszewski Z. *High-Resolution CMB Power Spectrum from the Complete ACBAR Data Set*. ApJ, vol. 694, pages 1200–1219, April 2009. [8](#)
- Retzlaff J., Rosati P., Dickinson M., Vandame B., Rit   C., Nonino M., Cesarsky C. and GOODS Team . *The Great Observatories Origins Deep Survey. VLT/ISAAC near-infrared imaging of the GOODS-South field*. A&A, vol. 511, pages A50+, February 2010. [88](#)
- Riess A. G., Filippenko A. V., Challis P., Clocchiatti A., Diercks A., Garnavich P. M., Gilliland R. L., Hogan C. J., Jha S., Kirshner R. P., Leibundgut B., Phillips M. M., Reiss D., Schmidt B. P., Schommer R. A., Smith R. C., Spyromilio J., Stubbs C., Suntzeff N. B. and Tonry J. *Observational Evidence from Supernovae for an Accelerating Universe and a Cosmological Constant*. AJ, vol. 116, pages 1009–1038, September 1998. [127](#)
- Roberts M. S. and Haynes M. *Global Properties Along the Morphological Sequence from Im to Sa*. In G. Meylan & P. Prugniel , editeur, European Southern Observatory Conference and Workshop Proceedings, volume 49 of *European Southern Observatory Conference and Workshop Proceedings*, pages 197–+, January 1994. [22](#)
- Roberts M. S. and Haynes M. P. *Physical Parameters along the Hubble Sequence*. ARA&A, vol. 32, pages 115–152, 1994. [22](#), [51](#)
- Roberts M. S. *Integral Properties of Spiral and Irregular Galaxies*. AJ, vol. 74, pages 859–+, September 1969. [22](#)
- Roberts M. S. *M 31 and a Brief History of Dark Matter*. In A. H. Bridle, J. J. Condon, & G. C. Hunt , editeur, Frontiers of Astrophysics: A Celebration of NRAO’s 50th Anniversary, volume 395 of *Astronomical Society of the Pacific Conference Series*, pages 283–+, August 2008. [117](#)
- Robertson B., Bullock J. S., Cox T. J., Di Matteo T., Hernquist L., Springel V. and Yoshida N. *A Merger-driven Scenario for Cosmological Disk Galaxy Formation*. ApJ, vol. 645, pages 986–1000, July 2006. [33](#), [34](#), [35](#)

- Rodighiero G., Cimatti A., Gruppioni C., Popesso P., Andreani P., Altieri B., Aussel H., Berta S., Bongiovanni A., Brisbin D., Cava A., Cepa J., Daddi E., Dominguez-Sanchez H., Elbaz D., Fontana A., Förster Schreiber N., Franceschini A., Genzel R., Grazian A., Lutz D., Magdis G., Magliocchetti M., Magnelli B., Maiolino R., Mancini C., Nordon R., Perez Garcia A. M., Poglitsch A., Santini P., Sanchez-Portal M., Pozzi F., Riguccini L., Saintonge A., Shao L., Sturm E., Tacconi L., Valtchanov I., Wetzstein M. and Wieprecht E. *The first Herschel view of the mass-SFR link in high- z galaxies*. A&A, vol. 518, pages L25+, July 2010. [64](#)
- Rodrigues M., Hammer F., Flores H., Puech M., Liang Y. C., Fuentes-Carrera I., Nesvadba N., Lehnert M., Yang Y., Amram P., Balkowski C., Cesarsky C., Dannerbauer H., Delgado R., Guiderdoni B., Kembhavi A., Neichel B., Östlin G., Pozzetti L., Ravikumar C. D., Rawat A., di Serego Alighieri S., Vergani D., Vernet J. and Wozniak H. *IMAGES IV: strong evolution of the oxygen abundance in gaseous phases of intermediate mass galaxies from $z \sim 0.8$* . A&A, vol. 492, pages 371–388, December 2008. [75](#), [108](#)
- Rohlf K. and Kreitschmann J. *Dynamical mass modelling of the Galaxy*. A&A, vol. 201, pages 51–62, July 1988. [117](#)
- Sandage A. and Bedke J. The Carnegie Atlas of Galaxies. Volumes I, II. 1994. [14](#), [47](#), [53](#)
- Sandage A. and Tammann G. A. A revised Shapley-Ames Catalog of bright galaxies. 1981. [14](#)
- Sandage A., Freeman K. C. and Stokes N. R. *The Intrinsic Flattening of e , so , and Spiral Galaxies as Related to Galaxy Formation and Evolution*. ApJ, vol. 160, pages 831–+, June 1970. [25](#)
- Sandage A., Sandage M. and Kristian J. Galaxies and the Universe. 1975. [9](#), [14](#), [21](#)
- Sandage A. *The Classification of Galaxies: Early History and Ongoing Developments*. ARA&A, vol. 43, pages 581–624, September 2005. [23](#)
- Sanders D. B. and Mirabel I. F. *Luminous Infrared Galaxies*. ARA&A, vol. 34, pages 749–+, 1996. [54](#)
- Saracco P., Longhetti M., Severgnini P., Della Ceca R., Braito V., Mannucci F., Bender R., Drory N., Feulner G., Hopp U. and Maraston C. *The density of very massive evolved galaxies to $z \sim 1.7$* . MNRAS, vol. 357, pages L40–L44, February 2005. [26](#)

- Sargent M. T., Carollo C. M., Lilly S. J., Scarlata C., Feldmann R., Kampczyk P., Koekemoer A. M., Scoville N., Kneib J.-P., Leauthaud A., Massey R., Rhodes J., Tasca L. A. M., Capak P., McCracken H. J., Porciani C., Renzini A., Taniguchi Y., Thompson D. J. and Sheth K. *The Evolution of the Number Density of Large Disk Galaxies in COSMOS*. ApJS, vol. 172, pages 434–455, September 2007. [49](#)
- Scarlata C., Carollo C. M., Lilly S., Sargent M. T., Feldmann R., Kampczyk P., Porciani C., Koekemoer A., Scoville N., Kneib J.-P., Leauthaud A., Massey R., Rhodes J., Tasca L., Capak P., Maier C., McCracken H. J., Mobasher B., Renzini A., Taniguchi Y., Thompson D., Sheth K., Ajiki M., Aussel H., Murayama T., Sanders D. B., Sasaki S., Shioya Y. and Takahashi M. *COSMOS Morphological Classification with the Zurich Estimator of Structural Types (ZEST) and the Evolution Since $z = 1$ of the Luminosity Function of Early, Disk, and Irregular Galaxies*. ApJS, vol. 172, pages 406–433, September 2007. [46](#)
- Schade D., Lilly S. J., Crampton D., Hammer F., Le Fevre O. and Tresse L. *Canada-France Redshift Survey: Hubble Space Telescope Imaging of High-Redshift Field Galaxies*. ApJ, vol. 451, pages L1+, September 1995. [44](#), [48](#)
- Schade D., Lilly S. J., Le Fevre O., Hammer F. and Crampton D. *Canada-France Redshift Survey. XI. Morphology of High-Redshift Field Galaxies from High-Resolution Ground-based Imaging*. ApJ, vol. 464, pages 79–+, June 1996. [48](#)
- Schade D., Lilly S. J., Crampton D., Ellis R. S., Le Fèvre O., Hammer F., Brinchmann J., Abraham R., Colless M., Glazebrook K., Tresse L. and Broadhurst T. *Hubble Space Telescope Imaging of the CFRS and LDSS Redshift Surveys. III. Field Elliptical Galaxies at $0.2 < z < 1.0$* . ApJ, vol. 525, pages 31–46, November 1999. [27](#), [55](#)
- Scherrer R. J. *Resurrecting hot dark matter - Large-scale structure from cosmic strings and massive neutrinos*. PASP, vol. 100, pages 1364–1366, November 1988. [117](#)
- Schrabback T., Hartlap J., Joachimi B., Kilbinger M., Simon P., Benabed K., Bradač M., Eifler T., Erben T., Fassnacht C. D., High F. W., Hilbert S., Hildebrandt H., Hoekstra H., Kuijken K., Marshall P. J., Mellier Y., Morganson E., Schneider P., Semboloni E., van Waerbeke L. and Velander M. *Evidence of the accelerated expansion of the Universe from weak lensing tomography with COSMOS*. A&A, vol. 516, pages A63+, June 2010. [127](#)
- Schramm D. N. and Turner M. S. *Big-bang nucleosynthesis enters the precision era*. Reviews of Modern Physics, vol. 70, pages 303–318, January 1998. [126](#)
- Scott D. and Smoot G. *Cosmic Microwave Background Mini-Review*. ArXiv Astrophysics e-prints, January 2006. [117](#)

- Sellwood J. A. and Wilkinson A. *Dynamics of barred galaxies*. Reports on Progress in Physics, vol. 56, pages 173–256, February 1993. [94](#)
- Semelin B. and Combes F. *New multi-zoom method for N-body simulations: application to galaxy growth by accretion*. A&A, vol. 441, pages 55–67, October 2005. [31](#)
- Sersic J. L. Atlas de galaxias australes. 1968. [48](#), [84](#)
- Shandarin S. F. and Zeldovich Y. B. *The large-scale structure of the universe: Turbulence, intermittency, structures in a self-gravitating medium*. Reviews of Modern Physics, vol. 61, pages 185–220, April 1989. [116](#)
- Shaw M. A. and Gilmore G. *The luminosity distributions of edge-on spiral galaxies. I - A two-dimensional model and its application to NGC 891 and 4565*. MNRAS, vol. 237, pages 903–927, April 1989. [85](#)
- Shen S., Mo H. J., White S. D. M., Blanton M. R., Kauffmann G., Voges W., Brinkmann J. and Csabai I. *The size distribution of galaxies in the Sloan Digital Sky Survey*. MNRAS, vol. 343, pages 978–994, August 2003. [22](#)
- Sheth K., Regan M. W., Scoville N. Z. and Strubbe L. E. *Barred Galaxies at $z > 0.7$: NICMOS Hubble Deep Field-North Observations*. ApJ, vol. 592, pages L13–L16, July 2003. [13](#), [30](#), [95](#)
- Sheth K., Vogel S. N., Regan M. W., Thornley M. D. and Teuben P. J. *Secular Evolution via Bar-driven Gas Inflow: Results from BIMA SONG*. ApJ, vol. 632, pages 217–226, October 2005. [32](#)
- Sheth K., Elmegreen D. M., Elmegreen B. G., Capak P., Abraham R. G., Athanasoulas E., Ellis R. S., Mobasher B., Salvato M., Schinnerer E., Scoville N. Z., Spalsbury L., Strubbe L., Carollo M., Rich M. and West A. A. *Evolution of the Bar Fraction in COSMOS: Quantifying the Assembly of the Hubble Sequence*. ApJ, vol. 675, pages 1141–1155, March 2008. [31](#), [95](#), [99](#), [100](#)
- Shimasaku K., Fukugita M., Doi M., Hamabe M., Ichikawa T., Okamura S., Sekiguchi M., Yasuda N., Brinkmann J., Csabai I., Ichikawa S.-I., Ivezić Z., Kunszt P. Z., Schneider D. P., Szokoly G. P., Watanabe M. and York D. G. *Statistical Properties of Bright Galaxies in the Sloan Digital Sky Survey Photometric System*. AJ, vol. 122, pages 1238–1250, September 2001. [22](#)
- Simard L., Willmer C. N. A., Vogt N. P., Sarajedini V. L., Phillips A. C., Weiner B. J., Koo D. C., Im M., Illingworth G. D. and Faber S. M. *The DEEP Groth Strip Survey. II. Hubble Space Telescope Structural Parameters of Galaxies in the Groth Strip*. ApJS, vol. 142, pages 1–33, September 2002. [48](#), [49](#), [80](#), [84](#)

- Simien F. and de Vaucouleurs G. *Systematics of bulge-to-disk ratios*. ApJ, vol. 302, pages 564–578, March 1986. [21](#), [49](#), [91](#)
- Smail I., Dressler A., Couch W. J., Ellis R. S., Oemler Jr. A., Butcher H. and Sharples R. M. *A Catalog of Morphological Types in 10 Distant Rich Clusters of Galaxies*. ApJS, vol. 110, pages 213–+, June 1997. [45](#)
- Smoot G. F., Bennett C. L., Kogut A., Wright E. L., Aymon J., Boggess N. W., Cheng E. S., de Amici G., Gulkis S., Hauser M. G., Hinshaw G., Jackson P. D., Janssen M., Kaita E., Kelsall T., Keegstra P., Lineweaver C., Loewenstein K., Lubin P., Mather J., Meyer S. S., Moseley S. H., Murdock T., Rokke L., Silverberg R. F., Tenorio L., Weiss R. and Wilkinson D. T. *Structure in the COBE differential microwave radiometer first-year maps*. ApJ, vol. 396, pages L1–L5, September 1992. [117](#)
- Somerville R. S., Primack J. R. and Faber S. M. *The nature of high-redshift galaxies*. MNRAS, vol. 320, pages 504–528, February 2001. [33](#)
- Somerville R. S., Lee K., Ferguson H. C., Gardner J. P., Moustakas L. A. and Giavalisco M. *Cosmic Variance in the Great Observatories Origins Deep Survey*. ApJ, vol. 600, pages L171–L174, January 2004. [75](#)
- Springel V. and Hernquist L. *Formation of a Spiral Galaxy in a Major Merger*. ApJ, vol. 622, pages L9–L12, March 2005. [34](#)
- Springel V., Di Matteo T. and Hernquist L. *Modelling feedback from stars and black holes in galaxy mergers*. MNRAS, vol. 361, pages 776–794, August 2005. [34](#)
- Springel V., White S. D. M., Jenkins A., Frenk C. S., Yoshida N., Gao L., Navarro J., Thacker R., Croton D., Helly J., Peacock J. A., Cole S., Thomas P., Couchman H., Evrard A., Colberg J. and Pearce F. *Simulations of the formation, evolution and clustering of galaxies and quasars*. Nature, vol. 435, pages 629–636, June 2005. [123](#)
- Springel V., Frenk C. S. and White S. D. M. *The large-scale structure of the Universe*. Nature, vol. 440, pages 1137–1144, April 2006. [7](#)
- Springob C. M., Haynes M. P. and Giovanelli R. *Morphology, Environment, and the H I Mass Function*. ApJ, vol. 621, pages 215–226, March 2005. [22](#)
- Stewart K. R., Bullock J. S., Wechsler R. H. and Maller A. H. *Gas-rich Mergers in LCDM: Disk Survivability and the Baryonic Assembly of Galaxies*. ApJ, vol. 702, pages 307–317, September 2009. [107](#)

Stoughton C., Lupton R. H., Bernardi M., Blanton M. R., Burles S., Castander F. J., Connolly A. J., Eisenstein D. J., Frieman J. A., Hennessy G. S., Hindsley R. B., Ivezić Ž., Kent S., Kunszt P. Z., Lee B. C., Meiksin A., Munn J. A., Newberg H. J., Nichol R. C., Nicinski T., Pier J. R., Richards G. T., Richmond M. W., Schlegel D. J., Smith J. A., Strauss M. A., SubbaRao M., Szalay A. S., Thakar A. R., Tucker D. L., Vanden Berk D. E., Yanny B., Adelman J. K., Anderson Jr. J. E., Anderson S. F., Annis J., Bahcall N. A., Bakken J. A., Bartelmann M., Bastian S., Bauer A., Berman E., Böhringer H., Boroski W. N., Bracker S., Briegel C., Briggs J. W., Brinkmann J., Brunner R., Carey L., Carr M. A., Chen B., Christian D., Colestock P. L., Crocker J. H., Csabai I., Czarapata P. C., Dalcanton J., Davidsen A. F., Davis J. E., Dehnen W., Dodelson S., Doi M., Dombeck T., Donahue M., Ellman N., Elms B. R., Evans M. L., Eyer L., Fan X., Federwitz G. R., Friedman S., Fukugita M., Gal R., Gillespie B., Glazebrook K., Gray J., Grebel E. K., Greenawalt B., Greene G., Gunn J. E., de Haas E., Haiman Z., Haldeman M., Hall P. B., Hamabe M., Hansen B., Harris F. H., Harris H., Harvanek M., Hawley S. L., Hayes J. J. E., Heckman T. M., Helmi A., Henden A., Hogan C. J., Hogg D. W., Holmgren D. J., Holtzman J., Huang C.-H., Hull C., Ichikawa S.-I., Ichikawa T., Johnston D. E., Kauffmann G., Kim R. S. J., Kimball T., Kinney E., Klaene M., Kleinman S. J., Klypin A., Knapp G. R., Korienek J., Krolik J., Kron R. G., Krziesiński J., Lamb D. Q., Leger R. F., Limmongkol S., Lindenmeyer C., Long D. C., Loomis C., Loveday J., MacKinnon B., Mannery E. J., Mantsch P. M., Margon B., McGehee P., McKay T. A., McLean B., Menou K., Merelli A., Mo H. J., Monet D. G., Nakamura O., Narayanan V. K., Nash T., Neilsen Jr. E. H., Newman P. R., Nitta A., Odenkirchen M., Okada N., Okamura S., Ostriker J. P., Owen R., Pauls A. G., Peoples J., Peterson R. S., Petravick D., Pope A., Pordes R., Postman M., Prosapio A., Quinn T. R., Rechenmacher R., Rivetta C. H., Rix H.-W., Rockosi C. M., Rosner R., Ruthmansdorfer K., Sandford D., Schneider D. P., Scranton R., Sekiguchi M., Sergey G., Sheth R., Shimasaku K., Smee S., Snedden S. A., Stebbins A., Stubbs C., Szapudi I., Szkody P., Szokoly G. P., Tabachnik S., Tsvetanov Z., Uomoto A., Vogeley M. S., Voges W., Waddell P., Walterbos R., Wang S.-i., Watanabe M., Weinberg D. H., White R. L., White S. D. M., Wilhite B., Wolfe D., Yasuda N., York D. G., Zehavi I. and Zheng W. *Sloan Digital Sky Survey: Early Data Release*. AJ, vol. 123, pages 485–548, January 2002. [27](#)

Strateva I., Ivezić Ž., Knapp G. R., Narayanan V. K., Strauss M. A., Gunn J. E., Lupton R. H., Schlegel D., Bahcall N. A., Brinkmann J., Brunner R. J., Budavári T., Csabai I., Castander F. J., Doi M., Fukugita M., Györy Z., Hamabe M., Hennessy G., Ichikawa T., Kunszt P. Z., Lamb D. Q., McKay T. A., Okamura S., Racusin J., Sekiguchi M., Schneider D. P., Shimasaku K. and York D. *Color Separation of Galaxy Types in the Sloan Digital Sky Survey Imaging Data*. AJ, vol. 122, pages 1861–1874, October 2001. [22](#), [29](#)

- Sunyaev R. A. and Zeldovich Y. B. *Small scale entropy and adiabatic density perturbations - Antimatter in the Universe*. Ap&SS, vol. 9, pages 368–382, December 1970. [116](#)
- Thomas P. A., Colberg J. M., Couchman H. M. P., Efstathiou G. P., Frenk C. S., Jenkins A. R., Nelson A. H., Hutchings R. M., Peacock J. A., Pearce F. R. and White S. D. M. *The structure of galaxy clusters in various cosmologies*. MNRAS, vol. 296, pages 1061–1071, June 1998. [5](#), [121](#), [122](#)
- Tikhonov A. V., Gottlöber S., Yepes G. and Hoffman Y. *The sizes of minivoids in the local Universe: an argument in favour of a warm dark matter model?* MNRAS, vol. 399, pages 1611–1621, November 2009. [119](#)
- Tinsley B. M. *Correlation of the dark mass in galaxies with Hubble type*. MNRAS, vol. 194, pages 63–75, January 1981. [22](#)
- Treu T., Stiavelli M., Casertano S., Møller P. and Bertin G. *The Evolution of Field Early-Type Galaxies to $z \sim 0.7$* . ApJ, vol. 564, pages L13–L16, January 2002. [55](#)
- Tully R. B. and Fisher J. R. *A new method of determining distances to galaxies*. A&A, vol. 54, pages 661–673, February 1977. [66](#), [68](#)
- van den Bergh S., Abraham R. G., Ellis R. S., Tanvir N. R., Santiago B. X. and Glazebrook K. G. *A Morphological Catalog of Galaxies in the Hubble deep Field*. AJ, vol. 112, pages 359–+, August 1996. [55](#)
- van den Bergh S., Cohen J. G., Hogg D. W. and Blandford R. *Caltech Faint Galaxy Redshift Survey. XIV. Galaxy Morphology in the Hubble Deep Field (North) and Its Flanking Fields to $Z=1.2$* . AJ, vol. 120, pages 2190–2205, November 2000. [55](#)
- van den Bergh S., Cohen J. G. and Crabbe C. *Caltech Faint Galaxy Redshift Survey. XV. Classifications of Galaxies with $0.2 < Z < 1.1$ in the Hubble Deep Field North and its Flanking Fields*. AJ, vol. 122, pages 611–620, August 2001. [66](#)
- van den Bergh S. *A Preliminary Liminosity Classification for Galaxies of Type Sb*. ApJ, vol. 131, pages 558–+, May 1960. [19](#)
- van den Bergh S. *A Preliminary Luminosity Clssification of Late-Type Galaxies*. ApJ, vol. 131, pages 215–+, January 1960. [19](#)
- van den Bergh S. *A new classification system for galaxies*. ApJ, vol. 206, pages 883–887, June 1976. [20](#), [21](#)
- van den Bergh S. *Ten Billion Years of Galaxy Evolution*. PASP, vol. 114, pages 797–802, August 2002. [31](#), [38](#)
- van den Bergh S. *What are S0 Galaxies?* ApJ, vol. 694, pages L120–L122, April 2009. [9](#)

- van Dokkum P. G. and Ellis R. S. *On the Assembly History of Early-Type Galaxies in the Hubble Deep Field-North*. ApJ, vol. 592, pages L53–L57, August 2003. 55
- Vega Beltrán J. C., Pignatelli E., Zeilinger W. W., Pizzella A., Corsini E. M., Bertola F. and Beckman J. E. *Kinematics of Gas and Stars Along the Hubble Sequence*. Ap&SS, vol. 276, pages 509–516, March 2001. 22
- Velazquez H. and White S. D. M. *Sinking satellites and the heating of galaxy discs*. MNRAS, vol. 304, pages 254–270, April 1999. 32
- Verheijen M. A. W. *The Ursa Major Cluster of Galaxies*. In M. Persic & P. Salucci, editeur, *Dark and Visible Matter in Galaxies and Cosmological Implications*, volume 117 of *Astronomical Society of the Pacific Conference Series*, pages 190–+, 1997. 67
- Verheijen M. A. W. *The Ursa Major Cluster of Galaxies: TF-relations and dark matter*. PhD thesis, PhD thesis, Univ. Groningen, The Netherlands, (1997), 1997. 67
- Verheijen M. A. W. *The Ursa Major Cluster of Galaxies. V. H I Rotation Curve Shapes and the Tully-Fisher Relations*. ApJ, vol. 563, pages 694–715, December 2001. 143
- Vogt N. P., Forbes D. A., Phillips A. C., Gronwall C., Faber S. M., Illingworth G. D. and Koo D. C. *Optical Rotation Curves of Distant Field Galaxies: Keck Results at Reshifts to Z approximately 1*. ApJ, vol. 465, pages L15+, July 1996. 66, 69
- Vogt N. P., Phillips A. C., Faber S. M., Gallego J., Gronwall C., Guzman R., Illingworth G. D., Koo D. C. and Lowenthal J. D. *Optical Rotation Curves of Distant Field Galaxies: Sub-L Systems*. ApJ, vol. 479, pages L121+, April 1997. 66
- Walker I. R., Mihos J. C. and Hernquist L. *Quantifying the Fragility of Galactic Disks in Minor Mergers*. ApJ, vol. 460, pages 121–+, March 1996. 32
- Weiner B. J., Willmer C. N. A., Faber S. M., Melbourne J., Kassin S. A., Phillips A. C., Harker J., Metevier A. J., Vogt N. P. and Koo D. C. *A Survey of Galaxy Kinematics to $z \sim 1$ in the TKRS/GOODS-N Field. I. Rotation and Dispersion Properties*. ApJ, vol. 653, pages 1027–1048, December 2006. 140
- Werk J. K., Jangren A. and Salzer J. J. *Luminous Compact Blue Galaxies in the Local Universe*. ApJ, vol. 617, pages 1004–1016, December 2004. 65
- White S. D. M., Frenk C. S. and Davis M. *Clustering in a neutrino-dominated universe*. ApJ, vol. 274, pages L1–L5, November 1983. 118

- White S. D. M. *Angular momentum growth in protogalaxies*. ApJ, vol. 286, pages 38–41, November 1984. [37](#)
- Wilson G., Cowie L. L., Barger A. J. and Burke D. J. *Star Formation History since $z=1.5$ as Inferred from Rest-Frame Ultraviolet Luminosity Density Evolution*. AJ, vol. 124, pages 1258–1265, September 2002. [64](#)
- Wright S. A., Larkin J. E., Barczys M., Erb D. K., Iserlohe C., Krabbe A., Law D. R., McElwain M. W., Quirrenbach A., Steidel C. C. and Weiss J. *Integral Field Spectroscopy of a Candidate Disk Galaxy at $z \sim 1.5$ Using Laser Guide Star Adaptive Optics*. ApJ, vol. 658, pages 78–84, March 2007. [109](#)
- Wright S. A., Larkin J. E., Law D. R., Steidel C. C., Shapley A. E. and Erb D. K. *Dynamics of Galactic Disks and Mergers at $z \sim 1.6$: Spatially Resolved Spectroscopy with Keck Laser Guide Star Adaptive Optics*. ApJ, vol. 699, pages 421–440, July 2009. [109](#)
- Yamauchi C., Ichikawa S.-i., Doi M., Yasuda N., Yagi M., Fukugita M., Okamura S., Nakamura O., Sekiguchi M. and Goto T. *Morphological Classification of Galaxies Using Photometric Parameters: The Concentration Index versus the Coarseness Parameter*. AJ, vol. 130, pages 1545–1557, October 2005. [45](#)
- Yang Y., Flores H., Hammer F., Neichel B., Puech M., Nesvadba N., Rawat A., Cesarsky C., Lehnert M., Pozzetti L., Fuentes-Carrera I., Amram P., Balkowski C., Dannerbauer H., di Serego Alighieri S., Guiderdoni B., Kembhavi A., Liang Y. C., Östlin G., Ravikumar C. D., Vergani D., Vernet J. and Wozniak H. *IM-AGES. I. Strong evolution of galaxy kinematics since $z = 1$* . A&A, vol. 477, pages 789–805, January 2008. [38](#), [74](#), [75](#), [76](#), [137](#), [139](#), [140](#)
- Yang Y., Hammer F., Flores H., Puech M. and Rodrigues M. *A surviving disk from a galaxy collision at $z = 0.4$* . A&A, vol. 501, pages 437–443, July 2009. [36](#), [109](#)
- Yoachim P. and Dalcanton J. J. *Structural Parameters of Thin and Thick Disks in Edge-on Disk Galaxies*. AJ, vol. 131, pages 226–249, January 2006. [38](#)
- Zel’dovich Y. B. *Physics of Our Days: the “hot” Model of the Universe*. Soviet Physics Uspekhi, vol. 9, pages 602–617, April 1967. [116](#), [119](#)
- Zel’Dovich Y. B. *Gravitational instability: An approximate theory for large density perturbations*. A&A, vol. 5, pages 84–89, March 1970. [116](#)
- Zeldovich Y. B. *A hypothesis, unifying the structure and the entropy of the Universe*. MNRAS, vol. 160, pages 1P–+, 1972. [124](#)
- Zheng X. Z., Hammer F., Flores H., Assémat F. and Pelat D. *HST/WFPC2 morphologies and color maps of distant luminous infrared galaxies*. A&A, vol. 421, pages 847–862, July 2004. [34](#), [50](#), [51](#), [80](#), [91](#), [92](#)

- Zheng X. Z., Hammer F., Flores H., Assémat F. and Rawat A. *HST/WFPC2 morphologies and bar structures of field galaxies at $0.4 < z < 1$* . A&A, vol. 435, pages 507–519, May 2005. [30](#), [50](#), [51](#), [66](#), [95](#)
- Zwicky F. *On the Masses of Nebulae and of Clusters of Nebulae*. ApJ, vol. 86, pages 217–+, October 1937. [117](#)

The Evolution of the Hubble Sequence: morpho-kinematics of distant galaxies

Abstract: The main objective of my thesis was to provide us, for the first time, with a reliable view of the distant Hubble sequence, and its evolution over the past 6 Gyr. To achieve this goal, we have created a new morphological classification method which (1) includes all the available observational data, (2) can be easily reproduced, and (3) presents a negligible subjectivity. This method allows us to study homogeneously the morphology of local and distant galaxies, and has the main advantage of presenting a good correlation between the morphological type and dynamical state of each galaxy.

The first step has been to study the evolution of galaxies using the IMAGES survey. This survey allowed us to establish the kinematic state of distant galaxies, to study the chemical evolution of galaxies over the past 8 Gyr, and to test important dynamical relations such as the Tully-Fisher relation. Kinematics is, indeed, a crucial information needed to guarantee a robust understanding of the different physical processes leading to the present day Hubble sequence. Using Integral Field Spectroscopy, which provides a complete kinematic diagnosis, we have been able to test our new morphological classification against the kinematic state of each galaxy. We found that the morpho-kinematic correlation is much better using our classification than other morphological classifications. Applying our classification to a representative sample of galaxies at $z \sim 0.6$, we found that 4/5 of spiral galaxies are rotating disks, while more than 4/5 peculiar galaxies are not in a dynamical equilibrium.

Applying our morphological classification to a representative sample of both local and distant galaxies, having equivalent observational data, we obtained a Hubble sequence both in the local and distant Universe. We found that spiral galaxies were 5/2 times less abundant in the past, which is compensated exactly by the strong decrease by a factor 5 of peculiar galaxies, while the fraction number of elliptical and lenticular galaxies remains constant. It strongly suggests that more than half of the present-day spirals had peculiar morphologies, 6 Gyr ago.

Finally, I present further studies concerning the history of individual galaxies at $z < 1$, combining kinematic and morphological observations. I also present the first ever-estimated distant baryonic Tully-Fisher relation, which does not appear to evolve over the past 6 Gyr. In the coming years, our morphological classification and these studies will be extended to galaxies at $z \gg 1$, thanks to the future ELTs.

Keywords: Galaxy Formation and Evolution - Galaxy Morphology and kinematics.
